Assessment of Disease Progression in the Rare Disease Alkaptonuria by Quantitative Image Analysis

Thesis submitted in accordance with the requirements of the University of Liverpool for the degree of Doctor of Philosophy

by **Leah Frances Taylor**

April, 2018

ACKNOWLEDGMENTS

I would first and foremost like to express the greatest thanks to my number one supervisor Professor Jim Gallagher. Firstly, for giving me the opportunity to undertake this PhD and secondly, for his consistent support and guidance throughout the time I have been a part of his lab. I can honestly say it has been a pleasure to be a part of your group. I could not have felt more supported along the way with you and Jane who have looked after me like a daughter. I would also like to thank Jane for all the proof reading she has done for me, especially for correcting my awful grammar! I would also like to thank you both for pushing me to further my career and for supporting me to make the best decisions for my future. For this I will be forever thankful.

To Professor Ranganath I owe a huge thank you for always believing in me and supporting me and my work. Without your input, support and guidance this thesis would not have been possible.

Thank you to Dr Nathan Jeffery for his invaluable imaging knowledge and for giving me the opportunity to demonstrate Anatomy alongside my PhD. Thanks also to the following people; Sobhan Vinjamuri for facilitating my work in the nuclear medicine department; Mark Baker, for his hard work providing me with the patient scans and teaching me how to use the sophisticated software in the nuclear medicine department; Eftychia Psarelli for her invaluable guidance on statistical analysis.

A very important thank you goes to the AKU patients without whom this PhD would not have been possible. My gratitude for this work also goes to the Royal Liverpool University Hospital and The University of Liverpool for providing the funding for this work.

My next thanks go to my fellow colleagues. Hazel Sutherland for always being there for me. Your support was invaluable, you have been a true friend. A 'not so big' thanks goes to Pete and Dr Craig for taking the 'mick' out of me constantly for three years! However, I would not have expected anything less! You two have provided me with many laughs and have taught me not to take life too seriously, which I think is a very important lesson to learn…. even if I did want to punch your lights out for it.

Eddie and Brendan. We have shared many happy times together including lots of eating, drinking and introducing our friend to Western society, I know for that he will be forever grateful! There are lots of new members of Jim's group now including Juliette and Eman that I have had the pleasure of working with, I thank you all too for your support.

Finally, I would like to thank my family and friends. Firstly, I would like to thank my Mum & Barry and my Dad & Sue for supporting me both emotionally and financially throughout my life and always supporting my decisions and guiding me to make the right choices. Mum, thank you for your unconditional love and always having my back through thick and thin. I know I can always count on you anytime, anywhere. Dad,

thank you for everything especially your sense of humour and your ‘happy go lucky’ attitude to life. I have learnt to be more like this because of you. Without your support I would not be where I am today. Having said that, I am fully aware that you still haven’t got a clue about what I have spent the last three and a half years doing!

Thank you to my sister Ceri for always supporting me and teaching me how to be tough and to never give up. Thank you for listening to many of my talks however, I can still bet that I can put you to sleep as soon as I start talking. That is a skill!

I am especially grateful to my Gran and Nan for always showing interest in what I do and always being proud of me. I know that Grandad and Taid would be proud too. Thank you to my Aunty Karen for being a great walking partner and keeping me knowledgeable about health and wellbeing. I would also like to thank the rest of my family for always looking after me and supporting what I do.

Last, but not least, thank you to my best friends, Nicky and Kate. As nuts as you are I want to thank you for being such good friends to me and for always supporting me through the good, the bad and the ugly! Thank you for the laughs and the good times. Here is to many more great times ahead!

A big thank you also goes to all my good friends in Liverpool, Preston and back at home for your support, company and laughter. Long may this continue.

The support I have received throughout my life as well as the academic support I have been lucky enough to receive throughout this PhD has all had a massive part to play in this achievement. For this I will be forever thankful. I hope this thesis and everything I continue to do makes you all proud.

Leah

ABSTRACT

Alkaptonuria (AKU) arises from a genetic deficiency of homogentisate 1,2 dioxygenase (HGD) an enzyme involved in tyrosine metabolism. AKU is characterised by high circulating homogentisic acid (HGA) some of which is deposited as ochronotic pigment in connective tissues, mainly cartilage, leading to multisystemic damage dominated by premature severe osteoarthropathy.

Pathological changes in the spine as a result of ochronosis can be imaged using fluorine-18 labelled sodium fluoride positron emission tomography (^{18}F-NaF PET). This imaging modality allows quantitative assessment of focal bone remodelling by measuring the uptake of ^{18}F into the hydroxyapatite crystal of bone and calcified cartilage. The mean standardised uptake value (SUVm), a mathematically derived ratio of tissue radioactivity in a region of interest (ROI) and the decay corrected injected dose per kilogram of the patient's body weight has common place in oncology. The functional changes that ^{18}F-NaF PET detects have led to this modality being re-evaluated for its advantages in skeletal diseases such as osteoarthritis and AKU.

AKU patients underwent a variety of clinical testing and imaging including ^{18}F-NaF PET scanning at the Royal Liverpool University Hospital. Semi-quantitative analysis of the PET scans was utilised to investigate the anatomical distribution of increased ^{18}F uptake. Quantitative SUVms were also obtained as a measure of Fluoride uptake in the bony vertebrae and cartilaginous intervertebral discs (IVD). Other clinical data were taken from the case notes for correlation.

The anatomical distribution of increased ^{18}F uptake was confirmed to primarily affect the weight bearing joints. The quantitative SUVm methodology revealed a striking variation between AKU and control SUVms in the IVDs thought to represent calcification of the IVDs in AKU. The mechanism proposed is that calcium hydroxyapatite or calcium pyrophosphate dihydrate are deposited in the fibrocartilaginous IVDs in AKU due to biochemical alterations of the disease. ^{18}F binds to the calcium deposits resulting in high SUVms compared to the control. The SUVms obtained from the vertebrae in both AKU and control patients are similar across the lumbar and thoracic spine suggesting that generalised rates of bone turnover in AKU and control patients are comparable.

With age the AKU SUVms of the IVDs followed an interesting trend (the inverted ‘U’ shaped trend) that was strikingly different to that of the control group that appears to remain stable with age. It is proposed that the AKU trend demonstrates the process of disc degeneration. In the bony vertebrae, an age-related decline in SUVm was observed in both AKU and control groups, thought to represent reduced bone turnover with age.

Correlations were made with the IVD SUVms and other clinical data. Reduced vertebrae SUVm and increased IVD SUVm were found to be associated with higher clinical scores, pain scores, excessive spinal curvature angles, lower BMD T-scores and spinal flexibility measurements. The proposed reason for this is primarily due to reduced BMD with age and spinal arthropathy associated with calcified IVDs.

All in all, this thesis has provided new insights into spinal arthropathy in AKU. The utilisation of novel quantitative techniques demonstrated in this thesis can be used to aid in clinical interpretation of PET scans as well as providing a measure of disease severity and to analyse disease progression and response to therapy.

ABBREVIATIONS

AC - Articular cartilage

ACC - Articular calcified cartilage

AKU - Alkaptonuria

AKUSSI – Alkaptonuria severity score index

AT – Anatomical threshold

B-AT – Bone-anatomical threshold

BMD – Bone mineral density

BQA - Benzoquinone acetic acid

C-AT – Cartilage-anatomical threshold

CT – Computed tomography

DEXA – Dual-energy x-ray absorptiometry

DICOM – Digital imaging and communications in Medicine

ECM - Extracellular matrix

ENT – Ear, nose and throat

EO - Endochondral ossification

^{18}F-NaF – Fluorine-18- labelled Sodium Fluoride

FDA – Food and Drug Administration

HA - Hyaluronan

HAC - Hyaline articular cartilage

HDMPs - High density mineralised protrusions

HGA - Homogentisic acid

HGD - Homogentisate 1,2-dioxygenase

HPPA - 4-hydroxyphenylpyruvic acid

HPPD - 4-hydroxyphenylpyruvate dioxygenase

HT1 - Tyrosinemia type 1

IL-11 – Interleukin 11

IO - Intramembranous ossification

ITM -Interterritorial matrix

IVD - Intervertebral disc

JPEG – Joint photographic experts group

KL – Kellgren and Lawrence

LC-MS/MS- Liquid chromatography tandem mass spectrometry

MIP – Maximum intensity projection

MRI – Magnetic resonance imaging

NAC- National Alkaptonuria Centre

NIH - National Institute of Health

NTBC - Nitisinone

OA - Osteoarthritis

PA view- Posteroanterior view (X-Ray)

PACS – Picture archiving and communication systems

PCM – Pericellular matrix

PET – Positron emission tomography

QCT – Quantitative computer tomography

RA – Rheumatoid arthritis

RLBUHT- Royal Liverpool and Broadgreen University Hospital Trust

ROI – Region of interest

RGB – Red, green, blue

SB -Subchondral bone

SEM – Standard error of the mean

s-HGA - serum homogentisic acid

SOFIA - Subclinical ochronotic features in alkaptonuria

SONIA1 - Suitability of nitisinone in alkaptonuria 1

SONIA2 - Suitability of nitisinone in alkaptonuria 2

SPECT - Single-photon emission computed tomography

SUV- Standardised uptake value

SUVm – Mean standardised uptake value

TM – Territorial matrix

TSC – Trans axial, sagittal, coronal

TIFF – Tagged image file format

TOF – Time of flight

u-HGA- urine homogentisic acid

WHO – World Health Organisation

3D - Three dimensional

TABLE OF CONTENTS

LIST OF FIGURES

CHAPTER 1

CHAPTER 2

CHAPTER 3

CHAPTER 4

CHAPTER 5

CHAPTER 6

LIST OF TABLES

CHAPTER 1

CHAPTER 2

CHAPTER 6

1.0 INTRODUCTION

1.1 Alkaptonuria

Alkaptonuria (AKU) is a rare autosomal recessive disorder that arises due to a genetic deficiency of homogentisate 1, 2 dioxygenase (HGD), an enzyme involved in tyrosine metabolism resulting in the inability to fully metabolise tyrosine and phenylalanine. Loss of activity of the HGD enzyme results in high circulating levels of homogentisic acid (HGA) (Figure 1.1). Oxidative conversion of HGA leads to the production of a melanin-like polymer, this is termed ochronosis (Figure 1.2) (1). HGA is excreted via the urinary system causing urine to darken upon exposure to air (2). However, some HGA is deposited over time in connective tissues leading to the formation of ochronotic pigment which causes multisystemic damage dominated by premature severe osteoarthropathy (2,3).

1.1.1 History

The earliest reported case of alkaptonuria dates back to 1500 B.C of an Egyptian mummy named *Harwa.* Biochemical and radiographical analysis of the hip and knee joints and intervertebral discs were used to confirm the diagnosis (4–6). The first clinical case of alkaptonuria was reported in 1584, when Scibonius reported a case of a school boy in good health who passed urine "as black as ink" and coined the term 'black urine disease' (7). Schenck reported the same findings in a Carmelite monk. The term "alkaptonuria" was first used in 1859 by Boedeker to describe the discolouration of urine due to the unusual reducing properties of a compound it contained (4). He named this compound 'alkapton' derived from the Arabic word 'alkali' and a Greek word meaning "to suck up oxygen greedily" (4,8,9). The term

ochronosis was first described by Virchow in 1866 after discovering black pigmented articular cartilage of a 67-year-old man. He examined the pigment microscopically and found the pigment was actually yellow/brown (ochre) in colour leading him to describe the findings as ochronosis (10). Wolkow and Bauman identified HGA as the causative compound by 1891 (9). Albrecht, made the link between between AKU and ochronosis in 1902, when he explained that AKU results in ochronosis over a number of years. In 1908 Archibald Garrod brought AKU into the spotlight in his Croonian lectures when he used the disease to illustrate his theory of 'the inborn error of metabolism' (11,12). He provided evidence of the dynamic nature of metabolism demonstrating that normal metabolic pathways can be made variant by mendelian inheritance. He identified a familial pattern of inheritance and concluded that an inherited biochemical abnormality must result in the passage of an abnormal intermediate in the urine. Garrod identified that AKU was a recessive disorder and thus became the first genetic disease to conform to mendelian autosomal recessive inheritance. Garrod's lectures today are considered as landmarks in the history of genetics, medicine and biochemistry, and his contribution to understanding AKU is by far the most important in the history of the disease (11). Almost half a century after Garrod identified that AKU conformed to mendelian inheritance, La Du and colleagues discovered that AKU was a result of the deficiency of an enzyme involved in the tyrosine and phenylalanine metabolic pathway and called this enzyme HGD (13).

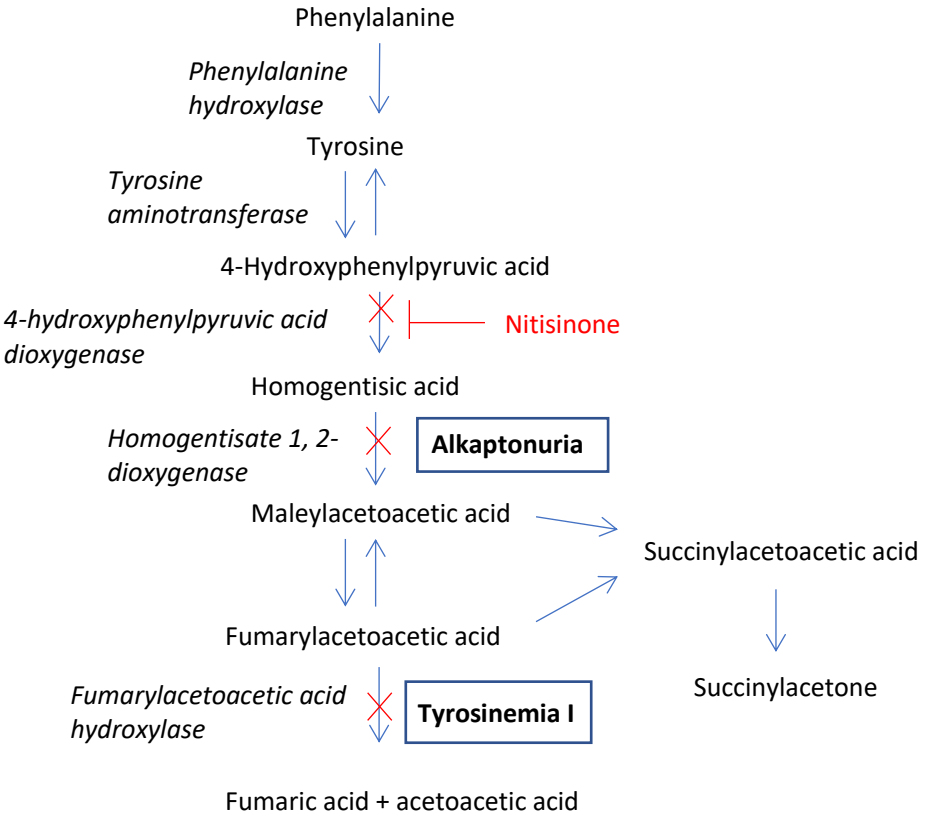

Figure 1.1 The tyrosine metabolic pathway. The biochemical defect in alkaptonuria is the deficiency of the enzyme homogentisate 1,2 dioxygenase. The drug nitisinone inhibits the enzyme 4-hydroxyphenylpyruvic acid dioxygenase blocking production of homogentisic acid and downstream metabolites (Adapted from (14)).

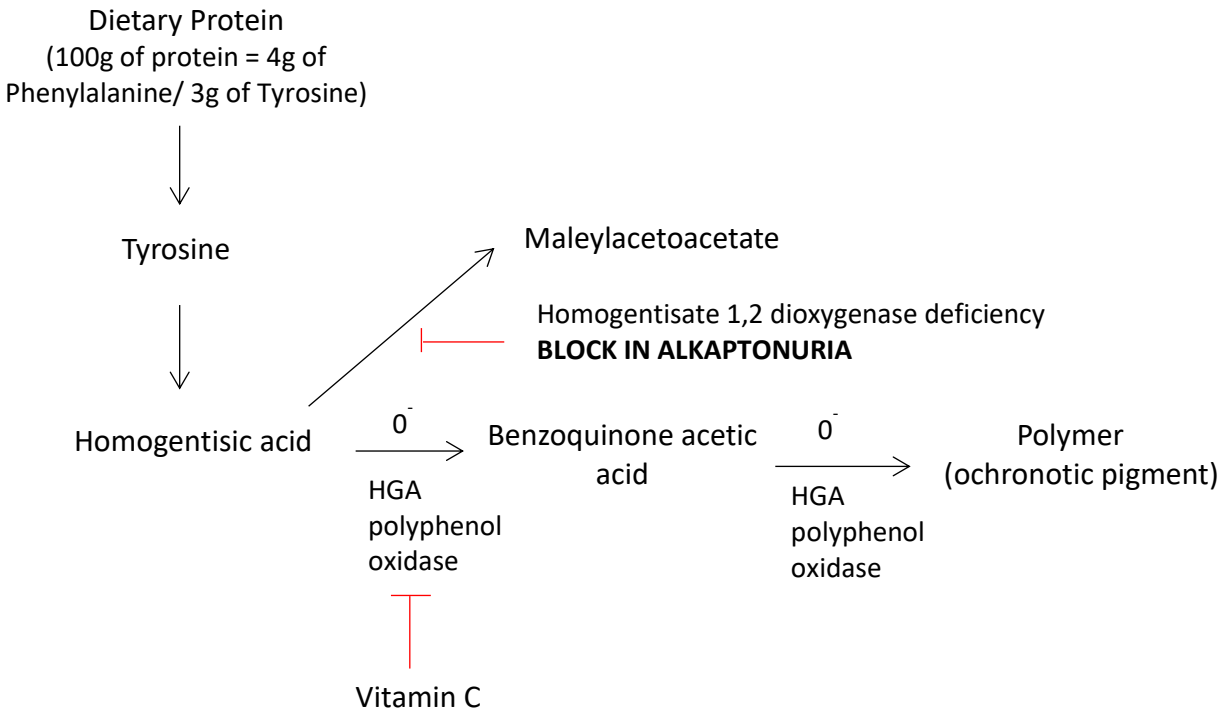

Figure 1.2 Formation of ochronotic pigment. Protein is metabolised via homogentisic acid (HGA) to maleylacetoacetate. Deficiency of the enzyme homogentisate 1,2 dioxygenase in alkaptonuria leads to increased HGA. Oxidative conversion of HGA to benzoquinone acetic acid leads to the production of ochronotic pigment that binds to connective tissues (Adapted from (3)).

1.1.2 Epidemiology

A review of AKU cases worldwide in 1962 found that 600 patients had been identified to have AKU across 35 countries. To date some 950 patients have now been identified worldwide across 40 countries. Today the incidence of AKU is approximately 1 in every 250,000 to 1 million live births and is therefore classified as an ultra-rare

disease (8,9). Hotspots have been identified in Slovakia, Dominican Republic, Jordan and India, with the highest incidences found in the North-West region of Slovakia reaching greater than 1:20,000. A possible reason for this is genetic isolation and the founder effect (loss of genetic variation) due to living in isolated hamlets (15). Also consanguineous marriages may explain the increased incidence in countries such as Jordan and India (8,13,16). The reason for this can be explained by the offspring of a consanguineous marriage receiving two defective gene copies derived from a common ancestor (17). High numbers of novel mutations of the HGD gene have been identified in Slovakia and Jordan demonstrating the high incidence of the disease in these countries (18). Research suggests that reporting of new cases of AKU has increased due to the increased awareness of the features of the disease. However, the number of cases worldwide is much less than what we might expect based on the incidence (8).

1.1.3 Genetic defect

AKU arises due to a genetic deficiency of the enzyme HGD. HGD converts HGA into maleylacetoacetate and has a major role in the catabolism of tyrosine and phenylalanine (Figure 1.1). Fernandez-Canon *et al*., 1996 (19) identified that the enzymatic loss in AKU is caused by mutations within the HGD gene. The human HGD gene is a single copy gene, spanning 54,363 bp of genomic sequence and is mapped to chromosome 3q13.33 (1). The HGD transcript is split into 14 exons ranging from 35 – 360 bp that encodes the HGD protein (20,21). The crystalline structure of the HGD protein has been resolved and the protein is composed of 445 amino acids that

forms a dimer of trimers giving rise to a functional hexamer (22). Northern blot hybridisation shows expression of HGD in the liver, prostate, small intestine, colon and kidney. The first human HGD mutations were described by Fernandez-Canon (19) in Spanish AKU families and were found to have missense mutations. To date 149 different HGD variants have been identified, of which 116 are mutations and 33 are polymorphisms (23). The mutations are spread throughout the entire gene with some prevalence in exons 3,6,7,8 and 13. Missense mutations are the most common followed by splicing, frameshift, nonsense, deletions and expansion. It has been identified that some mutations are spread throughout the world and some are specific to certain countries where there are hotspots of AKU e.g. Slovakia, India and Jordan (20). There is currently no genotype-phenotype correlation due to the complex hexameric structure of the enzyme.

1.1.4 Homogentisic acid

HGA is a small water-soluble molecule. It is an intermediate in the catabolism of tyrosine and phenylalanine (Figure 1.1). HGA is usually broken down by HGD into maleylacetoacetic acid in the liver, however in AKU the enzymatic deficiency of HGD results in a build-up of HGA. Upon oxidation (addition of NaOH or in the presence of O_2) HGA forms the highly reactive benzoquinone acetic acid (BQA). BQA polymerises to form the pigmented polymer termed ochronosis (24). HGA has also been found to be present in a bacterial plant pathogen as well as in yeast of which it has been associated with the production of brown pigment and has been identified as a precursor of melanin synthesis (25).

1.1.5 Clinical Presentation

AKU is characterised by three distinct features; homogentisic acidurea, ochronosis and ochronotic osteoarthropathy and tissue damage. The first feature to be detected from birth is the high concentrations of HGA in urine. HGA oxidises in air (or alkalinisation) and turns black. This feature is pathognomonic to AKU and leads to 21% of patients being diagnosed with the condition before the age of 1 (8). However, darkening may not occur for several hours so this often goes unnoticed by the patient (26). Chromatographic testing of urine samples for the presence of HGA is the gold standard for diagnosis. Plasma HGA concentrations in AKU patients ranges from 0.018 – 0.165mM, compared to 0.014 – 0.071μM in the non AKU patient. Additionally genetic testing would determine if the patient was homozygous or compound heterozygous for the condition (1,8). The reason urine turns black in AKU is a result of oxidative conversion of the excess HGA to benzoquinone acetic acid, and this in turn forms a melanin like polymer that results in the urine slowly turning black (Figure 1.2). The HGA that is not excreted undergoes oxidation and polymerisation in connective tissues of skeletal, cardiovascular and ocular systems, leading to a pathological blue-black discolouration termed ochronosis (7).

Black pigmentation of the sclera and the pinna of the ear are two of the most obvious features externally, however these features are not commonly seen before age 25-30. Pigmentation of the ear and eyes has been reported in 70% and 50% of AKU patients respectively. Pigmentation of bodily fluids including perspiration leads to the discolouration of skin. Discolouration of the hands, nose and gums has also been documented (7,8). Continued polymerisation of HGA in tissues, specifically cartilage

over time, leads to rapid early onset osteoarthropathy around the third to fourth decade of life.

Ochronotic arthropathy primarily affects the axial and weight bearing joints. Both synovial and intervertebral joints are affected. The first clinical symptom often starts in the spine as lower back pain (17). In a study of 163 cases of AKU, the spine was found to be involved in 159 patients compared to much lower frequencies of involvement found in the knee and hip (27). Radiological observations of the spine include wafer-like disc calcification, IVD space narrowing with vacuum phenomenon (radiolucent collection of gas), osteophyte formation and in most severe cases fusion of vertebrae (17,26). Symptoms worsen from the fourth decade and include progressive kyphoscoliosis and impaired spinal mobility. This has been shown to cause secondary effects on pulmonary inflation, disc herniation and cord compression (1).

Involvement of the large weight bearing joints usually occurs several years after the spinal changes. The knees, hips and shoulders are most frequently involved with relative sparing of the small joints of the hands and feet in most cases (28). Radiographic observations of the large peripheral joints are similar to that of osteoarthritis (OA) including, joint space narrowing, subchondral bone (SB) sclerosis and osteophytosis, and as a result AKU is often misdiagnosed as OA (17). Ochronotic arthropathy is crippling and inevitably leads to the patient requiring multiple joint replacements. By the age of 55, 50% of AKU patients have undergone at least one joint replacement (29).

AKU is often diagnosed intraoperatively when a blackened joint is exposed (30). Autopsy results from a 74-year-old female with AKU who died of disseminated ovarian cancer revealed extensive osteoarthropathy. The patient had undergone surgery to replace both knee joints, both hip joints and the left shoulder joint and had OA of both ankles and the right shoulder. Thoracic scoliosis and lumbar lordosis was evident and marked pigmentation on the annulus fibrosus of the IVDs was observed with bony bridging between vertebral bodies. OA of the shoulder was identified with extensive bony exposure and a narrow rim of pigmented cartilage and debris present (31). In AKU the pigmented tissues often become weak and brittle and are susceptible to chipping and splintering hence the pigmented debris present at autopsy. This process results in rapid joint deterioration coupled with inflammatory processes in some cases (17).

Apart from joint damage other manifestations of AKU include renal, salivary gland, prostate and gall bladder stones. Ligament and tendon calcification and ruptures have also been documented (8). Osteopenia and fractures are less common but have been documented. Fisher *et al*. (4) documented a case of a 69 year old AKU patient presenting with a low trauma fracture of the distal femur, and distal radius. She had no other contributing risk factors that may have predisposed her to fractures such as vitamin D deficiency, osteoporosis or history of osteoporotic fractures. Bone changes are thought to be less common in frequency and severity than cartilage changes. This is thought to be due to the remodelling properties of bone limiting the ability to reduce the cross linking of the collagen fibrils that result in connective tissue failure (4).

The cardiac manifestations of AKU are not un-common. Many studies have documented pigmentation associated with the cardiac valves and atherosclerotic plaques. At autopsy Helliwell *et al*. (31) found prominent pigmentation of the mitral valve as well as calcification and mild fusion of the aortic valve therefore AKU is a predisposing factor for valve calcification, stenosis and regurgitation. Patients with AKU exhibit a high frequency of aortic valve involvement acquiring this condition in the seventh to eighth decade of life. The aortic sinus region also contained pronounced pigmentation. Interestingly no pigmentation was observed in the venous components of circulation and the tricuspid valve and the pulmonary valve showed minimal pigmentation. It was proposed that pigmentation of the aortic and mitral valves as well as the carotid sinus region is due to the high blood pressure and turbulent blood flow that is associated with those structures and that deposition of pigment may be linked to areas of high blood pressure and other haemodynamic factors. It is still unclear whether the pigment alone causes increased stiffening of the valve or whether it is a result of pigment related damage to the collagen fibres. Echocardiographic screening is recommended for all AKU patients (32). Currently there is no effective licenced therapy to treat AKU. Joint replacements and pain relief are offered to help ease the pain but do not combat the cause.

1.1.6 The Initiation of ochronotic pigmentation (the exposed collagen hypothesis)

The pathogenesis of ochronosis is still not fully understood and it wasn't until recently that possible mechanisms to explain the initiation of pigmentation were elucidated. In 2009 Taylor *et al*. (33,34) described the relationship between HGA and fibrillar

collagen suggesting there was a binding site for HGA on collagen. Taylor *et al*. identified that pigmentation is initiated in the pericellular matrix surrounding chondrons of the articular calcified cartilage. Further studies revealed that tissues are initially resistant to pigmentation but become susceptible following mechanical or biochemical damage to the extracellular matrix such as repetitive mechanical loading, chemical attack and ageing (35). It is proposed that the collagen fibre has sites which HGA can bind to, however these are protected in healthy collagen by proteoglycans (Figure 1.4). Following mechanical or biochemical damage, proteoglycans are lost, and these binding sites become exposed and available for HGA to attach. The initial binding of HGA is comparable to a nucleation event; once HGA has bound there is rapid deposition of HGA as an ochronotic polymer. Binding of HGA to collagen results in stiffening of the fibre leading to further mechanical damage. This process results in progressive ochronosis (Figure 1.4) (13). This process is thought to be as a result of ageing and is thought to occur in non-AKU connective tissues also.

1.1.7 Pathogenesis of Joint Destruction

Initial pigmentation is laid down in individual chondrocytes and their territorial matrix within the calcified cartilage. Pigmentation spreads to other chondrons within the calcified cartilage and proliferates through the hyaline cartilage. Pigmented hyaline cartilage becomes stiff and shields the underlying bone from normal mechanical loading leading to aggressive resorption of the subchondral plate by osteoclasts resulting in degeneration of the joint (Figure 1.3) (13,35,36).

1.1.8 Diagnosis

Currently, the diagnosis of AKU is based on the detection of a significant amount of HGA in a urine sample by gas chromatography-mass spectrometry analysis. The amount of HGA excreted per day in urine in individuals with alkaptonuria is usually between 1-8 g compared to 20-30 mg in an individual without AKU. Genetic testing is required to determine if the individual is homozygous or compound heterozygous. Identification of biallelic pathogenic variants confirms the diagnosis and allows family studies and counselling (1,37).

Once the HGD pathogenic variants have been identified in an alkaptonuric family member, prenatal testing and preimplantation genetic diagnosis for a pregnancy at increased risk for the disease are optional (37).

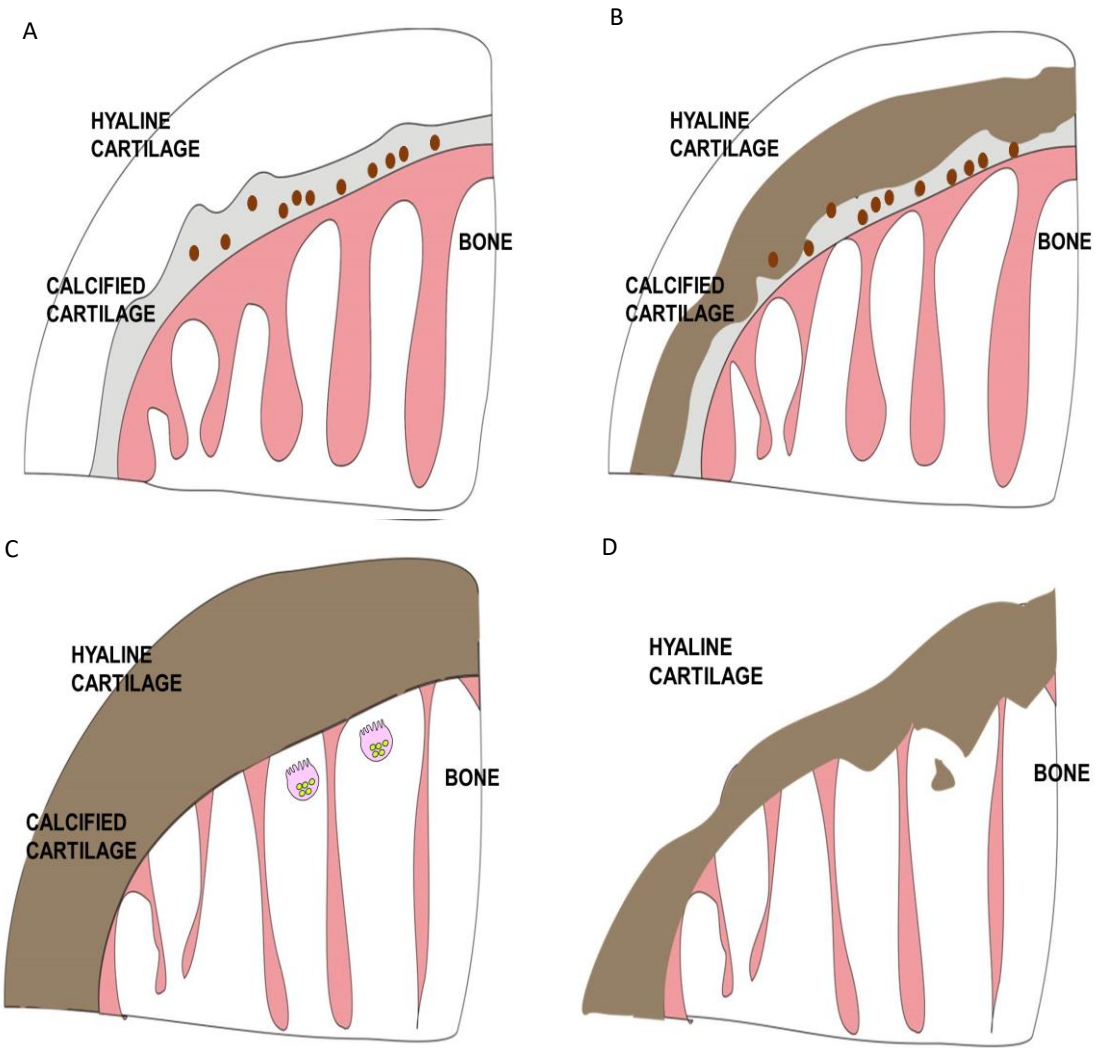

Figure 1.3 Progression of ochronosis in the joint. A) Ochronotic pigment is laid down within individual chondrocytes within the calcified cartilage. B) Ochronosis spreads to other chondrons in the calcified cartilage and proliferates through to the hyaline cartilage. C) Ochronotic cartilage shields the underlying bone from normal mechanical loading, leading to resorption of the subchondral plate by osteoclasts. D) Despite the increased stiffness the pigmented shell of the remaining articular cartilage fails catastrophically leading to rapid onset severe osteoarthropathy. Taken from (3), evidence from (2).

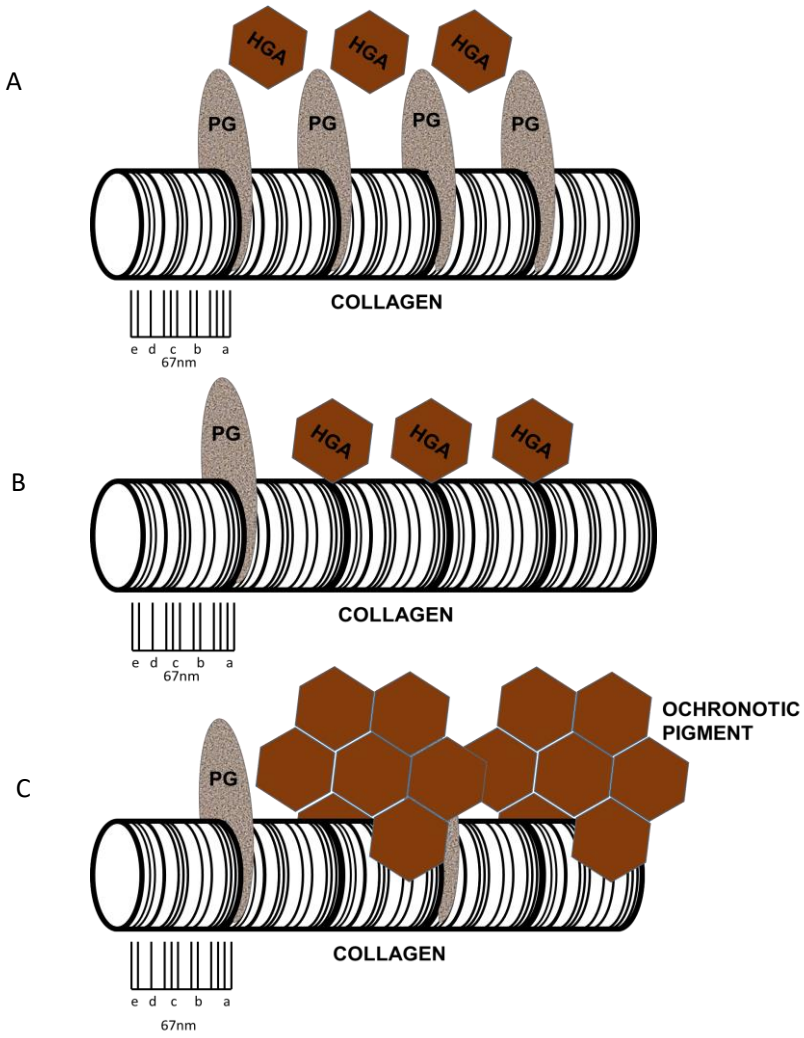

Figure 1.4 The initiation of ochronotic pigment - the exposed collagen hypothesis. A) Homogentisic acid (HGA) is present in the extracellular environment however cannot bind to the collagen fibril due to the protective proteoglycans (PG). B) Protective PG are lost as a result of repetitive mechanical loading, chemical attack and or ageing and this exposes the collagen fibril to attack from small molecules such as HGA. C) In AKU the initial binding of HGA to the collagen fibril is comparable to a nucleation event followed by rapid deposition of HGA as an ochronotic polymer. This binding results in the collagen fibril becoming stiff and leading to further mechanical damage. This leads to a downward cascade of increasing pigment deposition and ochronosis (38). Taken from (13) evidence from (35).

1.1.9 Therapy

Several therapeutic approaches have been tried to treat AKU with little effect. Currently there is no effectively therapy licenced to treat AKU. The only available treatments focus on reducing the symptoms, and do not tackle the intrinsic cause (1). Palliative management of AKU includes joint replacement therapy, physiotherapy and pain management (8). Table 1.1 summarises all the therapies that have been tried in AKU.

1.1.9.1 Vitamin C

Vitamin C was first used to treat AKU in 1940 by Sealock *et al*. (39). He reported that Vitamin C therapy delayed the darkening of urine presumably by preventing the oxidation of HGA. Studies have shown that Vitamin C acts by blocking the conversion of HGA to benzoquinone acetic acid (BQA) by inhibiting the enzyme HGA polyphenol oxidase (Figure 1.2) [8]. BQA is an intermediary product in the formation of ochronotic pigment, therefore the hypothesis was that preventing the oxidative conversion of HGA to BQA would prevent ochronosis. Wolff *et al*. (40) reported that the administration of relatively large amounts of Vitamin C resulted in the disappearance of BQA in the urine. However, it did not change the amount of HGA excreted. It was also found that HGA concentration doubled after administration of Vitamin C in young infants and the authors proposed that this was due to activation of the enzyme hydroxyphenylpyruvate dioxygenase (HPPD) that converts 4-hydroxyphenylpyruvic acid (HPPA) to HGA (Figure 1.1) (40). Other studies found that Vitamin C caused HGA production to increase, contributing to the production of renal

oxalate stones, increasing their risk of developing these further. This evidence confirms that Vitamin C is not an effective treatment in AKU.

1.1.9.2 Low Protein Diet

Reducing dietary intake of protein seems the most logical form of treatment. By reducing dietary intake of phenylalanine and tyrosine this will reduce the amount of HGA produced, therefore reducing ochronosis. Haas *et al*. (41) from the Netherlands found a significant decrease in the excretion of HGA with a low protein diet of 1 g/kg per day however this was age dependant. They found that children below the age of twelve had reduced HGA production but above the age of twelve there was no effect. They concluded that protein restriction in older patients is probably useless but restriction should be advised in younger patients. This would require strict specialist supervision during growth periods to ensure adequate levels of essential amino acids, vitamins and minerals are available for growth (1). Another report from the Netherlands described reduced joint pain after receiving a low protein diet in children (42). Other studies also reported no change in HGA excretion with protein restriction (9). Approximately only 6% of dietary protein is degraded via HGA, however, nearly all HGA is produced by dietary intake of protein. Additionally reducing dietary protein is very hard to comply with long term and it appears small reductions in protein intake do not have a noticeable effect (1). It was concluded that restricting protein intake was not the most appropriate treatment option.

1.1.9.3 Nitisinone

Nitisinone, 2-(2-nitro-4-triflurомethylbenzoyl)cyclohexane-1,3-dione (NTBC), a very effective herbicide, is a potential disease modifying therapy for AKU. Nitisinone acts by inhibiting the enzyme HPPD (HPPD coverts HPPA into HGA), therefore blocking the production of the culprit HGA (Figure 1.1). It is administered orally and has high affinity for HPPD in the liver (1). Nitisinone has been used since 1992 for the rare disease tyrosinemia type 1 (HT1) and has proven to be well tolerated long and short term. Nitisinone operates several steps before the defect in HT1 and the dosage given is 1-2mg/kg body weight. Nitisinone acts on the very reaction that causes AKU therefore it was proposed that a lower dosage may be required. An early study revealed the dose to treat AKU was 30-fold lower than that used to treat HT1 (43). Current experience with nitisinone in AKU is limited. Suwannarat *et al*. (14) at the NIH investigated the safety and efficacy of nitisinone in a study of 9 AKU patients over a period of 4 months. A dose of 2.1mg was given, and this was shown to decrease urinary HGA concentrations by 95% (from an average of 4.0 to 0.2g/day) and increase plasma tyrosine levels 11-fold (from 68 μmol/L to 760 μmol/L). The tyrosinemia did not cause any corneal toxicity, and six out of seven patients that received nitisinone reported decreased pain in their joints (14).

In a second study Introne *et al*. (44) conducted a three year randomised therapeutic NIH trial of nitisinone (2.1mg/day) on 40 AKU patients. Nitisinone was shown to reduce mean urinary HGA by 98% (from 5.1 to 0.125 g/day). Mean plasma HGA levels reduced by 95% from 5.74 to 0.306 mg/l. Hip rotation was used as the defining parameter to determine the efficacy of the drug, however the results were

inconclusive from a rheumatological aspect (44). Ranganath *et al*. (45) suggested one possible reason for this could be that an optimal dose was not used. Ranganath and his team conducted a dose response study to investigate the effect of nitisinone on urinary HGA (SONIA 1). The study had 5 groups of patients each containing 8 patients and the 5 dosages were 0,1,2,4, and 8mg. A clear dose-response relationship was observed at 4 weeks, the adjusted geometric mean u-HGA in 24 hours was 31.53mmol, 3.26mmol, 1.44mmol, 0.57mmol for the 1mg, 2mg, 4mg and 8mg doses, respectively. The 8mg dose daily was most effective, corresponding to a mean reduction of u-HGA of 98.8% compared with baseline. No safety concerns were reported in this short study, however the long-term safety and efficacy of the drug is not fully understood so a 2mg dose is what is usually prescribed in clinic today (45).

Life-long therapy is required to maintain reduced levels of HGA. The pathophysiological and clinical significance of tyrosinemia is not fully understood, however it can cause corneal irritation as well as other serious side effects such as thrombocytopenia, leukopenia and porphyria which are associated with neurological complications such as tremor, ataxia, delayed development and intellectual impairment (8).

1.1.9.4 Other treatments

A variety of options are available to treat AKU and these are summarised in Table 1.1. Lifestyle counselling can be beneficial. Siblings with the same mutation and gender can have very different symptoms. Assessing lifestyle choices can have a positive impact on symptoms. Minimising joint loading in all areas of life is likely to be

important. Physiotherapy is used to increase joint motion and activity. Pain control is vital but often is only partially effective. A wide variety of drugs are prescribed to tackle the pain such as paracetamol, non-steroidal anti-inflammatories, opioids, anticonvulsants, local anaesthetics and gabapentin. Physical modalities are also used such as acupuncture, nerve blocks and trans-cutaneous nerve stimulation. Organ transplantation has been associated with resolving AKU however it is not justified in a disease where longevity is rarely affected. Multiple joint replacement therapy and spinal surgery are inevitable and are often required multiple times throughout life (1).

Nitisinone is most effective in reducing the causative agent however it is imperfect because it is acting as a metabolic block and therefore causes secondary effects on tyrosine levels. A perfect treatment would involve replacing the missing enzyme by utilising gene or enzyme replacement therapy. This would result in decreasing HGA without affecting the rest of the tyrosine metabolic pathway. However, there are potentially fatal complications with this therapy. The HGD enzyme would have to be delivered to the exact location of tyrosine metabolism within the hepatocytes of the liver to be successful. If the HGD enzyme was present in the blood and the extracellular fluid this would result in succinylacetone to spontaneously form from maleylacetoacetate and fumarylacetoacetate (Figure 1.1). These products are toxic and highly mutagenic resulting in serious complications as the enzymes required to break these products down would not be present unlike in the liver (8).

Table 1.1 Information regarding the various, current and future therapies to treat AKU. Adapted from (8,1).

Treatment	Summary
Vitamin C	Efficacy unproven, HGA production increases, may worsen the condition
Low protein diet	Efficacy in adults unproven, compliance difficult
Lifestyle counselling	Underused, lack of evidence base
Physiotherapy	Underused
Pain control	Widely used, palliative, incompletely effective
Organ replacement	Unjustified in a disease with normal lifespan
Palliative surgery	Effective but invasive
<u>HGA lowering therapies:</u> Nitisinone Enzyme replacement Gene replacement	 Not shown to alter outcomes, increases tyrosine Not yet available Not yet available

1.1.10 Assessment

AKU is present from birth however these patients experience an asymptomatic pre-ochronotic phase from birth up until around the third decade of life. This delay in ochronotic deposition is still not fully understood. A major difficulty in clinical research is the lack of suitable quantifiable methodology to describe disease severity (46). Until recently, most descriptions of AKU were qualitative and there was no methodology to quantify the disease, or to define an objective measure of disease severity. Without an appropriate method to quantify the disease, clinicians were unable to make comparisons of disease severity between patients. This issue has been rectified recently with the introduction of the AKU severity score index (AKUSSI). This score is based on a quantitative, validated, multidisciplinary assessment that can be used for patient assessment in the AKU clinical trials (1).

The AKUSSI quantifies the clinical features of AKU systematically in a standardised manner. Table 1.2 is the AKUSSI which represents the clinical features that are scored and summed to derive a composite score. The features of AKU are broken down into three categories, features due to excess circulating HGA (prostate, kidney, salivary and gall stones), features due to ochronosis (ear/eye pigmentation, teeth and skin pigment, osteopenia, ENT features and cardiac valve disease) and features due to damage of connective tissue (fractures, tendon/ligament/muscle ruptures, as well as spinal and joint disease). The early appearing features were scored lower and the latter appearing features were scored higher (46). A questionnaire based severity score index, has also been described and is easy to use and could be used at any hospital around the world.

Table 1.2 AKUSSI table. Features shown in the table are scored and summed up to derive a composite score. This score represents the totality of clinical features of AKU. The modality regarding how clinical features are scored is shown red. The scores given for each feature are in brackets depending on the severity or if the feature is present.

AKUSSI **Name** **dob** **Gender** **RQ**

Feature	Score						Feature	Score					
	V1	V2	V3	V4	V5	V6		V1	V2	V3	V4	V5	V6
Eye Pigment R Eye Nasal * PHOTOS							L Eye Nasal * PHOTOS						
R Eye Temporal * PHOTOS							L EyeTemporal * PHOTOS						
Ear Pigment (Present = 2; Marked 4) **RIGHT** PHOTO							Present = 2; Marked 4) **LEFT** ear						
Prostate Stones (4 per episode) ULTRASOUND or History (Features of AKU report)							**Kidney Stones (4 per episode)** ULTRASOUND or History of features of AKU report						
Osteopenia (4) CT Densitometry or DEXA BMD							**Fracture (8 per #) HISTORY in AKU Report**						
Aortic sclerosis (6), Aortic stenosis (mild, moderate, severe) (8,10,12) CARDIOLOGY REPORT OR ECHOCARDIOGRAM													
Hearing impairment (4) HISTORY in AKU Report							**Muscle** rupture (8 per rupture)) HISTORY **in AKU Report**						
Ligament rupture (8 per rupture) HISTORY							**Tendon** rupture (8 per rupture) HISTORY **in AKU Report**						
ALL CLINICAL FEATURES ONLY													
Clinical joint pain score (1 for each large joint area; 14 large joint areas) HISTORY **in AKU Report**													
Scintigraphic scan joint score (2 for each large joint; 14 large joints areas) REPORT PETCT OR ISOTOPE SCAN													
Number of arthroscopies (2 for each) HISTORY **in AKU Report in Treatments**													
Number of joint replacements Each joint 4 (Max 10 large joints) HISTORY **in AKU Report in Treatments**													
NON SPINE JOINT AGGREGATE SCORES													
Clinical Spinal pain score (2 each for cervical, thoracic, lumbar, sacroiliac) HISTORY **in AKU Report**													
Kyphosis (4) XRAY REPORT OR RHEUMATOLOGY							Scoliosis (4) XRAY REPORT						

1.2 AKU Society and the National Alkaptonuria Centre

The AKU society was founded in 2003 by an AKU patient Robert Gregory and Professor L. Ranganath. The AKU society is a patient group, with a foundation of a partnership between patient and doctor. The aim of this society is to research possible treatments, connect AKU patients from across the world, and to help patients and their families live with the disease (47,48). Communications with the UK Department of Health suggested approaching National Specialised Services with the idea of founding a Centre of Excellence for AKU patients to provide expert care to all

patients with AKU. In 2012 the Robert Gregory National Alkaptonuria Centre (NAC), was established by the NHS Highly Specialised Services Commissioning Group at the Royal Liverpool University Hospital. The NAC delivers expert care and advice from leading experts in the field. The NAC provides off-label nitisinone to patients who receive annual check-ups and follow up blood, and urine tests post nitisinone. Patients confirmed with alkaptonuria are commenced on 2 mg dose of nitisinone that they take on alternative days, for three months with daily dose thereafter. Monitoring and clinical assessments are performed annually. Currently 58 patients with AKU have been enrolled at the NAC for treatment with nitisinone. Twenty-three females (mean age 53 years, range 22-75) and 35 males (mean age 48 years, range 22-70). The NAC is an on-going service that is transforming the lives of AKU patients through patient support, community building and medical research (47,48).

1.3 DevelopAKUre

Research into the use of nitisinone in AKU started in the 1990's however, the results were underpowered and were not statistically significant. A goal for the AKU society was to further investigate the efficacy of nitisinone (48). In 2012 a series of international clinical trials was founded called the DevelopAKUre consortium with Sobi (the pharmaceutical company with the licence for nitisinone) (49). The DevelopAKUre consortium is coordinated by Professor L. Ranganath, at the Royal Liverpool University Hospital. Two other clinical sites are involved outside of the UK; The National Institute of Rheumatic Disease, Piestany, Slovakia and Hospital Necker and Institute Necker in France. The objective is to study the efficacy and safety of nitisinone to obtain marketing authorisation for the treatment of AKU. The duration

of DevelopAKUre is approximately 75 months, and is due to conclude in 2019 (49). If nitisinone is proven to be effective in AKU, the consortium will apply for marketing authorisation and approval of Nitisonone by the European Medicines Agency. DevelopAKUre involves three studies, a dose response study called 'Suitability of Nitisinone in Alkaptonuria 1' (SONIA 1), an efficacy study called 'Suitability of Nitisinone in Alkaptonuria 2 (SONIA 2) and a cross sectional study called 'Sub-clinical Ochronotic Features in Alkaptonuria (SOFIA) (49).

1.3.1 Suitability of Nitisnone in Alkaptonuria 1 (SONIA 1)

This study was designed to identify the most appropriate dose of nitisinone to be used over a patient's lifetime, as well as the most effective dose in reducing HGA levels. Forty patients were recruited for the trial and were split up into five age dependent groups of eight. Each group received varying doses of nitisinone (0mg, 1mg, 2mg, 4mg, and 8mg). SONIA 1 began in May 2013, and lasted 4 weeks (45). Two centres were involved, the Royal Liverpool University Hospital and the National Institute of Rheumatic Disease, Piestany. The 8mg dose showed the least variability and was found to reduce urinary HGA levels down by on average 99.4%, as well as reducing serum HGA to undetectable levels in 7/8 patients (45,50).

1.3.2 Suitability of Nitisinone in Alkaptonuria 2 (SONIA 2)

This study is designed to test whether nitisinone slows down the progression of the disease in AKU. SONIA 2 commenced in 2014 and is expected to finish in 2019. 138 patients were enrolled and were randomly divided into two equal groups of 69. One group receives nitisinone (10mg/day) and the other group does not. This trial is based across three clinical sites in Liverpool, Piestany and Paris. Patients attend their allocated test centre a total of six times, each visit lasting up to 4 days. SONIA 2 aims to elucidate the impact of nitisinone on HGA levels in the body over a period of 4 years; this will define whether nitisinone has a positive impact on HGA levels and whether it is safe long term. If nitisinone is proven to be beneficial in the treatment of AKU the DevelopAKUre consortium will apply for a drug license for AKU (49,50).

1.3.3 Subclinical Ochronotic Features in Alkaptonuria (SOFIA)

This study is an observational cross-sectional study that commenced early 2017. SOFIA is designed to investigate the onset of ochronosis and to define the best time to begin treatment with nitisinone. Thirty patients (15 males, 15 females) were recruited for SOFIA from a range of ages. They were split into 8 age groups (16-20, 21-25, 26-30, 31-35, 36-40, 41-45, 45-50, 50+) with 4 patients in each group (2 males, 2 females). This trial will involve study patients visiting the clinical site in Liverpool for three days where a series of tests will be performed including urine tests, blood tests, MRI scan, ear cartilage biopsy and gait analysis. All samples will be analysed for ochronosis, and will be compared with 30 healthy volunteers without AKU (49,50).

1.4 Cartilage

Cartilage is an avascular, flexible connective tissue found throughout the body, providing support to adjacent tissues. Cartilage is devoid of blood vessels, lymphatics and nerves; it therefore derives oxygen and nutrients via diffusion. This results in cartilage having a limited capacity to repair (51). Cartilage is composed of chondrocytes, embedded within an extracellular matrix. Chondrocytes maintain and regulate the turnover of extracellular matrix (52). There are three different types of cartilage in the body, hyaline cartilage, fibrocartilage and elastic cartilage. These three types differ slightly in term of the structure and function (53). Hyaline cartilage is the most abundant type. It is found at the ventral ends of the ribs, the tracheal rings, larynx and bronchi and it also forms the articular surfaces of long bones (articular cartilage). Hyaline cartilage matrix consists of type II collagen and the glycosaminoglycan chondroitin sulphate and is covered externally by perichondrium, a fibrous membrane that contains vessels that provide oxygen and nutrition (except articular cartilage) (53). Fibrocartilage contains abundant collagen and fibrous tissue. Fibrocartilage is distinct in that it contains Type I and Type II collagen. Type I collagen provides considerable tensile strength and the ability to resist compressive forces, therefore fibrocartilage is found in regions requiring these properties such as the annulus fibrosus of the intervertebral discs, pubic symphysis, menisci of the knee and the temporomandibular articular disc. Lastly, elastic cartilage histologically looks similar to hyaline cartilage in that it contains type II collagen and chondroitin sulphate, however it also contains many elastic fibres that lie in a solid matrix, providing this type of cartilage with great flexibility that can withstand repeated bending. Elastic cartilage can be found in the pinna of the ear and the epiglottis (53).

1.4.1 Articular Cartilage Structure

Articular cartilage (AC) is highly specialised hyaline cartilage of diarthrodial joints. It functions to provide a smooth, lubricated surface for articulation, and to facilitate load transmission through the joint. Typically, AC is 2-5mm thick, and is completely avascular, aneural and is devoid of lymphatic drainage. AC is composed of chondrocytes embedded in a dense extracellular matrix (ECM) of water, collagen and proteoglycans and has a layered, organised structure (54). Morphologically AC is organised into four zones (Figure 1.5); the uppermost layer is the superficial (tangential) zone, immediately deep to this layer is the middle (transitional) zone, followed by the deep zone and calicifed zone. The superficial, middle and deep layers are un-mineralised and often referred to as the hyaline articular cartilage (HAC). The calcified zone is mineralised and is often referred to as the articular calcified cartilage (ACC) (52). AC provides an extremely smooth, firm yet deformable layer that increases contact area between bones and therefore reduces contact stress.

1.4.1.1 Superficial zone

The thin superficial zone acts to protect the deeper layers, and provides a gliding surface for articulation. The superficial zone makes up 10% to 20% of the overall HAC thickness. The collagen fibres (mainly collagen type II and IX) are packed tightly and arranged parallel to the articular surface (54). The chondrocytes are flattened and relatively high in number and express lubricin (essential for lubrication). This layer is in contact with the synovial fluid, and acts to resist shear, tensile and compressive forces. The integrity of this layer is paramount for the protection of the deeper layers, and is often the first layer to show changes in OA (Figure 1.5) (51).

1.4.1.2 Middle Zone

The middle zone provides an anatomical and functional bridge between the superficial and deep zones and represents approximately 40-60% of the overall HAC thickness. It contains obliquely orientated collagen fibrils and low density spherical chondrocytes embedded in dense ECM that is rich in proteoglycans such as aggrecan (54). The middle zone functions to resist compressive forces and transfers them from the superficial zone to the deeper zones (Figure 1.5) (52).

1.4.1.3 Deep Zone

The deep zone represents approximately 30% of the overall HAC volume, and contains the highest number of proteoglycans and the largest diameter of collagen fibrils. It therefore, functions to provide the greatest resistance to compressive forces. The collagen fibrils and spherical chondrocytes are arranged in vertical columns perpendicular to the joint surface. Cellular density is lowest in the deep zone

(approximately 1/3 the density of the superficial layer) however it contains the largest amount of aggrecan (Figure 1.5) (52,54).

1.4.1.4 Calcified zone

The calcified zone, also known as the ACC plays an integral role in securing the cartilage to bone by anchoring the collagen fibrils of the deep zone to the SB. The basophilic tidemark distinguishes the deep zone from the ACC. The cell population is scarce and the chondrocytes are hypertrophic and synthesise type X collagen that calcifies the surrounding matrix. Calcification of the matrix provides structural integrity important for shock absorption (51,54). The SB is located beneath the ACC and includes the subchondral plate (comprises the ACC and a thin cortical bone layer) and the underlying trabecular bone (Figure 1.5).

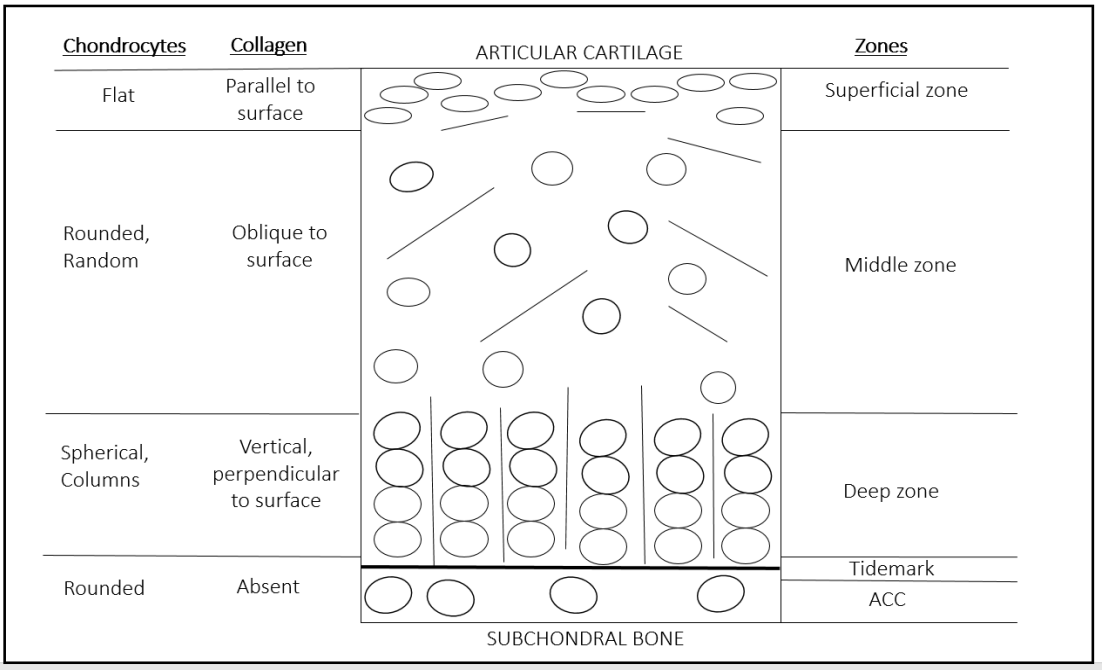

Figure 1.5 Zones and morphology of articular cartilage. Chondrocytes are flat and collagen fibres lie parallel to the surface in the superficial zone. Chondrocytes in the middle zone are rounded with random orientation and oblique collagen fibrils. Chondrocytes in the deep zone are spherical and orientated in columns with vertical collagen fibrils orientated perpendicular to the surface. The tidemark (represented by the thick black line) separates the hyaline articular cartilage (composed of the superficial, middle and deep zones) with the articular calcified cartilage (ACC). Chondrocytes in the ACC are rounded, and collagen and proteoglycans are absent. The ACC chondrocytes are hypertrophic and synthesise type X collagen, which upon release from the cell calcifies the surrounding matrix (Adapted from (52,54,55)).

1.4.2 Extracellular matrix

As well as the zonal regions, the ECM has distinct regions based on the proximity to the chondrocyte and collagen composition and organisation. The ECM can be divided into the pericellular, territorial and interterritorial regions (Figure 1.6) (54). The pericellular matrix (PCM) directly surrounds the chondrocyte and contains mainly proteoglycans and glycoproteins. This region is thought to play a functional role in initiation of signal transduction in response to load (56). The territorial matrix (TM) surrounds the pericellular matrix and is composed of a network of fine collagen fibrils that protect the chondrocytes against mechanical stresses. The interterritorial matrix (ITM) is the largest and is characterised by abundant proteoglycans and the random organisation of collagen fibres (Figure 1.6) (54).

AC contains between 65%-80% tissue fluid. Water is the most abundant component. The flow of water through the ECM and across the articular surface distributes oxygen and nutrients to the chondrocytes as well as providing lubrication (54). The dry weight of the ECM is composed of collagen, proteoglycans and a small number of lipids, phospholipids, non-collagenous proteins and glycoproteins (Figure 1.7). Collagen is the most abundant structural molecule in the ECM and accounts for up to 60% of the dry weight of cartilage. Type II collagen represents approximately 90% of the collagen within the ECM (54). Collagen types I, IV, V, VI, IX and XI are also present but in small amounts and help to stabilise the type II collagen fibrillar network. Collagen fibres provide tensile strength to the cartilage and provide a binding site for proteoglycans. Proteoglycans contribute 10% - 15% of the wet weight. Proteoglycans

are composed of a protein core with one or more glycosaminoglycan chains covalently attached that extend out from the core and remain separate due to the charge repulsion. AC contains many essential proteoglycans. The largest (250,000d) and most abundant is aggrecan. Aggrecan is highly glycosylated proteoglycan, composed of 90% carbohydrate derived from two types of glycosaminoglycan; chondroitin sulphate and keratin sulphate. Aggrecan interacts with hyaluronan (HA) via link proteins to form large protein aggregates (Figure 1.7). The entrapment of these large aggregates within the collagen matrix provides the unique mechanical properties of cartilage (52). Chondrocytes are the only cell type responsible for synthesising ECM as well as regulating ECM turnover, however they only represent 5% of the total volume of the cartilage (52).

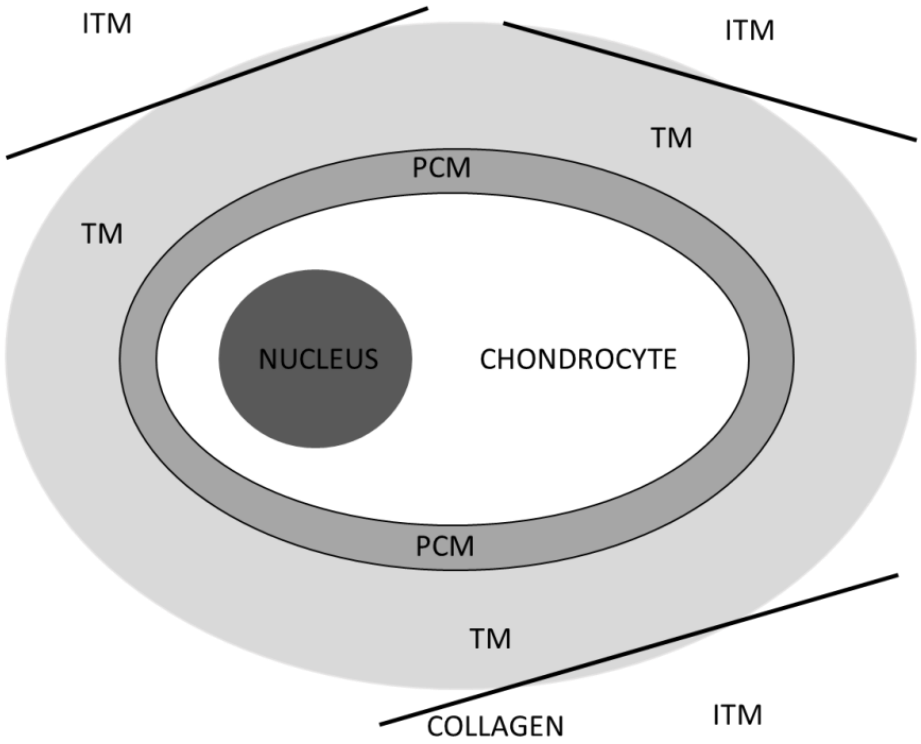

Figure 1.6 Chondrocyte structure. Chondrocytes are contained in lacunae containing extracellular fluid and are surrounded by pericellular matrix (PCM), together they are termed the 'chondron'. The territorial and interterritorial matrix constitutes the rest of the cartilage occupied by the chondrocytes. The territorial matrix (TM) surrounds the chondron and is highly basophilic due to the high number of proteoglycans and along with the interterritorial matrix (ITM) acts to dissipate load (55,57).

1.4.3 Chondrocytes

Chondrocytes are highly specialised, metabolically active cells found in cartilage that function to synthesise, maintain and repair ECM. Chondrocytes constitute approximately 2% of the total volume of AC and vary in number and size across the various zones of AC (54). Each chondrocyte establishes a specific microenvironment and is responsible for the turnover of ECM in its immediate vicinity. The chondrocyte and pericellular matrix forms a functional unit called an 'chondron' (58). Rarely do chondrocytes form cell-to-cell contacts for direct signal transduction, however they are responsive to a variety of stimuli including growth factors, cytokines, mechanical load and hydrostatic pressures (59). Under normal physiological conditions chondrocytes maintain ECM, however when cartilage becomes damaged, chondrocytes respond by secreting inflammatory cytokines (including interleukin 1 and tumor necrosis factor -α) that result in increased synthesis of metalloproteinases that in turn break down ECM (60). The ageing process also influences the organisation of chondrocytes, their response to external factors and therefore the composition of the ECM that ultimately results in degradation of the articular surface. This results in OA, and is accelerated by injury or disease. OA affects approximately 60% of men and 70% of women older than 65 years (52,61), and it has been forecast that 25% of the adult population (18 years and older) will be affected by the disease by the year 2020 (62).

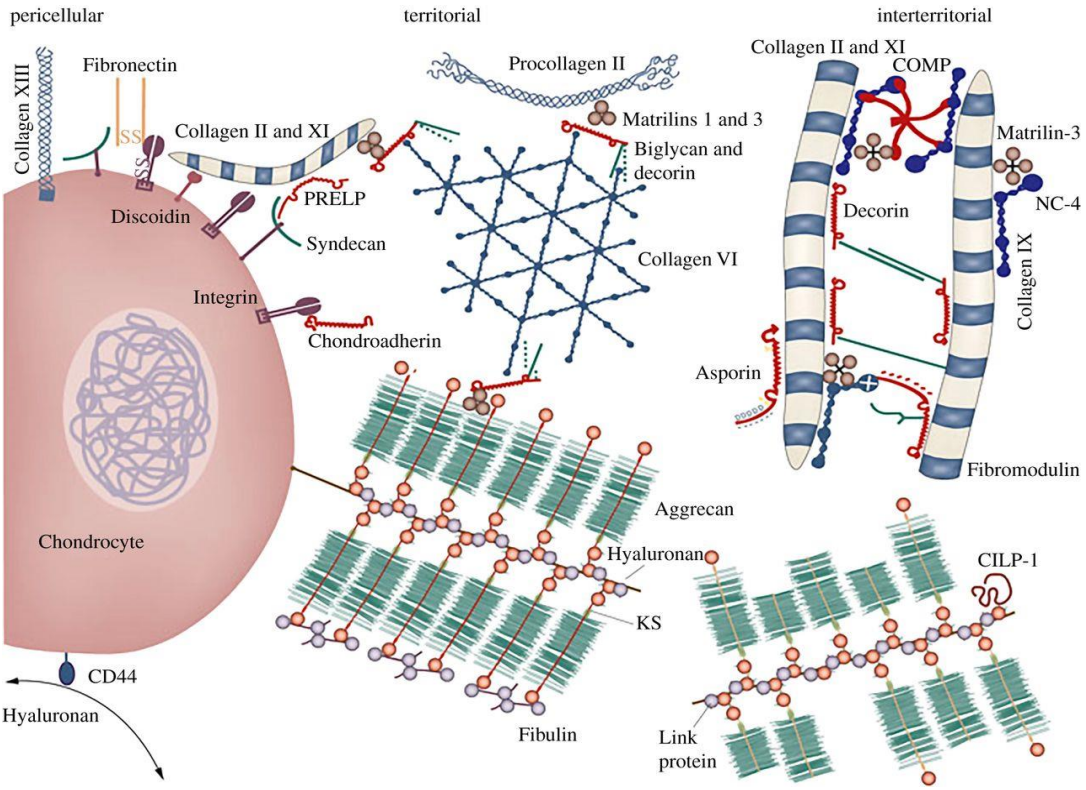

Figure 1.7 The molecular arrangement of extracellular matrix in cartilage. ECM is composed of collagen, proteoglycans and a small number of lipids, phospholipids, non-collagenous proteins and glycoproteins. Collagen is the most abundant structural molecule in the ECM and accounts for up to 60% of the dry weight of cartilage. Type II collagen represents approximately 90% of the collagen within the ECM. Collagen types I, IV, V, VI, IX and XI are also present but in small amounts and help to stabilise the type II collagen fibrillar network. Proteoglycans contribute to 10%- 15% of the wet weight. Proteoglycans are composed of a protein core with one or more glycosaminoglycan chains covalently attached that extend out from the core. AC contains many essential proteoglycans. The largest (250,000d) and most frequent is aggrecan. Aggrecan is highly glycosylated proteoglycan, composed of 90%

carbohydrate derived from two types of glycosaminoglycan; chondroitin sulphate and keratin sulphate (KS). Aggrecan interacts with hyaluronan via link proteins to form large protein aggregates. The entrapment of these large aggregates within the collagen matrix provides the unique mechanical properties of cartilage (52) (Image taken from (63)).

1.4.4 Collagen

Collagen is the most abundant macromolecule in ECM and accounts for approximately 60% of the dry weight of cartilage. Fifteen distinct collagen types have been identified and despite their structural diversity all have the characteristic triple helix, composed of three α-polypeptide chains (64). Type II collagen represents 95% of the total collagen in the ECM, however types I, IV, V, VI, IX and XI are also present but at much lower frequencies. Type II collagen consists of three α1(II)- polypeptide chains containing a glycine residue every third position resulting in a 'Gly-X-Y' repeat, X being proline and Y being hydroxyproline to provide stability via hydrogen bonds along the chain (65). This triple helical structure provides AC with impressive shear and tensile properties, stabilising the matrix. Type I collagen is the most abundant collagen in bone forming 90% of the organic mass. The collagen I triple helix is formed by a heterotrimer of two identical α1(I)- chains and one α2(I)- chain. Type I collagen provides tensile strength and torsional stiffness and provides bone with great load bearing qualities (64). The biosynthesis of collagen is a complex, multistep process involving intra and extracellular processes. The first step of collagen biosynthesis is transcription of the collagen genes within the nucleus producing mRNA. The ribosome bound mRNA is then translated into procollagen α-chains in the rough

endoplasmic reticulum. The proline and lysine residues are then hydroxylated forming hydroxyproline and hydroxylysine residues respectively (requiring vitamin-C). Hydroxyproline is necessary for intermolecular hydrogen bonds essential for the stability of the triple helix. Hydroxylysine is responsible for the cross linking of collagen molecules during fibril formation. Glucose and galactose are added to the hydroxyl group of lysine (glycosylation). The hydroxylated and glycosylated pro-peptides form the triple helix, and the procollagen is transported to the golgi complex where they are packaged into secretory vesicles for further processing. From here the procollagen trimers are secreted out into the extracellular space and the procollagen is cleaved at the C- and N-propeptides by specific enzymes forming tropocollagen. The final stage involves self-assembly of tropocollagen into fibrils and cross linkage of the collagen fibril for stabilisation (64,65).

1.5 Bone

Bone is characterised by its strength and rigidity, providing support and protection for the body, as well as the power to regenerate and repair itself. Unlike cartilage, bone is highly vascular with a high cell content, allowing bone to adapt to changing mechanical demands (modelling) and to repair and regenerate following injury. Bone also undergoes remodelling to remove old bone with new, stronger bone, preserving bone strength (66). Gross inspection of bone has revealed two forms of bone tissue, cortical or compact bone which is dense, solid and surrounds the marrow space, and trabecular or cancellous bone that is found interspersed in the bone marrow compartment, composed of a honeycombed-like network of trabeculae. Cortical and trabecular bone have the same matrix composition. However, the mass of cortical bone matrix per unit volume is much greater. Cortical bone is usually limited to the outer shell of bone providing rigid articular surfaces, and is described as having an outer periosteal and inner endosteal surface. Trabecular bone has a much larger surface area and is found internally (67). Although cortical and trabecular bone have the same composition, the differences in arrangement and distribution facilitate the varied mechanical properties of different bones.

Another categorisation of bone is based on the pattern of collagen forming the osteoid. Again, there are two types, woven bone which is characterised by disorganised and irregular arrangement of collagen fibres, and lamellar bone which is characterised by organised, parallel alignment of collagen fibrils organised into sheets. This structure gives lamellar bone great mechanical strength. Woven bone lacks this organised structure and is produced when osteoblasts lay down osteoid

rapidly. This occurs in all foetal bones during development as well as in fracture healing, however the woven bone is later reorganised into lamellar bone. Lamellar bone makes up almost all of a healthy adult skeleton (68). The arrangement of lamellae varies depending on the specific bone. The organisation of trabecular and the periosteal and endosteal surfaces of cortical bone, the lamellae form continuous circumferential layers located parallel to the bony surfaces. The central regions of cortical bone however are arranged in concentric cylinders around neurovascular channels called Haversian canals. Mineralisation is a gradual process that slows over time. Immature woven bone mineralises faster than lamellar bone. In cortical bone lamellae take on the form of cylindrical osteons. These structures mineralise from inside out, therefore the concentration of mineral is highest in the older peripheral layers and lowest in the inner newest layers (68).

1.5.1 Bone Formation

Bone formation or ossification occurs by two distinct processes during foetal development; intramembranous ossification (IO) and endochondral ossification (EO). IO is initiated by mesenchymal stem cells resulting in bone being laid down in the primitive connective tissue or mesenchyme. This process occurs in the skull, clavicle, and mandible. IO also occurs in the healing process of compound fractures. EO is the formation of bone from a hyaline cartilage precursor. This process occurs in the long bones and involves the ossification of bone in two different anatomical regions (primary ossification centre located in the centre of the diaphysis, and the secondary ossification centres located at both epiphyses) followed by the formation of AC and

epiphyseal plate. This process is essential during the natural healing of long bones (66,68).

1.5.2 Bone Matrix

Calcified bone matrix is a composite material made up of organic and inorganic parts. The organic component constitutes approximately 25% of the wet weight of bone, the inorganic component constitutes approximately 70% with water contributing to approximately 5% of the remaining wet weight of bone. The organic component primarily consists of collagen type I (approximately 90%) and other structural proteins such as proteoglycans and glycoproteins. This gives bone its form and ability to resist tension (66). The inorganic or mineral component consists of hydroxyapatite (99%) giving bone its hardness, rigidity and strength and is the main reason bone is seen on radiographs. Bone mineral also has an important carbonate component and a small amount of calcium phosphate (67). Hydroxyapatite [$Ca_{10}(PO_4)_6(OH)_2$] is the chief mineral salt of bone, contributing to approximately a quarter of the volume and half of the mass of adult bone. Hydroxyapatite is deposited along the collagen fibril where the crystals are packed close together. The major ions in bone mineral are calcium, phosphate, hydroxyl and carbonate. Fluoride ions can substitute for hydroxyl ions (as in ^{18}F PET imaging) and carbonate can substitute for hydroxyl or phosphate ions. The calcium and inorganic phosphate are derived from nutritional sources obtained from blood plasma. Calcium phosphate matures through several steps to produce hydroxyapatite (66).

1.5.3 Bone cells

The cellular components of bone are associated with specific functions. Osteoblasts form new bone, osteocytes maintain bone, and osteoclasts resorb bone. Bone cells originate from two cell lines: a mesenchymal stem cell line where osteoblasts and osteocytes develop and a haematopoietic stem cell line where osteoclasts develop. Osteoblasts are mononucleated cells that line up along the surfaces of new bone and are responsible for the deposition of new bone matrix. They are also responsible for the regulation of osteoclasts in response to systemic hormones such as parathyroid hormone and local cytokines (66,67). As the osteoblasts secrete bone matrix some of them ultimately get trapped giving rise to osteocytes which gradually stop secreting osteoid. Osteocytes are mononucleated and represent terminally differentiated osteoblasts. Osteocytes are the most abundant cell in bone and constitute 90% of cells in the mature skeleton. They are thought to act as mechanosensors instructing osteoblasts when and where to make new bone and instructing osteoclasts when and where to resorb it. They are also thought to play a role in regulating the response of bone to mechanical loading (69,70). Osteoclasts are multinucleated cells responsible for resorbing bone matrix. Unlike osteoblasts and osteocytes, osteoclasts are derived from the hematopoietic stem-cell precursor and contain abundant mitochondria and lysosomes. Osteoclasts have an extremely efficient method to destroy bone matrix, they migrate to the bone surface and resorb bone via a phagocytic method by establishing an acidic environment to solubilise bone matrix and then secreting acid proteases to degrade the remaining matrix (67).

1.5.4 Bone Remodelling

Bone remodelling is the process whereby bone is continually renewing itself throughout life. Bone remodelling is a lifelong active and dynamic process that relies on the correct balance between bone formation by osteoblasts and bone resorption by osteoclasts. These two functions are tightly coordinated, and vital to maintain bone homeostasis. When this coupling is lost the skeleton can become compromised. An increase in osteoclast activity or a decrease in osteoblast activity leads to reduction in bone loss and osteoporosis. In contrast osteopetrosis is the result of failure of osteoclasts to resorb bone leading to increased bone mass (71).

Bone remodelling maintains the structural integrity of the bone and serves its metabolic function of storing calcium and phosphorus. Remodelling also allows the substitution of infantile bone for the stronger organised adult bone, removal and repair of micro fractured or ischaemic bone, acts to maintain correct calcium homeostasis, as well as responding to mechanical loading (thus bone is laid down in areas experiencing increases in load to provide increased strength) (66). The bone remodelling cycle includes a series of highly controlled steps involving osteoblasts and osteoclasts. The first phase is the activation phase where different inputs such as microfracture, an increase in mechanical loading detected by osteocytes, or factors released in the bone microenvironment activate quiescent osteoblasts (lining cells). The next phase is the resorption phase where osteoclasts adhere to the bone surface and begin to dissolve the bone followed by the reverse phase where the debris produced during matrix degradation is removed. The final stage is the formation

phase where osteoblasts produce new bone matrix initially as non-calcified osteoid then promoting mineralisation (71).

1.5.5 Subchondral bone

SB is the zone of epiphyseal bone beneath the ACC and includes the subchondral plate and underlying trabecular bone (Figure 1.5). The subchondral plate includes the ACC and thin layer or cortical bone. SB is a key player in protecting the joint due to its important shock absorbing and supportive functions to the joint and has been shown to attenuate 30% of the joint load, providing a mechanical base for cartilage (72). SB not only provides important mechanical support to cartilage but it provides important nutrients and facilitates removal of waste products. SB undergoes constant adaptation in response to alterations in the biomechanical environment including increases in mechanical loading due to increased body mass, weakened muscles with age and joint instability due to injury (73). SB is known to be extremely important in the pathogenesis of OA and has been used as a key target for treatment. SB changes have also been associated with ochronotic arthropathy in AKU.

1.5.6 Osteoarthritis

OA is the most common degenerative joint disease in the world and is characterised by loss of AC, SB remodelling and osteophyte formation. OA is a polymorphic disease presenting with a variety of clinical symptoms including chronic pain, joint instability, stiffness and radiographic joint space narrowing (62). The aetiology of OA is multifactorial, and several risk factors have been linked to the pathogenesis such as

ageing, menopause, joint injuries, genetic predisposition and obesity. Ageing is considered as one of the most common risk factors. Collagen fibre network stiffens with age resulting in a gradual loss of proteoglycan and water content, this predisposes collagen fibrils to damage via physiological mechanical loading during daily activities (73). Additionally ageing chondrocytes are associated with increased oxidative stress resulting in cell senescence and altered mitochondrial function as well as reduced repair response (62). SB undergoes changes during the OA process including, increased bone turnover, microfractures, angiogenesis and in later stages bone sclerosis subsequently leading to alterations in the mechanical properties of overlying cartilage. SB stiffness is thought to decrease the viscoelastic properties resulting in a reduction in shock absorbing qualities of SB and leading to extra mechanical loading being distributed to cartilage. This ultimately destroys the joint (72). With such a multifactorial aetiology the molecular mechanisms are still to be fully understood. Hence this is why there is still no treatment to restore degraded cartilage or to stop the progression of OA.

1.5.7 Osteoarthritis and Alkaptonuria

Rare diseases have been a neglected area of study in OA research. It is widely recognised that research into rare diseases can provide us with valuable lessons that apply to much more common disorders. Often rare diseases have extreme phenotypes and disease progression is often much more rapid and predictable making it easier to identify the pathological changes. Investigating AKU (characterised by rapid early onset osteoarthritis) has already provided important

lessons in the understanding of OA however, more work is needed to fully understand the initiation and progression of both disorders. Although AKU is a metabolic disorder and the mechanism of joint destruction being due to the molecule HGA resulting in ochronosis, there are many parallels between the pathophysiology of OA and AKU (74). Age related changes lead to alterations in the organisation and composition of the ECM. In AKU HGA is the culprit whereas in non-AKU joints, reaction with sugar molecules leads to the production of advanced glycation end-products. This leads to a stiffening effect on the collagen fibrils resulting in a reduction in the ability to resist mechanical loading leading to structural damage. These changes are initiated in the calcified cartilage, then they spread through to the hyaline cartilage resulting in aberrant transmission of mechanical loading to bone ultimately resulting in resorption of the subchondral plate (74). Knowledge gained from AKU research of great significance is the identification of high density mineralised protrusions (HDMPs). Studies using AKU tissue samples and the AKU mouse model revealed microanatomical cracks in the subchondral plate termed HDMPs that have never been previously identified. Later these changes were identified for the first time in OA indicating that they are widespread in OA too (13,75). Future research aims to make a significant contribution to the development of effective therapies and identification of novel biomarkers for OA.

1.5.8 Intervertebral disc anatomy

The IVD is a fundamental building block of the spine located between adjacent vertebrae in the vertebral column (Figure 1.8). Each IVD forms a fibrocartilaginous

joint allowing slight movement and flexibility of the spinal column. The function of the IVDs is to act as shock absorbers and to transmit and absorb mechanical loading down the spine (76). The IVDs occupy one-third of the height of the spinal column in a healthy adult and are approximately 3-5mm in height in the cervical region, 7mm in the thoracic region and 10mm in the lumbar region with a diameter of approximately 4cm in the lumbar region (77). The healthy IVD consists of three components: the central gelatinous nucleus pulposus; an outer fibrous ring, the annulus fibrosus; and the cartilaginous endplate that connects to the vertebral body.

The annulus fibrosus consists of several (15-25) layers of concentric lamellae composed of type I and type II collagen. Type I collagen is organised around the periphery of the disc where it provides mechanical strength. Elastin fibres lie between the lamellae thought to help the disc return to its original arrangement after bending (77).

The central nucleus pulposus contains collagen fibres, that are organised randomly and elastin fibres that are arranged radially embedded in a highly hydrated aggrecan containing gel (77). The nucleus pulposus functions to aid in distributing pressure evenly across the disc and acts as a shock absorber (78). The IVD is often likened to articular cartilage and resembles this in many ways, particularly in the biochemical components present.

The third morphologically distinct region is the cartilage endplate, a thin horizontal layer usually less than 1mm thick of hyaline cartilage. This interfaces the disc and the

vertebral body. The collagen fibres within the cartilage end plate run horizontally and parallel to the vertebral bodies (78).

The healthy IVD is avascular but contains some nerves, mainly restricted to the outer lamellae. The endplates, like other hyaline cartilage are completely avascular and aneural in a healthy adult. The capillaries, that originate in the vertebral bodies, terminate just above the cartilaginous endplate. Nutrients including HGA in AKU patients, must then diffuse from the capillaries through the endplate and the dense extracellular matrix of the annulus fibrosus and the nucleus pulposus to the cells, which may be as far as 8mm from the capillary bed (77).

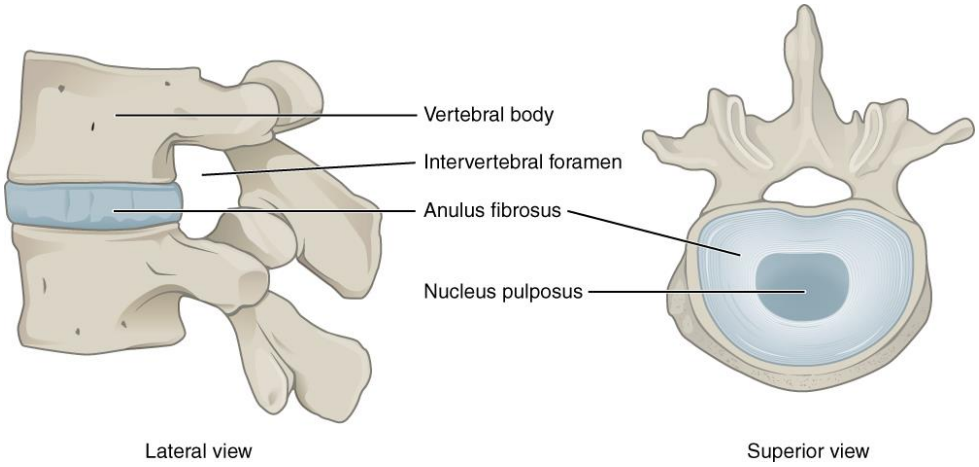

Figure 1.8 Anatomy of the intervertebral disc. The IVD is a fundamental building block of the spine located between adjacent vertebrae in the vertebral column. Each IVD forms a fibrocartilaginous joint allowing slight movement and flexibility of the spinal column. The healthy IVD consists of three components: the central gelatinous nucleus pulposus; an outer fibrous ring, the annulus fibrosus; and the cartilaginous endplate that connects to the vertebral body. Taken from (68).

1.5.9 Intervertebral disc degeneration

IVD degeneration has been identified as one of the leading causes of back pain and motor deficiency. IVD degeneration is thought to be due to both age-related changes and tissue damage caused by multiple stresses. With age the nucleus pulposus dehydrates and its shock absorbing capacity reduces (76). The annulus fibrosus also weakens and is more likely to tear resulting in herniations. The end plates progressively thin and lead to sclerosis of the subchondral plate. The most significant biochemical change to occur in disc degeneration is the loss of proteoglycan which has a major effect on the discs loading properties (76). With loss of proteoglycan, the osmotic pressure of the disc falls and the disc is less able to maintain hydration under load resulting in the discs bulging. Importantly the loss of proteoglycan with degeneration links in with the exposed collagen hypothesis of AKU described by Taylor *et al*. where it has been suggested that tissues are initially resistant to the deposition of HGA due to the protective proteoglycans present. Following mechanical damage to the IVDs the protective proteoglycans are lost and HGA is able to bind to exposed collagen resulting in pigmentation, stiffening and further mechanical damage (76,79).

The clinical features of a degenerating IVD are typically a reduction in disc height, structural deterioration, loss of lumbar lordosis and widespread calcification (76,79). Patients with ochronotic arthropathy usually present with lower back pain as a result of disc deterioration as the initial joint manifestation of AKU. Symptoms worsen from the fourth decade leading to painful spinal disease resulting in spinal stenosis and often changes to the curvature of the spine (kyphosis and scoliosis) (1).

1.5.10 Diagnostic imaging in OA

Plain radiography remains the gold standard for diagnosis of OA. Many attempts have been made to develop diagnostic criteria to define OA. The first formalised radiographic classification of OA was introduced by Kellgren and Lawrence (KL) in 1957, and was later accepted by the World Health Organisation (WHO) in 1961. They developed a five-grade classification scheme to define the severity of OA ranging from 0 – 4, with grade 0 signifying no OA, and grade 4 signifying severe OA (80). Table 1.3 demonstrates the KL classification scale for OA severity. This classification scale is widely used in research and in clinical practice.

Table 1.3 Kellgren-Lawrence radiographic classification scale for OA severity. Grades range from 0-4, 0 reflects no arthritic features present and 4 reflects severe osteoarthritis (Adapted from (80)).

Grade	Description
0	No radiographic features of OA
1	Doubtful narrowing of joint space, possible osteophyte development
2	Possible narrowing of joint space, definite osteophytes
3	Definite narrowing of joint space, moderate multiple osteophytes, some subchondral sclerosis, possible joint deformity
4	Marked narrowing of joint space, large osteophytes, severe subchondral sclerosis, definite joint deformity.

1.6 Medical Imaging in AKU

Medical imaging refers to several different technologies that are used by a clinician to visualise both the morphology and the function of the human body to diagnose, monitor and treat medical conditions. Medical imaging is utilised routinely for all AKU patients that attend the NAC and the SONIA 2 clinical trial. These AKU patients undergo the following investigations annually; X-ray of the spine, bone mineral density testing (DEXA scan) or quantitative computer tomography (QCT), Tc99m isotope bone scintigraphic scan or ^{18}F-NaF PET/CT scan (post 2016), whole body MRI as well as echocardiogram and abdominal ultrasound (46). These images are repeated annually for each patient documenting longitudinal pathological changes.

1.6.1 History of medical imaging

120 years ago, physicians could only rely on external signs and symptoms to diagnose and treat a patient. If they needed to look inside, surgery was the only option. This changed in November 1895 when X-rays were first discovered, this remains the most important discovery in the history of medical technology and enabled physicians and medical professionals to obtain images of inside the body for the first time (81). Wilhelm Conrad Röntgen, a German professor of physics discovered the X-ray by chance. Röntgen discovered this with an early cathode ray tube, he noticed that the invisible rays could penetrate some solid objects (human flesh) better than others (bone and metal). He first introduced the radiographs at the Würzburg Physical Medical Society, where he sent a report with the famous X-ray picture of a hand and wedding ring, believed to be his wife's Bertha. Röntgen was a pioneer in medical

imaging, the most important of his findings was that he identified the ability of various materials of the same thickness to transmit X-rays and this is dependent on their densities, he found also that the ability of samples of the same material to transmit X-rays depends on their thickness; an increase in thickness of the material decreases the transmission of the rays, and he found that photographic plates are sensitive to X-rays (82).

The commercialisation and mass production of X-ray tubes spread worldwide quickly after his work was published and Roentgen was later awarded the first Nobel Prize in Physics in 1901 (83). By the 1920's Fluoroscopy was introduced. Radio-opaque barium swallow or enema was administered, this enabled the radiologist to visualise motion through the gastrointestinal tract. Planar radiographs represent the anatomy in projections, so that the anatomical structures of the region scanned are superimposed on top of each other. X-rays therefore poorly depict small changes in density between tissues (81). X-ray tomography was later introduced in the 1940's that sparked great fascination within the medical community. This imaging modality allowed visualisation of sections through the body without superimposition. X-ray tomography produces 'tomograms' that display the anatomy slice by slice. This was achieved by rotating the X-ray tube around the patient so that only the desired slice of tissue stayed in focus.

The first computer was made in 1946, and by 1970s Allan MacLeod Cormack and Godfrey Newbold Hounsfield invented computed tomography (CT), pairing the discovery of X-rays with the development and refinement of computational techniques (83). They were awarded the Nobel Prize for Physiology or Medicine in

1979. The first CT scan was performed in 1971, where an X-ray tube rotated around the patient and various detectors detected X-rays that were not absorbed, refracted or reflected as they passed through the body. Early computers took all night to process the images that today takes a few milliseconds (82).

The risks of imaging using radiation were realised including the increased risk of developing cancer in the future. In 1973 Paul. C. Lauterbur an American Chemist, published his work on magnetic resonance imaging (MRI) that does not utilise X-rays. He utilised resistive magnets with weak magnetic fields producing images initially with low spatial resolution, however the soft tissue discrimination was seen to be superior to that of CT (84). In the late 1970's Peter Mansfield an English Physicist developed the echo-planar imaging technique that would lead to clearer scans that take seconds rather than hours. In 2003 Paul Lauterbur and Peter Mansfield were awarded the Nobel Prize for Physiology or Medicine for their discoveries of MRI (83).

1.6.2 Radiography

Plain radiographs form the most basic, least expensive imaging tests carried out on patients with arthropathy. Radiographs have a useful role in symptomatic joint disease and highlight destructive lesions such as osteophytes, subchondral sclerosis and cysts. Radiography can also illustrate joint space width which determines AC loss as well as cartilage calcification (85).

1.6.2.1 Basic principles of radiography

Radiography has been used for over 120 years since Röntgen discovered X-rays in 1895. X-rays are a form of electromagnetic radiation which consist of high-energy photons (86). X-rays are produced in an X-ray tube consisting of a glass envelope, filament cathode, a copper anode and a tungsten target (Figure 1.9). The cathode is the source of electrons; the electrons are accelerated towards the target by applying a high voltage between the anode and the cathode. When the electrons hit the tungsten target they decelerate rapidly creating X-ray emissions (86). The X-rays are passed through the patient and detected by the X-ray sensitive film located behind the patient (Figure 1.10). X-rays are absorbed by the material they pass through in differing amounts depending on the density and composition of the material. As the X-ray beam is passed through the body, some X-rays are absorbed or scattered attenuating the beam. Structures of high density (bone) cause high X-ray attenuation therefore appear lighter on the radiographic film and structures with low density (fat/air) cause less X-ray attenuation and appear darker on the film (87). Traditionally X-ray images were exposed onto photographic film and were processed in a dark room, today radiographic images are produced digitally using computed radiography or digital radiography. The digital images are sent straight to the viewing workstations and can be manipulated (images can be magnified, brightness/contrast can be altered and measurements can be taken) for better interpretation. Many medical imaging departments employ large data storage devices known as picture archiving and communication systems (PACS) this digitally stores all the images (including all other imaging modalities) allowing instant recall and display of patient scans (88).

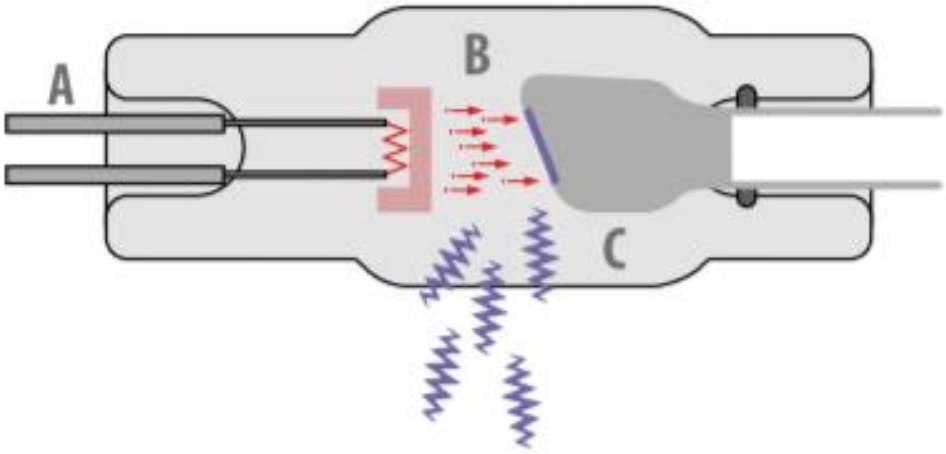

Figure 1.9 Generation of X-rays in an X-ray tube consisting of A – cathode, B – Tungsten target (blue line), C – anode. The cathode is the source of the electrons (red arrows); the electrons are accelerated towards the target (B) by applying a high voltage between the anode (C) and the cathode (A). When the electrons hit the tungsten target they decelerate rapidly creating X-ray emissions (blue jagged lines) (Taken from (86)).

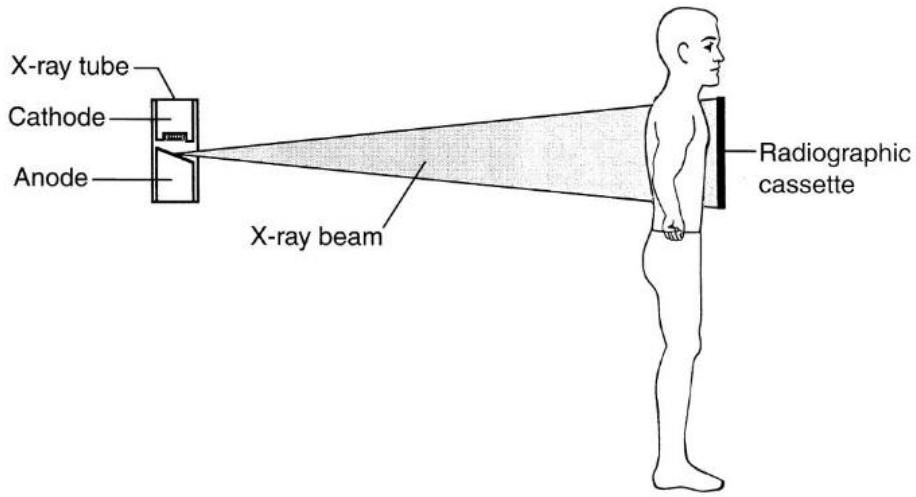

Figure 1.10 Set up of a chest radiograph. Posteroanterior X-ray where the X-ray beam originates from the X-ray tube passes through the patient and strikes the radiographic film (Taken from (87)).

1.6.3 Bone densitometry

Until recently plain radiographs were used to determine bone density, however this was an estimation and bone loss was not observed until bone loss exceeded 25-30% of its density. This led to finding more sophisticated methods of measuring bone density with the ability to detect early changes. The two most common tools used to measure bone mineral density (BMD) are dual-energy x-ray absorptiometry (DEXA) and quantitative computer tomography (QCT). These techniques are used to diagnose osteoporosis and to evaluate the risk of fracture. These imaging modalities are carried out routinely in both the NAC and the SONIA 2 clinical trial as it is widely recognised that changes in cartilage composition have direct implications for bone in AKU. The NAC patients have bi-annual QCT scans, and the SONIA 2 patients have

annual DEXA scans. In AKU it is proposed that chronic arthritis can impair bone architecture which then may predispose AKU patients to fractures (89). It is still however under debate as to whether bone lesions cause osteoarthritis or whether cartilage disease results in bone lesions, extensive research is still ongoing to understand this further.

1.6.3.1 Basic principles- DEXA

DEXA has long been used as the gold standard in the clinical diagnosis of osteoporosis. DEXA determines BMD in two dimensions and is based on the emission of two X-rays of two distinct energies (90). The fundamental principle of DEXA is the measurement of X-ray transmission through the body at high and low energies and the assumption that the body is a two-compartment model made up of bone mineral and soft tissue. The two X-ray beams of differing intensities are used to differentiate between bone and soft tissue. The ratio of attenuation of the two photon energies is analysed in anatomical sites containing bone and areas just containing soft tissue. The ratio of attenuation in areas of soft tissue can then be subtracted away leaving just the BMD (91,92).

BMD is measured in g/cm^2, however it is more commonly referred to as the T-score. It is expressed as the number of standard deviations above or below the mean BMD of a healthy 30-year old adult (peak bone density) of the same sex and ethnicity as the patient. Figure 1.11 represents a DEXA report of an AKU patient. Table 1.4 illustrates the WHO definitions of BMD levels. Osteoporosis is defined as a T-score equal to or below -2.5, Osteopenia as a T-score of below or equal to -1.0 and normal

BMD is equal to one standard deviation above or below that of a healthy adult (91). No upper reference value has been proposed as the adverse effects of increased BMD have been poorly studied. DEXA at the lumbar spine and femoral neck are the routine sites chosen to measure BMD. Spinal degeneration such as IVD calcification, osteophyte formation as well as abdominal aortic calcification has been shown to result in a false reading of increased BMD in DEXA. Yu *et al*. (93) reported that BMD measured by DEXA was significantly higher in patients with spinal degenerative joint disease changes than in those without. Spinal degeneration is inevitable in AKU and clinically presents around the fourth decade of life. This defines why it may be problematic to used DEXA as clinical findings may indicate osteoporosis, whilst the DEXA report may indicate BMD is normal (94).

1.6.3.2 Basic principles - QCT

QCT measures BMD using an X-ray computed tomography scanner containing a calibration standard to convert Hounsfield units into BMD values. The sites most commonly measured to determine BMD are the lumbar spine and hip (95). QCT is more costly and requires more ionising radiation than DEXA but has numerus advantages. This method yields volumetric 3D measurements of BMD as well as providing a measurement of trabecular and cortical bone density which is due to the difference in attenuation values of trabecular and cortical bone (95). This method has the ability to spatially separate highly responsive cortical bone from less responsive trabecular bone. This is useful because trabecular bone loss is affected earlier and to a greater degree than cortical bone. QCT is therefore likely to detect low BMD earlier in the spine than DEXA. Artificially high BMD due to spinal degeneration such as

calcification and osteophyte formation can therefore be avoided (94). QCT yields both BMD in g/cm³ and T-scores however, the WHO definition of osteoporosis (Table 1.4) is specific to DEXA and should not be applied to QCT. It is important to note that QCT T-scores cannot be used to compare with DEXA T-scores. More often than not the QCT T-score results in a lower T-score than that of the DEXA report. It has been reported that a DEXA T-score of -2.5 equals an average T-score of -3.4 in QCT, therefore DEXA is currently the only method to diagnose osteopenia or osteoporosis from T-scores (96). This is due to a variety of factors such as the physiological effects of ageing and the menopause, the technical effects of increased mineral density due to osteophytes and aortic calcification, increased BMI as well as bone size (94). These effects will be discussed further in Chapter 5.

Table 1.4 World Health Organisation definitions of bone mineral density levels. BMD- bone mineral density, SD- standard deviation (Adapted from (91)).

Level	Definition
Normal	BMD within 1 SD of the young adult mean
Osteopenia	BMD is between 1 and 2.5 SD below the young adult mean
Osteoporosis	BMD is 2.5 SD or more below the young adult mean

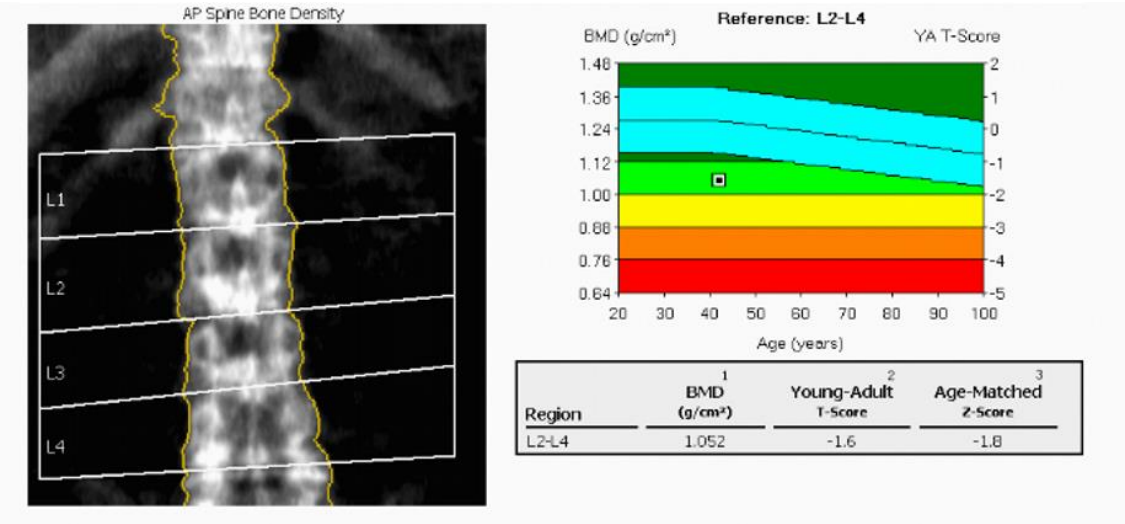

Figure 1.11 Dual-energy X-ray absorptiometry report. BMD is measured in g/cm³ of bone. The young adult T-score value represents how BMD compares to a healthy 30-year old adult of the same sex and ethnicity (values of +1 or -1 represent normal BMD, values between -1 and -2.5 indicate osteopenia, values below -2.5 indicate osteoporosis). Age matched Z score compares BMD to others of the same age as the patient.

1.6.4 Computed tomography

CT is considered more sensitive than conventional X-ray imaging due to high spatial resolution and high contrast between low attenuating cartilage and high attenuating bone. Whole body CT and arthrography are utilised in AKU to determine cartilage damage and cartilage loss in the major joints affected. CT arthrography is excellent at depicting cortical bone and soft tissue calcifications as well as subchondral bone sclerosis and osteophytes associated with severe changes of OA (85).

1.6.4.1 Basic Principles - CT

The word tomography is derived from the Greek word *tomos*, meaning slice. This definition demonstrates the fundamental limitations of the radiograph and represents the downfall that anatomical structures are viewed in a single plane and superimposed on top of each other. This led to the development of CT; an imaging modality whereby cross sectional images are obtained using X-rays (97). A CT scanner produces serial images that represent the X-ray attenuation of the various structures of the body. In CT scanning the patient is passed through a rotating gantry that has an X-ray tube on one side and a set of detectors on the other side (86). A fan shaped beam of X-rays is produced as the gantry spins around the patient and thousands of sectional views of the body are generated that are reconstructed into 2D cross sectional images. CT scans can be acquired very quickly and have a much higher resolution than conventional X-rays providing far more detailed images. The data captured by the scanner is digitally converted into reconstructed images using various algorithms (88). The individual volume elements that make up the image are represented as 2D pixels that correspond to the attenuation properties of that area (represented as Hounsfield units (HU)). In CT water is assigned an attenuation value of 0 HU, structures that are less dense than water have negative values (e.g. air = -1000 HU, fat = -120 HU), structures that are more dense have positive values (e.g. muscle = 40 HU, bone = 500 HU). As in plain X-rays high density objects such as bone cause more attenuation of the X-rays and are therefore displayed as white or light grey, and the lower density tissues such as fat and air are displayed as dark grey or black (88).

1.7 Nuclear Medicine

Nuclear medicine involves the application of radioactive substances in the diagnosis and treatment of disease. The purpose of radionuclide imaging is to obtain a picture of the distribution of the radioactive-labelled tracer around the body after it has been administered (either orally or intravenously). The emissions from the radioactive tracers are detected by cameras externally and are then converted into an image. Nuclear medicine in AKU uses phosphate analogues to visualise bone metabolism, changes of which occur in response to alterations in cartilage composition and structure (89). Positron emissions tomography (PET) is a branch of nuclear medicine where a positron-emitting radionuclide is injected into the subject. Fluoride 18-labelled PET imaging provides a unique non-invasive method to visualise bone metabolism, and molecular and cellular changes in affected joints. Changes in bone metabolism occur before clear morphological signs in OA and AKU, therefore PET imaging can be used to detect early pathological changes. PET also has a common place in oncology, used to diagnose bony metastasis as well as assess response to therapy (98,99). Hybrid imaging techniques involving fusion of PET data with CT data provide the clinician with cross-sectional functional and anatomical information used for more accurate diagnosis (89).

PET imaging has superior spatial resolution compared to other functional imaging techniques such as SPECT (single-photon emission computed tomography). SPECT is similar to PET in that it utilises radiotracers and detects gamma rays however, SPECT radionucleotides directly emit gamma radiation without annihilation. The coincident detection of the photons in PET imaging provides more radiation event localisation

therefore better spatial resolution. SPECT imaging is performed using the gamma camera and acquires multiple 2D images that are reconstructed into a 3D images. PET imaging is performed using PET/CT scanner and acquires 4D images (100).

1.7.1 History of Nuclear Medicine

The development of nuclear medicine has been a multidisciplinary effort due to advances in physics, mathematics, chemistry, computer science and biology (101). The discovery of X-rays in 1895 lead to Henri Becquerel's discovery of 'mysterious rays'. Becquerel used salt of uranium and potassium and he noticed once exposed to sunlight the salt emitted radiation that blackened a photographic plate. This inspired many scientists to investigate this further and in 1897 Marie and Pierre Curie tried to isolate the substances that emitted these rays in doing so they discovered polonium and radium. They coined the term and confirmed the existence of 'radioactivity' (102). In 1909 Sir Ernest Rutherford demonstrated what happens to an element during radioactive decay. Positron emission tomography (PET) is a branch of nuclear medicine that utilises the detection of a pair of gamma rays that are emitted indirectly by a positron-emitting radiotracer.

The history of PET dates back to the late 1920's, where the discovery of the positron, artificial radiation, invention of the cyclotron and recognition of radionuclides were among the important advances (101). In the 1950's Hal Anger developed the first gamma camera; the Anger scintillation camera, a 2D planar detector that produces a 2D projection image. Radon, developed the mathematical method to reconstruct projections in 1917 however, it was the 1970's before its use in medical imaging came

to light. The first PET system was built in the 1970's and used for phantom studies. The first human PET system was built soon after by Phelps and Hoffman *et al*. in 1975 followed by Sokoloff *et al*. producing the first true image of the human brain in 1976 (86). PET imaging continued to advance from here, in 2000 Beyer *et al*. conducted the first PET/CT scan marrying together both functional and anatomical information. Furthermore the development of technology and computer based algorithms enhanced image resolution and improved the use of PET as a clinical tool that has contributed to more accurate diagnosis of many diseases (103).

1.7.2 Positron emission tomography- physical principles

Proton rich isotopes decay via positron emission, in which a proton in the nucleus decays into a neutron, and a positron and neutrino (104). Upon administration of the radiotracer the radioactive atom decays resulting in a positron being ejected from the nucleus. The positron travels a few millimetres before colliding with an electron resulting in an annihilation event producing two 511 KeV photons that travel in opposite directions. PET image acquisition is based on the simultaneous (coincident) detection of these two photons (Figure 1.12). The PET scanner consists of many photon detectors that are positioned surrounding the subject. During a PET scan millions of coincident detections are detected, that are reconstructed into electrical signals providing information about the distribution of the radiotracer (105).

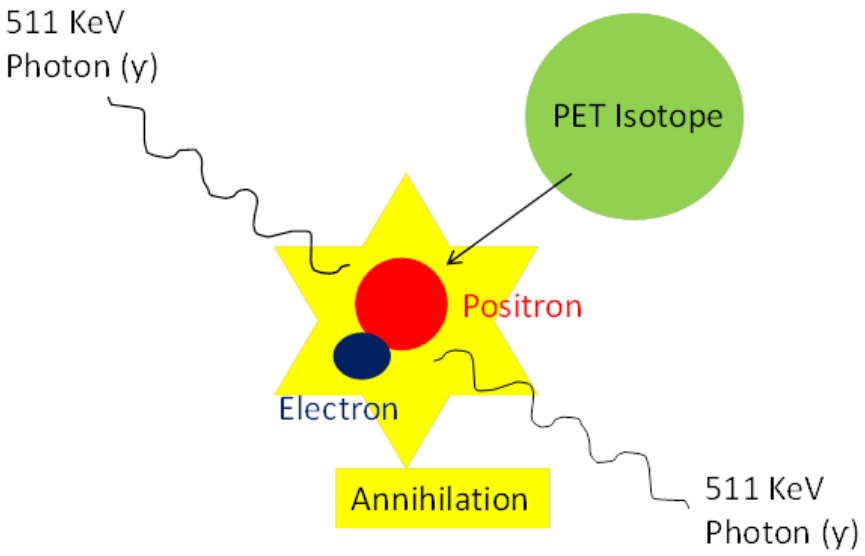

Figure 1.12 Positron emission schematic. The PET isotope injected into the patient decays via positron emission. The positron is emitted from the nucleus and travels a few millimetres before colliding with an electron. This results in an annihilation event producing two 511 KeV photons that travel in opposite directions from one another (Adapted from (105)).

1.7.3 Bone imaging radiopharmaceuticals

Absorption of fluoride by bone, dentine and enamel was first discovered in 1940 followed by the introduction of ^{18}F-labelled sodium fluoride (^{18}F-NaF) by Blau *et al*. in 1972. ^{18}F-NaF became widely used as a bone imaging agent and was approved by the U.S. Food and Drug Administration (FDA) in 1972 (106). ^{18}F-NaF gained popularity due to its high skeletal uptake and rapid blood clearance resulting in high bone-to-background ratio in a short space of time. Images can be obtained less than one hour after intravenous administration due to the relatively short half-life (Table 1.5).

Although ^{18}F-NaF was the first widely used bone imaging agent it quickly fell into disuse. One limitation of ^{18}F bone imaging was the requirement of imaging with high energy rectilinear scanners equipped with thick Sodium Iodide crystals due to the high energy (511 KeV) annihilation photons. Logistical challenges of the 110 minute half-life of ^{18}F-NaF , the introduction of cheaper radiopharmaceuticals (technetium-Tc-99m) and the development of the Anger gamma camera designed for the 140 KeV photons of Tc-99m resulted in the FDA withdrawing its approval in 1975 (107). The widespread availability of Tc-99m generators resulted in Tc-99 labelled bone imaging agents to become the most commonly performed imaging procedure in nuclear medicine.

The challenges associated with ^{18}F-NaF imaging were reassessed in 1992 when Dahlbom *et al*. (108) used ^{18}F-NaF in the development of a whole-body PET technique that demonstrated increased spatial resolution, and greater photon capture due to coincident detection of photons. ^{18}F-NaF whole body PET skeletal imaging was later introduced in 1993 with early studies showing promising results for both malignant and metabolic bone disorders. This led to the FDA re-issuing approval of ^{18}F-NaF for skeletal imaging in 2000 (106). Since then the development of combined PET/CT scanners, ease of production in a cyclotron (previously ^{18}F-NaF was produced in a nuclear reactor with a two-step reaction) coupled with shortages of Tc-99m generators, has led to ^{18}F-NaF being the preferred bone imaging agent once again (109).

As a skeletal imaging agent ^{18}F-NaF has superior skeletal kinetics compared to Tc-99m including faster blood clearance and two-fold higher bone uptake providing superior

bone-to-background ratio. This along with the added benefits of the PET scanner provides better spatial resolution, greater sensitivity and higher image quality (110) (Table 1.6). Furthermore, PET imaging allows quantitative measurements of NaF uptake that cannot be generated from other imaging modalities. Measurements that represent the uptake of NaF in a particular region of interest (ROI) can be used to assess the progression of disease and response to therapies (106).

Table 1.5 Comparison between the characteristics of ^{18}F-NaF and Tc-99m MDP bone imaging agents (Adapted from (106)).

Characteristic	^{18}F-NaF	Tc-99m
Radiotracer half-life	110 min	6 hr
Emissions	511 KeV annihilation photons	140 KeV photon
Spatial resolution (mm)	3-6	4-15
Organ receiving highest dose	Bladder	Bone
Patient dose (mSv)	4.4-8.9	4.2-6.3
Time to imaging after injection	30-60 minutes	3-6 hr
Technique	PET	SPECT Anger camera

1.7.3.1 Mechanism of ^{18}F-NaF uptake

Fluorine 18 is produced in a cyclotron by bombarding ^{18}O-enriched water with high energy protons (111). Fluoride is well known to be taken up by bone mineral. The pharmacokinetics of ^{18}F-NaF uptake essentially depend on the rates of bone uptake and elimination from the circulation via renal excretion. ^{18}F-NaF is administered

intravenously and the images are acquired 60 minutes' post injection (112). ^{18}F-NaF localises to bone and is distributed throughout the skeleton. The principle uptake mechanism involves absorption of ^{18}F-NaF into the hydroxyapatite crystal of bone where substitution of $^{18}F^-$ for OH^- groups occurs. This results in covalent binding to hydroxyapatite ($Ca_{10}(PO_4)_6OH_2$) to form fluorapatite compounds ($Ca_{10}(PO_4)_6F_2$) (111). Uptake is higher in new bone (osteoid) due to the higher availability of binding sites (109). The rate of ^{18}F uptake into bone therefore reflects the amount of actively mineralising bone present and closely resembles bone metabolism. Uptake in cartilage is seen in patients with calcification in the IVDs where ^{18}F can bind to form fluoroapatite.

Radiotracer delivery and localisation to bone depends on regional blood flow and the extraction rate of bone. Changes in radiotracer kinetics therefore relate to osteoblastic activity and or bone vascularity (110). Increased vascularity and bone turnover are both seen in osseous and metabolic diseases. Radioactive NaF clears biexponentially in plasma ensuring that only 10% of the administered dose remains after one hour. Soft tissue activity therefore should be minimal and reflects the amount of circulating ^{18}F in the blood pool, hence good-quality images. Excretion of ^{18}F is via the urinary tract. Kidneys, ureters and bladder should be visible in the absence of renal insufficiency and urinary obstruction will cause increased tracer localisation proximal to the site of obstruction. Physiologic uptake of ^{18}F in the skeleton is generally uniform in adults, and areas of increased localisation of tracer uptake reflects increased bone metabolism at that site (113).

Table 1.6 Advantages of ^{18}F-NaF PET for studying bone tracer kinetics (Adapted from (110)).

^{18}F-NaF Advantages
Superior spatial resolution of PET scanner
^{18}F-NaF shows rapid bone uptake
^{18}F-NaF clears rapidly from blood
High bone to soft tissue background
^{18}F-NaF easily generated in cyclotron by irradiation of ^{18}O-enriched water
PET scanners widely available

1.7.4 Quantitative measurement of ^{18}F-NaF – SUVm

Quantitative measurements in PET imaging are used as a tool to supplement visual interpretation providing a method that is less user-dependant and can be used for intra- and inter-patient comparisons. Today, uptake measurements are most widely used in oncology to assess response to therapies and to distinguish degrees of pathology (114). ^{18}F-NaF PET has been applied to several kinds of bone disorders as ^{18}F-NaF binds to both osteoblastic and osteolytic lesions. Uptake values have been investigated for the early detection of OA (115). The standardised uptake value (SUV) is a common method of expressing the uptake of PET tracers. The SUV is a measure of radioactivity in a region of interest, normalised against injected activity and the subject's body weight. The calculation can be seen in Figure 1.13 where the SUV is defined as the activity concentration in the ROI (kBq/mL) as measured by the PET scanner divided by the decay corrected injected dose of ^{18}F-NaF divided by the patient body weight (kg) that acts as a surrogate for the distribution volume of tracer (116). If all the injected ^{18}F-NaF is retained and uniformly distributed throughout the

body, the SUV will be 1g/ml under the assumption that 1ml of tissue weighs 1g. Larger SUVs represent proportionally higher concentrations of radiotracer. The uptake is represented by pixel or voxel intensity value in the ROI, which is then converted into the activity concentration (117). SUV can be expressed as SUVm (mean SUV in ROI), SUVmin (minimum SUV in ROI) or SUVmax (maximum SUV in ROI). SUVs have been described in the literature as quantitative measurements of disease state. SUVs can be used to assess disease progression and response to therapy and has more recently been proposed as a diagnostic tool.

$$SUV = \frac{r}{(a / w)}$$

Figure 1.13 Standardised uptake value calculation. Where 'r' is the radioactivity concentration (kBq/ml) in a ROI, divided by 'a' the decay corrected injected dose (kBq) divided by body weight (kg) (118).

1.7.4.1 SUV measurements in osteoarthritis

PET imaging has been applied to OA for the visualisation of bone metabolism. Currently plain X-ray is the gold standard for diagnosing OA, however it is realised that functional abnormalities can exist without radiographic evidence. ^{18}F-NaF PET has been shown to detect early changes in OA by identifying areas of accelerated bone remodelling associated with OA pathology. Kobayashi *et al*. (115) measured the SUV at the hip and revealed accelerated bone remodelling in late-stage OA. The SUVm was significantly associated with the radiographic stage of OA (KL grade), as well as the severity of pain. These authors suggested that hip pain may be related to subchondral bone abnormality caused by mechanical stress (115).

The molecular kinetics of ^{18}F-NaF PET is based on bone metabolism, other studies have assessed the use of 18-F fluorodeoxyglucose (^{18}F-FDG), utilised to visualise inflammation by detecting accelerated glucose metabolism. However, 18F-FDG has been shown to be more suitable for the detection of soft tissue inflammation as seen in synovitis or rheumatoid arthritis. Several studies have stated that there is no specific SUV that defines either benign or malignant lesions (119). However Kobayashi *et al*. (120) stated that a SUVm of 6.4 can be used to predict OA incidence or progression. SUVm has been used in the literature over SUVmin or max as the mean SUV in the ROI provides a better representation of the uptake in that site. The utilisation of SUVs in AKU has not previously been investigated. Considering the pathology of OA is comparable to that of AKU, it can be appreciated that these quantitative measurements could be beneficial in assessing AKU disease pathology as well as in the clinical trials to assess response to nitisinone.

Currently AKU patient ^{18}F-NaF scans are analysed as part of the AKUSSI (Table 1.2) to assess the extent and burden of arthropathy. The scans are assessed by a nuclear medicine consultant and a visual assessment of the whole skeletal system is conducted, involving mapping of the various large joints with arthritic changes. The 14 large joint areas scored include the hips, knees, ankles, feet, shoulders, elbows, hands including wrists. Spine involvement was also scored and included the cervical, thoracic and lumbar regions. The nuclear medicine consultant gives a score of 1 if there is increased tracer uptake at that anatomical site, and gives a score of 0 if there is normal uptake. These scores are then fed into the AKUSSI and contributes to an overall composite score of disease severity (46). Additionally an index of the relative activity of arthropathy is also given by visual assessment of the intensity of skeletal uptake, for example the scoring ranges from 0-3, where 0 = normal, 1 = mild, 2 = moderate and 3 = intense uptake (89). The AKUSSI describes the extent of disease manifestations but does not quantify disease burden. This thesis introduces for the first time, quantitative SUV measurements of bone and cartilage to assess disease state and progression in AKU.

1.7.5 Maximum Intensity Projection

A maximum intensity projection (MIP) image is a method of visualisation where the voxels with the highest intensity are projected on to a two-dimensional image. This method displays bone and contrast material - filled structures preferentially and other low attenuation structures are not well visualised. This method is useful clinically to visualise areas of high uptake of ^{18}F into the skeleton or calcified tissues.

2.0 MATERIALS AND METHODS

2.1 ETHICAL APPROVAL

Ethical approval for the NAC was approved by the Health and Life Sciences Committee on Research Ethics, University of Liverpool for 'analysis of data from the National Alkaptonuria Service which could help us better understand AKU' (reference:0310), dated 26/05/2017.

Ethical approval for the SONIA 2 clinical trial was granted by the National Research Ethics Service (REC reference: 13/NW/0567), dated 17/9/2013.

2.2 PATIENT GROUPS

2.2.1 NAC

Forty three adult AKU patients (17 females, 26 males) with a mean age of 49 (SD±14.8 range 21-74) attended the National Alkaptonuria Centre in the Royal Liverpool University Hospital, Liverpool, England for baseline tests in 2012. A plethora of assessments and tests are carried out including the following; blood samples, urine samples, X-Ray, MRI, DEXA, PET/CT, ultrasound (abdomen and pelvis), clinical eye photographs, ear cartilage biopsies and echocardiograms. Patients all received 2mg of off-label nitisinone daily after the baseline visit. Twenty two of the forty three patients have attended the NAC annually for four visits after baseline providing longitudinal analysis of nitisinone.

2.2.2 SONIA 2

AKU patients were recruited for the SONIA 2 clinical trial in 2014/15. 138 patients in total were enrolled, 69 of which were randomly selected to receive nitisinone (10mg/day). The 138 patients are based across three trial sites; Liverpool, Paris and Piestany. The Liverpool site has 41 patients attending (16 females, 25 males) with a mean age of 51 (SD±10.9 range 30-68) at baseline. Only the Liverpool patients were analysed for the purpose of this thesis. Data was available for visit 1 (baseline) and visit 3 (1-year post nitisinone/no treatment).

2.2.3 CONTROL GROUP

Ten female non-metastatic breast cancer patients were used as a control group with a mean age of 62 (SD±13.8 range 43-84). These patients had undergone ^{18}F-NaF PET scanning to determine suspected bony metastasis. Exclusion criteria included active arthropathy of the spine, hips or shoulders.

Table 2.1 Patient demographic characteristics for the 4 groups of patients analysed.

Patient Group	SONIA 2 – AKU	NAC – AKU	NAC – AKU 4 visits	CONTROL
Number of patients	n= 41	n=43	n=22	n=10
Male: Female	25:16	26:17	13:9	0:10
Mean age (±SD)	51 (±10.9)	49 (±14.8)	47 (±16.1)	62 (±13.8)
Age range	30-68	21-74	21-75	43-84
Chapters analysed in:	Chapter 4 Chapter 6	Chapter 3	Chapter 5	Chapter 4 Chapter 5

2.3 PET/CT PROTOCOL

Two hundred Mbq of ^{18}F-fluoride was injected into the patient intravenously by direct venepuncture or intravenous catheter. Whole body PET and low dose CT views were acquired 60 minutes' post injection.

2.4 ^{18}F-NaF PET THRESHOLD APPLICATION

2.4.1 IMAGE TYPE

Maximum intensity projection (MIP) PET images were used for the threshold application study. MIP PET images are 3D reconstructions of PET data representing the maximum pixel value on every view. This method displays bone and calcified tissue preferentially providing a clearer image by blocking low attenuating structures like soft tissue that may occlude visualisation.

2.4.2 IMAGEJ SOFTWARE

ImageJ (1.49j) is a public domain, Java-based image processing program developed at the National Institute of Health. ImageJ can display, edit, analyse and process 8-bit, 16-bit, 32-bit and RGB files and can read many file formats e.g. TIFF, JPEG, DICOM including stacks (121).

2.4.3 HISTOGRAM ANALYSIS

Baseline 8-bit MIP PET images of the 43 NAC patients were imported into Image J (1.49j). A histogram plot was created for each patient to analyse the distribution of pixel values within the image. The pixel values within the image ranged from 0-255

(0 = black, 255= white) (Figure 2.1). A large proportion of the pixel values in the image are white representing the background as demonstrated by the large spike around 245, a small spike can be seen at pixel value 0 representing the areas of high uptake of ^{18}F into bone and calcified tissue.

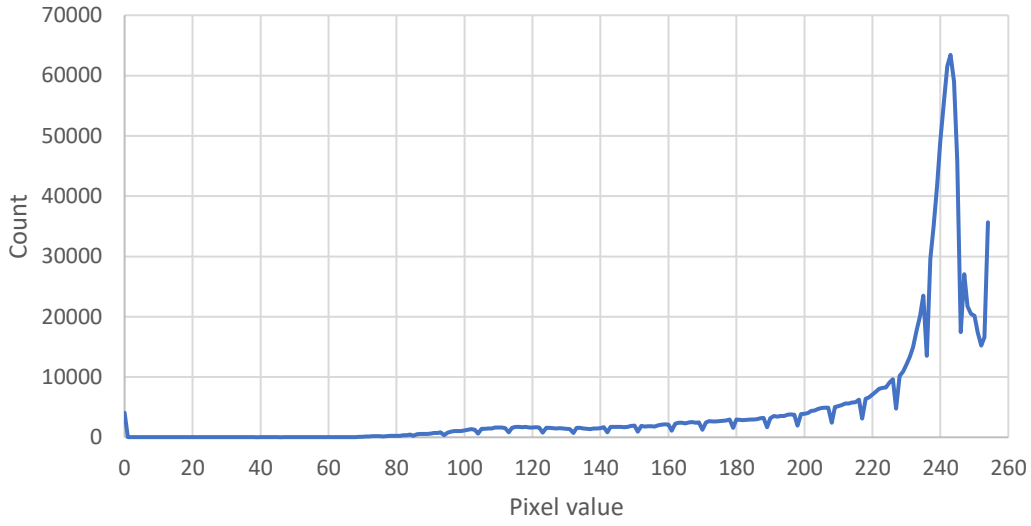

Figure 2.1 Histogram plot of MIP PET image pixel value distribution. Pixel values ranging from 0 – 255 (0 = black, 255 = white) (NAC patient 9).

Another histogram was created to further analyse the small spike at 0 as this represented the areas of high uptake of ^{18}F thought to be associated with disease pathology (Figure 2.2A). A threshold value was then identified from the histogram and the pixel value was selected on the graph where the pixel counts start to increase (position indicated by the red line- pixel value 70) (Figure 2.2A). A threshold value was identified this way for every patient.

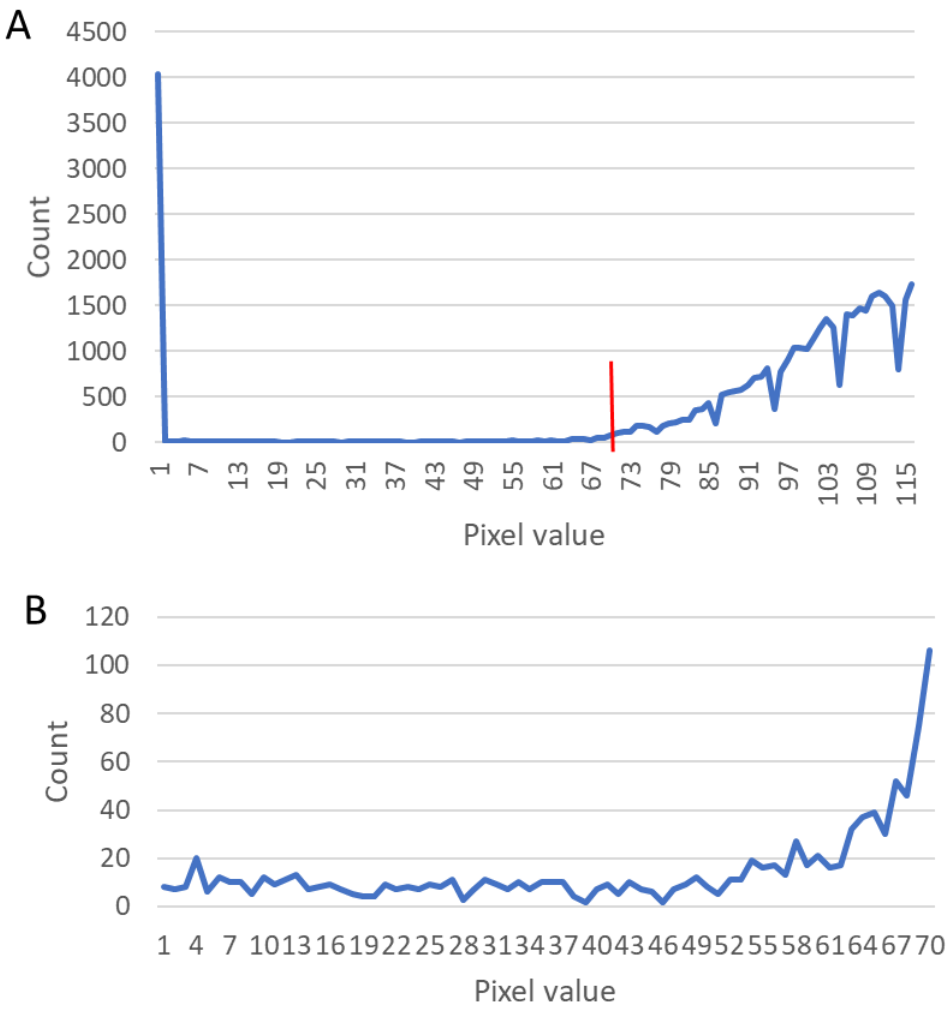

Figure 2.2 Histogram plot of MIP PET image pixel value distribution analysing the darkest pixels in the image (0 = black 255 = white). A- represents the spike at zero and demonstrates the threshold applied to the point on the graph where the pixel values start to increase (threshold value indicated by the red line – value of 70). B- demonstrates the counts in between pixel values 1 to 70.

2.4.4 THRESHOLD APPLICATION

After obtaining a threshold value from each patient's histogram plot (as described in section 2.4.3) this value was applied to the MIP PET image using ImageJ (Figure 2.3). The pixel values above the threshold value can be seen highlighted in red for easy visualisation in Figure 2.3. These pixel values were then considered as regions of increased uptake of ^{18}F at that anatomical region.

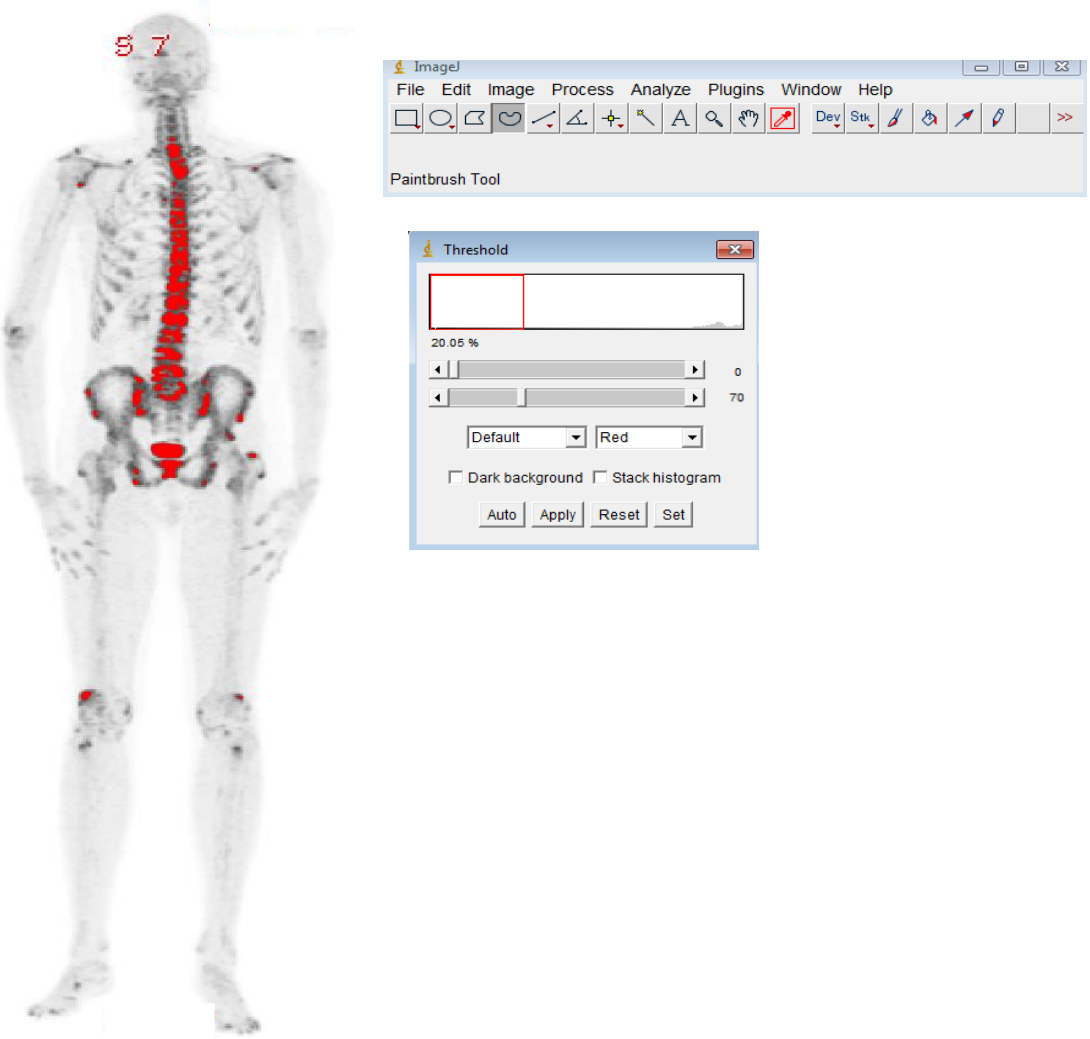

Figure 2.3 Threshold application. 8-bit ^{18}F MIP PET image with a threshold value of 70 applied. The pixel values highlighted in red are identified as pixels above the threshold value.

2.4.5 ANATOMICAL SCORING

The thresholded MIP PET images were then assessed anatomically. Both cartilage and bone were analysed for increased tracer uptake (pixels above threshold were considered as increased tracer uptake) and they were scored for the presence of pixel values above threshold. Figure 2.4 illustrates uptake of ^{18}F into cartilage and bone of the spine demonstrating that the quality of these ^{18}F MIP PET images enabled easy identification of bone and cartilage. The following anatomical regions were analysed, for the bony anatomy; the calcaneus, talus, midfoot, forefoot, tibia, fibula, patella, femur, hip, sacrum, vertebrae (L5-C1), scapulae, humerus, radius, ulna, carpal, metacarpal/ phalanges, clavicle and sternum. These regions were scored 0 or 1 (0= if no pixels were present above threshold 1= if pixels were identified above threshold (red)). For the cartilage, the joints of the foot, ankle, knee, hip, sacroiliac joint, intervertebral discs (S1/L5 – C1/C2), shoulder, elbow, wrist, hand were scored 0 or 1 as described above. Figure 2.5 represents a labelled skeletal map demonstrating the various cartilaginous joints and bones analysed. This method aims to remove any subjectivity in observing regions of increased tracer uptake associated with disease pathology.

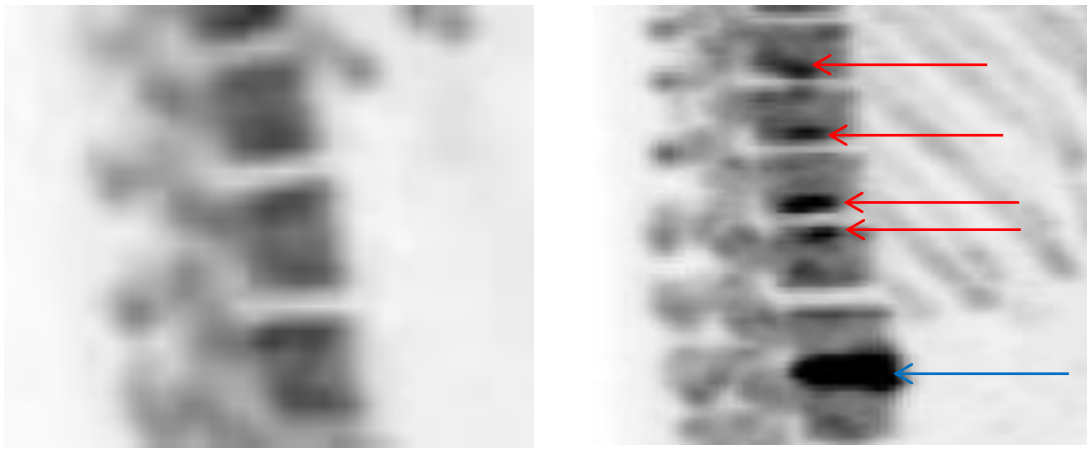

Figure 2.4 ^{18}F MIP PET images of lumbar vertebrae and intervertebral discs. Left image- control spine indicating healthy IVDs and vertebrae. IVDs appear light grey on the image due to few gamma photons. In contrast the vertebrae appear darker due to more gamma photons in these regions (^{18}F binds to bone). Right image – AKU spine demonstrating increased uptake in the end plates of the vertebrae, as well as the cartilage of the IVD (red arrows indicate increased tracer uptake in the bony vertebrae, blue arrow indicates increased tracer uptake in the intervertebral disc). The quality of the ^{18}F MIPs allows confident identification of cartilage and bone.

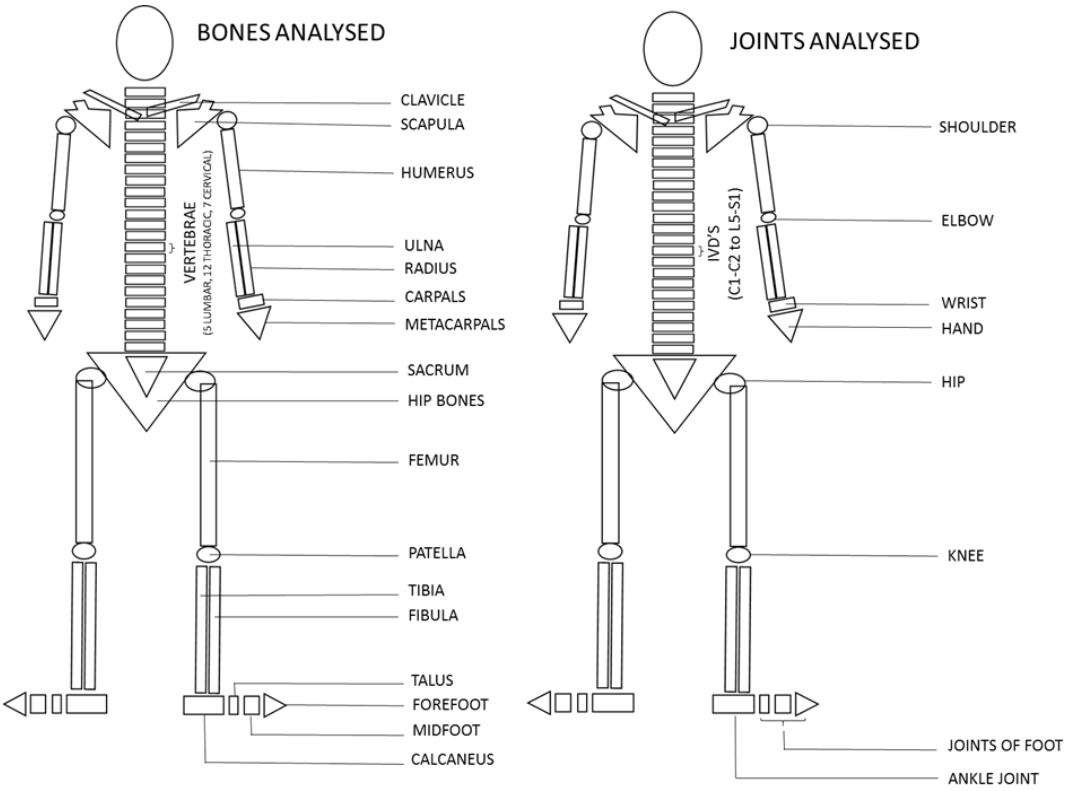

Figure 2.5 Labelled skeletal map of a human skeleton. Left image demonstrates the various bones assessed. Right image demonstrates the various cartilaginous joints assessed.

2.4.6 CARTILAGE-ANATOMICAL THRESHOLD SCORE

Cartilage anatomical threshold (C-AT) score represents a summation of all the cartilage scores (based on pixel values present above threshold) from the following joints; foot, ankle, knee, hip, S1-L5 - C2-C1 IVD (24 IVDs), shoulder, elbow, wrist and hand. A total of 32 joints were scored to give a maximum C-AT score of 32 (a score of one was given if increased uptake was observed in either right or left joint, if uptake was observed in both joints no extra score was given).

2.4.7 BONE-ANATOMICAL THRESHOLD SCORE

Bone anatomical threshold (B-AT) score represents a summation of all the bone scores (based on pixel values present above threshold) from the following bones; calcaneus, talus, midfoot, forefoot, tibia, fibula, patella, femur, hip, sacrum, L5-C1 vertebrae (24 vertebrae), scapula, humerus, radius, ulna, carpal, metacarpal/phalanges, clavicle and sternum. A total of 42 bones scored to give a maximum B-AT score of 42 (a score of one was given if increased uptake was observed in either right or left specific bone, if uptake was observed in both no extra score was given).

2.4.8 TOTAL ANATOMICAL-THRESHOLD SCORE

The total anatomical threshold (AT) score was added up to correlate with the total clinical score (based on the AKUSSI). The reason for this correlation was to see if the threshold methodology (Section 2.4.3, 2.4.4, 2.4.5) correlated with the nuclear medicine report assessed by the consultant (2.4.6). The total AT score was created by adding up the scores from the following joints (shoulder, elbow, wrist and hand, hip, knee, ankle, foot and lumbar, thoracic and cervical spine) to give a maximum total AT score of 10. Lumbar, thoracic and cervical spine was scored 1 if there were pixels above threshold identified in any of the vertebrae in the region, also right and left joints were not distinguished. If increased uptake was observed in one joint a score of 1 was given irrespective of if the other joint was affected too, exactly comparable to the total clinical score. Other anatomical regions analysed were excluded from this analysis as they were not scored as part of the AKUSSI.

2.4.9 TOTAL CLINICAL SCORE

The total clinical score is based on the AKUSSI. The nuclear medicine consultant scores the MIP PET images 'by eye' scoring each large joint and spine based on increased uptake at that site. Increased uptake (subject to consultant's opinion) is given a score of 1 in each large joint (shoulder, elbow, wrist and hands, hip, knee, ankle, foot and lumbar, thoracic and cervical spine). Right and Left joints were not distinguished in this score at baseline. Therefore, if increased uptake was observed in either the right or left joint a score of 1 was given, no extra scores were given if both joints were involved. These scores were added up to give a total clinical score that could be a maximum value of 10.

2.5 OBTAINING THE STANDARDISED UPTAKE VALUE

2.5.1 HERMES HYBRID VIEWER 1.4

The medical imaging software Hermes hybrid viewer version 1.4 (Hermes medical solutions, Stockholm, Sweden) was accessed in the nuclear medicine department in the Royal Liverpool and Broadgreen University Hospital Trust, England. This diagnostic imaging software was used to view the PET/CT scans as well as to obtain the SUVms for Chapters 4 and 5.

2.5.2 MEASURING THE MEAN STANDARDISED UPTAKE VALUE – SPINE

Hermes hybrid viewer 1.4 was opened, the appropriate patient was uploaded and whole-body PET and the time of flight (TOF) files were opened. The trans-axial, sagittal, coronal and CT (TSC+CT) views were selected to view the images (Figure 2.6). The centre of selected vertebrae and IVDs was defined by counting the number of CT slices the structure extended and selecting the middle slice. The triangulation point was used to align all viewing planes along the same axis and was placed in the middle slice at the centre of the vertebrae and IVDs (Figure 2.7). The circular region of interest (ROI) tool with a diameter of 1cm was selected (0.785cm^2). The ROI was placed in the appropriate anatomical location in the trans-axial PET image (in the centre of appropriate vertebrae or IVDs) (Figure 2.8) and the SUV (mean, minimum and maximum values) was automatically calculated for each ROI.

2.5.3 MEASURING THE STANDARDISED UPTAKE VALUE – HIP AND SHOULDER

Hermes hybrid viewer 1.4 was opened, the appropriate patient was uploaded and whole-body PET and TOF files were opened. The trans-axial view was selected for each of the three modalities (CT, PET/CT and PET) as seen in Figure 2.9. The triangulation point was placed in the centre of the hip joint where the head of the femur articulates with the acetabulum and ROIs (0.5cm diameter, 0.196cm^2) were placed in the acetabulum, head of femur and the AC, SUVms were obtained for each location (Figure 2.9). N.B. SUVms could only be obtained from the PET data so the ROIs were placed in the PET scan as seen in Figure 2.8. The triangulation point was then moved to the centre of the shoulder joint where the head of the humerus

articulates with the glenoid fossa and ROIs (0.5cm diameter, 0.196cm^2) were placed in the glenoid fossa, head of the humerus and the AC (Figure 2.10), and SUVms were obtained for each location. Exclusion criteria for this analysis included bilateral hip and/or shoulder replacements. The right shoulder and hip were chosen for analysis. If the right side was replaced the left side was measured.

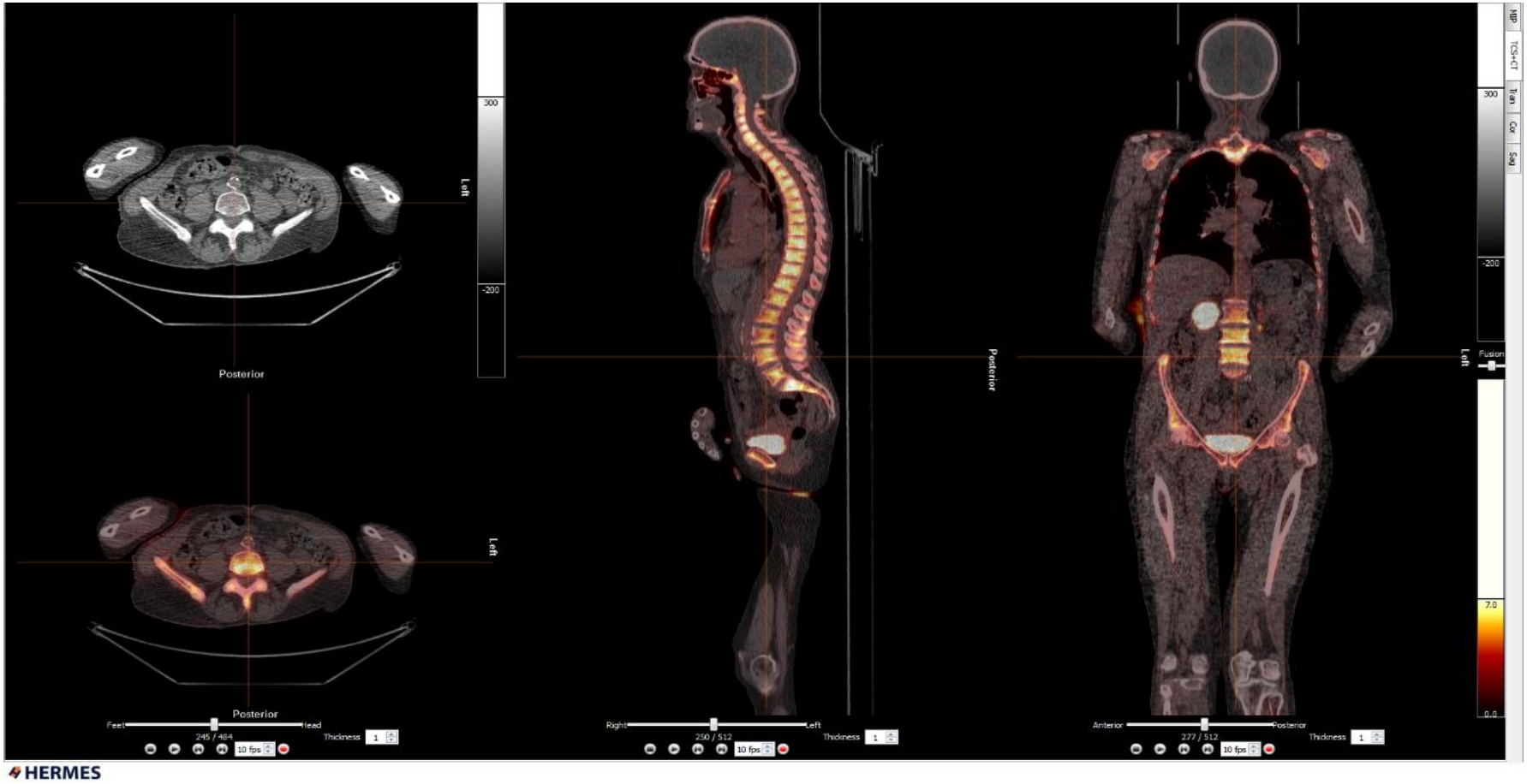

Figure 2.6 ^{18}F-NaF PET/CT scan showing trans-axial (far left), sagittal (middle), coronal (far-right) and CT (top left image) views. The triangulation point can be seen placed in the centre of the fourth lumbar vertebrae (triangulation point is the point where the vertical and horizontal lines intersect). When selected, this brings the triangulation point into view in each plane.

Figure 2.7 ^{18}F-NaF PET/CT sagittal view of spine. Triangulation point (intersection of the orange lines) selected in the centre of the vertebrae (on the left) and in the centre of the IVD (on the right).

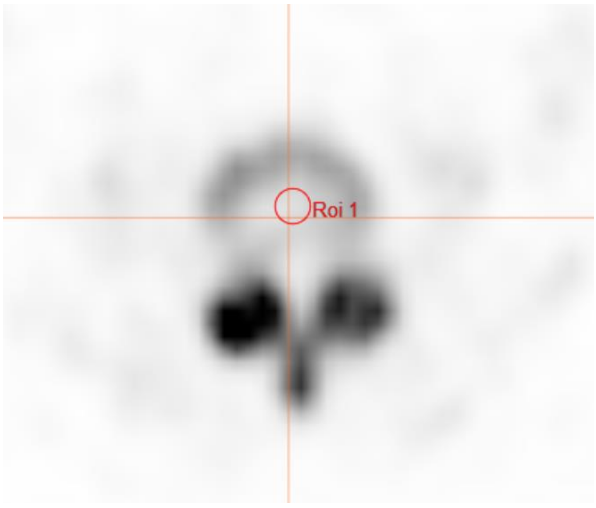

Figure 2.8 ^{18}F-NaF PET trans axial view with ROI placed in the centre of the IVD. Triangulation point placed in appropriate position as shown in Figure 2.7, the ROI (1cm in diameter, 0.785cm^2) was then placed in the trans-axial PET image.

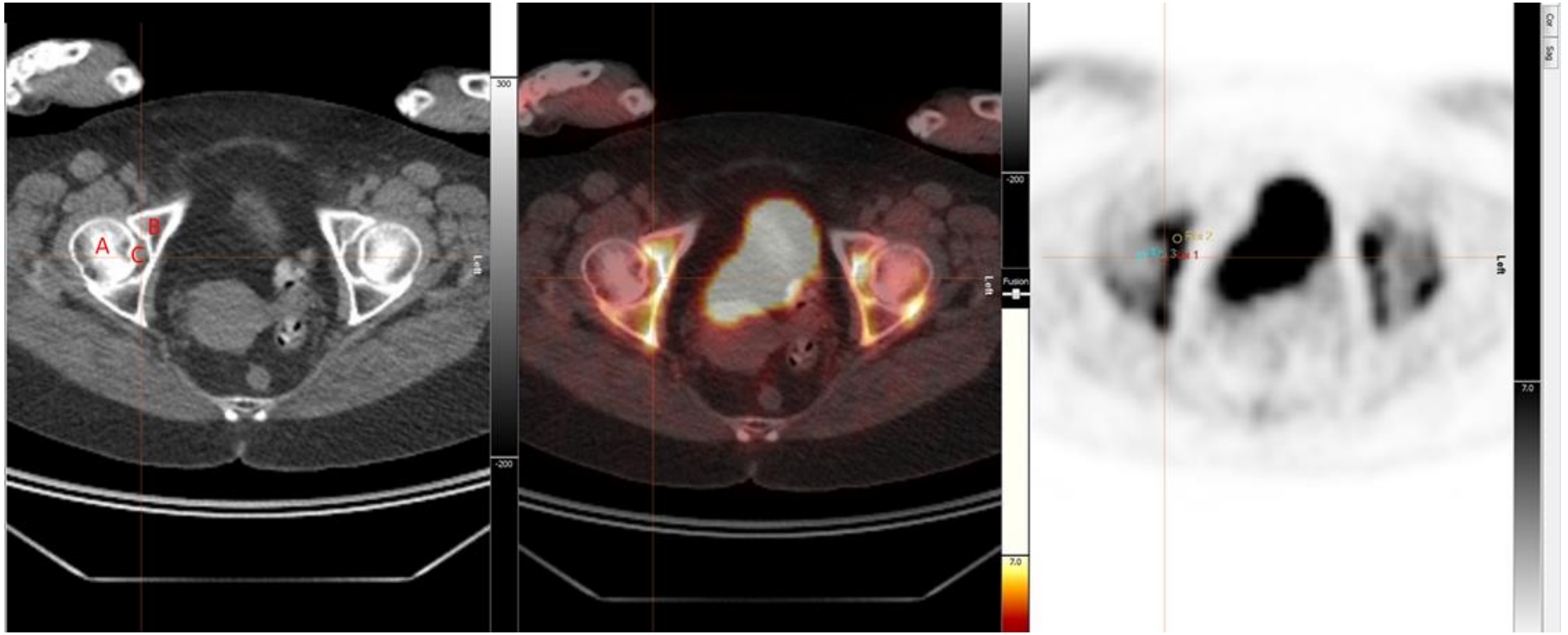

Figure 2.9 ^{18}F-NaF PET/CT trans-axial section through the hip joint demonstrating ROIs placed in the head of femur (A), acetabulum (B) and the articular cartilage (C). Left image: CT, middle image: PET/CT, right image: PET data showing ROIs (0.5cm in diameter, 0.196cm^2) in the acetabulum, head of femur and AC. (ROIs could only be measured using the PET data to obtain SUVms).

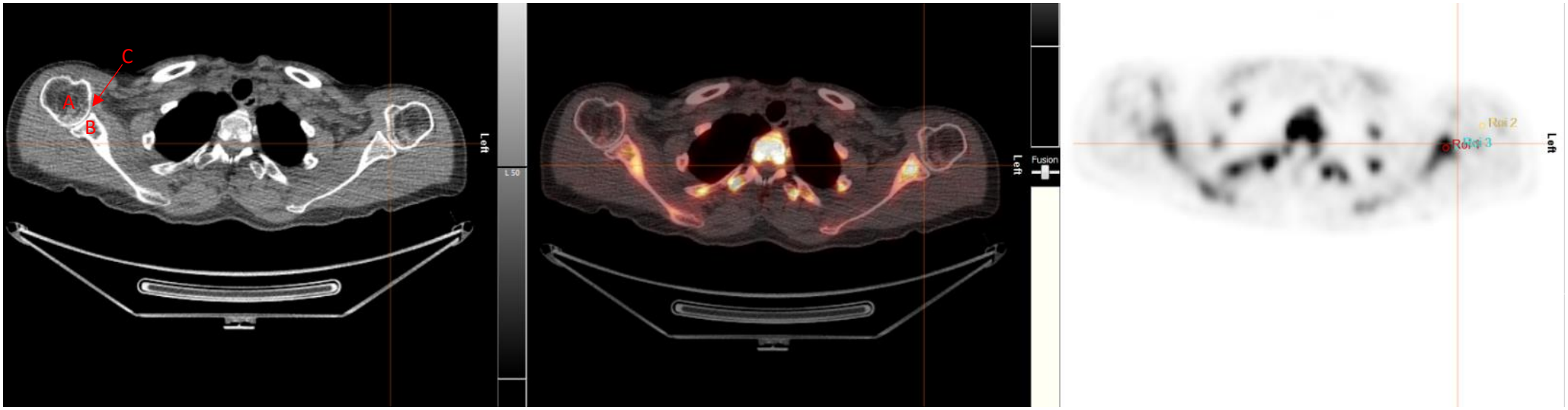

Figure 2.10 ^{18}F-NaF PET/CT trans-axial section through the hip joint demonstrating ROIs placed in the head of the humerus (A), glenoid fossa (B), and articular cartilage (C). Left image: CT, middle image: PET/CT, right image: PET data showing ROIs (0.5cm in diameter, 0.196cm^2) in the head of humerus, glenoid fossa and AC.

2.6 COBB ANGLE MEASURMENTS

Cobb angles are used to standardise spinal curvatures. Thoracic kyphosis is the outward curvature of the thoracic spine. Normal thoracic kyphosis ranges from 20-45 degrees, hyperkyphosis exceeds 45 degrees (122). Lumbar lordosis is the inward curvature of the lumbar spine. There is no defined measurements that determine hyper or hypo lumbar lordosis as muscular strength, flexibility and BMI all affect this angle (123). Scoliosis is defined as a lateral curvature of the spine of 10 degrees or more to the right or left (124). Spinal kyphosis, lordosis and scoliosis Cobb angles were measured for all SONIA 2 patients using the picture archiving and communications system (PACS) software. X-Ray and MRI images were electronically stored and accessed via PACS, and Cobb angles were generated for both scans for each patient. Access to the PACS system was via the Royal Liverpool and Broadgreen University Hospital Trust computer.

2.6.1 X-RAY SCOLIOSIS MEASUREMENTS

Whole body posteroanterior (PA) X-Ray view was selected to analyse scoliosis. Using the Cobb angle tool the end vertebrae of the curve were selected and lines were drawn to demarcate the vertebrae that lie at the upper and lower limits of the curve (the vertebrae that tilt the most towards the apex of the curve) (Figure 2.11A). The Cobb angle was automatically generated measuring the intersection of the two lines drawn. Scoliosis is clinically defined as a spinal curvature of more than 10 degrees to the right or left (124).

2.6.2 X-RAY THORACIC KYPHOSIS AND LUMBAR LORDOSIS MEASUREMENTS

Lateral X-ray view was selected to measure thoracic kyphosis and lumbar lordosis Cobb angles. Using the Cobb angle tool the lower border of the twelfth thoracic vertebrae (T12) and the upper border of the fourth thoracic vertebrae (T4) were selected to define thoracic kyphosis (125) (Figure 2.11B). The Cobb angle was automatically generated by measuring the intersection between the lines selected. Normal kyphosis ranges from 20-45 degrees, hyper kyphosis is defined as more than 45 degrees (122). Lumbar lordosis was measured from the lower border of the fifth lumbar (L5) vertebrae and the upper border of the first lumbar vertebrae (L1). Lumbar hyperlordosis is not defined by a Cobb angle (Figure 2.11B).

2.6.3 MRI THORACIC KYPHOSIS AND LUMBAR LORDOSIS MEASUREMENTS

Thoracic kyphosis and lumbar lordosis Cobb angles were also measured on MRI (Figure 2.11C). The MRI whole spine was selected using the PACS and the methodology of measuring thoracic kyphosis and lumbar lordosis was exactly as described in section 2.6.2.

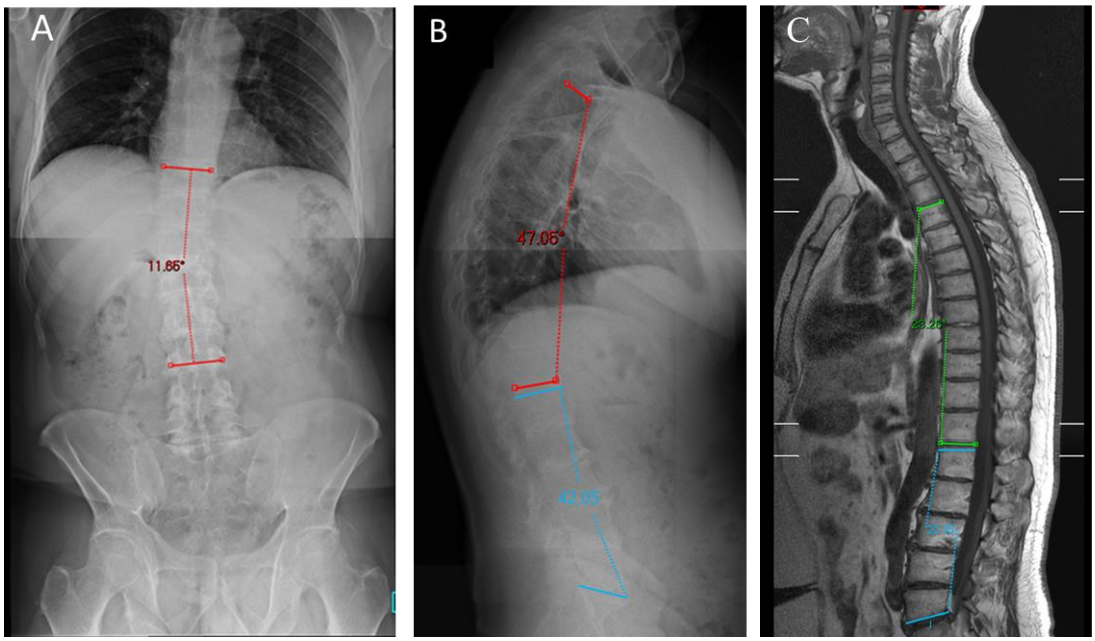

Figure 2.11 PA X-Ray (A), lateral X-Ray (B) and T1 weighted whole spine MRI-sagittal view (C) to measure scoliosis, thoracic kyphosis and lumbar lordosis Cobb angles. Figure A demonstrates scoliosis Cobb angle, the lines are drawn at the upper and lower limits of the curve and the angle is automatically generated. Figure B demonstrates the kyphosis Cobb angle (red lines) where the lines are drawn at the lower border of thoracic vertebrae number 12, and the upper border of thoracic vertebrae number 4 and the lumbar lordosis Cobb angle (blue lines) where the lines are drawn at the lower border of the fifth lumbar vertebrae and the upper border of the first lumbar vertebrae. Figure C demonstrates the thoracic kyphosis (T4-T12) (green lines) and lumbar lordosis (L1-L5) (blue lines) Cobb angles in MRI.

2.7 SPINAL FLEXIBILITY MEASUREMENTS

2.7.1 LUMBAR SIDE FLEXION MEASUREMENTS

Lumbar side flexion was measured by a senior physiotherapist at the RLBUHT. Lumbar side flexion was measured by firstly asking the patient to stand up straight against the wall with their shoulders back and feet 12 inches apart. The distance between the tip of the middle finger and the floor was measured on the left and right sides. The patient was then asked to side flex and then the physiotherapist applied slight over pressure to push the patient further into the range, the distance between the tip of the finger and the floor was re-measured on both the left and right sides to obtain the passive range of motion. The difference between the two measurements on both the right and the left was calculated reflecting passive lumbar side flexion of the patient to the right and to the left in cm (126,127). The passive range of movement determines the maximum amount of movement possible at the joint, and is usually higher than the active range of movement which is the distance before the physiotherapist applies the slight over pressure to push the patients further into the range. The passive range of motion was used for analysis in this thesis.

2.7.2 CERVICAL SPINE ROTATION MEASURMENTS

Cervical spine rotation was measured by a senior physiotherapist at the RLBUHT. Cervical spine rotation was measured by firstly asking the patient to stand up straight against the wall with their shoulders back in a neutral position with the head facing forwards. The distance between the gnathion (midpoint of the lower border of the

mandible) of the chin to the lateral aspect of the acromion of the scapula was measured with the head looking straight forwards on both the right and left sides. The patient was then asked to turn their head to the right side with the physiotherapist applying over pressure to push the patient further into the range. The distance between the gnathion and lateral aspect of the acromion was re-measured and the difference between the two values was then calculated to obtain the value for passive cervical spine rotation. These measurements were then repeated on the left (126,127).

2.8 STATISTICAL ANALYSIS

All statistical analysis was carried out using *Stats Direct* statistical software (Version: 3.0.171). The data was plotted using *Stats Direct* to see if the data was normally distributed using the Kolmogorov-Smirnov (K-S) test. The K-S test produces a p value, if $p>0.05$ the data is assumed to be normally distributed. Histograms were plotted to confirm these distributions. Parametric tests were carried out on normally distributed data. Non-parametric tests were carried out on non-normally distributed data.

2.8.1 PARAMETRIC TESTS

Independent samples t-tests were carried out to compare the means of a normally distributed interval dependant variable for two independent groups. Paired (samples) t-test were carried out to compare means from the same individual. The result of these tests provided p values a $p\leq0.05$ was statistically significant. A $p\leq0.05$

typically indicates strong evidence against the null hypothesis, so the null hypothesis is rejected. The null hypothesis states that there is no relationship between two measured phenomena.

2.8.2 NON-PARAMETRIC TESTS

Wilcoxon-Mann-Whitney test is a non-parametric analog to the independent samples t-test and was used when the dependant variable was not normally distributed. The Wilcoxon signed rank sum test is the non-parametric version of a paired samples t-test. This test was used when the distribution was not normally distributed.

2.8.3 REGRESSION ANALYSIS

2.8.3.1 Multiple linear regression

A multivariate statistical technique was used to examine the linear correlations between two or more independent variables and a single dependent variable. Multiple linear regression analysis was used to compare control and AKU patients SUVm (in thoracic and lumbar vertebrae and IVDs) with age. The outcome variable was mean lumbar/thoracic IVD/vertebrae. The grouping variable was either V1 (AKU) vs control group, or V3 (AKU) vs control group and the other variable tested was age.

2.8.3.2 Simple linear regression and Pearson's correlation

Simple linear regression and Pearson's correlation was used to test the correlation between two variables. Pearsons r value defines the strength of the relationship, and

has a value between +1 and -1, where 1 is total positive linear correlation, 0 is no correlation and -1 is total negative correlation. The p value defines the significance level of the correlation ($p \leq 0.05$ is statistically significant). The R^2, the coefficient of determination is a statistical measure of how close the data are fitted to the regression line which was plotted on the graphs.

2.8.4 TREND LINES

Trend lines were added to graphs using Excel. The distribution of the data was assessed and the most appropriate trend line was selected based on the distribution. A linear trend line was applied when the data set had a simple linear correlation. In situations where the data did not indicate a linear relationship, polynomial models were tested. The criteria for selecting a polynomial fit was as follows:

1. In situations where the relationships were hypothesised to be curvilinear. For example, the relationship between uptake of ^{18}F into the lumbar and thoracic IVDs (Figure 4.12 and 4.13), as discussed in Section.
2. A visible inspection indicated the data are bivariate, for example the inverted 'U' shaped trends shown in Figure 4.12 and 4.13.
3. When an inspection of residuals reveals that a linear model is not appropriate

Where appropriate a second order polynomial line was applied to data that had one peak or trough.

3.0 SKELETAL DISTRIBUTION OF INCREASED ^{18}F PET UPTAKE IN PATIENTS WITH ALKAPTONURIA

3.1 INTRODUCTION

Early osteoarthropathy is an inevitable consequence of AKU resulting in considerable pain and suffering in peak adulthood due to premature joint and spinal disease. Weight bearing joints are thought to be predominantly affected due to increased mechanical damage (1). The purpose of this study was to investigate the natural history of alkaptonuria using the novel imaging modality ^{18}F-NaF PET. A semi-quantitative approach was used to assess the anatomical distribution of osteoarthropathy with age.

Plain X-Ray is still the gold standard imaging modality to diagnose arthritic disease, however it is realised that functional abnormalities can exist without radiographic evidence. ^{18}F-NaF PET is a valuable tool to detect functional skeletal involvement and is routinely used in diagnosing skeletal metastatic disease. However, more recently it has been utilised in identifying arthropathy in OA and in AKU. ^{18}F-NaF PET provides highly sensitive, three-dimensional imaging of the skeleton with advantages such as high spatial resolution, superior image quality and hybrid PET/CT imaging providing accurate anatomical localisation (89). Upon injection of the radiotracer ^{18}F covalently binds to hydroxyapatite crystals of newly forming bone and therefore reflects the amount of actively mineralising bone present and closely resembles bone metabolism (110). A positive or abnormal scan manifests itself as an area of increased radiotracer uptake and reflects the increased osteogenic activity at that site. Radiotracer delivery is also dependent on regional blood flow therefore the scan also provides an index of vascularity of bone (89). Increased osteogenic activity and

vascularity are features of a degenerating joint due to the inflammatory and healing processes that occur in response to injury hence why this imaging modality is useful in AKU (89).

Until recently there has been a lack of semi-quantifiable methodology to describe AKU disease severity. The AKUSSI attempts to assess all features of AKU in a standardised manner producing a composite score representing the totality of clinical features. Table 1.2 represents the AKUSSI. The ^{18}F-NaF PET scans are analysed by an experienced nuclear medicine consultant. The large joint areas scored are the shoulder, elbow, wrist and hands, hip, knee, ankle, foot and the cervical, thoracic and lumbar spine based on increased uptake at that site. Increased uptake is given a score of 1 in each large joint and a score of zero is given if the joint has normal uptake. These scores are then fed into the AKUSSI and contribute the final aggregated score. It is important to note that this scoring is based on the opinion of the nuclear medicine consultant and therefore is subjective. This work attempts to develop a semi-quantitative method that demarcates the boundary between increased tracer uptake and normal bone uptake that could be used as an alternative or a complementary non-subjective method to score the ^{18}F-NaF PET scans by the clinician.

3.2 DESIGN OF STUDY

3.2.1 PATIENT GROUP

43 adult patients (17 females, 26 males, mean age 49, SD±14.8, range 21-74) from the National Alkaptonuria Centre (see section 2.2.1) underwent ^{18}F-NaF PET scanning. Baseline (pre-nitisinone) PET images were analysed for each patient (see section 2.3 for PET protocol). Patients were included only if a whole-body MIP scan was present. Five patients (Patients 9,11,23,27,30) were excluded from the correlation with the clinical score as the AKUSSI analysis was not available.

3.2.2 IMAGE ANALYSIS

Baseline 8-bit MIP PET images of the 43 NAC patients were imported into Image J (1.49j). A histogram plot was created for each patient to analyse the distribution of pixel values within the image. A threshold was applied (as described in 2.4.4) highlighting the pixel values that represent increased tracer uptake that are associated with AKU disease pathology.

3.2.3 ANATOMICAL SCORING

The MIP PET images were then analysed anatomically (as described in section 2.4.5) and were scored based on the presence or absence of pixel values above threshold. A score of 0 or 1 was given (0= no pixels present above threshold, 1= at least one pixel identified above threshold in the various anatomical regions). Pixels above threshold represent increased tracer uptake at that site associated with disease pathology. This method aims to remove any subjectivity in observing regions of increased tracer uptake associated with disease pathology.

3.3 RESULTS

Each patient was scored for the presence or absence of pixels above the threshold value in the various anatomical locations. Both cartilaginous joints and bones were analysed. For the bony anatomy the calcaneus, talus, midfoot, forefoot, tibia, fibula, patella, femur, hip, sacrum, vertebrae (L5-C1), scapulae, humerus, radius, ulna, carpal, metacarpal/ phalanges, clavicle and sternum were scored 0 or 1 (0= if no pixels were present above threshold 1= if pixels were identified above threshold). For the cartilaginous joints, the joints of the foot, ankle, knee, hip, sacroiliac joint, intervertebral discs (S1/L5 – C1/C2), shoulder, elbow, wrist and hand were scored 0 or 1 as described above. The percentage incidence of increased tracer uptake (pixel values above threshold) was calculated and plotted on a skeletal map (Figure 2.5 shows a skeletal map of regions analysed) demonstrating the bones and joints most affected by the disease. The percentage incidence was calculated by adding up the scores from all patients at each anatomical site. The cohort was split into five age dependant groups (21-30 n=8, 31-40 n=5, 41-50 n=7, 51-60 n=12, 61-70+ n=11) to assess distribution with age.

3.3.1 SKELETAL DISTRIBUTION OF INCREASED ^{18}F UPTAKE WITH AGE IN THE BONES OF THE SKELETON

Figure 3.1 demonstrates the skeletal distribution of increased ^{18}F PET uptake in the bones of the skeleton. The highest incidences of increased tracer uptake were found in the hip, sacrum and thoracic and lumbar vertebral bodies (93%, 64%, 73% and 80% incidence respectively) (Figure 3.1). The lowest incidences were found in the bones

of the lower limb (averaging 26% incidence in the femur, patella, tibia, fibula, forefoot, midfoot, talus and calcaneus) and very low in the bones of the upper limb (averaging 12% incidence in the humerus, radius, ulna, carpals, metacarpals and phalanges) (Figure 3.1).

Figure 3.2 illustrates the percentage incidence of increased ^{18}F uptake with age represented as a skeletal map. When looking at the overall distribution and percentage incidence, there does not seem to be a clear trend with age. The percentage incidence of increased ^{18}F uptake overall across all bones scored was lowest in the 41-50 age group, followed by the 61-70+ and 21-30 age groups. The 31-40 and the 51-60 age groups had the highest overall increased tracer uptake.

When looking at the number of bones affected the youngest age group had the least amount of areas involved and the oldest age group has the highest number of areas involved. Increased uptake in the hip seems to be high across all age groups. Uptake in the feet and hands are generally low across all age groups. The youngest age groups (21-30 and 31-40) have the highest percentage incidence in the spine, sacrum and the hip bones. The bones of the upper limb are very low across the three youngest age groups and this is the case for the oldest two age groups except the humerus which increases to 61-80% incidence. Uptake in the bones of the lower limb is variable between the age groups ranging from very low in the 21-30 and 41-50 age groups, and increasing to moderately high in the 31-40 and 51-60 and 61-70+ age groups.

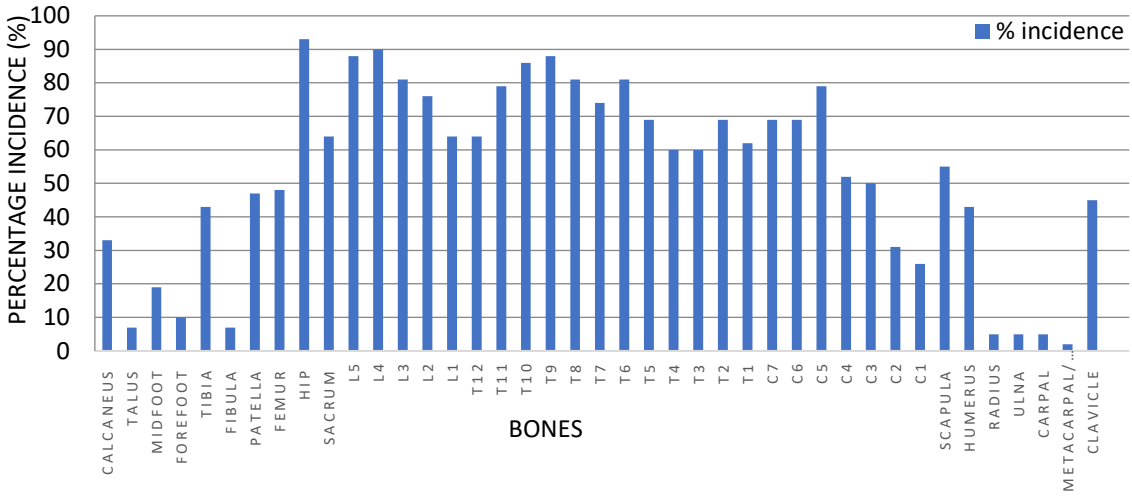

Figure 3.1 Percentage incidence of increased ^{18}F uptake in the bones of the skeleton. Percentage incidence = the number of patients identified to have increased tracer uptake at a specific anatomical site as a percentage. n=43 (17 females, 26 males, mean age 49, SD±14.8, range 21-74).

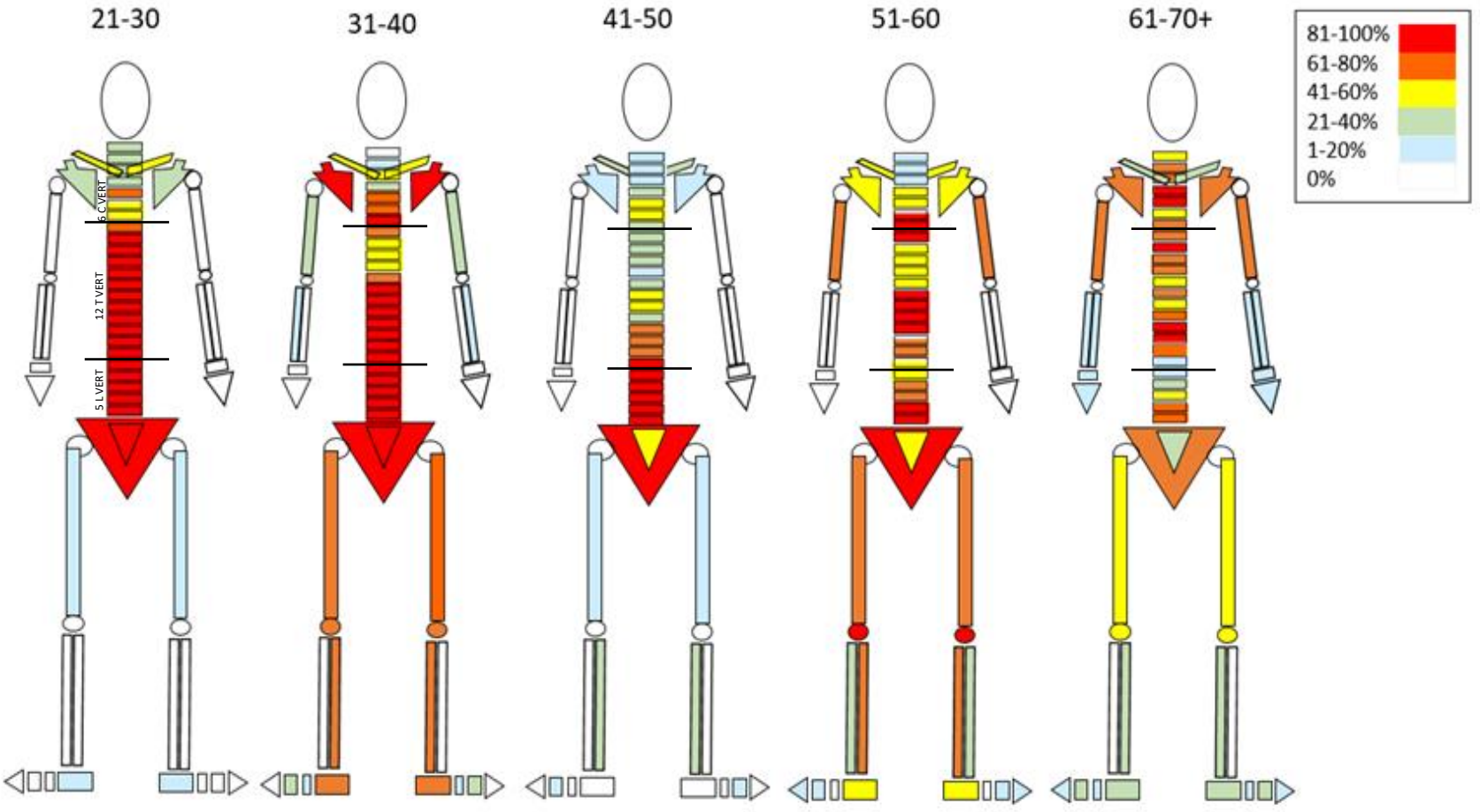

Figure 3.2 Skeletal distribution of increased ^{18}F PET uptake with age in the bones of the skeleton represented on a skeletal map. Colour scale representing the percentage incidence of ^{18}F uptake (red= 81-100% incidence, orange= 61-80% incidence, yellow= 41-60% incidence, green= 21-40% incidence, blue= 1-20% incidence, white= 0% incidence.) Vertebrae: 5 lumbar, 12 thoracic and 7 cervical. See Figure 2.5 for a labelled skeletal map of the bones analysed. n=43 (17 females, 26 males, mean age 49, SD±14.8, range 21-74). Age groups: 21-30 n=8, 31-40 n=5, 41-50 n=7, 51-60 n=12, 61-70+ n=11.

Figure 3.3 illustrates the percentage incidence of increased ^{18}F uptake in the lumbar vertebrae with age. The percentage incidence is very high across all age groups (100% in the 20-30, 31-40, 41-50 and reduces slightly in the 51-60 age group and further reduces in the 61-70+ age group). The percentage incidence reduces by 22% across all five lumbar vertebrae between the age group 41-50 to 51-60 and then drops by a further 29% between the age group 51-60 to the oldest age group (61-70+) (Figure 3.3).

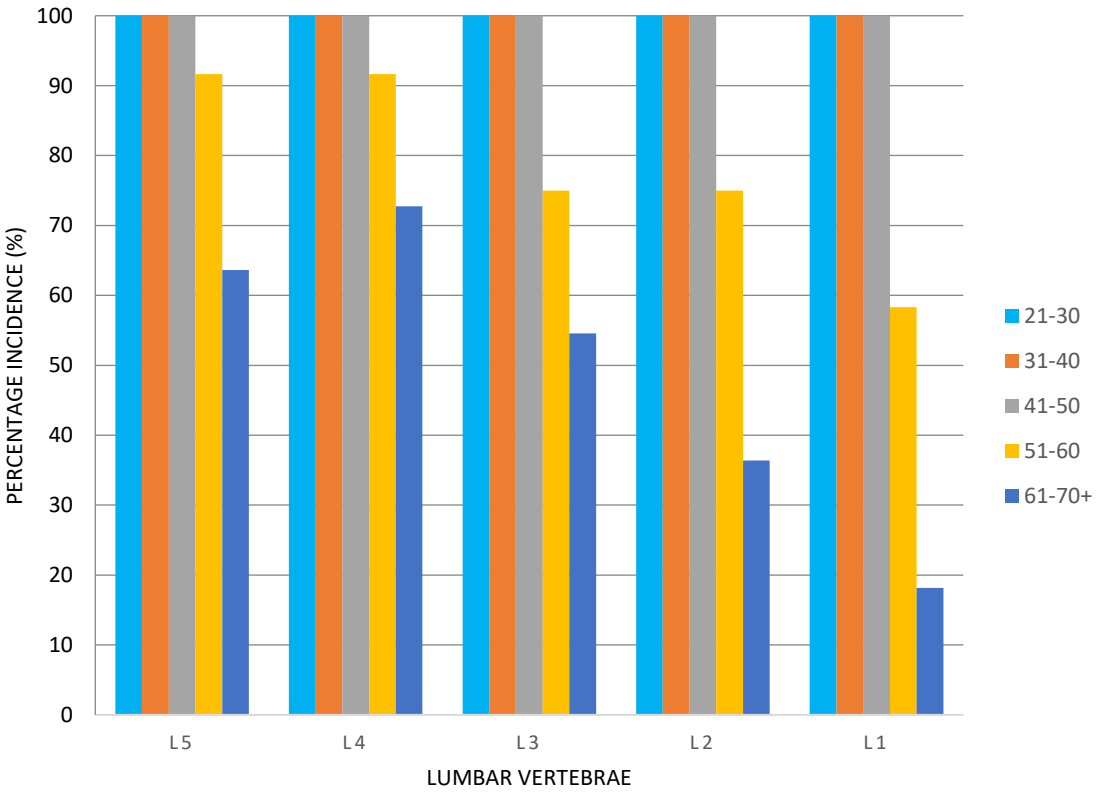

Figure 3.3 Percentage incidence of ^{18}F uptake in the lumbar vertebrae with age. Five lumbar vertebrae (L5- fifth lumbar vertebrae, L4- fourth lumbar vertebrae, L3- third lumbar vertebrae, L2- second lumbar vertebrae, L1- first lumbar vertebrae). n=43 (17 females, 26 males, mean age 49, SD±14.8, range 21-74). Number of patients in each age group: 21-30 n=8, 31-40 n=5, 41-50 n=7, 51-60 n=12, 61-70+ n=11.

Figure 3.4 represents the percentage incidence of increased ^{18}F uptake in the thoracic vertebrae with age across three youngest age groups (21-30, 31-40, 41-50). The general trend is a reduction in percentage incidence across the thoracic vertebrae with age. The youngest age group (21-30) can be seen having the highest incidence, with a mean percentage of 94% across all thoracic vertebrae. The incidence then reduces to 76% across all thoracic vertebrae in the 31-40 age group, and down to 57% across all thoracic vertebrae in the 41-50 age group. The incidence can also be seen gradually decreasing along the spine from T12 to T1. The percentage incidence of increased ^{18}F uptake is highest in the lower thoracic vertebrae and this can be seen to reduce up the spine from T12 to T1 across all age groups. In the three age groups the percentage incidence is reduced from 100% at T12 down to 63% (21-30), 67% (31-40) and 40% (41-50) at T1 respectively.

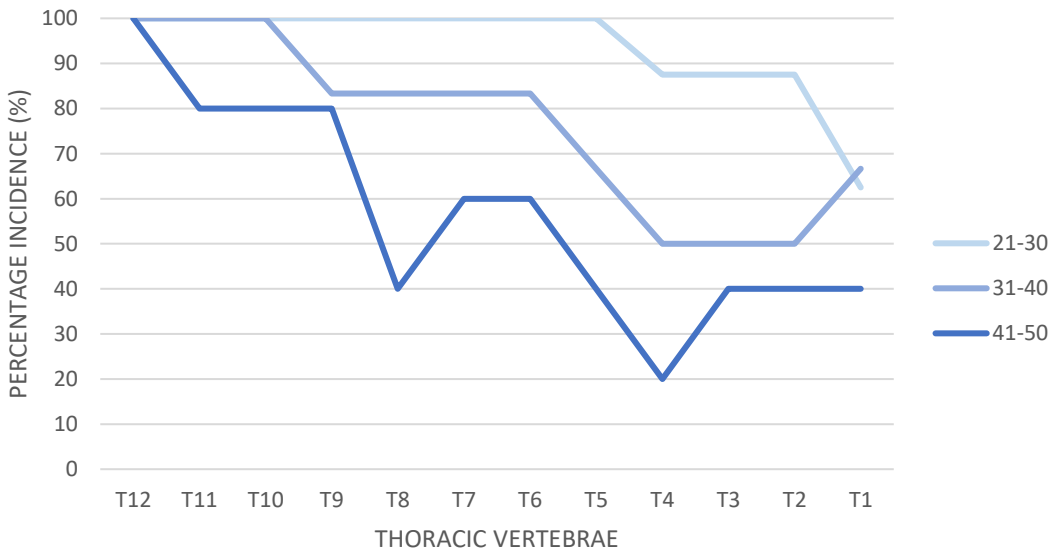

Figure 3.4 Percentage incidence of ^{18}F uptake in the thoracic vertebrae with age in the youngest patient groups. Twelve thoracic vertebrae (T1-T12). n=43 (17 females, 26 males, mean age 49, SD±14.8, range 21-74). Number of patients in each age group: 21-30 n=8, 31-40 n=5, 41-50 n=7.

The percentage incidence in the thoracic spine in the oldest two age groups (51-60 and 61-70+) (Figure 3.5) does not follow the same trend as Figure 3.4, where a reduction in percentage incidence with age was observed in the younger age groups. The two oldest age groups follow a fluctuating trend with low incidence at the lower limits of the thoracic spine followed by increased incidence ascending by 3-4 vertebrae followed by another dip observed around the mid thoracic spine and again another increase in incidence towards the upper limits of the thoracic spine (Figure 3.5).

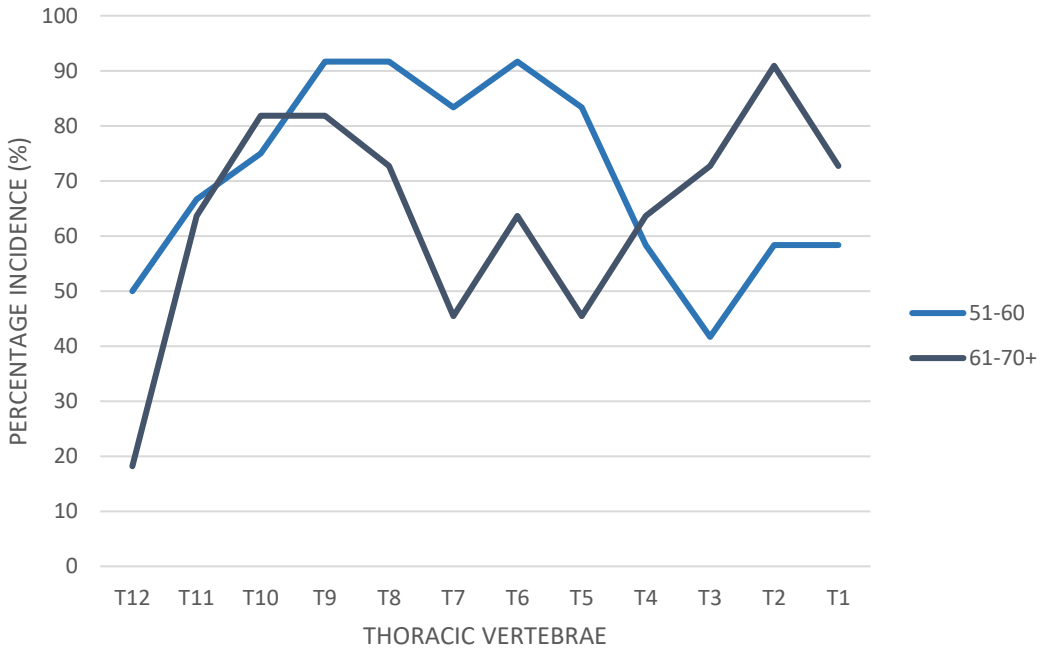

Figure 3.5 Percentage incidence of ^{18}F uptake in the thoracic vertebrae in the oldest patient groups. Twelve thoracic vertebrae (T1-T12). n=43 (17 females, 26 males, mean age 49, SD±14.8, range 21-74). Number of patients in each age group: 51-60 n=12, 61-70 n=11.

Figure 3.6 demonstrates the percentage incidence of increased ^{18}F uptake in the cervical vertebrae. The percentage incidence of increased ^{18}F uptake in the cervical vertebrae decreases along the spine from C7 to C1, this general trend can be seen across all five age groups. It is also evident that the oldest two age groups (51-60 and 61-70+) generally have the highest incidences of increased ^{18}F uptake compared to the younger age groups (21-30, 31-40 and 41-50). This contradicts the trend of the lumbar (Figure 3.3) and thoracic vertebrae (Figure 3.4) that found a decrease in the percentage incidence with age.

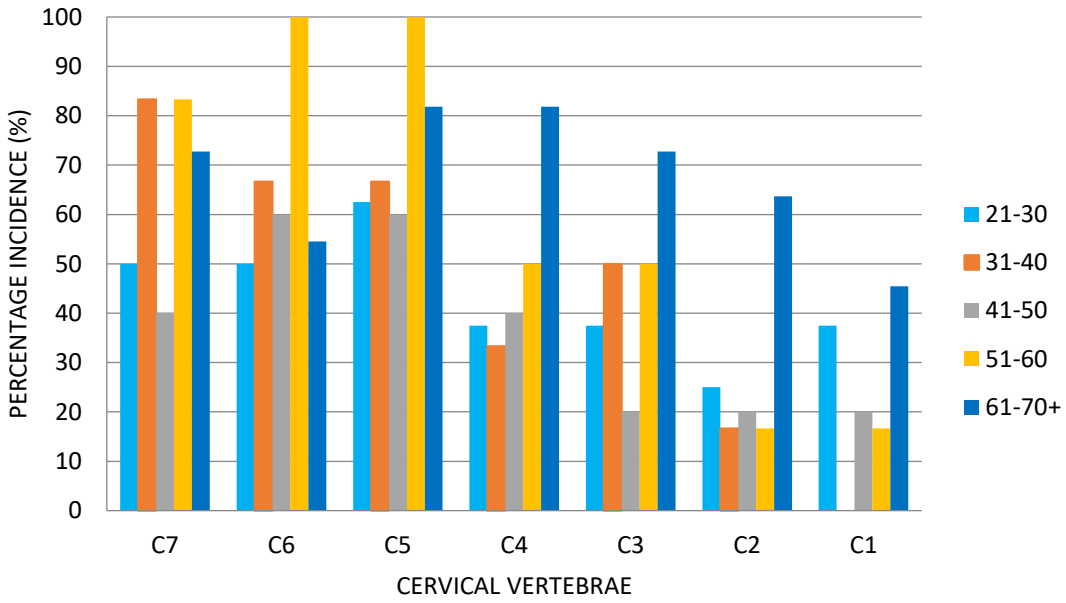

Figure 3.6 Percentage incidence of increased ^{18}F uptake in the cervical vertebrae with age. Six cervical vertebrae (C1-C6). n=43 (17 females, 26 males, mean age 49, SD±14.8, range 21-74). Number of patients in each age group: 21-30 n=8, 31-40 n=5, 41-50 n=7, 51-60 n=12, 61-70+ n=11.

3.3.2 SKELETAL DISTRIBUTION OF INCREASED ^{18}F UPTAKE WITH AGE IN CARTILAGINOUS JOINTS

The highest percentage incidences of increased ^{18}F uptake in cartilage was found in the joints of the foot, knee, hip and shoulder with incidences of 52%, 65%, 52% and 48% respectively. The remaining cartilaginous joints had low incidence of increased ^{18}F uptake of less than 20% incidence across the remaining joints scored (Figure 3.7). Figure 3.8 demonstrates the percentage incidence of increased tracer uptake with age in the 5 age groups. It is clear with increasing age; the more cartilaginous joints are affected with increasing percentage incidences. In the youngest age group (21-30), two joint areas (hip and foot) were identified to have increased tracer uptake compared to every joint analysed in the oldest age group (61-70). Figure 3.9 represents this data on a skeletal map.

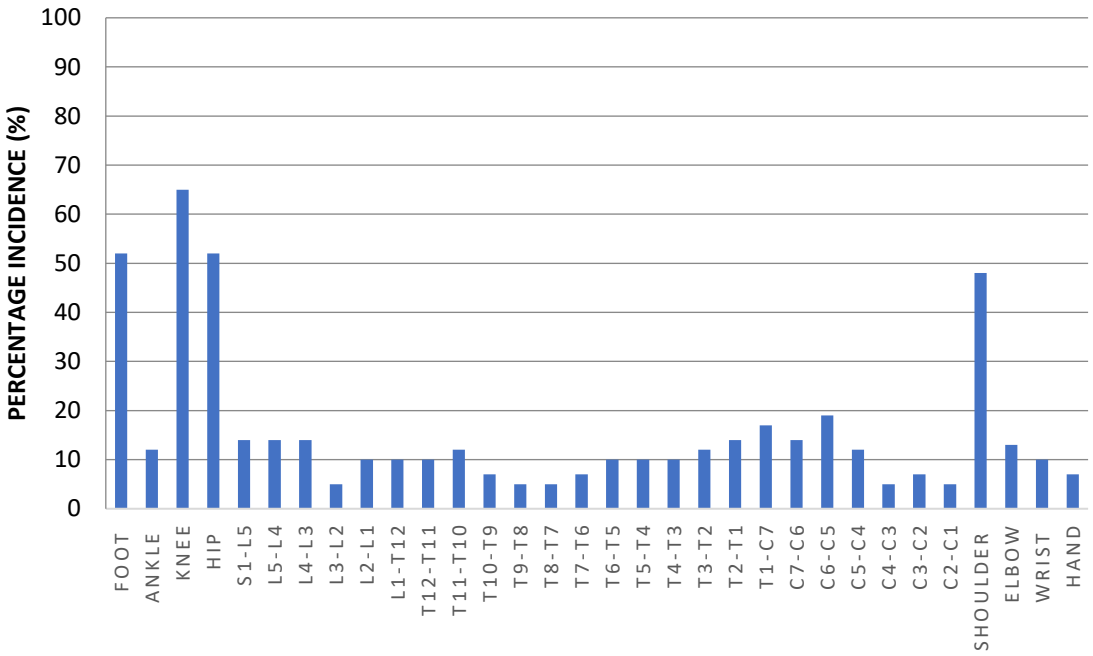

Figure 3.7 Percentage incidence of increased ^{18}F PET uptake in cartilaginous joints. Intervertebral discs denoted by the vertebrae they lie between e.g. L5-L4 IVD located between L5 and L4 vertebrae. Foot represents joints in the feet except the ankle. Hand represents all joints in the hand except the wrist. n=43 (17 females, 26 males, mean age 49, SD±14.8, range 21-74).

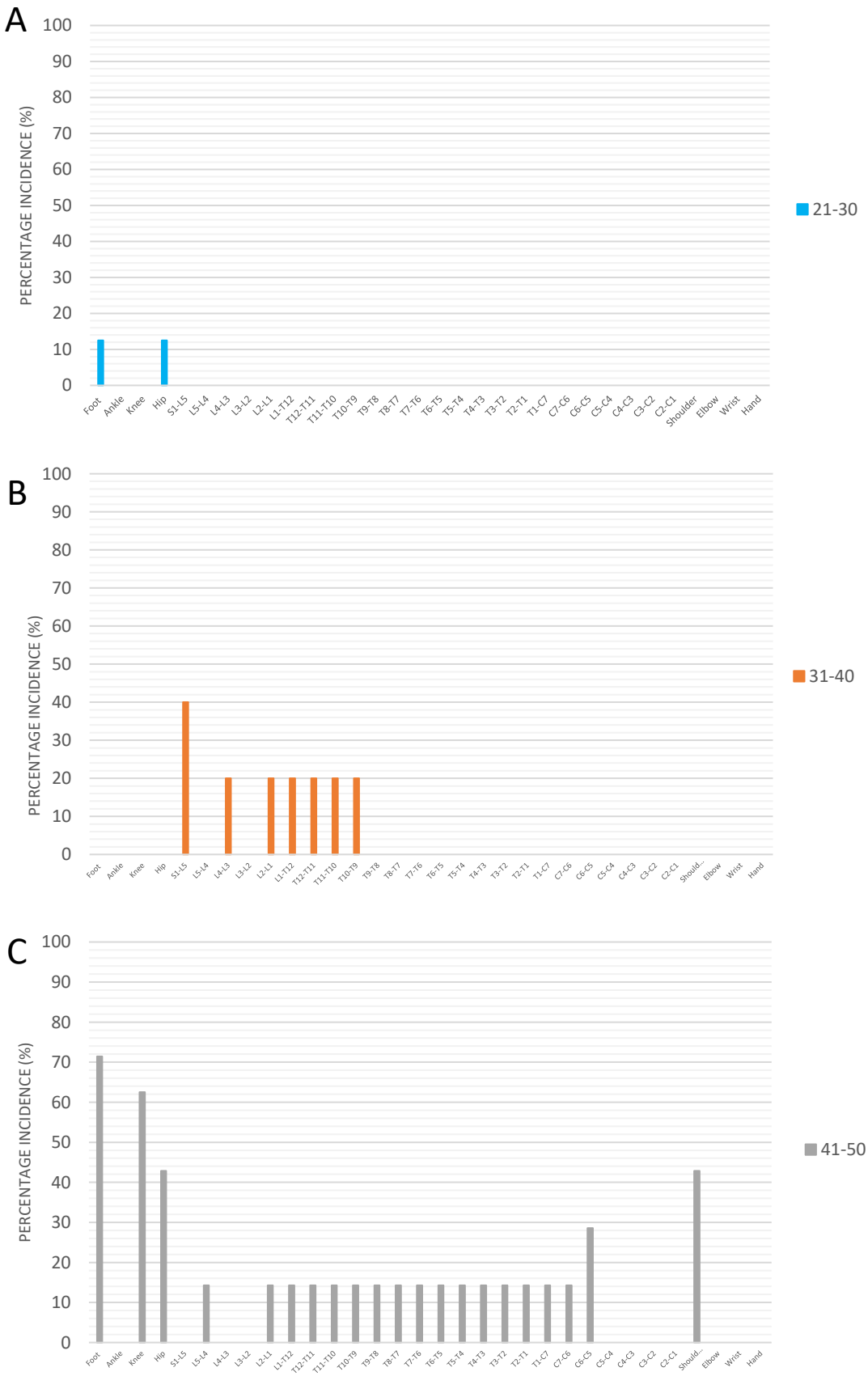
A
B
C
PERCENTAGE INCIDENCE (%)
100
90
80
70
60
50
40
30
20
10
0
21-30
31-40
41-50
Foot
Ankle
Knee
Hip
S1-L5
L5-L4
L4-L3
L3-L2
L2-L1
L1-T12
T12-T11
T11-T10
T10-T9
T9-T8
T8-T7
T7-T6
T6-T5
T5-T4
T4-T3
T3-T2
T2-T1
T1-C7
C7-C6
C6-C5
C5-C4
C4-C3
C3-C2
C2-C1
Shoulder
Elbow
Wrist
Hand

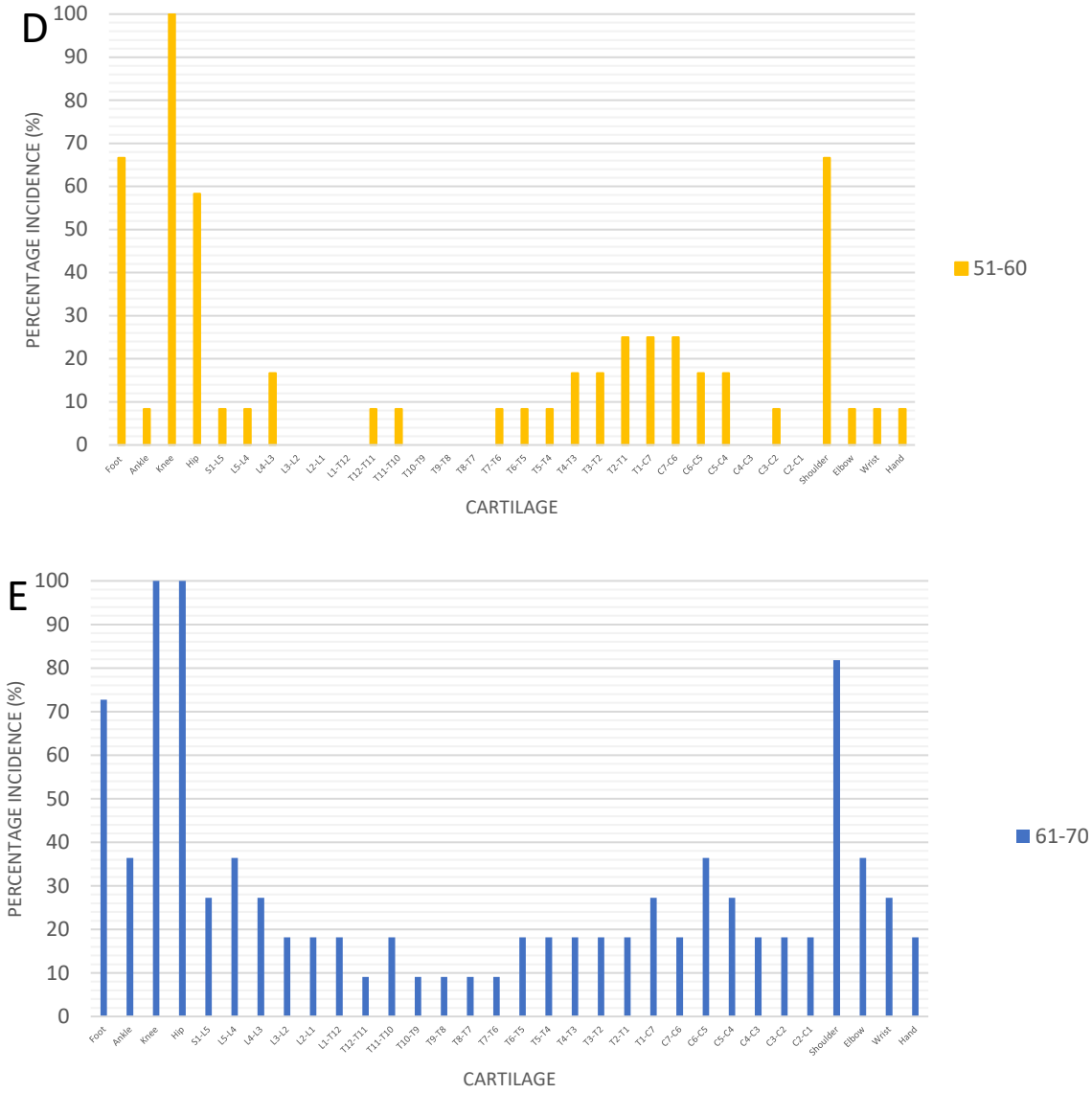

Figure 3.8 Percentage incidence of increased ^{18}F uptake in the cartilaginous joints by age. n=43 (17 females, 26 males, mean age 49, SD±14.8, range 21-74). Number of patients in each age group: (A) 21-30 n=8, (B) 31-40 n=5, (C) 41-50 n=7, (D) 51-60 n=12, (E) 61-70+ n=11.

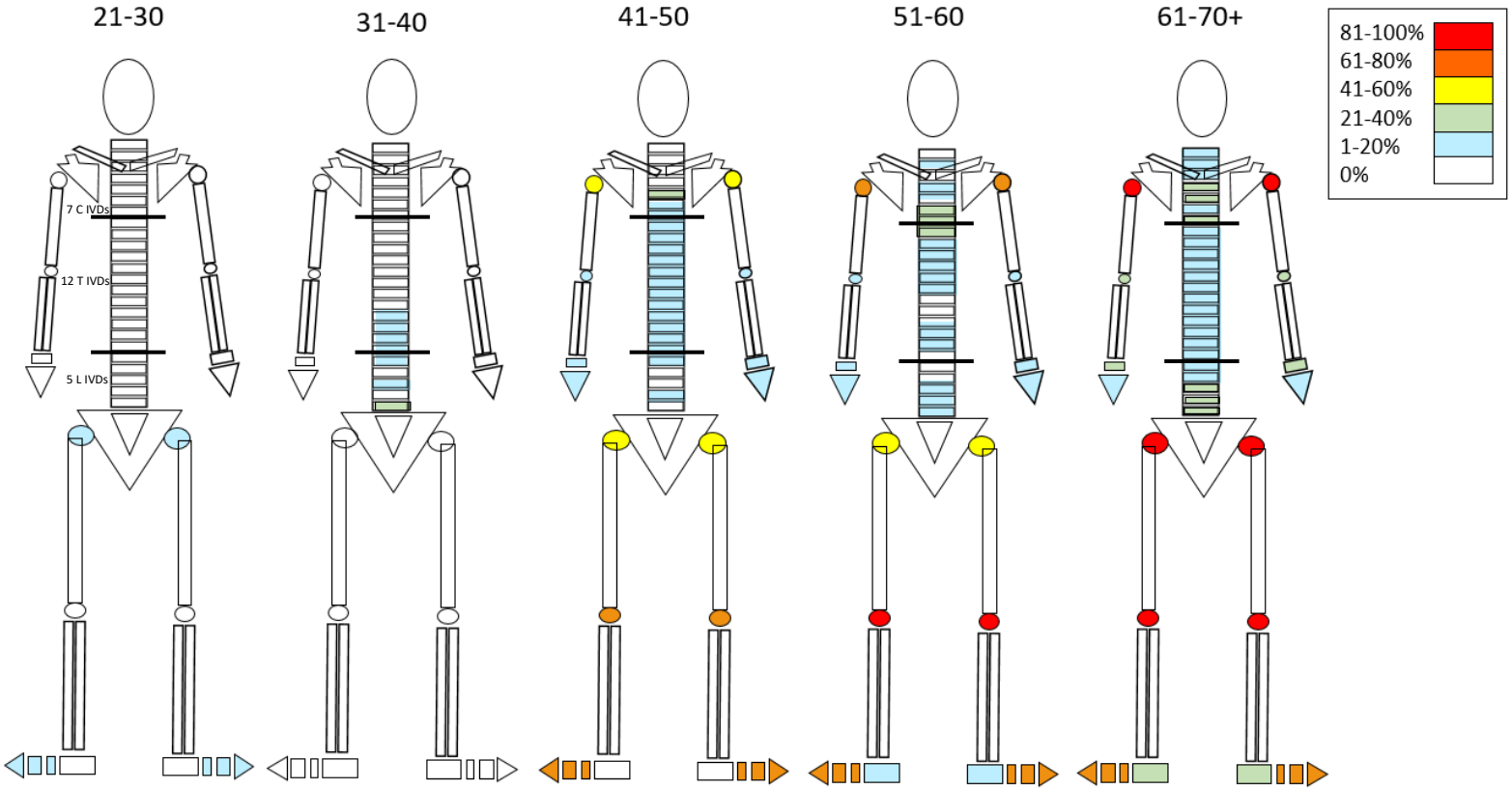

Figure 3.9 Skeletal distribution of increased ^{18}F PET uptake with age in the cartilaginous joints of the skeleton. Colour scale representing the percentage incidence of ^{18}F uptake (red= 81-100% incidence, orange= 61-80% incidence, yellow= 41-60% incidence, green= 21-40% incidence, blue= 1-20% incidence, white= 0% incidence or not analysed). IVDs: 5 lumbar, 12 thoracic and 7 cervical. See Figure 2.5 for a labelled skeletal map of the joints analysed. n=43 (17 females, 26 males, mean age 49, SD±14.8, range 21-74). Age groups: 21-30 n=8, 31-40 n=5, 41-50 n=7, 51-60 n=12, 61-70+ n=11.

The percentage incidence of ^{18}F uptake in the knee joint, hip joint and shoulder joint increases with age (Figure 3.10). No increased uptake of ^{18}F was identified in the shoulder and knee joints in the two youngest age groups (21-30 and 31-40) and very low incidence was found in the hip (12.5% incidence in the 21-30 age group, 0% incidence for the 31-40 age group). From the age group 31-40 the percentage incidence of ^{18}F uptake increases in all three joints. In the shoulder joint the percentage incidence increases from 0% in the two youngest age groups to 43% in the 41-50 age group, then further increases to 67% in the 51-60 age group and increases again reaching 82% in the oldest age group. In the knee the same trend is seen; an exponential increase from 0% in the youngest two age groups followed by an increase up to 63% in the 41-50 age group, reaching 100% incidence in the 51-60 and 61-70 age groups. In the hip low incidences were found in the youngest two age groups (13% in the 21-30 age group and 0% in the 31-40 age group) followed by exponential increase to 43% in the 41-50 age group, 58% in the 51-60 age group, reaching 100% in the 61-70 age group.

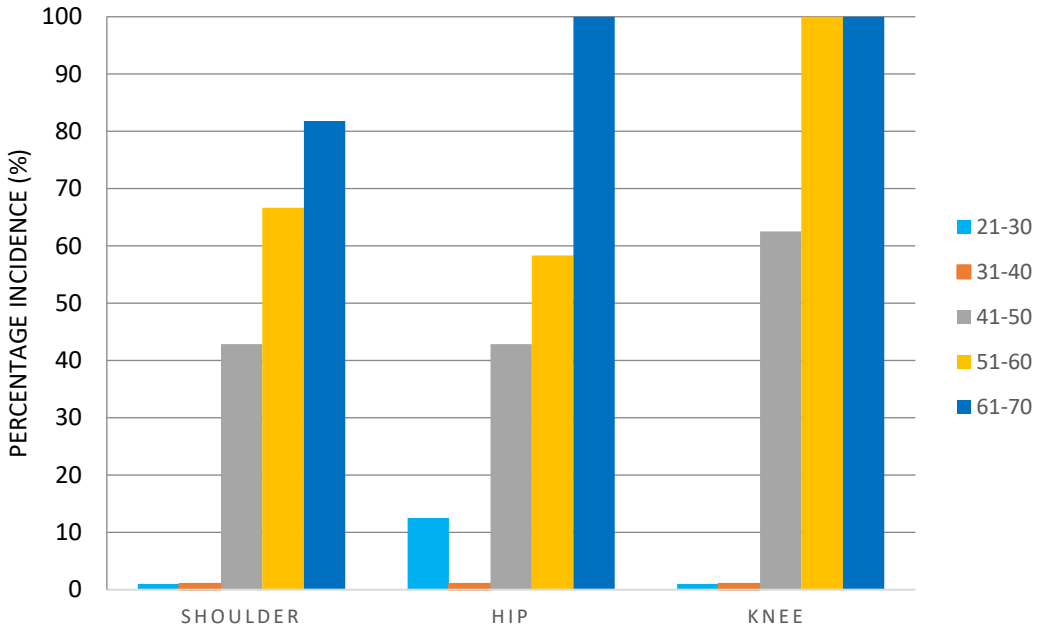

Figure 3.10 Percentage incidence of increased tracer uptake in the shoulder, hip and knee joints with age. n=43 (17 females, 26 males, mean age 49, SD±14.8, range 21-74).

3.3.3 CARTILAGE ANATOMICAL THRESHOLD SCORE WITH AGE

The C-AT score (summation of all joints scored, explained in section 2.4.6) was correlated with age (Figure 3.11). Regression analysis found a positive statistically significant correlation ($r=0.487$, $p<0.001$). This supports the findings illustrated in Figures 3.8 and 3.9 that demonstrate an increase in the percentage incidence of increased tracer uptake with age in the cartilaginous joints.

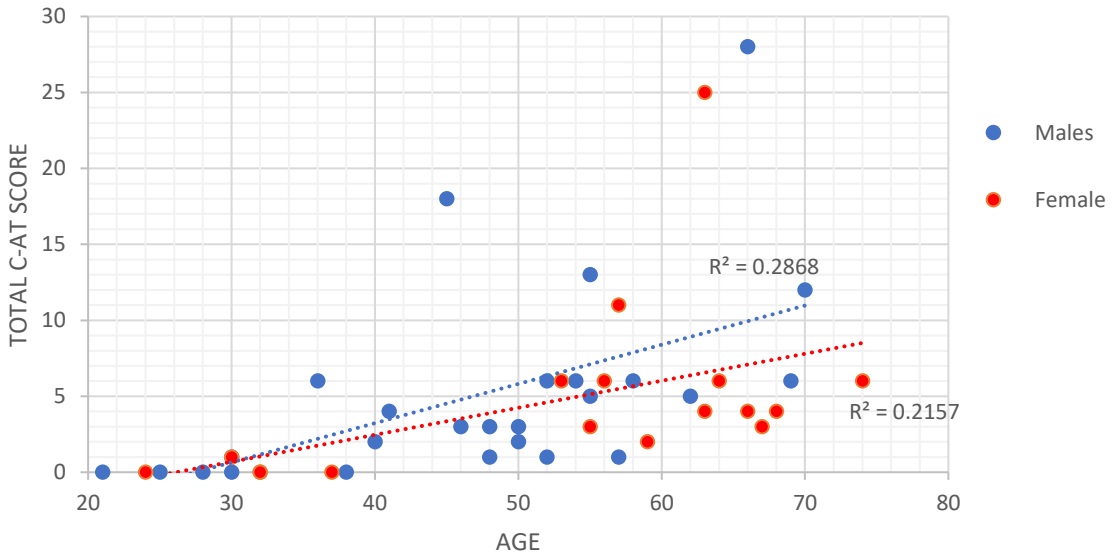

Figure 3.11 Correlation between cartilage anatomical threshold (C-AT) score with age. 32 Joints summated to produce the C-AT score as explained in section 2.4.6. Maximum score of 32. A positive statistically significant correlation was found (r=0.487, p<0.001). n=43 (17 females, 26 males, mean age 49, SD±14.8, range 21-74).

3.3.4 BONE ANATOMICAL THRESHOLD SCORE WITH AGE

The B-AT score is the summation of all bone scores measured (explained in section 2.4.7). No correlation was found between the B-AT score and age (r=0.0004, p>0.05) (Figure 3.12). This supports the findings summarised in Figure 3.2, with no obvious trend between overall increased uptake and age. However, in contrast Figures 3.3 and 3.4 demonstrate a general reduction in increased tracer uptake in the spine with age.

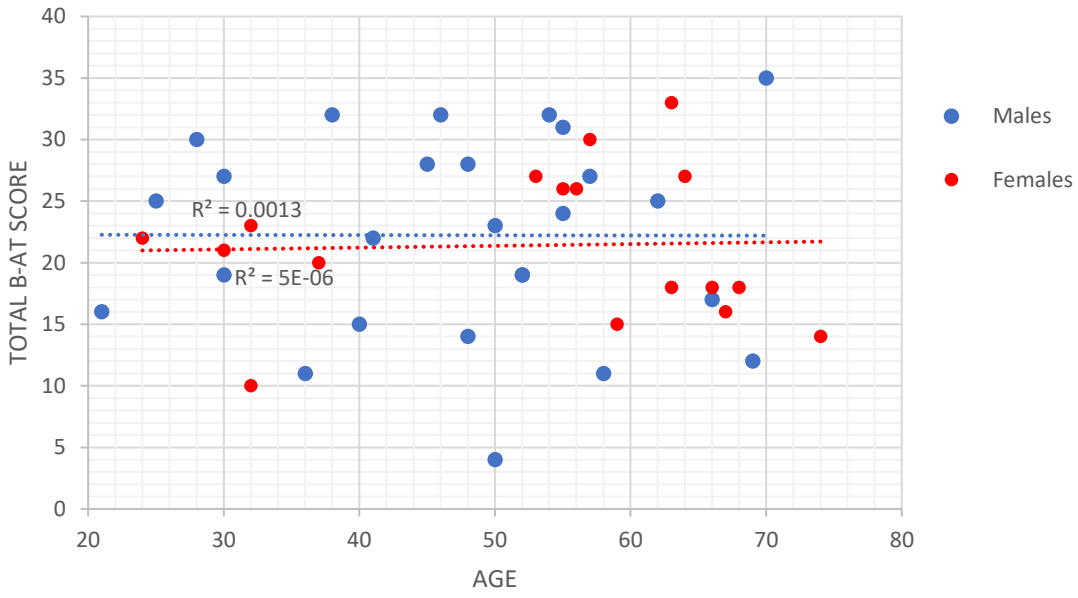

Figure 3.12 Scatter plot showing the correlation between bone anatomical threshold (B-AT) score and age. 42 Joints summated to produce the B-AT score as explained in section 2.4.7. Maximum score of 42. No statistically significant correlation found (r=0.0004, p>0.05). n=43 (17 females, 26 males, mean age 49, SD±14.8, range 21-74).

3.3.5 TOTAL CLINICAL SCORE vs TOTAL ANATOMICAL THRESHOLD SCORE

Correlations were also made with the total clinical score obtained from the AKUSSI (section 2.4.9) with the total anatomical threshold score (section 2.4.8) to assess the anatomical threshold methodology (section 2.4). A positive statistically significant correlation (r=0.881, p<0.001) was found between total clinical score versus the total anatomical threshold score (Figure 3.13). Positive statistically significant correlations were also identified between the total anatomical threshold score with age (r=0.888, p<0.001) and the total clinical score with age (r=0.956, p<0.001) (Figures 3.14 and 3.15 respectively).

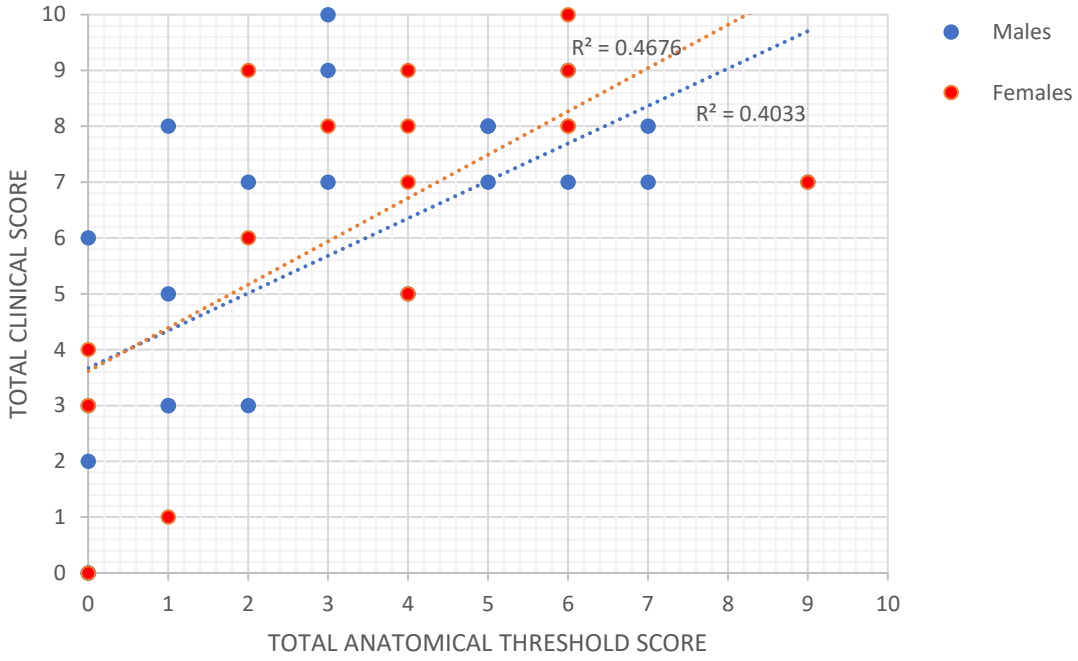

Figure 3.13 Correlation between the total clinical score and total anatomical threshold score. Total clinical score (explained in section 2.4.9) maximum value of 10, total anatomical threshold score (explained in section 2.4.8) maximum value of 10. Positive statistically significant correlation ($r=0.881$, $p<0.001$). n=38.

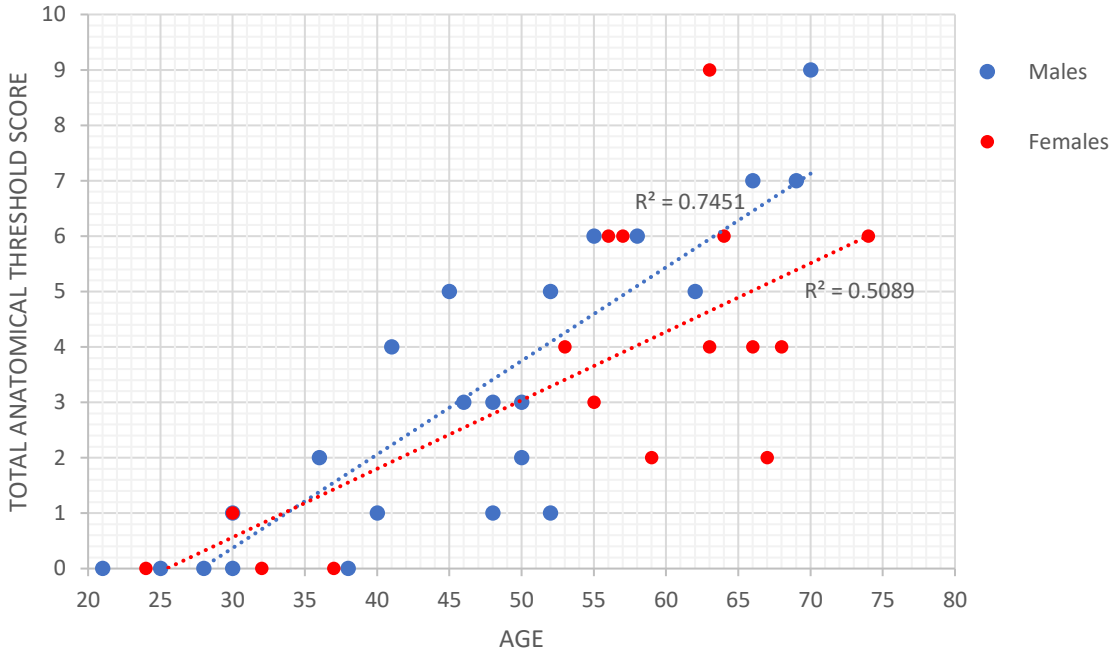

Figure 3.14 Correlation between the total anatomical threshold score with age. Total anatomical threshold score explained in section 2.4.8. Positive statistically significant correlation ($r=0.888$, $p<0.001$). n=43 (17 females, 26 males, mean age 49, SD±14.8, range 21-74).

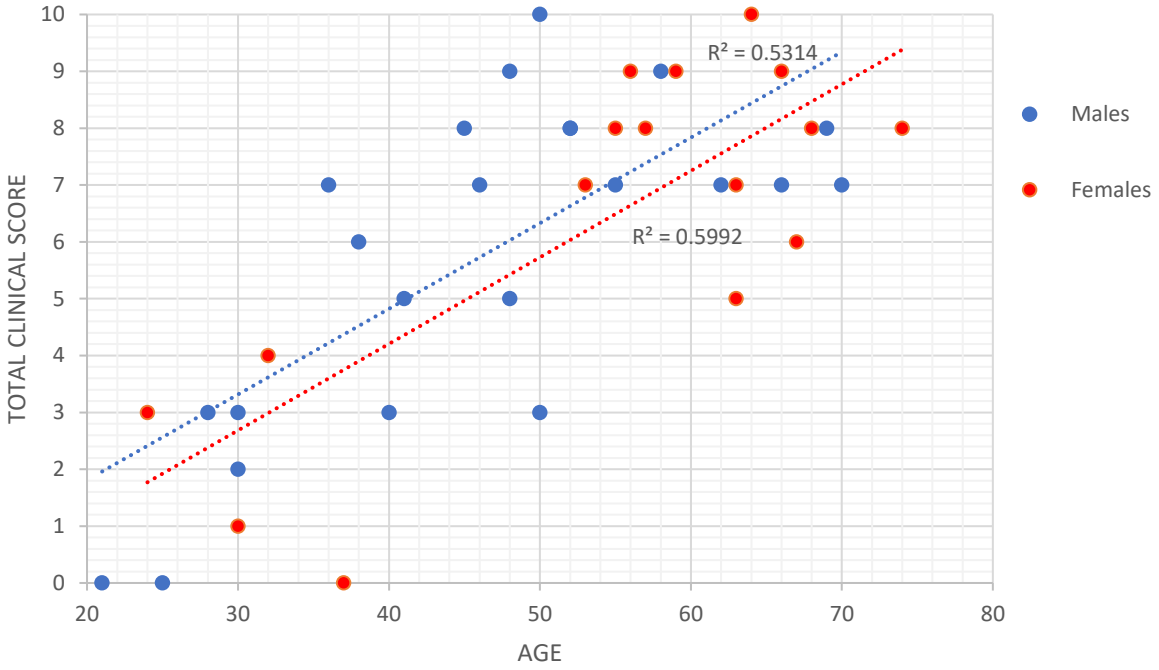

Figure 3.15 Correlation between the total clinical score with age. Total clinical score explained in section 2.4.9. Positive statistically significant correlation (r=0.956, p<0.001). n=38.

3.4 DISCUSSION

^{18}F has been utilised as a bone imaging radionuclide since the 1960's. Although ^{18}F-NaF was the first widely used bone imaging agent it quickly fell into disuse. Limitations included, logistical challenges of the 110 minute half-life of ^{18}F-NaF , the introduction of cheaper radiopharmaceuticals such as technetium (Tc-99m) and the development of the Anger gamma camera designed for the 140 KeV photons of Tc-99m resulted in the FDA to withdraw its approval in 1975 (107). The challenges associated with ^{18}F-NaF imaging were reassessed in 1992 when Dahlbom *et al*. (108) used ^{18}F-NaF in the development of a whole-body PET technique that demonstrated increased spatial resolution and greater photon capture due to coincident detection of photons. During the past decade nuclear imaging with ^{18}F-NaF PET has re-emerged as an attractive, specific, non-invasive method of detecting bone metabolism in osseous diseases (109). The development of combined PET/CT scanners, ease of production in a cyclotron (previously ^{18}F-NaF was produced in a nuclear reactor with a two-step reaction) coupled with shortages of Tc-99m generators, has led to ^{18}F-NaF being the preferred bone imaging agent once again (109). The pharmacokinetics of ^{18}F-NaF depends on both bone uptake and elimination from the circulation. Uptake of ^{18}F into the skeleton reflects the amount of actively mineralising bone present and resembles bone metabolism (109). The principle uptake mechanism involves ^{18}F being deposited onto the crystalline structure of hydroxyapatite of newly forming bone by exchanging fluoride with hydroxyl ions forming fluorapatite (109,128). The application of ^{18}F-NaF PET to detect areas of increased bone remodelling and inflammation has been demonstrated in many studies in various osseous diseases (110,115,129,130). X-ray is the gold standard for imaging arthritic changes in OA.

Pathological changes appear with the progression of the disease and are graded depending on the extent of involvement (KL grading scale see Table 1.3). However, often functional abnormalities occur before clear radiographic signs appear (115). Functional PET imaging has been shown to identify these early changes. Kobayashi *et al*. (115), demonstrated the use of ^{18}F-NaF PET in detecting bone remodelling in early stage osteoarthritis (OA) of the hip. Increased ^{18}F uptake was found to be associated with increased radiographic stage of OA (KL grading scale) and the severity of hip pain. They proposed this could be useful in deciding on a treatment strategy in early stage OA. Watanabe *et al*. (129) demonstrated the coupling of inflammation and accelerated bone turnover in rheumatoid arthritis (RA) using ^{18}F-FDG and ^{18}F-NaF PET/CT. They found that accumulation of ^{18}F-NaF correlated with clinical assessment and physical disability in RA. Frost *et al*. (130) demonstrated the effect of the antiresorptive drug risedronate on lumbar vertebrae bone metabolism in OA measured by ^{18}F-NaF PET. They found that osteoclastic and osteoblastic activity displayed a significant decrease after 6 months on risedronate due to the close coupling of bone resorption and bone formation, demonstrating the effects of the treatment. These studies demonstrate the usefulness of ^{18}F-NaF PET in the detection and treatment of metabolic bone diseases.

In AKU HGA deposition over time results in ochronosis of connective tissues including cartilage (36). It is understood that HGA deposition within cartilage alters the mechanical properties within the tissue leading to aberrant transmission of mechanical loading to bone resulting in resorption of the subchondral plate and calcified cartilage. The end stage of the pathogenesis of ochronosis in the joint is

failure. Secondary to this the cartilage becomes calcified and becomes visible on the PET images due to ^{18}F binding to the calcifications forming fluorapatite. It is understood that ochronotic cartilage becomes stiff, it is not yet fully understood whether the calcifications form inside the ochronotic cartilage or if they are forming on the surface despite this the calcifications must be accessible for ^{18}F to bind. It is unknown if binding of ^{18}F is altered by the presence of ochronotic pigment although it is agreed that the weight bearing joints are predominantly affected by the disease possibly due to mechanical damage (1). AKU has pathological parallels with OA therefore ^{18}F-NaF PET imaging can be utilised in AKU. This is the first study to date that looks at the distribution of ^{18}F-NaF PET in the rare disease AKU.

3.4.1 INCREASED ^{18}F UPTAKE IN BONE - MECHANICAL LOADING

In bone the highest incidences of increased ^{18}F signal was found in the hip, sacrum, thoracic and lumbar vertebrae (93%, 64%, 73% and 80% respectively) (Figure 3.1). These bones are classically weight bearing bones and it has been proposed that there is a link between mechanical stress and ^{18}F uptake. It was demonstrated by Kobayashi *et al*. (115) that mechanical loading enhances interleukin 11 (IL-11) gene expression that stimulates osteoblast differentiation. The function of IL-11 is believed to be inhibition of Dickkopf 1 and 2, which are inhibitors of Wnt signalling. Wnt signalling has been shown as an important regulatory pathway in osteogenic differentiation. Induction of Wnt signalling promotes bone formation, while inactivation leads to osteopenia. If bone formation is promoted this increases the availability of hydroxyapatite for ^{18}F to bind. It is believed that a reduction in IL-11 with age may be one of the factors contributing to osteoporosis (131,132).

Sanchez *et al*. (133) also demonstrated a link between mechanical stress and increased expression of genes involved in bone remodelling and bone formation in human osteoblasts. This chapter has demonstrated that the non-weight bearing bones of the upper limb had very low incidences averaging 12% in comparison to the bones of the lower limb and foot that had an average incidence of 26% (Figure 3.1). This supports the theory that weight bearing bones experiencing mechanical loading are associated with increased bone formation and increased ^{18}F uptake.

Win *et al*. (117) described the uptake of ^{18}F in various skeletal sites in a control population and found that different skeletal sites have different amounts of fluoride uptake. The proposed reason for this variation is the composition of bone at different sites. They found that ^{18}F tends to have greater deposition in the axial skeleton (e.g. vertebrae and pelvis) than in the appendicular skeleton (limbs), this supports the results described in this chapter where the highest incidences were found in the hip, sacrum and lumbar and thoracic spine (Figures 3.1 and 3.2).

3.4.2 INCREASED ^{18}F UPTAKE IN BONE- VASCULARITY

Uptake of ^{18}F in bone depends on regional blood flow, osteoblastic activity and renal clearance (117). Trabecular bone is highly vascular and contains abundant red marrow, which may explain the increased incidence of ^{18}F uptake in the vertebrae and hip that contain mostly trabecular bone in contrast to relatively lower trabecular bone in the long bones of the limbs (Figure 3.1) (134).

3.4.3 INCREASED ^{18}F UPTAKE IN THE VERTEBRAE

Interestingly the incidence of increased ^{18}F uptake in the lumbar vertebrae decreases with age (Figure 3.3). This trend can also be seen in the three youngest age groups in the thoracic vertebrae (Figure 3.4). It has been described that with age there is a reduction in red marrow and an associated decrease in perfusion to bone (134). Reduced perfusion to bone would result in reduced ^{18}F transport to that area. This may explain the reduction in the incidence of ^{18}F uptake with age. It is widely agreed that BMD decreases with age. Riggs *et al*. (135) found that bone diminution in the vertebrae began in young adulthood and was linear with increasing age. A reduction in BMD with age may explain the reduction in the incidence of increased ^{18}F uptake with age; if there is less hydroxyapatite available, less fluorapatite can form. Not only does the incidence of ^{18}F reduce with age in the spine but it also reduces up spine from T12-T1 (Figure 3.4). The larger bones located towards the lower ends of the spine have more of a weight-bearing role, therefore have increased uptake compared to the smaller bones located further up. The cervical vertebrae follow a similar trend where the percentage incidence of ^{18}F uptake decreases as you travel up the spine from C7-C1 (Figure 3.6). However, in the cervical vertebrae, generally the oldest two age groups (51-60 and 61-70+) have higher incidences of ^{18}F signal compared to the younger age groups (21-30, 31-40, and 41-50). Interestingly, pain in the cervical region has been reported in older patients with AKU. Generally lower incidences were seen in the cervical and upper thoracic spine compared to the lower thoracic spine and lumbar vertebrae in the youngest three age groups (Figure 3.2), this could be due to the reduced mechanical load experienced by the cervical vertebrae compared to the lower thoracic and lumbar vertebrae.

3.4.4 BONE ANATOMICAL THRESHOLD SCORE WITH AGE

No correlation ($r=0.0004$, $p>0.05$) was identified between the B-AT score with age (Figure 3.12) suggesting that when looking at the overall skeletal distribution of increased ^{18}F uptake there is no direct trend with age (Figure 3.2). A reduction in increased uptake of ^{18}F with age was expected due to a reduction in bone turnover, BMD and vascularity associated with ageing, however this trend was not evident. It is thought that increased ^{18}F uptake is individual to the patient depending on where the disease affects them and at what stage in time. AKU can affect all cartilaginous joints although each patient can present differently, with different joints being affected and at different severities. Plotting the incidence of increased ^{18}F uptake per patient and correlating the results with the clinicians notes to obtain information like pain scores, and radiographic signs may provide a better representation of uptake in bone for each patient and this would test the reliability of the method.

3.4.5 PATHOGENESIS OF INCREASED ^{18}F UPTAKE IN CARTILAGE

AKU is primarily a cartilage disease with secondary effects in bone. It is therefore not surprising that we have identified uptake in cartilage as well as bone. In terms of the pathophysiology of AKU, HGA is deposited in individual chondrocytes within the calcified cartilage. With time ochronosis spreads through to the hyaline cartilage causing it to become stiff, resulting in aberrant transmission of mechanical loading to bone. This leads to resorption of the subchondral plate including calcified cartilage and bone. This results in destruction of the joint where pigmented cartilage becomes impacted on the underlying trabecular bone and embedded in the marrow space (3).

3.4.6 INCREASED UPTAKE OF ^{18}F IN CARTILAGE

High incidence of ^{18}F uptake was found in the joints of the foot, knee, hip and shoulder joints with incidences of 52%, 65%, 52% and 48% respectively. Low incidences (less than 20%) were found in the rest of the cartilaginous joints scored (Figure 3.7). The incidence of ^{18}F uptake was found to increase with age in the three large joints (shoulder, hip and knee) and was found to reach 100% in the hip and knee in the oldest age group (61-70) (Figure 3.10). The hip and the knee are largely weight bearing joints experiencing large amounts of mechanical loading. It is therefore not surprising that these joints have been found to be most affected by AKU. A positive statistically significant correlation ($r=0.487$, $p<0.001$) was identified between the C-AT score with age (Figure 3.11), this supports the findings illustrated in Figures 3.8 and 3.9 that demonstrate an increase in the percentage incidence of increased tracer uptake with age in cartilage.

Age related changes to cartilage results in the disarray of the extracellular matrix due to disruption of collagen fibrils and proteoglycans which is exacerbated by trauma. These changes render exposed collagen vulnerable to the reactive molecule HGA in AKU resulting in ochronosis (136). The uptake of ^{18}F in cartilage represents binding of ^{18}F to calcifications within the cartilage due to ochronosis. ^{18}F binds to newly formed hydroxyapatite; therefore, the uptake in cartilage must represent newly formed mineral forming within the cartilage. Chondrocalcinosis is a disease in which calcium pyrophosphate is deposited within cartilage leading to osteoarthritis. This disease process is characterised by chondrocyte hypertrophy, matrix mineralisation and many structural changes to the joint (136). Mineralisation within cartilage has been

documented in OA, especially in severe OA where deposition of calcium pyrophosphate and basic calcium phosphate crystals (including hydroxyapatite) have been frequently identified (137). It is proposed that this could also be the case in AKU due to the many parallels OA and AKU share. Uptake of ^{18}F in cartilage reflects the severity of AKU osteoarthropathy and confirms the anatomical distribution of increased ^{18}F uptake into cartilaginous joints that localise to areas of high mechanical loading. It therefore can be said that these areas are more susceptible to attack by HGA and mineral deposition within cartilage resulting in mechanical changes, eventually leading to multisystemic damage dominated by premature severe osteoarthropathy. Interestingly we found low incidence throughout all the IVDs, however these patients are known to suffer from spinal arthropathy. This could be due to the resolution of the ^{18}F MIP PET images not enabling differentiation between calcified IVDs and bone in the osteoarthritic spine seen in later stages of AKU.

3.4.7 ASSESSMENT OF METHODOLOGY

Correlations were made between the total clinical score and the total anatomical threshold score to assess the methodology (Figure 3.13). The total clinical scores were consistently higher than the total anatomical threshold scores and a positive statistically significant correlation ($r=0.881$, $p<0.001$) was identified. This suggests that the anatomical threshold method may not be sensitive enough to identify smaller increases in tracer uptake that reflects areas affected by the disease. Positive statistically significant correlations were also identified between the total anatomical threshold score with age (Figure 3.14) ($r=0.888$, $p<0.001$) and the total clinical score

with age (Figure 3.15) ($r=0.956$, $p<0.001$) demonstrating that both methods identified the same trend.

3.4.8 SUMMARY

Uptake of ^{18}F localises to hydroxyapatite crystals of newly formed bone and calcified cartilage that are exposed to high mechanical loading. Pigmentation of the AC associated with AKU causes stiffening, resulting in aberrant transmission of mechanical loading to subchondral bone, leading to altered bone remodelling. Secondary to this and with advancing disease progression, cartilage becomes calcified and identified as areas of increased ^{18}F uptake on the PET scans. The joints exposed to high mechanical loading are most susceptible to destruction via this process. With age the uptake in bone and cartilage follows opposite trends. The incidence of ^{18}F uptake in cartilage increases with age in the weight bearing joints due to mineralisation. However, the percentage incidence of ^{18}F uptake in bone decreases with age due to reduced bone turnover associated with ageing. This work demonstrates the sensitivity of ^{18}F PET scans in detecting the distribution of joint disease in AKU.

3.4.9 LIMITATIONS

The major limitations of this study are, firstly the data described in this chapter is based on pixel values, pixel values are a measure of intensity, however it is the amount ^{18}F uptake that is directly related to what is being observed, therefore uptake values are more appropriate. Secondly, when trying to identify small joints the resolution of the ^{18}F MIP PET images was not sufficient to differentiate between

cartilage and bone. This was especially evident in the osteoporotic spine where it was very difficult to distinguish between calcified IVDs and bone (Figure 3.16). Overlying CT data would help with anatomical localisation.

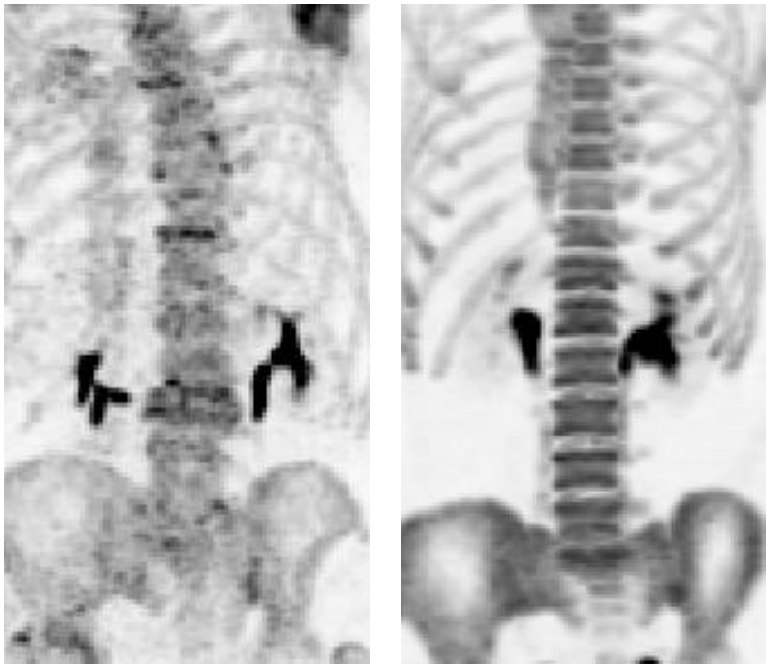

Figure 3.16 ^{18}F-NaF images of the spine in a non-arthritic and arthritic patient. Left image demonstrating severe arthropathy; uptake of ^{18}F-NaF is uniform throughout the spine, therefore very difficult to distinguish between IVD and bone. Right image demonstrating non-arthritic spine with bands of increased uptake in the vertebrae, with very little uptake in the IVDs.

3.4.10 FUTURE WORK

Future work is needed to develop quantitative measures of ^{18}F uptake within bone and cartilage which could be used to assess disease progression, and response to therapy. Utilising PET/CT will improve resolution and localisation of areas of increased ^{18}F uptake, this will enable precise localisation of anatomical regions such as vertebral end plates and IVDs.

4.0 APPLICATION OF ^{18}F-NaF PET STANDARDISED UPTAKE VALUE FOR THE DETECTION OF ARTHROPATHY IN AKU

4.1 INTRODUCTION

Chapter 3 of this thesis looked at the skeletal distribution of ^{18}F in AKU patients. The method used was based on the distribution of pixel values in the image. As described in the limitations section (3.4.9) the data described in Chapter 3 was based on pixel values. Pixel values are a measure of intensity. However, it is the amount of ^{18}F uptake that is directly related to what is being observed. Therefore, uptake values are more appropriate. Additionally, the anatomical localisation of the spine proved to be difficult to distinguish between bone and calcified IVDs due to the resolution of the image. This chapter resolves these issues by utilising measurements of radioactivity instead of pixel values, as well as utilising PET/CT for improved anatomical localisation.

Quantitative measurements in PET imaging are used as a tool to supplement visual interpretation providing a method that is less user-dependent and that can be used for intra and inter patient comparisons. Uptake measurements are used to assess response to therapies and to distinguish degree of pathology (114). ^{18}F-NaF PET has been used to visualise many bone disorders as ^{18}F-NaF binds to bone mineral associated with both osteoblastic and osteolytic lesions (115). ^{18}F-NaF PET scanning is routinely carried out annually as part of the NAC as well as for the SONIA 2 clinical trial (see sections 2.2.1 and 2.2.2).

The mean standardised uptake value (SUVm) is a common method of expressing the uptake of PET tracers. The SUVm is a measure of radioactivity in a region of interest, normalised against the injected activity and the subjects body weight. The SUVm is defined as the activity concentration in the ROI ((kBq/mL) as measured by the PET

scanner) divided by the decay corrected injected dose of ^{18}F-NaF (kBq) divided by the patient body weight (kg) that acts as a surrogate for the distribution volume of tracer (SUVm= radioactivity concentration / (decay corrected injected dose / body weight)) (116). If all the injected ^{18}F-NaF is retained and uniformly distributed throughout the body, the SUVm will be 1g/ml under the assumption that 1ml of tissue weighs 1g. Larger SUVms represent proportionally higher concentrations of radiotracer. The uptake is represented by pixel or voxel intensity value in the ROI, which is then converted into the activity concentration (117). PET imaging allows quantitative SUVm measurements allowing the clinician to quantify disease state, progression and response to therapy. More recently, SUVm measurements in ^{18}F-NaF PET have been reported to have potential as a diagnostic tool in OA (116). This chapter introduces for the first time, quantitative SUVm measurements of bone and cartilage to identify active spondyloarthropathy and to quantify disease state in AKU.

4.2 FEASIBILITY STUDY

A feasibility study was first undertaken to assess the viability and practicality of obtaining SUVm measurements from both cartilage and bone in the large joints and spine. The purpose was to objectively identify the strengths and weaknesses of the methodology and the feasibility of measuring small anatomical regions such as articular cartilage (AC).

4.2.1 DESIGN OF FEASIBILITY STUDY

Ten female non-metastatic breast cancer patients were used as a control group (mean age of 62, SD±13.8, range 43-84, see section 2.2.3) exclusion criteria included active arthropathy in the shoulder, hip and spine. Ten randomly selected female AKU (NAC) patients (mean age of 60, SD±6.47, range 52-72, section 2.2.1) were included for comparison. Hermes hybrid viewer (section 2.5.1) was utilised to obtain SUVms from the hip and shoulder (see section 2.5.3) and lumbar and thoracic spine (see section 2.5.2). The knee and ankle could not be included in this analysis as the control patients were not scanned below the knee. For the hip, the SUVm was obtained from the head of the femur, acetabulum and AC (ROI= 0.5cm diameter, 0.196cm^2). For the shoulder, SUVms were obtained from the head of the humerus, glenoid fossa and AC (ROI= 0.5cm diameter, 0.196cm^2). SUVms were also obtained from the centre of each thoracic (T1-T12) and lumbar (L1-L5) vertebrae, and from the centre of the corresponding IVD below (T1/T2 – L5-S1) (ROI= 1cm diameter, 0.785cm^2). The feasibility of measuring SUVms at these anatomical sites was assessed.

4.2.2 RESULTS OF FEASIBILITY STUDY

4.2.2.1 Mean standardised uptake value – Hip

The SUVm was obtained from AKU and control hip joints. The SUVm was measured in the AC, acetabulum and the head of femur. The triangulation point was placed at the centre of the hip joint. Figure 4.1 demonstrates the SUVm across the three anatomical regions within the hip joint in the individual AKU patients. It is apparent in Figure 4.1 when looking at patient 60B that the SUVm for the AC is strikingly higher (SUV = 23) compared to the other patients, with a mean SUVm of 3.7. The acetabulum and the head of the femur have low values and are relatively stable across all patients with a mean of 6.5, and 4.0 respectively. Generally, except patient 60B, the SUVms of the acetabulum and head of the femur are higher than that of the AC. There appears to be no trend in SUVms across the AC, acetabulum or the head of the femur with age (Figure 4.1).

Figure 4.2 demonstrates the SUVms within the AC, acetabulum and head of the femur in the individual control patients. The same trends can be seen in the control group as in the AKU group. The acetabulum of the hip consistently has the highest SUVms (averaging 7.3) across the three anatomical locations for each patient. The head of the femur has generally low SUVms across all patients (averaging 2.7), as does the SUVms for the AC (averaging 3.0) (Figure 4.2). There appears to be no definitive trend across the AC, acetabulum or the head of femur with age as found in the AKU group. Figure 4.3 demonstrates a comparison of the control and AKU SUVm in the three anatomical regions of the hip. This Figure shows that the AKU group have marginally higher SUVms in both the AC and the head of the femur demonstrated by the box

plot (X denotes the mean value), and slightly lower SUVms in the acetabulum. Independent t-tests revealed no statistically significant differences between AKU and control SUVm in the AC ($p>0.05$), acetabulum ($p>0.05$) or the head of the femur ($p>0.05$).

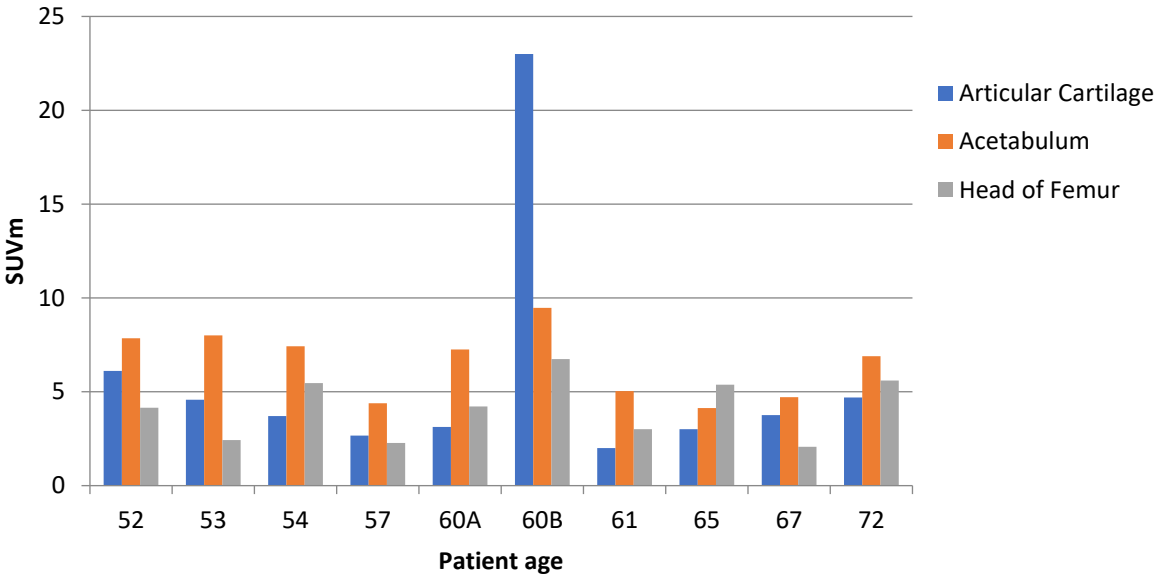

Figure 4.1 SUVm of the articular cartilage, acetabulum and head of femur in the AKU group with age. 10 female AKU patients (mean age of 60, SD±6.47, range 52-72). ROI = diameter 0.5cm 0.196cm^2, obtained from each anatomical location at the centre of the hip joint.

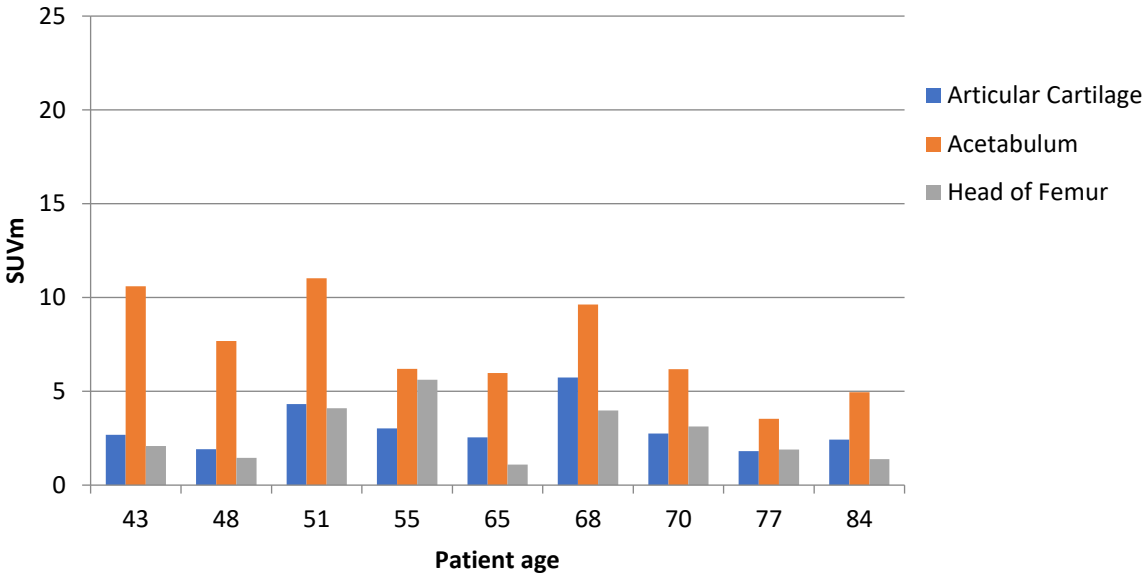

Figure 4.2 SUVm of the articular cartilage, acetabulum and head of femur in the control group with age. 9 female control patients (mean age of 62, SD±13.8, range 43-84). ROI = diameter 0.5cm, 0.196cm^2 obtained from each anatomical location (patient 83 was excluded due to active arthropathy in both hips).

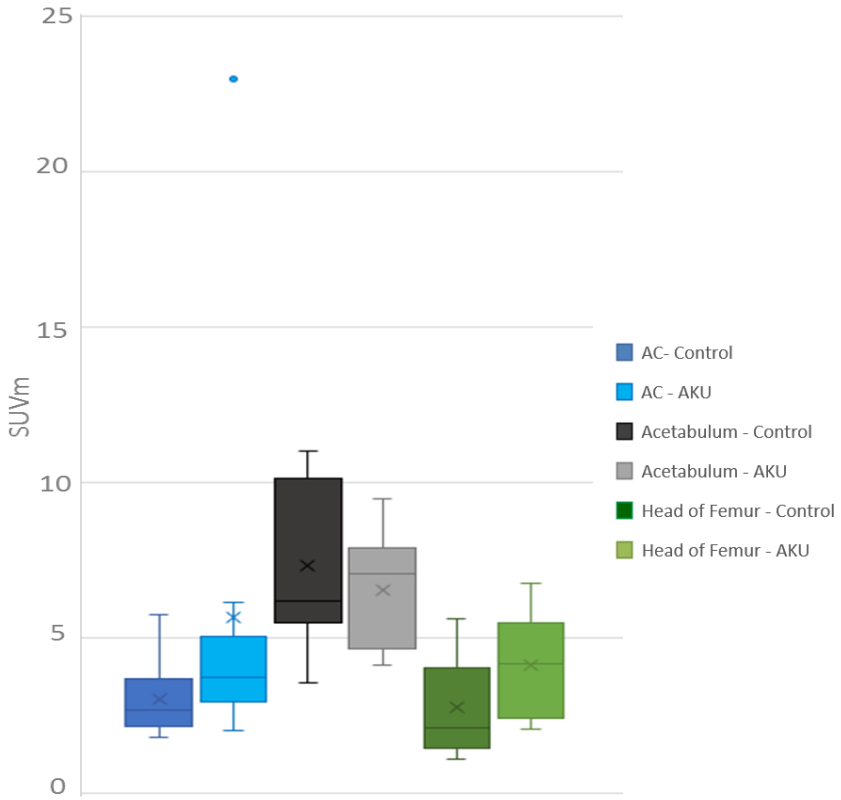

Figure 4.3 Box and whisker plot comparison of AKU and control SUVm in the articular cartilage, acetabulum and head of femur of the hip joint. Independent t-tests found no statistically significant differences between AKU and control in the articular cartilage ($p>0.05$), acetabulum ($p>0.05$) and the head of the femur ($p>0.05$). Box and whisker plot: height of box = interquartile range (upper quartile, lower quartile), X = mean value, line within box = median value. Whiskers show the range. Individual data points are plotted, the majority are hidden by the plotted boxes. Ten female control patients (mean age of 62, SD±13.8, range 43-84), Ten female AKU patients (mean age of 60, SD±6.47, range 52-72).

4.2.2.2 Standardised uptake value (mean) – Shoulder

SUVms were obtained from AKU and control shoulder joints. The SUVm was measured in the AC, glenoid fossa of the scapula and the head of the humerus, with the triangulation point placed at the centre of the shoulder joint. Figure 4.4 demonstrates the SUVm across the three anatomical regions within the shoulder joint in the individual AKU patients. Again, for patient 60B the SUVm for the AC is strikingly higher (SUVm= 27) than the other patients, who have a mean SUVm of 2.7. The glenoid fossa and the head of the humerus all have similar low values with a mean of 6.6 and 3.1 respectively across all AKU patients, this is similar to what was seen in the hip joint. Generally (except patient 60B), the SUVms of the glenoid fossa and head of the humerus are higher than that of the AC. The SUVm of the glenoid fossa is consistently higher than the AC and the head of the humerus, again reflecting what was observed in the corresponding regions of the hip. There appears to be no trend across the three anatomical regions with age.

Figure 4.5 demonstrates the SUVms within the AC, glenoid fossa and head of the humerus in the individual control patients. The glenoid fossa of the scapula consistently has the highest SUVms (mean = 6.1) across the three anatomical locations for each patient. The head of the humerus has generally low SUVms across all patients (mean = 2.0), as does the SUVms for the AC (mean = 2.2).

Figure 4.6 compares control and AKU SUVms across the three anatomical regions of the shoulder. This Figure shows that the AKU group had marginally higher SUVms compared to the control group across the three anatomical regions of the shoulder

joint demonstrated by the box plot (X denotes the mean values). However, independent t-tests revealed no statistically significant differences between AKU and control groups in the AC ($p>0.05$), glenoid fossa ($p>0.05$) and the head of the humerus ($p>0.05$). No trend was identified across the three anatomical regions with age in the control group.

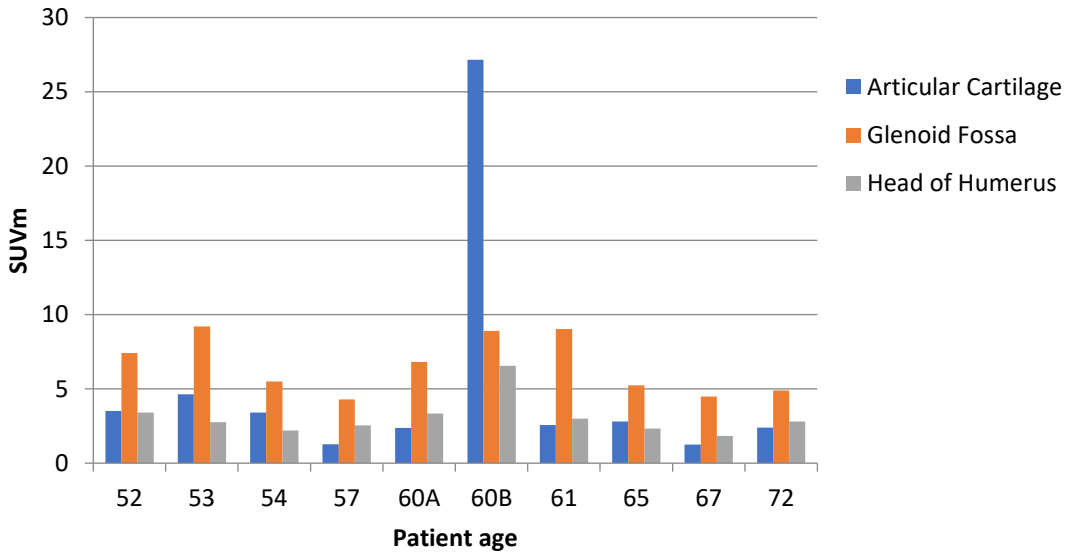

Figure 4.4 SUVm of the articular cartilage, glenoid fossa and head of the humerus of the shoulder in the AKU group with age. 10 female AKU patients (mean age of 60, SD±6.47, range 52-72). ROI = diameter 0.5cm, 0.196cm^2 obtained from each anatomical location at the centre of the shoulder joint.

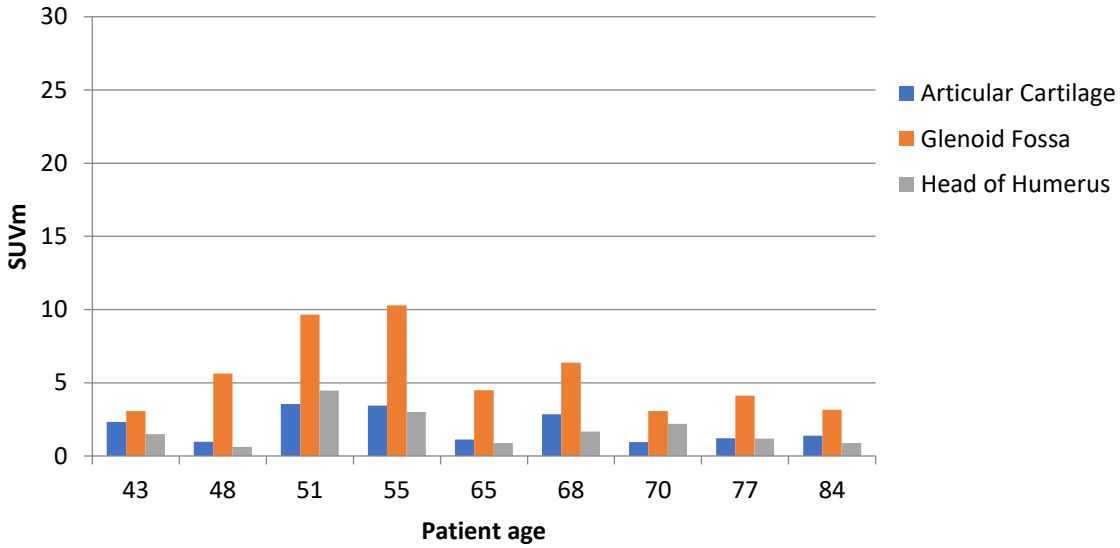

Figure 4.5 SUVm of the articular cartilage, glenoid fossa and head of humerus in the control group with age. 9 female control patients (mean age of 62, SD±13.8, range 43-84). Patient 83 was excluded due to active arthropathy in both shoulders. ROI = diameter 0.5cm, 0.196cm^2 obtained from each anatomical location at the centre of the shoulder joint.

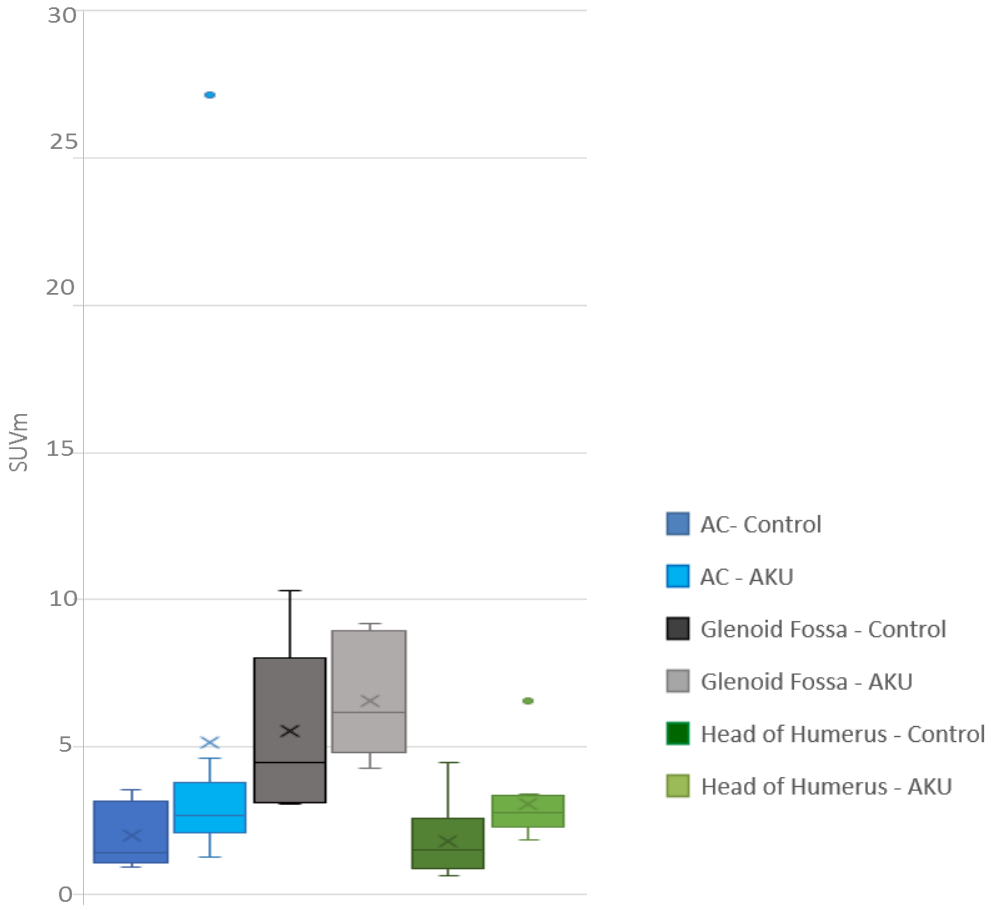

Figure 4.6 Box and whisker plot comparison of AKU and control SUVm in the articular cartilage, glenoid fossa and head of the humerus of the shoulder joint. Independent t-tests found no statistically significant differences between AKU and control in the articular cartilage ($p>0.05$), glenoid fossa ($p>0.05$) and the head of the humerus ($p>0.05$). Box and whisker plot: height of box = interquartile range (upper quartile, lower quartile), X = mean value, line within box = median value. Whiskers show the highest and the lowest value. Individual data points are plotted, the majority are hidden by the plotted boxes. Ten female control patients (mean age of 62, SD±13.8, range 43-84). Ten female AKU patients (mean age of 60, SD±6.47, range 52-72).

4.2.2.3 Standardised uptake value – Spine

Figure 4.7 demonstrates the SUVm across the lumbar and thoracic vertebrae in the AKU and control groups. Statistically there was no significant difference ($p>0.05$) between the SUVm of AKU vertebrae (mean SUVm=7.6, SD=1.3) and control vertebrae (mean SUVm=7.9, SD=0.6). There appears to be a gradual increase in SUVms in the AKU group along the vertebrae from L5-T1 ranging from 5.75 at the lower lumbar region to 10.05 at the upper thoracic region. The control group SUVms appear to be slightly more stable across the vertebrae ranging from 6.84 to 8.91.

Figure 4.8 demonstrates the SUVm across the lumbar and thoracic IVDs in the AKU and control groups. AKU IVDs are consistently higher compared to the control group with a mean SUVm of 12.01 (SD= 1.28) and 3.81 (SD=1.26) respectively. The control group SUVms across the IVDs ranged from 1.54-5.63 and the AKU IVDs ranged from 10.28- 14.95. No trend could be identified in the AKU group regionally along the spine reflected by the shallow fluctuations around SUVm of 12. A slight increase in SUVm is evident in the control group from L4/L3 IVD to T1/T2 rising from a SUV of around 2 to 6 ascending the spine. Independent t-tests identified a statistically significant difference ($p<0.01$) between AKU and control IVDs SUVms across all levels (Figure 4.8).

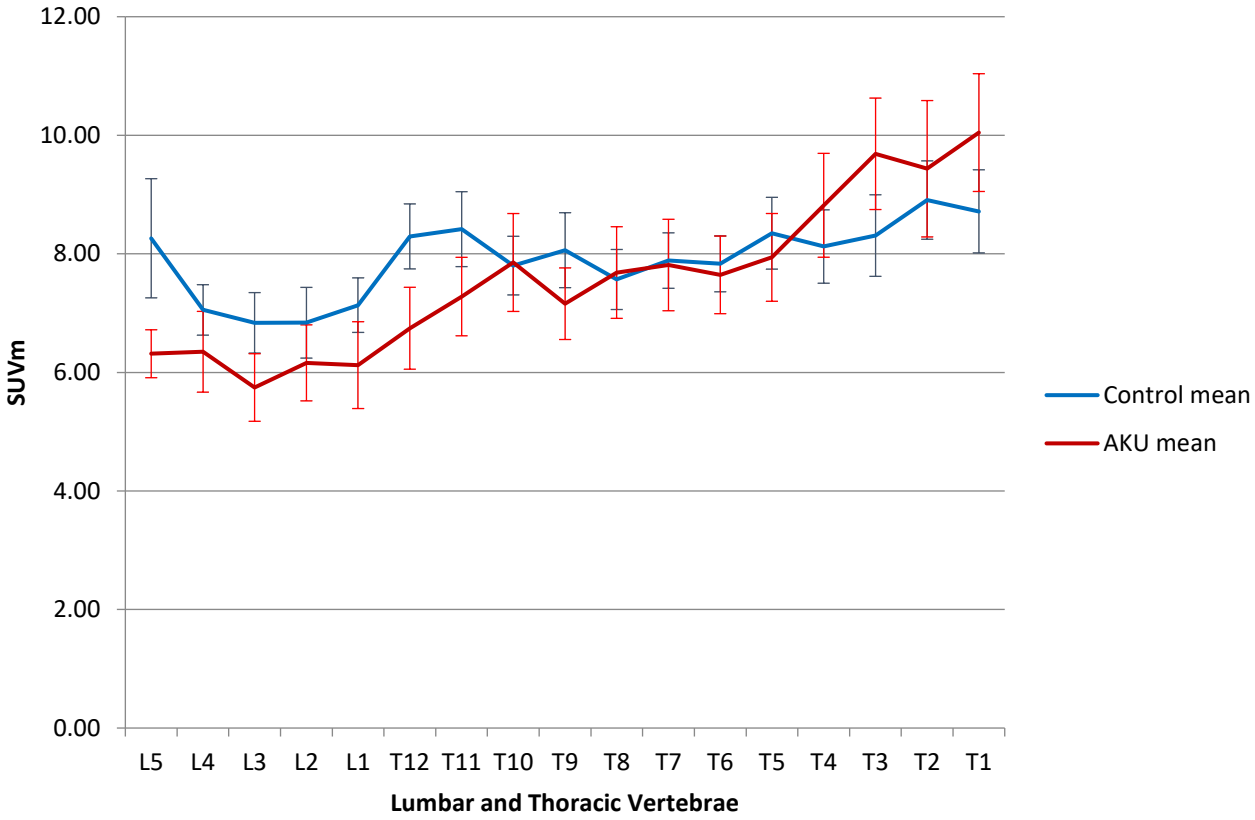

Figure 4.7 SUVm of mean lumbar and thoracic vertebrae in the AKU and control groups. SUVms obtained from the centre of the five lumbar (L1-L5) and the twelve thoracic (T1-T12) vertebrae. Independent sample t-tests and Wilcoxon-Mann-Whitney tests did not find any statistically significant differences between the SUVms of the control and AKU vertebrae across all levels ($p>0.05$). Ten female control patients (mean age of 62, SD±13.8, range 43-84). Ten female AKU patients (mean age of 60, SD±6.47, range 52-72).

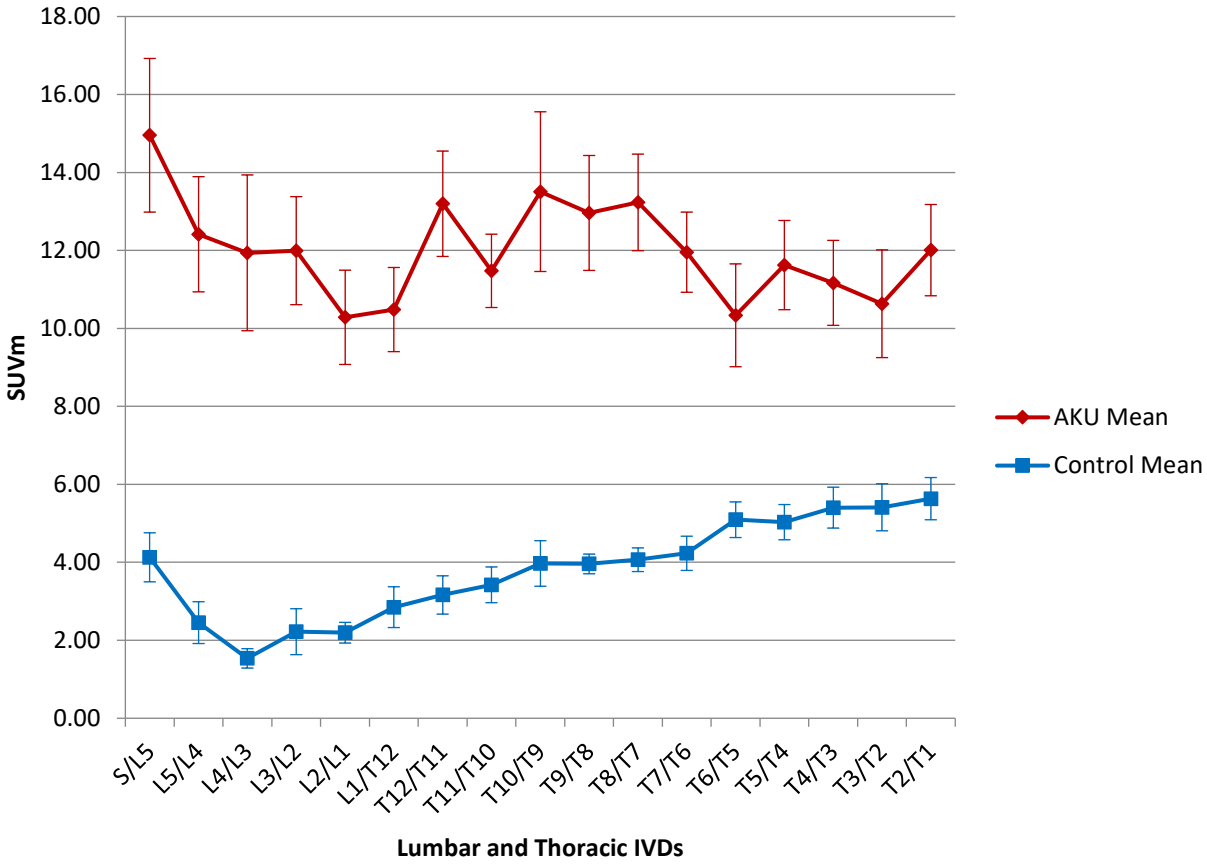

Figure 4.8 SUVm of mean lumbar and thoracic intervertebral discs in the AKU and control groups. SUVms obtained from the centre of the five lumbar (L1-L5) and the twelve thoracic (T1-T12) intervertebral discs. Independent t-test and Wilcoxon-Mann-Whitney tests identified statistically significant differences between the SUVms of the control and AKU IVDs at all levels ($p<0.01$). Ten female control patients (mean age of 62, SD±13.8, range 43-84). Ten female AKU patients (mean age of 60, SD±6.47, range 52-72).

4.2.3 DISCUSSION OF FEASIBILITY STUDY

This feasibility study was undertaken to evaluate the practicality and viability of obtaining accurate SUVms in the bone and cartilage of the hip (acetabulum, AC and head of femur), shoulder (glenoid fossa, AC and head of humerus) and the spine (thoracic and lumbar vertebrae and IVDs).

In terms of the methodology, obtaining the SUVms from the spine did not prove difficult. The IVDs were large enough in the thoracic and lumbar regions (IVD height approximately 7-10 mm) to ensure that the ROI was placed within the cartilaginous disc. The cervical region was excluded from the analysis for this reason, as the IVDs were too thin (less than 3-5mm), meaning that the SUVm did not reflect cartilage uptake alone**.** Statistically significant results were obtained when analysing the spine which provides confidence in the methodology (Figures 4.7 and 4.8). Figure 4.7 suggests that generalised rates of bone turnover within the thoracic and lumbar spine of the control and AKU groups are similar with no significant differences found (mean SUVm of AKU vertebrae = 7.6, and mean SUVm of control vertebrae = 7.9). This corresponds to the SUVs reported by Win *et al*. (116) who reported lumbar and thoracic SUVs in 11 normal vertebrae (SUV of 7.3) and Puri *et al*. (134) who reported SUVs of the lumbar spine in 12 healthy postmenopausal women (mean SUVm of 6). This therefore provides further evidence that this methodology is reliable and the results are in line with other published studies.

Figure 4.8 demonstrates the SUVms in the IVDs of the AKU and control groups, statistically significant differences were found at each level. The AKU group had much higher SUVms reflecting increased tracer uptake in the cartilage which has not been

previously identified in AKU. It is thought that this is the first time SUVms have been explored in cartilaginous IVDs. It is proposed that this is demonstrating calcification of the IVDs in AKU.

Obtaining the SUVms from the hip and shoulder proved more difficult. There was no problem obtaining SUVms from the bony acetabulum, glenoid fossa, head of femur and head of humerus when the triangulation point was placed at the center of the joint, as these structures were large and thick enough for the ROI (0.5cm diameter, 0.196cm^2) (Figures 2.9 and 2.10). However, the AC proved difficult to ensure the ROI was placed in cartilage alone without any bony tissue as normal AC diameter ranges from 0.2-0.5cm. AKU results in destruction of articular cartilage, therefore many patients had very thin AC in both the hip and shoulder joints. The smallest ROI available was 0.5cm and therefore in some patients with arthropathy it was difficult to ensure cartilage alone was measured. Additionally, the curvature of the joint influenced the reliability of placing the ROI within the cartilage, due to slices containing part cartilage and part bone. It is thought that these issues are reflected in the results (Figure 4.1, 4.2, 4.4 and 4.5) excluding patient 60B in the AKU group, and it is likely that the results of the AC reflected some bony uptake. After looking at the patient noted patient 60B had active arthropathy in both hips and shoulders.

After completing this feasibility study, we discovered issues with obtaining accurate SUVms within the AC of the hip and shoulder due to the nature of the very thin AC. Some very promising results were identified when analysing the SUVms of the IVDs between AKU and control groups. The AKU IVDs were found to have increased uptake of ^{18}F, thought to be the first time this phenomenon has been identified in AKU. As

this thesis is interested in looking at the differences in uptake of ^{18}F-NaF in both bone and cartilage the decision was made to exclude the shoulder and hip from any further analysis and to only study spinal arthropathy in a larger group of patients.

4.3 DESIGN OF STUDY

4.3.1 PATIENT GROUP

41 adult patients (16 females, 25 males, mean age 51, SD±10.9, range 30-68) from the SONIA 2 clinical trial (see section 2.2.2) underwent ^{18}F-NaF PET/CT imaging at baseline (V1), and again one year later (V3). V1 was carried out in 2014/15 pre-treatment and V3 one year later post-treatment (V2 was a safety visit at 3 months). One group receives 10mg of nitisinone, one group receives no treatment - the treatment and non-treatment groups are blinded until the end of the clinical trial in 2019 (see section 1.3.2 for more information). Ten non-metastatic breast cancer 'control' patients were used as a comparison (see section 2.2.3). These patients had undergone ^{18}F-NaF PET/CT to determine bony metastasis, of which all patients were reported as negative for any cancerous involvement.

4.3.2 MEASURING THE SUVms

Hermes Hybrid Viewer (see section 2.5.1) was used to measure the SUVms (section 2.5.2). Based on the results of the feasibility study, the SUVs obtained from all lumbar and thoracic vertebrae were not statistically different. It was therefore decided that the upper most, lower most and middle vertebrae and IVDs were analysed for the main study. The SUVm was obtained from the centre of three lumbar (L5, L3, L1) and

three thoracic (T1, T6, T12) vertebral bodies, and from the centre of the corresponding IVDs below (L5-S1, L3/L4, L1/L2, T12/L1, T6/T7, T1/T2). For the AKU group the SUVms were taken at baseline (V1) and again one year later (V3). For the control patients SUVms were measured for the single diagnostic scan, no follow up scans were available.

4.4 RESULTS

4.4.1 VERTEBRAE AND IVD SUVms

The SUVm was obtained from the lumbar and thoracic vertebrae (L5,L3,L1,T12,T6,T1) and IVDs (L5-S1, L3-L4, L1-L2, T12-L1, T6-T7, T1-T2) from both AKU and control subjects. Figure 4.9 demonstrates the mean SUVm across all AKU and control patients in the lumbar and thoracic vertebrae and IVDs (data is shown for both V1 and V3 for the AKU group). Statistically there was no significant difference across all vertebral levels ($p>0.05$) between the SUVm of the AKU vertebrae (mean SUVm =7.4) and control vertebrae (mean SUVm=7.58). In marked contrast, the AKU group has much higher SUVms in the IVDs compared to the control (mean = 11.6 and 3.81 respectively) (Figure 4.9). Independent t-test identified a statistically significant difference ($p<0.01$) between the AKU and control IVDs at every IVD level measured.

Paired t-tests were carried out to identify any changes between V1 and V3. Statistically there was no significant difference between V1 and V3 in the AKU group for both vertebrae ($p>0.05$) and IVDs ($p>0.05$) suggesting there has been no significant change in the SUVms over one year. It is clear when looking at AKU

vertebrae and IVDs that the vertebrae have consistently lower SUVms (mean SUVm = 7.58) than the IVDs (mean SUVm = 11.16), which was statistically significant at every level ($p<0.01$). When comparing the SUVms for the vertebrae and IVD in the control group, the opposite is seen. The SUV of the vertebrae (mean SUVm = 7.4) is consistently higher than the SUV of the IVDs (mean SUVm = 3.81). The control mean IVD SUVm was much lower in the control group (3.81) compared to what was found in the AKU group (11.16). This suggests that newly deposited mineral is being laid down in the IVDs in AKU due to calcification of the cartilage.

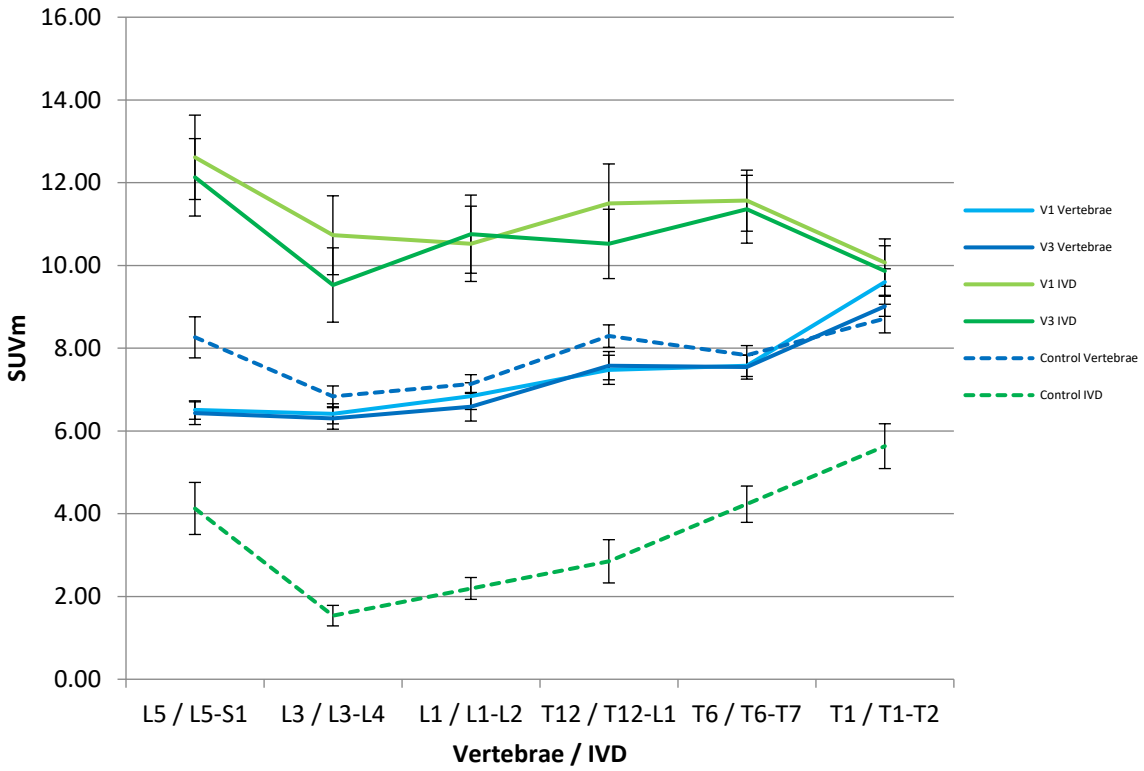

Figure 4.9 SUVm of mean lumbar and thoracic vertebrae and IVDs across all AKU and control patients. V1 = baseline visit, V3 = 1 year after V1. Vertebrae measured (L5, L3, L1, T12, T6, T1), IVDs measured (L5-S1, L3-L4, L1-L2, T12-L1, T6-T7, T1-T2). Independent t-tests and Wilcoxon-Mann-Whitney tests revealed statistically significant differences between AKU and control IVDs at every level ($p<0.01$). Paired t-tests revealed no significant differences between V1 and V3 in both the vertebrae and IVDs ($p>0.05$). n=41 AKU patients (16 females, 25 males, mean age 51, SD±10.9, range 30-68). V1 n=41, v3 n= 33. n=10 female control patients (mean age of 62, SD±13.8, range 43-84).

4.4.2 SUVm WITH AGE

The mean lumbar vertebrae (L5, L3, L1) SUVm was plotted for both visits (V1 and V3) against age for AKU and control groups (Figure 4.10). There is an obvious trend demonstrating a clear reduction in SUVm with age in both AKU and control groups. Generally, the youngest patients have the highest SUVms and the oldest have the lowest.

Paired t-tests revealed no significant difference ($p>0.05$) between the lumbar vertebrae SUVms for V1 and V3 in the AKU patients. The control mean lumbar vertebrae can be seen to have slightly increased SUVms compared to the AKU patients however independent t-tests revealed no significance between V1 and the control and V3 and the control ($p>0.05$).

The negative relationship with age was clear in both the AKU and control groups demonstrated by the regression lines. Multiple variate linear regression was applied to analyse the trend between the mean lumbar vertebrae SUVm with age in both AKU and control groups. Interestingly, age was found to be statistically significant to the mean lumbar vertebrae SUVm ($p<0.01$). Age affects mean lumbar vertebrae SUVm outcome negatively. For every year increase in age the SUVm decreases by 0.100 in both AKU and control groups.

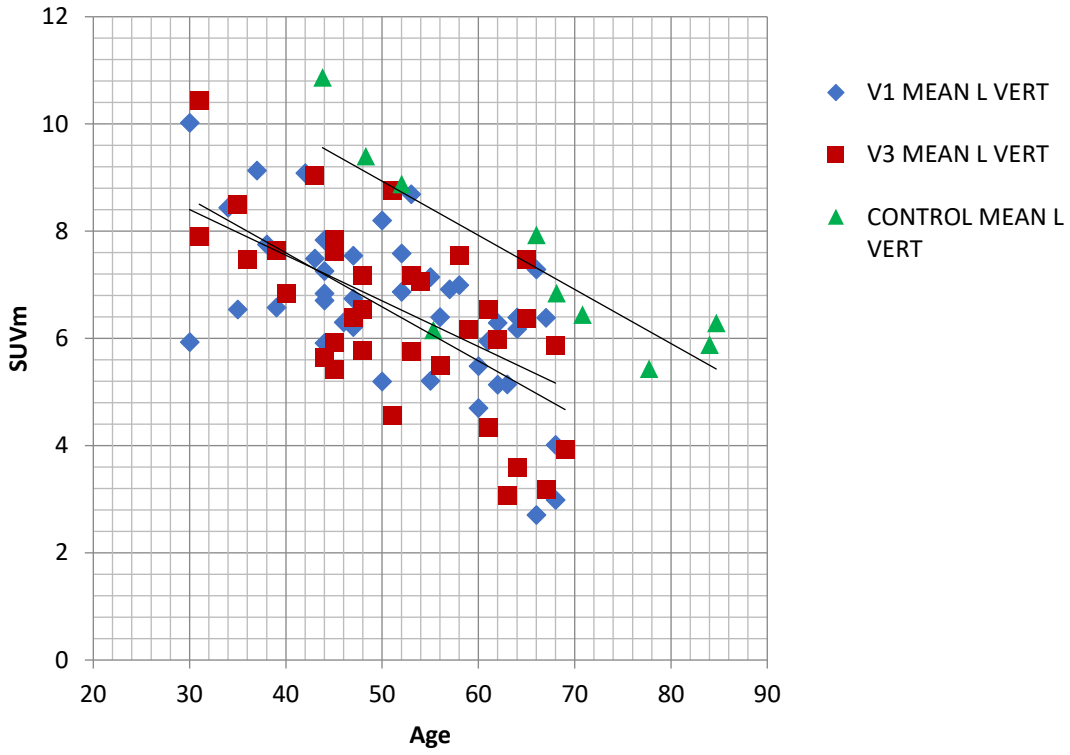

Figure 4.10 SUVm of mean lumbar vertebrae with age in individual AKU and control patients. V1 – baseline, V3 -1 year after V1. MEAN L VERT (SUV mean of mean lumbar vertebrae (of L5, L3, L1)). Paired t-tests revealed no significant differences between V1 and V3 mean lumbar vertebrae SUVm. Independent t-tests also revealed no statistically significant differences between the SUVms of AKU (V1 and V3) and the control group (control vs V1 $p>0.05$, control vs V3 $p>0.05$). Multiple linear regression analysis identified a significant difference ($p<0.01$) between age and mean lumbar SUVm in both control and AKU groups. n=41 AKU patients (16 females, 25 males, mean age 51, SD±10.9, range 30-68). V1 n=41, V3 n= 33. n=10 female control patients (mean age of 62, SD±13.8, range 43-84).

The mean thoracic vertebrae (T12, T6, T1) SUVm was plotted for V1 and V3 against age, the control group was added for comparison (Figure 4.11). A gradual reduction in SUVm can be seen with age in both AKU and control groups as seen in Figure 4.10. Paired t-tests revealed no significant difference ($p>0.05$) between the SUVms at V1 and V3. Independent t-tests also revealed no significant differences between the AKU group at visit 1 and 3 with the control ($p>0.05$).

Multiple variate linear regression analysis was conducted to analyse the trend in mean thoracic vertebrae SUVm with age in both AKU and control groups. As reported in the previous graph (Figure 4.10) age was found to be statistically significant to the mean thoracic vertebrae SUVm ($p<0.05$). Age has a negative effect on mean thoracic vertebrae SUVm, for every year increase in age the mean thoracic vertebrae SUVm reduces by 0.067 in both AKU and control groups.

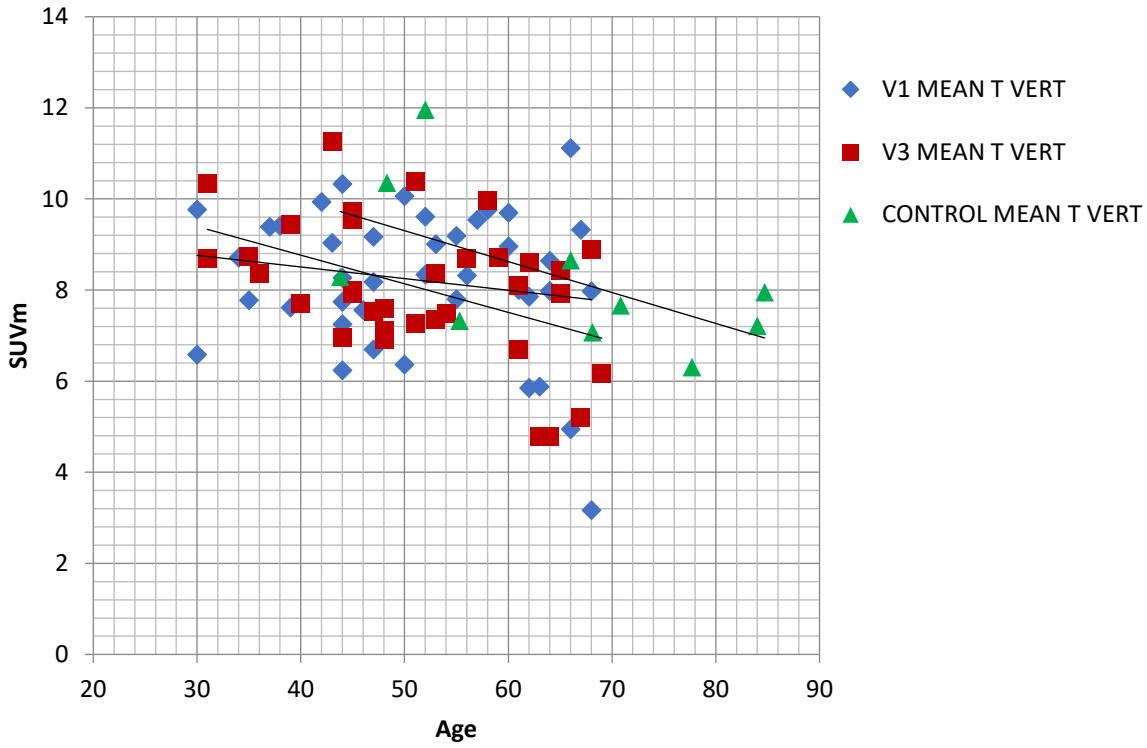

Figure 4.11 SUVm of mean thoracic vertebrae with age in individual AKU and control patients. V1 – baseline, V3 - 1 year after V1. MEAN T VERT (SUV mean of mean thoracic vertebrae (of T12, T6, T1)). Paired t-tests revealed no significant difference between V1 and V3 ($p>0.05$). Independent t-tests also revealed no significant differences between the SUVm of V1 and V3 with the control ($p>0.05$, $p>0.05$ respectively). Multiple linear regression analysis identified a significant difference ($p<0.05$) between age and mean thoracic SUVm in both control and AKU groups. n=41 AKU patients (16 females, 25 males, mean age 51, SD±10.9, range 30-68). V1 n=41, V3 n= 33. n=10 female control patients (mean age of 62, SD±13.8, range 43-84).

Figure 4.12 demonstrates the mean lumbar IVD SUVm with age in AKU and control groups. Paired t-tests revealed no significant difference between V1 and V3 in the AKU group ($p>0.05$). The SUVms of the control patients are consistently lower (SUVm = 2.5) compared to the AKU group (V1 SUVm = 11, V3 SUVm = 10). Independent t-tests revealed statistically significant differences between both V1 and V3 mean lumbar IVD with the control mean lumbar IVDs ($p<0.01$).

In the control group no trend was identified with age. In contrast, the trendline for the AKU group at both V1 and V3 shows a gradual increase in SUVm with age followed by a decline in the later years. The youngest AKU patients have the lowest SUVms (SUVm = below 5) that are in line with the SUVms of the control group. However, from the age of approximately 40 the SUVm can be seen to increase reaching a maximum SUV of 20 around the age of 50/55 years. From here, a general reduction in SUVm can be seen where the oldest patients (between 60 and 70) have a reduction in SUVms decreasing to values similar to that of the controls.

Multivariate linear regression found a significant difference between the AKU and control groups with age ($p<0.01$). In the AKU group the mean lumbar IVD SUVm increases by 0.238 every year, compared to no change in the control group. However, looking at the graph this trend in the AKU group does appear to stop around the age of 50/55.

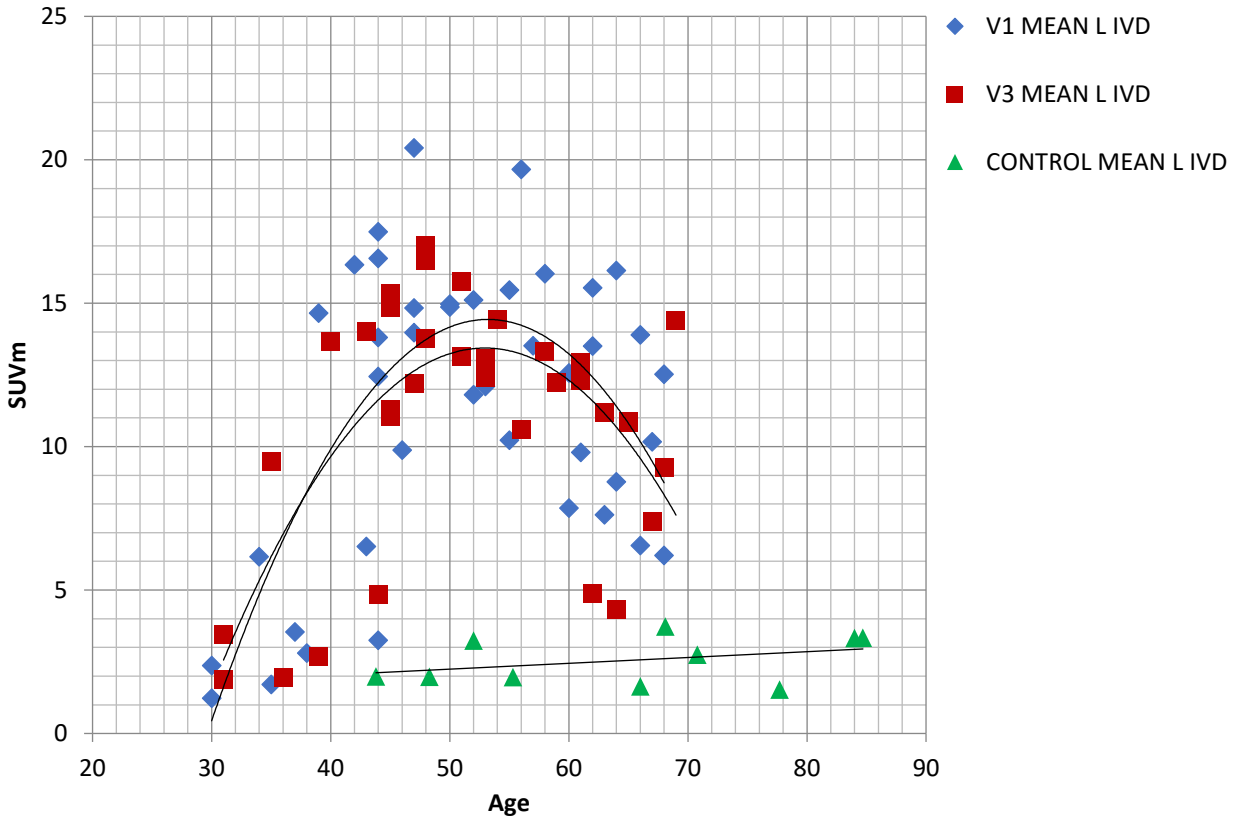

Figure 4.12 SUVm of mean lumbar IVDs with age in individual AKU and control patients. V1 – baseline, V3 - 1 year after V1. MEAN L IVD – SUV mean of mean lumbar IVD (L5/S1, T3/T4, L1/L2). Polynomial function was fitted to the AKU data (order 2 polynomial line used when the data has one hill), with R^2 values of V1 (R^2= 0.458) V2 (R^2= 0.435). Linear regression line for the control had a R^2 value of 0.133. Paired t-tests revealed no significant difference between V1 and V3 in the AKU group ($p>0.05$). Independent t-tests revealed statistically significant results between both V1 and V3 mean lumbar IVD SUVm with the control mean lumbar IVDs SUVm ($p<0.01$). Multivariate linear regression found a significant difference between the groups (AKU vs control) with age ($p<0.01$). n=41 AKU patients (16 females, 25 males, mean age 51, SD±10.9, range 30-68). V1 n=41, V3 n= 33. n=10 female control patients (mean age of 62, SD±13.8, range 43-84).

The same trend can be seen when looking at the SUVm of the mean thoracic IVDs in AKU and control groups (Figure 4.13). The youngest AKU patients have similar SUVms to the controls (control mean SUVm = 4). From the age of around 40 the SUVm of the AKU patients increases reaching a maximum of 18 around the age of 50-55 years. The oldest AKU patients (over the age of 60) have lower SUVms reducing towards the values of the controls as seen in Figure 4.12. There is a slight decrease in SUVm with age in the thoracic vertebrae of the control group.

No significant difference was found between the SUVms of V1 and V3 (paired t-test, $p>0.05$). Independent t-tests revealed significant differences between the mean thoracic IVD SUVm in the AKU groups (V1 and V3) compared to the control mean thoracic IVD SUVm ($p<0.01$).

Multivariate linear regression found a significant difference between the AKU and control groups with age ($p<0.01$). In the AKU group the mean thoracic IVD SUVm increases by 0.293 every year, compared to little change in the control group. However, looking at the graph this trend does appear to stop around the age of 50/55 consistent to what was described in Figure 4.12.

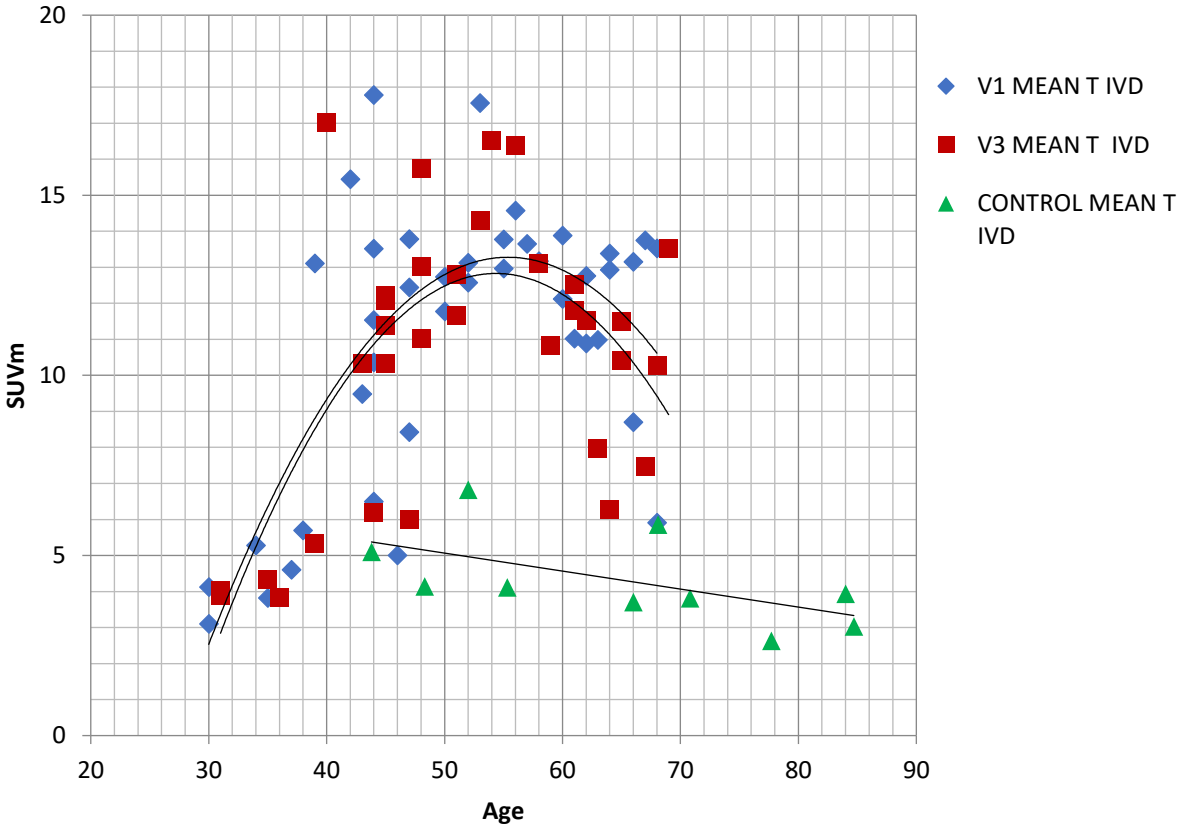

Figure 4.13 SUVm of mean thoracic IVDs with age in individual AKU and control patients. V1 (visit 1 – baseline) V3 (visit 3 - 1 year after V1). MEAN T IVD – SUV mean of mean thoracic IVD (T12/L1, T6/T7, T1/T2). Polynomial (order 2) regression lines = V1 (R^2= 0.497) V2 (R^2= 0.458). Linear regression line - control (R^2= 0.331). Paired t-tests revealed no significant difference between V1 and V3 mean thoracic IVD SUVm. Independent t-tests revealed statistically significant results between both V1 and V3 mean thoracic IVD SUVm with the control mean lumbar IVD SUVm ($p<0.01$). Multivariate linear regression found a significant difference between the groups (AKU and control) with age ($p<0.01$). n=41 AKU patients (16 females, 25 males, mean age 51, SD±10.9, range 30-68). V1 n=41, V3 n= 33. n=10 female control patients (mean age of 62, SD±13.8, range 43-84).

4.4.3 GENDER AND SUV

Figure 4.14 demonstrates the SUVm across the lumbar and thoracic vertebrae and IVDs in males and females. The SUVms across the lumbar and thoracic vertebrae are very similar in males and females. Independent t-test identified no significant difference between the vertebrae SUVms of the males and females at all vertebral levels (mean $p>0.05$). The SUVms across the lumbar and thoracic IVDs can be seen to be consistently higher compared to the vertebrae. The male group can be seen to have higher SUVms consistently across the lumbar and thoracic IVDs compared to the female group. However, independent t-tests found no statistically significant differences across all levels (mean $p>0.05$).

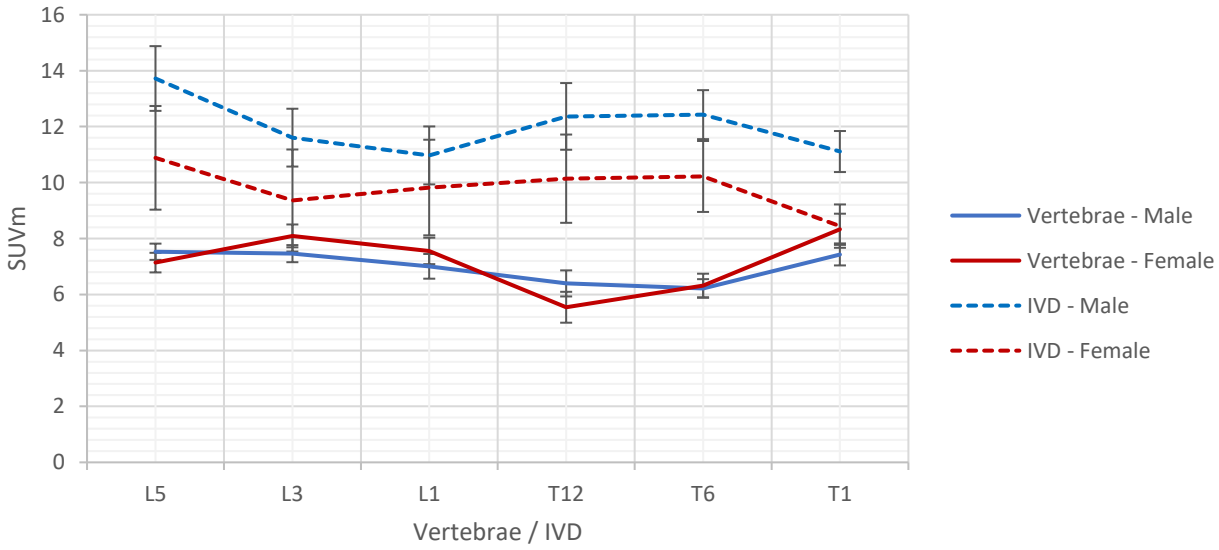

Figure 4.14 SUVm of mean lumbar and thoracic vertebrae and IVDs in males and females. Independent sample t-tests revealed no statistically significant differences between the vertebrae ($p>0.05$) and IVDs ($p>0.05$) at every level of males and females. n=41 AKU patients (16 females, 25 males, mean age 51, SD±10.9, range 30-68).

4.4.4 INDIVIDUAL CHANGE IN SUV OVER ONE YEAR

The AKU patients were separated into four age-dependent groups to look at the individual change in SUVm over one year in the vertebrae and IVDs. Figure 4.15 demonstrates the individual patient changes in the mean lumbar vertebrae SUVm at V1 and V3 in four age groups (30-39, 40-49, 50-59, 60-70). The red lines demonstrate a reduction in SUVm over one year, the blue lines demonstrate an increase in SUVm and green lines represent no change in SUVm. It is evident in graph A that the youngest patients have little change in SUVm over one year, with the other three age groups (Figure 4.15 B, C and D) having more of a change demonstrated by the steeper lines. In the 40-49-year-old age group there appears to be more of a reduction in SUVm over the one-year period, however, in the oldest two age groups patients can be seen to have either a reduction or increase in SUVm at equal rates. It is clear that the youngest age group has the highest SUVms and the oldest age group has the lowest SUVms supporting the age-related trend shown in Figure 4.10.

Figure 4.16 demonstrates the individual patient changes in the mean thoracic vertebrae SUVm at V1 and V3 in four age groups. It is clear in the youngest patients (Figure 4.16 A) that there is little change if any in SUVms across the two visits equivalent to what was found in the lumbar vertebrae (Figure 4.15 A). In the next age group (Figure 4.16 B) the results are more variable with some patients having an increase some having a decrease and some having no change in SUVm. The oldest two age groups (Figures 4.16 C and D) have more patients with a reduction in SUVm over one year. Comparable to what was seen in the lumbar vertebrae the youngest age group has the highest SUVms and the oldest age group has the lowest SUVms

supporting what was found in Figure 4.11 that demonstrates a reduction in SUVm with age.

The same analysis was carried out on the lumbar and thoracic IVDs. Figure 4.17 demonstrates the individual mean lumbar IVDs at V1 and V3 in the four age groups. In terms of the change in SUVm over one year, the youngest age group has mostly little change, with the oldest three age groups having more of a change over one year like we have seen in the lumbar and thoracic vertebrae. The oldest age group has the biggest changes in SUVms over the one-year period. The 40-49 age group (Figure 4.17 B) has more patients having a reduction in SUVm over one year. The next age group (Figure 4.17 C), the majority of patients appear to have a slight increase in SUVm across the visits. The oldest age group (Figure 4.17 D) has patients increasing and decreasing equally. Looking at the SUVms the youngest age group has the lowest values; the 40-49 group reaches the highest SUVms and the oldest age group can be seen reducing back to lower values. This supports the trend that was seen in Figure 4.12, that demonstrates the youngest patients have the lowest SUVms followed by an exponential increase in SUVm up to around the age of 45-50 followed by a plateau at around the age group 50-60 then followed by a steady decline in the oldest patients.

A very similar trend can be seen in Figure 4.18 that demonstrates the mean thoracic IVDs SUVm at V1 and V3 in four age groups. Again, little change is seen in the youngest age group (Figure 4.18 A), with more of a change seen in the other three age groups. The patents in the oldest age group (Figure 4.18 D) mostly have a reduction in SUVm over the one-year period. In terms of SUVms the youngest

patients have the lowest SUVms, the age group 50-59 have the highest SUVms and the oldest age group can be seen having lower SUVms. This confirms the findings in Figure 4.13 that demonstrates the youngest patients have the lowest SUVms followed by an exponential increase up to around the age of 50, followed by a plateau up to around the age of 60, followed by a steady decline in the oldest patients.

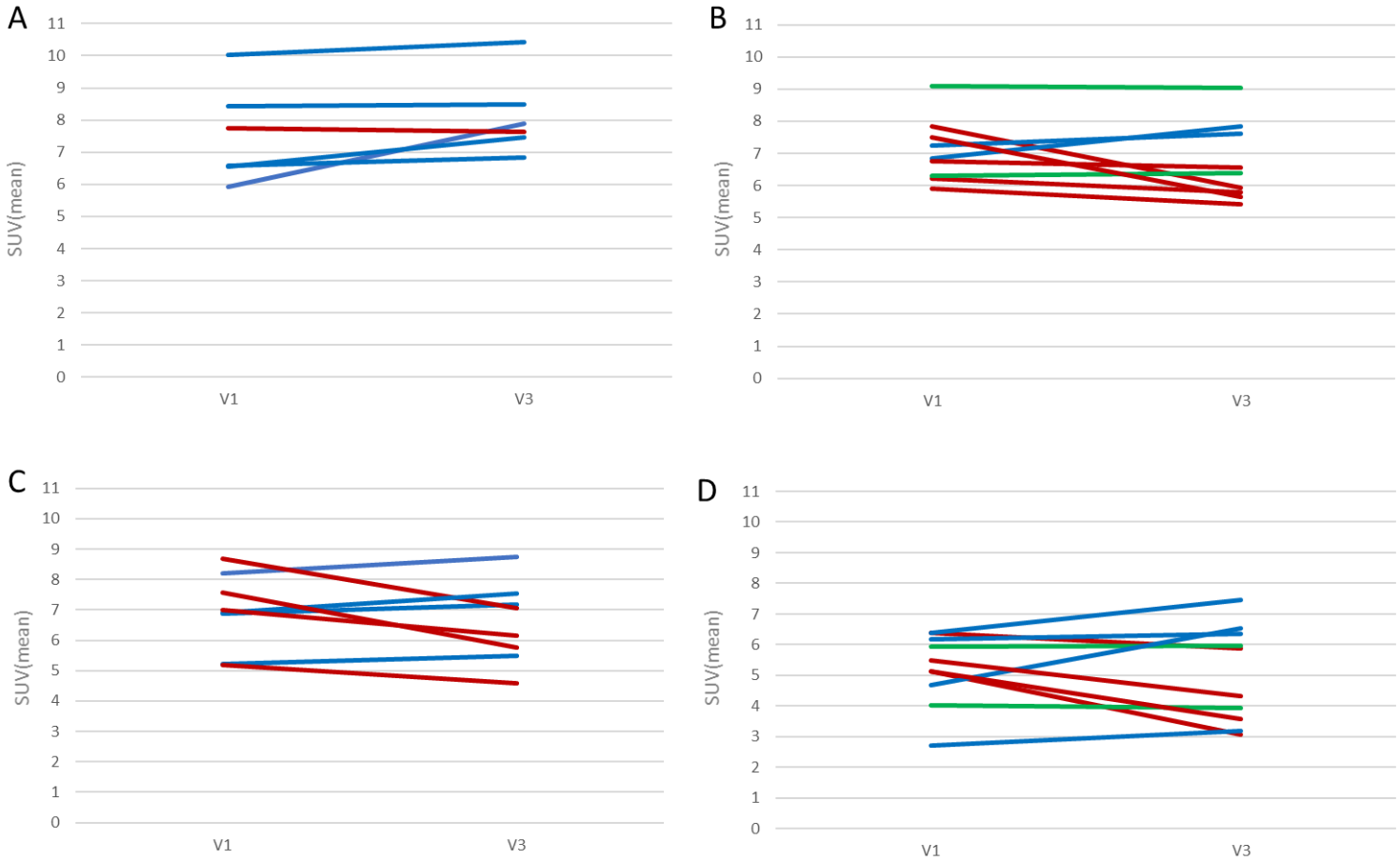

Figure 4.15 Individual patient mean lumbar vertebrae SUVm at V1 and V3 in four age groups. A - 30-39 years (n=6), B - 40-49 years (n=9), C - 50-59 years (n=8) D- 60-70 (n=10). Red = decrease in SUV across V1 and V3, Blue = increase in SUV, Green = no change in SUV.

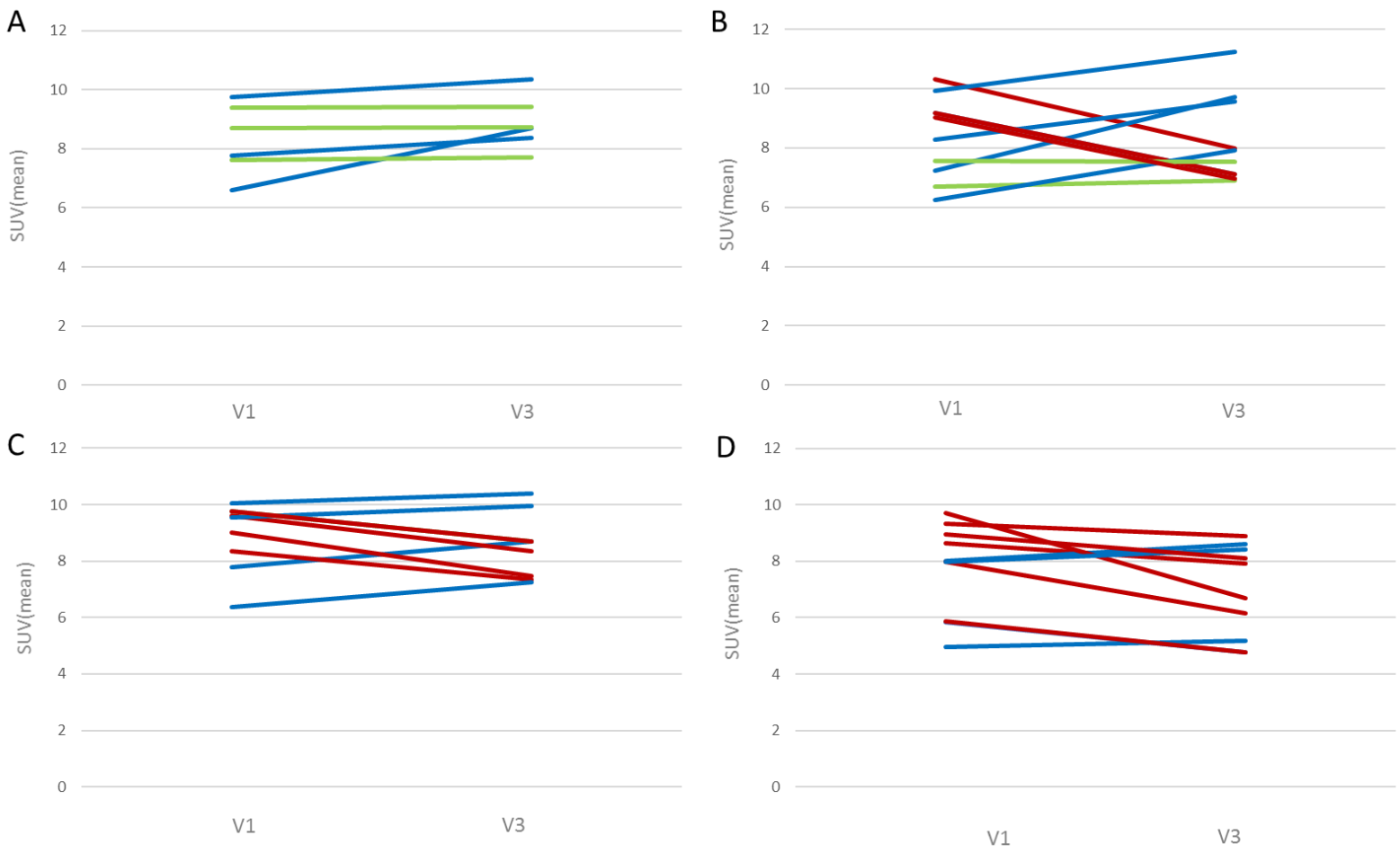

Figure 4.16 Individual patient mean thoracic vertebrae SUVm at V1 and V3 in four age groups. A - 30-39 years (n=6), B - 40-49 years (n=9), C - 50-59 years (n=8) D- 60-70 (n=10). Red = decrease in SUV across V1 and V3, Blue = increase in SUV, Green = no change in SUV.

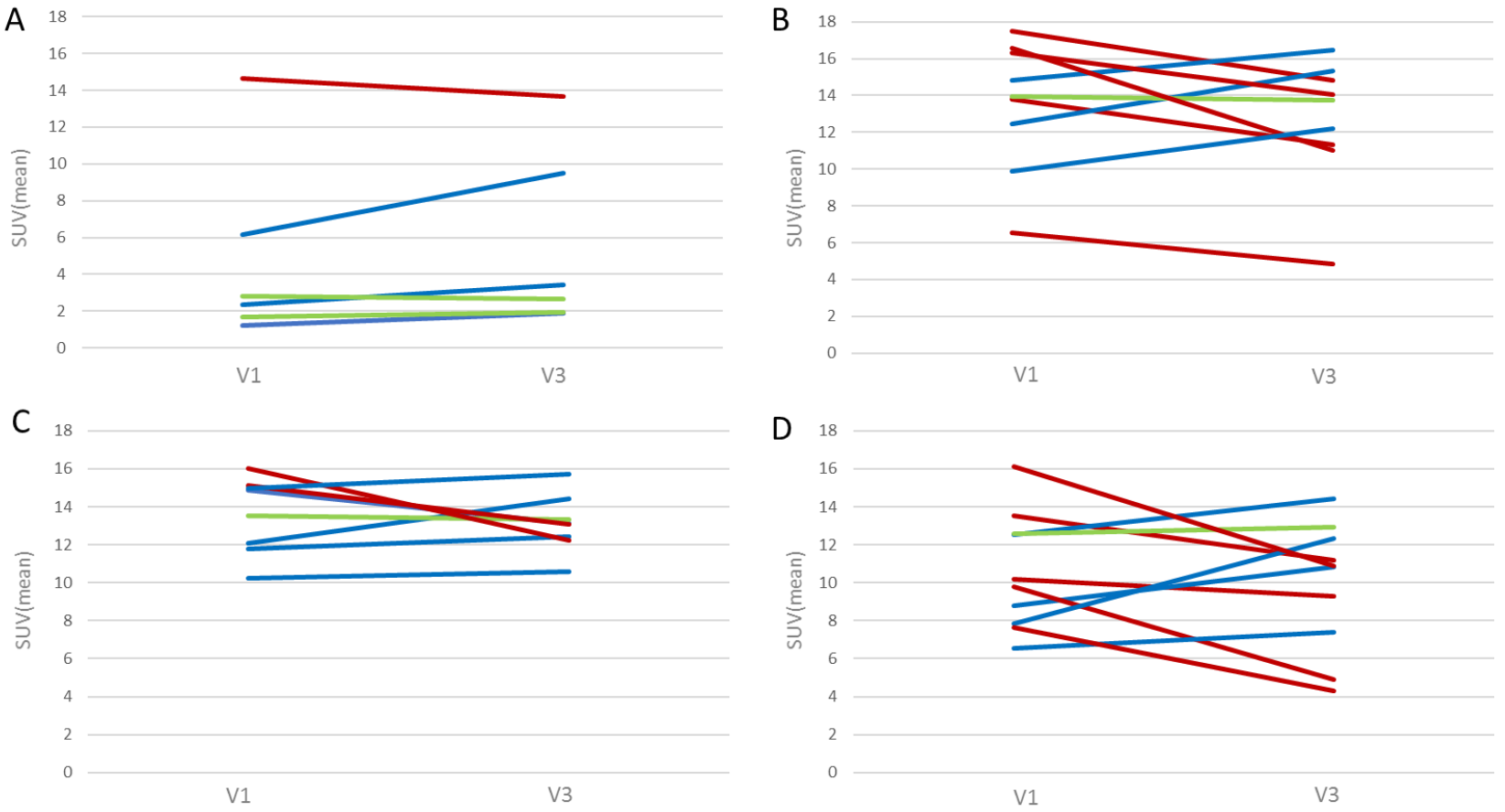

Figure 4.17 Individual patient mean lumbar IVD SUVm at V1 and V3 in four age groups. A - 30-39 years (n=6), B - 40-49 years (n=9), C - 50-59 years (n=8) D- 60-70 (10). Red = decrease in SUV across V1 and V3, Blue = increase in SUV, Green = no change in SUV.

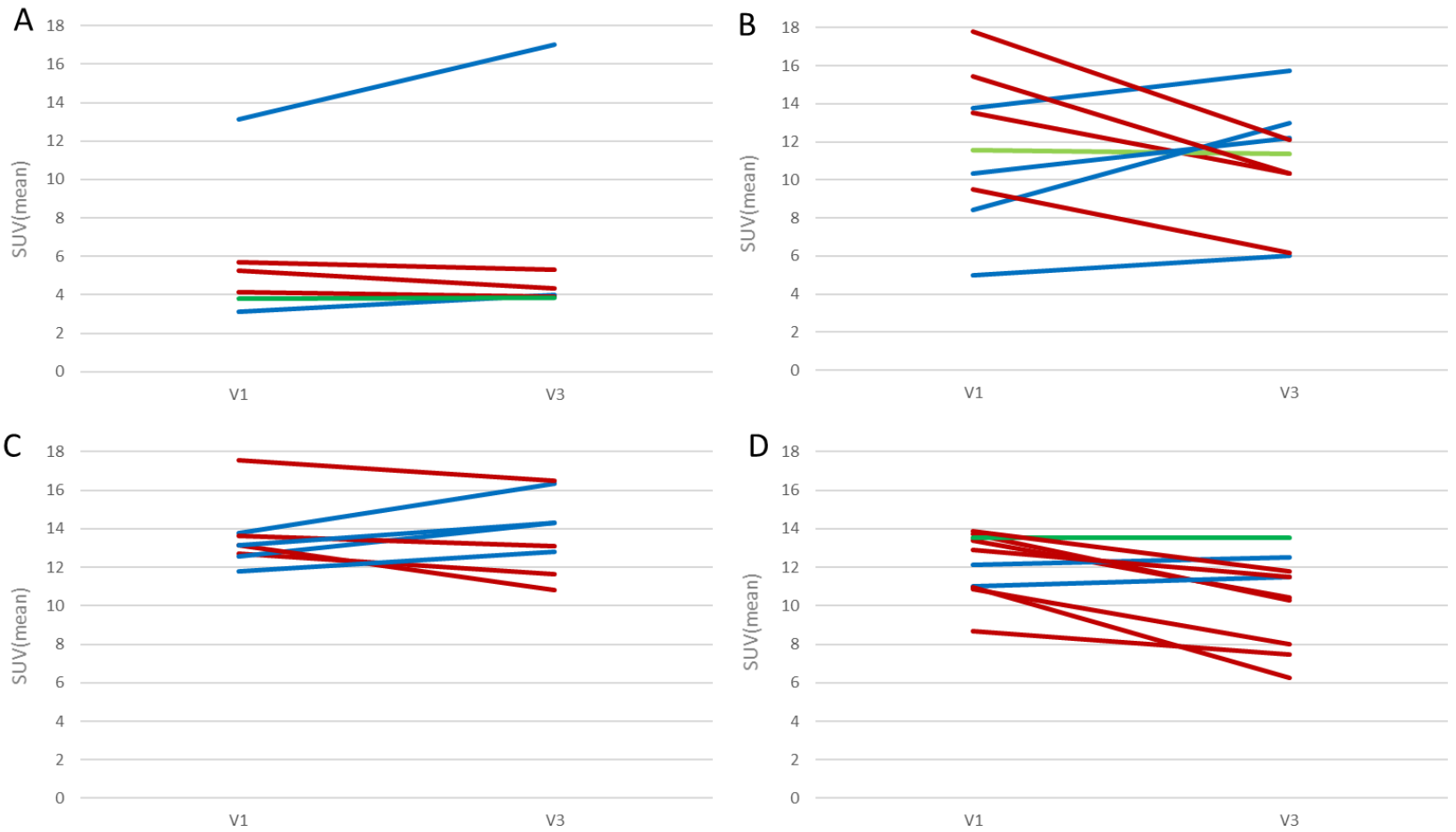

Figure 4.18 Individual patient mean thoracic IVD SUVm at V1 and V3 in four age groups. A - 30-39 years (n=6), B - 40-49 years (n=9), C - 50-59 years (n=8) D- 60-70 (n=10). Red = decrease in SUV across V1 and V3, Blue = increase in SUV, Green = no change in SUV.

4.5 DISCUSSION

In this chapter, the nuclear medicine imaging technique ^{18}F-NaF PET has been utilised to measure ^{18}F uptake in the thoracic and lumbar vertebrae and IVDs in AKU and control patients. The aim was to determine if there was a difference in bone metabolism, and/or cartilage composition/structure in AKU patients compared to control patients. ^{18}F-NaF was utilised because of its superior skeletal kinetics compared to other radioisotopes such as Tc-99m including faster blood clearance and two-fold higher bone uptake providing superior bone-to-background ratio. Additionally, the PET scanner provides better spatial resolution, greater sensitivity and superior image quality (110) (Table 1.6). Furthermore, and of more significance to this chapter PET imaging allows quantitative measurements of ^{18}F-NaF uptake that cannot be generated from other imaging modalities.

The pharmacokinetics of ^{18}F-NaF uptake essentially depends on the rates of bone uptake and elimination from the circulation via renal excretion. ^{18}F-NaF is absorbed into the hydroxyapatite crystal of bone where substitution of $^{18}F^-$ for OH^- groups covalently binds to hydroxyapatite ($Ca_{10}(PO_4)_6OH_2$) to form fluorapatite compounds ($Ca_{10}(PO_4)_6F_2$) (111). Uptake generally is higher in new bone (osteoid) due to the higher availability of binding sites (109). The rate of ^{18}F uptake into bone therefore reflects the amount of actively mineralising bone present and closely resembles bone metabolism. Radiotracer delivery and localisation to bone depends on regional blood flow and the extraction rate of bone. Changes in radiotracer kinetics therefore relate to osteoblastic activity and or bone vascularity (110). Increased vascularity and bone turnover are both seen in osseous and metabolic diseases. Areas of increased

localisation of tracer uptake reflect increased bone metabolism at that site, although physiologic uptake of ^{18}F in the skeleton is generally uniform in adults (113).

Quantitative measurements in PET imaging are used as a tool to supplement visual interpretation providing a method that is less user-dependent and that can be used for comparison between patients. The mean standardised uptake value (SUVm) is a common method of expressing the uptake of PET tracers. The SUVm is a measure of radioactivity in a region of interest, normalised against injected activity and the subject's body weight (Figure 1.13). If all injected ^{18}F is retained and uniformly distributed the SUV should be 1g/ml; larger SUVms represent proportionally higher uptake of ^{18}F at that specific site. This chapter investigates the SUVm of the lumbar and thoracic vertebrae and IVDs in AKU and control patients.

4.5.1 Discussion of feasibility study and SONIA 2 results

The feasibility study described at the start of this chapter identified and described the accuracy and robustness of the method of obtaining accurate SUVms representative of cartilage and bone in the spine. Figure 4.8 demonstrates the mean lumbar and thoracic IVD SUVm in the control and AKU groups. The SUVms were strikingly higher in the AKU group averaging SUVm of 12.01 across the IVDs compared to a mean SUVm of 3.8 in the control IVDs. Statistically significant differences were identified at each IVD level ($p<0.01$). In contrast, when analysing the vertebrae, the SUVms were similar to the control and the data points overlapped with no significant differences identified (Figure 4.7). This data was representative of ten AKU and ten control patients. The main study of this chapter was to repeat this analysis on a larger

cohort of AKU patients; 41 SONIA 2 patients were recruited and analysed. Five lumbar and twelve thoracic vertebrae and IVDs were measured in the feasibility study and the results across the vertebrae and IVDs were consistent (as seen in Figures 4.7 and 4.8). Therefore, only three lumbar and three thoracic vertebrae were measured in the main study (the lower-most, middle and upper-most vertebrae of that region). Figure 4.9 illustrates the results of the SONIA 2 data. The SUVms for the SONIA 2 IVDs were in line with the values identified in the feasibility study averaging SUVm of 11.6 compared to SUVm of 12.01 in the feasibility study. Again, independent t-tests revealed statistically significant differences ($p<0.01$) between AKU and control IVDs at every level. Additionally, the vertebrae SUVms also corresponded very accurately with the results of the feasibility study, with a mean SUVm of 7.4 in the SONIA 2 group and 7.6 in the feasibility study. These results demonstrate the robustness of the method and reliability of the results.

4.5.2 IVD SUVm

AKU patients with ochronotic arthropathy usually present with lower back pain resulting from disc degeneration as the initial joint manifestation of AKU. Symptoms worsen from the fourth decade leading to painful spinal disease often resulting in spinal stenosis (1). Therefore, it is not surprising that a significant difference between the SUVm of IVDs was identified in AKU patients compared to controls. The SUVms of the AKU IVDs are three times higher than that of the control (Figures 4.8 and 4.9). It is understood in AKU that IVDs become calcified as part of the disease pathophysiology. Calcification of IVDs is a consistent feature reported in many AKU

case reports along with disc space narrowing, loss of lumbar lordosis and in severe cases osteophytes (79,138–141). Jebaraj *et al*. (142) states that disc calcifications in spinal ochronosis usually occur as lamellar calcifications of the nucleus pulposus which begins in the lumbar disc and ascends the spine. They described the calcifications as calcium hydroxyapatite crystals or calcium pyrophosphate dihydrate crystals and suggested it was due to the biochemical alterations of the disease. IVD calcification or chondrocalcinosis occurs with age and the prevalence has been previously reported as 5-6% of the general adult population through conventional radiography. The prevalence in AKU has not been described but is considered a well-known radiological feature (143). Calcification in the discs likely accounts for the increased uptake of ^{18}F observed in AKU demonstrated by the increased SUVm. It is proposed that ^{18}F is binding to the calcium hydroxyapatite crystals / calcium pyrophosphate dihydrate crystals in the IVDs hence why fluoride uptake can be measured in these regions. The control patients have low uptake of ^{18}F in the discs due to IVDs being avascular and healthy IVDs not containing calcified deposits. Interestingly the SUVms of the IVDs were significantly higher than the vertebrae at every level in AKU patients suggesting that IVDs are more actively mineralising than bone. A possible reason for this is that ^{18}F binds preferentially to newly laid down hydroxyapatite in the IVDs due to the higher availability of binding sites due to active disease processes.

4.5.3 Vertebrae SUVm

^{18}F binds to hydroxyapatite in bone to form fluorapatite. The uptake of NaF into bone depends on the blood flow to the area, regional osteoblastic activity and renal clearance. The rapid uptake of ^{18}F occurs preferentially at high osteoblastic activity where bone remodelling is greatest. The spinal vertebrae are an ideal site for quantitative assessment of bone metabolism as the spine has a greater turnover of bone than other skeletal sites. This is due to factors such as the spine is subjected to mechanical stress which enhances interleukin 11 expression which stimulates osteoblast differentiation. This leads to increased bone turnover and increased osteoblastic activity which results in high ^{18}F uptake (117). Additionally, the vertebrae consist of mostly trabecular bone which is highly vascularised and is less dense compared to cortical bone, thus trabecular bone has higher SUVms compared to cortical bone.

The results of this study revealed that the SUVms of AKU vertebrae (SUV = 7.4) were very similar to control vertebrae (SUVm = 7.58) suggesting that generalised rates of bone turnover in AKU and control patients are very similar. This reflects that bone turnover in AKU is normal. It is believed that this is the first time SUVm measurements have been reported for AKU patients even though, there are several reports of SUVs of the spine in the normal skeleton. Win *et al*. (116) reported SUVs in the cervical, thoracic and lumbar vertebrae in 11 normal patients (excluding patients with abnormal renal function, history of cancer or metabolic bone disease). Interestingly, the SUVs for the vertebrae in this study were very similar to the results of this chapter. Win *et al*. (118) reported the mean SUV(max) of the thoracic and lumbar

vertebrae to be 7.31, which was very similar to the SUVm of the thoracic and lumbar vertebrae of the AKU and the control patients analysed in this study which had SUVms of 7.4 and 7.5 respectively. Puri *et al*. (134) also reported SUVs of the lumbar vertebrae in 12 post-menopausal women, they reported the mean SUV to be 6 corresponding to the results we have reported. These findings provide confidence in the method and quality of the results reported in this chapter.

In terms of the SUVms along the spine, the SUVms are slightly higher in the thoracic vertebrae compared to the lumbar vertebrae (Figures 4.7 and 4.9) and appear to slightly increase up the spine from L5-T1. This was also found by Kaneta *et al*. (144) who reported SUV measurements of normal thoracic and lumbar vertebrae using SPECT/CT Tc-99m. The SUVm gradually increased from the lower lumbar spine to the upper thoracic spine however this was not statistically significant. This finding is unexpected given that the lumbar vertebrae have the highest mechanical forces acting on them, and therefore increased bone turnover compared to areas of the spine with fewer forces acting upon them. It was expected that the lumbar vertebrae would have the highest SUVms. A possible reason for this could be the thoracic spine has increased axial forces acting upon it due to its flexibility. Additionally, in AKU the lumbar spine is known to be affected by osteoarthropathy to a higher extent than the thoracic spine. The end stage of spinal arthropathy results in spinal fusion. This could result in reduced SUVms due to low bone turnover at sites of bony fusion, due to less new mineralisation.

4.5.4 Vertebrae SUVm with age

This chapter describes a reduction in SUVm with age in the thoracic and lumbar vertebrae in both AKU and control groups (Figures 4.10 and 4.11). Essentially this means less mineral available for fluoride to bind and or decreased blood flow. This supports what was found in the previous chapter where a reduction in the percentage incidence of increased ^{18}F uptake with age was described in the lumbar vertebrae (Figure 3.3) as well as the thoracic vertebrae (Figure 3.4). This is consistent with the literature. Win *et al*. (116) found a negative trend in SUV(max) with age in the T5, T7, T12 and L2 vertebrae but without statistical significance. It is widely agreed that bone deteriorates in composition, structure and function with age. In the first three decades of life bone turnover is coupled very tightly maintaining a steady state between bone resorption and bone formation. Peak bone mass is reached around the age of 20 in women and older in men. After this bone turnover continues at a slower rate resulting in a steady reduction in bone mass (145).

The menopause in women greatly increases bone resorption due to low levels of oestrogen, accelerating bone loss. Daly *et al*. (146) conducted a ten-year population based observational study and reported that the annual percentage rate of loss in forearm BMD was 1.5 to 2.0-fold higher in females compared to males over the age of 60. Therefore, a reduction in BMD results in less hydroxyapatite for ^{18}F to bind, therefore resulting in a lower SUVms.

A reduction in red marrow is associated with ageing. Chen *et al*. (147) identified that the rate of vertebral bone marrow perfusion revealed a significant decrease in

subjects older than 50 years. Females were found to have a marked decrease in marrow perfusion compared to males over the age of 50. Reduced perfusion to bone due to reduced vascularity was proposed to result in a reduction of ^{18}F that is transported to that area resulting in lower SUVms and it was expected that females would have a reduction in SUVm for this reason. Figure 4.14 demonstrates the gender differences in SUVms in the vertebrae and IVDs. No statistical difference was identified between the vertebrae SUVms between males and females demonstrating no differences in uptake ^{18}F. A study by Aliberti *et al*. (148) assessed bone metabolism in ochronotic patients by evaluating bone turnover markers and bone mass. They described an imbalance in bone metabolism, leading to osteopenia or osteoporosis in ochronotic patients and hypothesised that HGA deposited into the bone matrix and osteocytes plays a pathophysiological role in accelerating bone loss. Figure 4.10 demonstrates the reduction in SUVm with age in the lumbar vertebrae. It can be seen that the AKU group have reduced SUVms compared to the control across all ages which could be due to reduction in BMD exacerbated by the disease process.

4.5.5 IVD SUVm with age

The AKU SUVms of the IVDs display an interesting trend (Figure 4.12 and 4.13); 'inverted U' curve on the graph, demonstrating the SUVm increasing from the youngest patients up to around the age of 50. At this point the curve plateaus up to around the age of 60 and then reduces again in the oldest patients. This trend is evident in both the lumbar and thoracic IVDs in both V1 and V3. The 30-40-year-old patients have low IVD SUVms in line with the control group. From the age of 40 a sharp increase is observed in SUVms, this age corresponds to the age of the onset of

arthritic pain, of which starts first in the spine. It is proposed that this increase in SUVm at this age could correspond to the deposition of hydroxyapatite / calcium pyrophosphate dihydrate crystals. By the age of 60-70 the IVDs may well be fused in some cases, or deposition is reduced reflecting the reduction in SUVm in the late stages of the disease. The previous chapter found low incidences throughout the IVDs and there was no trend with age. This was suggested to be due to the resolution of the ^{18}F MIP images, inhibiting accurate identification of the IVDs and the bony vertebrae. The results of this chapter demonstrate for the first time the process of disc calcification, illustrated by changes in radiotracer uptake in AKU.

4.5.6 Gender and SUVm

Little has been published regarding gender differences in SUVms in the spine. Figure 4.14 demonstrates vertebral and IVD SUVms of males and females. From this graph, it is clear that there is no difference between the thoracic and lumbar vertebrae between males and females, however when looking at the SUVms of the IVDs, males seem to have higher SUVms than females at each vertebral level, however this was not statistically significant. A possible reason for this could be that males generally weigh more than females therefore have increased forces acting through the spine. Additionally, increased weight may compress the discs to a higher extent in males. Win *et al*. (116) demonstrated a positive correlation between SUVm and weight and explained that increased weight puts mechanical stress on the spine, this results in increased osteoblastic activity therefore increased ^{18}F uptake. Kaneta *et al*. (144) commented on gender differences in the vertebrae of normal spines, and reported that males had higher SUVms compared to females and suggested this was due to

males having higher BMD than females. This was despite the mean age of the males being 5 years older than the females therefore this finding was thought to be significant.

4.5.7 Individual changes in SUVm

It is clear from Figures 4.9 - 4.13 that there is no significant difference between the SUVms of V1 and V3 in the lumbar and thoracic vertebrae or IVDs. Figures 4.15 – 4.18 demonstrate individual changes in SUVms across V1 to V3 in the vertebrae and IVDs. The individual comparisons try to shed light on what is happening over a period of 1 year on an individual basis in the IVDs and vertebrae with age. The results are generally very varied, some patient's SUVms increase some decrease and some are unchanged. It is hoped that once the SONIA 2 clinical trial has ended, and the additional visits have been analysed some interesting trends may be identified as the patients will have been taking the drug for a longer period. Additionally, the treatment group will be revealed so any changes in response to nitisinone can be analysed. The patients that show a reduction in SUVm over one year may be on the drug and those that are increasing may be the no treatment group. This data suggests that there appears to be a possibility of change after one year, in the clinic patients report improvement in symptoms soon after taking nitisinone therefore a change in SUVm could demonstrate this. This will be elucidated in 2019.

4.5.8 Limitations of the SUVm

Due to the relatively high radiation exposure of PET imaging it is unethical to scan healthy patients to use as controls. The control group used in this thesis to compare SUVms with AKU patients is all female ranging from 43-84 years of age. These patients were all positive for breast cancer who underwent PET scanning due to suspected bony metastasis. No male scans were available, additionally there were no patients available younger than 43 years of age due to the nature of the disease. This therefore is a limitation as the control data represents females some of which may be post-menopausal, so this is a caveat particularly when comparing young males.

There are many factors affecting quantitation using SUVms, that the radiologist is responsible for. These are described as biological factors and technical factors (149,150). The main biological factor includes the uptake duration between injection and scan. This linearly affects SUVm, increasing over time. The half-life of ^{18}F is 110 minutes, therefore all patients are scanned 60 minutes post injection (or as close to this as feasibly possible) in order to maintain consistency and to minimise variability between patients (149). Additionally, synchronisation of clocks is imperative for accurate radioactive decay calculations. Technical factors include residual activity in the syringe after patient injection. The SUVm calculation (Figure 1.12) takes into account the injected dose, therefore the residual activity in the syringe must be incorporated to avoid error in SUV (ignoring the residual activity introduces underestimation of SUV by approximately 2%) (150). The SUVm calculation also normalises for body weight; patient weight therefore must be measured on a

calibrated scale. Finally, correct data entry and quality of administration is vital to obtain accurate readings.

4.5.9 Summary

^{18}F-NaF PET imaging allows quantitative measurements of tissue radioactivity. The SUV is a common method of expressing the uptake of ^{18}F into calcified tissues. This chapter has revealed the variation between AKU and control SUVms in the vertebrae and IVDs and its use in detecting areas of arthropathy in AKU. The results of this chapter have described a significant difference between AKU and control IVD SUVms due to calcification of the IVDs in AKU. It has been proposed that calcium hydroxyapatite or calcium pyrophosphate dihydrate are deposited in the fibrocartilaginous IVDs in AKU due to biochemical alterations of the disease. ^{18}F binds to these calcium deposits in AKU resulting in high SUVms. With age the IVD SUVms follow an interesting trend (inverted 'U'). SUVms of the youngest patients are in line with that of the control. The SUVm increase exponentially then plateau at around the age of 55, before steadily declining again after the age of 60. This increase in SUVm illustrates the deposition of calcifications in the disc, the plateau illustrates maximum turnover, and the decline illustrates a reduction in turnover due to possible fusion of the vertebrae. Bone metabolism appears to be unaffected by the disease demonstrated by very similar SUVms between the AKU and control vertebrae measurements. A decline in vertebral SUVm was observed with age in both AKU and control groups. The AKU group was found to have lower SUVms with age reflecting reduced BMD that appears to be exacerbated by the disease process.

This chapter demonstrates the feasibility and utility of measuring vertebrae and IVD SUVms to identify active arthropathy and to quantify disease state in AKU. This methodology will provide clinicians with a quantitative tool to aid in visual interpretation of scans and to aid in assessing inter and intra patient differences.

4.5.10 Further work

Now we have established the application of the SUVm as a quantitative tool to measure spinal arthropathy in AKU, next we want to assess if the SUVms can accurately track changes longitudinally in a group of patients receiving treatment.

5.0 PROGRESSION OF SPINAL ARTHROPATHY IN RESPONSE TO NITISINONE IN AKU MONITORED BY ^{18}F-NaF STANDARDISED UPTAKE VALUE

5.1 INTRODUCTION

In Chapter 4 it was demonstrated that SUVms can be used to identify active arthropathy in the spine and to quantify disease state in AKU. The utility of SUVms in a clinical setting could provide clinicians with a quantitative tool to aid visual interpretation of scans and to aid in assessing inter and intra patient differences. In this chapter, the aim was to utilise this quantitative measurement to track disease progression in AKU longitudinally and to see if any trends could be identified in response to nitisinone (all patients analysed in this chapter all receive nitisinone).

AKU is characterised by a deficiency of the enzyme HGD that functions to break down HGA. Nitisinone is a potential disease modifying therapy for AKU. It acts by inhibiting the enzyme HPPD (HPPD converts HPPA into HGA) therefore blocking the production of the culprit molecule HGA (Figure 1.1). The NAC provides off-label nitisinone (2mg) to patients that attend the service. Annual assessments are included in this service where the patients undergo a variety of tests and scans to monitor HGA and tyrosine levels as well as tracking the progression of the disease in terms of pain, ochronotic arthropathy and monitoring the other clinical manifestations associated with AKU such as cardiac and ocular involvement.

This chapter utilises quantitative SUVm measurements in the spine (vertebrae and IVDs) across five visits, each with a year in between with the aim of determining if the same trends could be identified in this patient group as described in the previous chapter on the SONIA 2 patients. Correlations with clinical scores obtained from the ^{18}F-NaF PET scan, pain scores obtained from the patient questionnaire and other data

such as CTX-1 concentrations and quantitative CT densitometry (QCT) T-scores will define whether this SUVm data correlates well with other tests.

In recent years, cellular components of the bone matrix have been identified and categorised as either markers of bone formation or resorption. Although these markers have been used in research for a long time they are only now being recognised as tools in the clinical management of bone disease (151). C-terminal telopeptide 1 (CTX-1), measured in serum, is a marker of bone resorption and is a by-product of collagen degradation. This data will be used along with QCT T-scores of bone densitometry to explore the correlations with other methods of monitoring AKU pathophysiology. This 5-year longitudinal data should provide an insight into the progression of the disease, and possibly the effect of nitisinone.

5.2 DESIGN OF STUDY

5.2.1 PATIENT GROUP

58 patients enrolled at the NAC for treatment with nitisinone, of which 22 adult patients (9 females, 13 males, mean age 47, SD±16.05, range 21-75) attended the centre and undergone ^{18}F-NaF PET/CT imaging annually for five consecutive visits. It is these 22 patients that were included in this chapter. The first visit was baseline, pre-treatment, the consecutive four visits, each patient received 2mg of nitisinone daily. Not every one of the patients were present for every visit, V1 n=19, V2 n=16, V3 n=22, V4 n=18, V5 n=11. Ten non-metastatic breast cancer patients were used as non-AKU control for comparison. These patients had undergone ^{18}F-NaF PET to determine bony metastasis, all of which were reported as negative. The ten control patient data was only available for a single diagnostic scan and there were no follow up scans available.

5.2.2 MEASURING THE SUVms

Hermes hybrid viewer (see section 2.5.1) was used to measure SUVms (section 2.5.2). The SUVm was obtained from the centre of three lumbar (L5, L3, L1) and three thoracic (T1, T6, T12) vertebral bodies, and from the centre of the corresponding IVDs below (L5-S1, L3/L4, L1/L2, T12/L1, T6/T7, T1/T2). The SUVms were obtained for each visit (visit 1-5) to assess any longitudinal changes.

5.2.3 CORRELATIONS (QCT, CTX-1 AND PAIN SCORES)

Correlations were made with the SUVm data to see if other parameters that measure AKU symptoms correlate. Data was extracted from the NAC case notes from the baseline visit (pre-nitisinone). Lumbar and femur QCT T-scores were extracted for each of the patients (for more information see section 1.6.3.2) as well as serum CTX-1 (ug/L). Spinal pain scores that ranged from 0-10, 0= no pain, 10= most severe pain, were also extracted from the patient questionnaire.

5.3 RESULTS

5.3.1 COMPARISON BETWEEN LUMBAR AND THORACIC VERTEBRAE AND IVD SUVms

The SUVm was obtained from the centre of lumbar (L5, L3, L1) and thoracic (T12, T6, T1) vertebrae and corresponding IVDs below (L5-S1, L3/L4, L1/L2, T12/L1, T6/T7, T1/T2). Figure 5.1 shows the mean lumbar and thoracic vertebrae and IVD SUVm comparison between visit 1 and visit 5 in the NAC patient group (n=22). When comparing this graph to Figure 4.9 in the previous chapter, the trend is not as obvious. The results from Figure 4.9 demonstrate a clear difference between the AKU vertebrae and IVDs, with the AKU vertebrae having consistently lower SUVms (7.4) than the IVDs (11.6). However, when looking at Figure 5.1 there is no clear difference between vertebrae and IVDs. The SUVms for IVDs for V1 and V5 (9.0 and 8.8 respectively) are only slightly higher than that of the vertebrae (V1=8.2 and V5=7.4) across the vertebral levels. Paired t-tests revealed no statistical significances between V1 and V5 SUVms in both the vertebrae and IVDs across all vertebral levels.

Figure 5.2 demonstrates the mean lumbar and thoracic vertebrae and IVD SUVms across five annual visits in the NAC patient group. It is clear from the graph that the SUVm of the IVDs in the lumbar and thoracic region (mean SUVm across the visits = 9.1 and 9.5 respectively) are higher than that of the vertebrae (mean SUVm across the visits = 7.04 and 8.1 respectively). Paired t-tests revealed a statistically significant difference between both the lumbar and thoracic IVDs and vertebrae at visit 4 only. This trend supports what was found in Chapter 4 (Figure 4.9). The mean lumbar and thoracic SUVm measurements are generally consistent across the five visits in both

the vertebrae and IVDs when the mean data is plotted, suggesting that there is little change in SUVm in both the vertebrae and the IVDs over the 4 years on nitisinone. Paired t-tests revealed no significant changes across each of the visits.

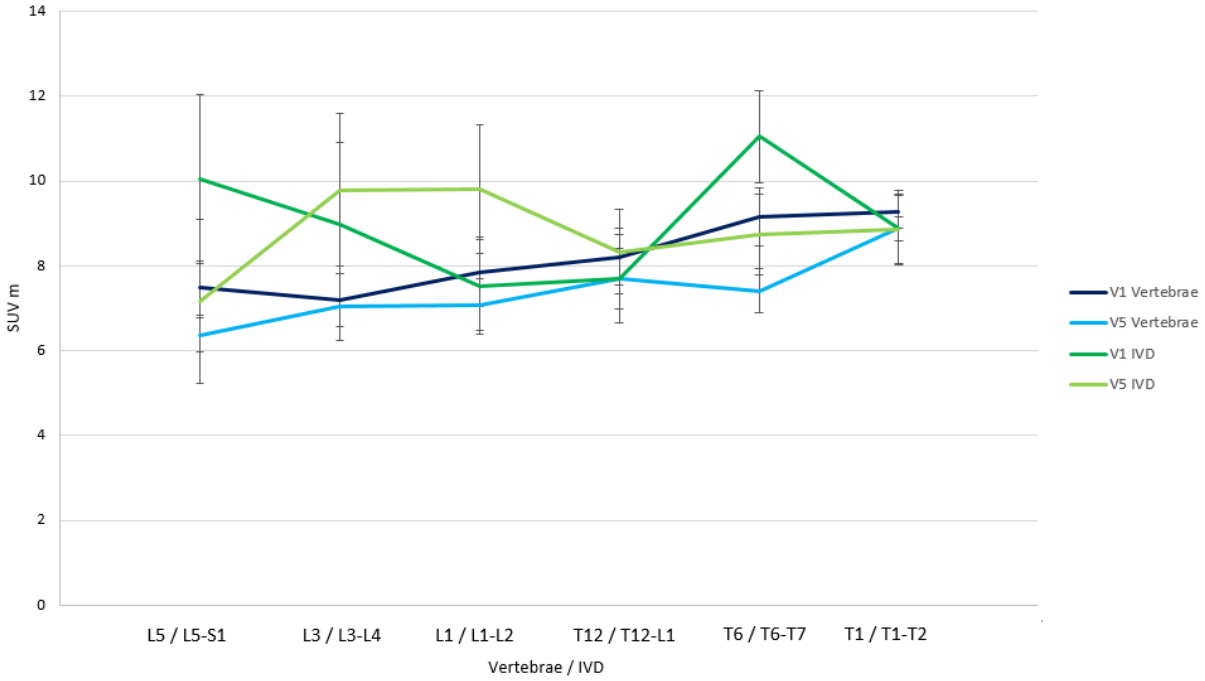

Figure 5.1 Mean lumbar and thoracic vertebrae and IVD SUVm comparisons between visit one and visit 5. V1 = baseline, V5 = 4 years on nitisinone. Vertebrae measured (L5, L3, L1, T12, T6, T1), IVDs measured (L5-S1, L3-L4, L1-L2, T6-T7, T1-T2). Paired t-tests revealed no significant differences between V1 and V5 SUVms in both the vertebrae and the IVDs across all vertebral levels. n=22 AKU patients (9 females, 13 males, mean age 47, SD±16.05, range 21-75). V1 n=19, V5 n=11.

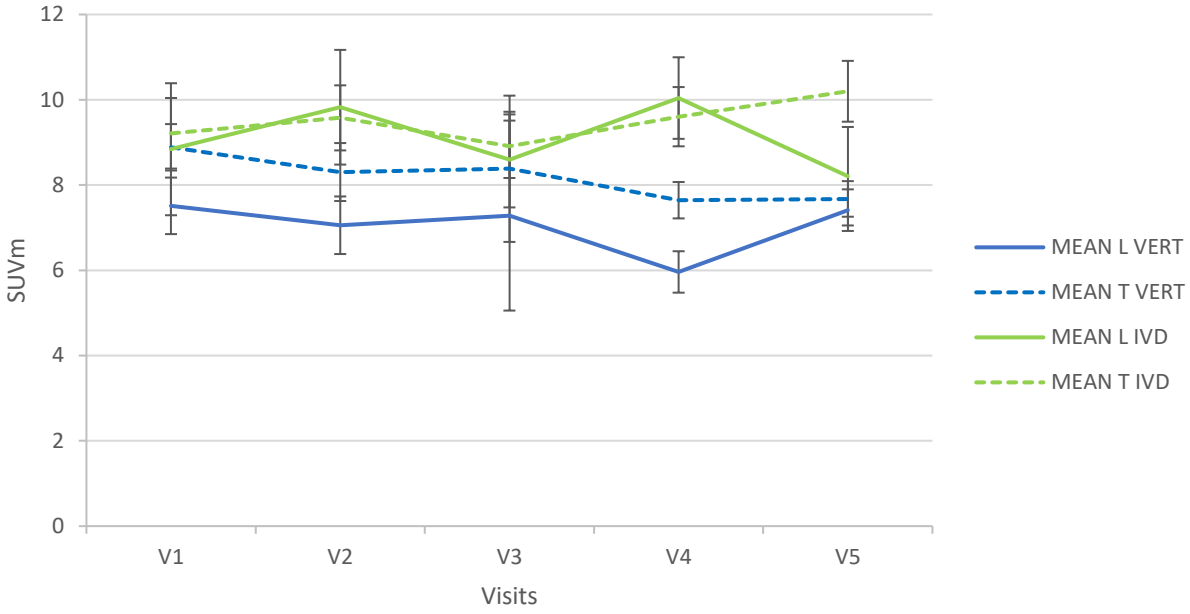

Figure 5.2 Mean AKU lumbar and thoracic vertebrae and IVD SUVm across 5 annual visits. Each visit was one year apart, V1 (Visit 1) = baseline (pre-nitisinone), V2, V3, V4 and V5 each with a year in-between on nitisinone. Paired t-tests revealed a significant difference between lumbar vertebrae and IVDs ($p<0.05$), and thoracic vertebrae and IVDs ($p<0.05$) at visit 4 only. n=22 AKU patients (9 females, 13 males, mean age 47, SD±16.05, range 21-75). V1 n=19, V2 n=16, V3 n=22, V4 n=18, V5 n=11.

5.3.2 SUVm WITH AGE

The AKU and control mean lumbar IVD SUVm was plotted against age (Figure 5.3). The AKU patients were plotted for each visit; V1- V5 (Figure 5.3 A-E). The control patients were plotted against V1 only however, will be used as a comparison across the five visits. Polynomial (second order) lines were fitted to the AKU data for each graph. The youngest patients have low IVD SUVms that are in line with the SUVm of the controls. With age IVD SUVm increases reaching the highest values around the age of 60. From here the SUVm declines. Due to the lower number of patients in this

group the trend is not as convincing as was seen in the previous chapter. However, the trend is reminiscent of what was seen in Figures 4.12 and 4.13 with a bigger patient number (41 patients). In contrast to the control data, there is an obvious difference in the trend of SUVm with age between the two groups where the control data consistently has low SUVm measurements across all ages. Independent t-tests revealed a significant difference between the mean lumbar IVD SUVm compared to the control group ($p<0.01$). This supports what was found in Figure 4.12. In terms of change in SUVm across the visits the maximum values that are seen around the age of 60 reduces upon each visit from V1 to V5. The maximum values in visit 1 (Figure 5.3A) reach a maximum SUVm of 24, by visit 2 (Figure 5.3B) the maximum values have reduced to 21, by visit 3 (Figure 5.3C) they have reduced to 18, and by visits 4 (Figure 5.3D) and 5 (Figure 5.3E) the maximum values are 15 and 16 respectively.

Figure 5.4 demonstrates the AKU and control mean thoracic IVD SUVm with age. The same trend is observed in the thoracic IVDs (Figure 5.4) however, is not as convincing as what was seen in Figure 4.13 in the previous chapter. In terms of change in the thoracic SUVm across the visits the highest SUVm is seen at V1 with a SUVm of 19 (Figure 5.4A), by V2 the highest value is around 15 (Figure 5.4B) and this further reduces to 13 in V5 (Figure 5.4E). Independent t-tests revealed a significant difference between the mean thoracic SUVm of the AKU and control group ($p =< 0.01$).

The lumbar and thoracic vertebrae SUVm were analysed across the five visits. Figure 5.5 demonstrates the mean lumbar vertebrae SUVm with age in individual AKU and control patients. A negative statistically significant correlation was identified

between SUVm and age in both AKU ($p<0.001$) and control ($p<0.01$) patients, with the youngest patients having the highest SUVms and the oldest patients having the lowest SUVms. This confirms what was found in the previous chapter (Figure 4.10). The control mean lumbar vertebrae have slightly increased SUVms compared to the AKU patients across the ages however, independent t-tests revealed no significant difference between the two groups ($p>0.05$). This supports what was found in the previous chapter (Figure 4.10). In terms of change across the visits, there appears to be very little change in the distribution of the data from V1 to V5 indicating that nitisinone may be arresting the progression of the disease.

Figure 5.6 demonstrates the mean thoracic vertebrae SUVm in individual AKU and control patients. Figure 5.6 shows the same trend as described in the previous chapter (Figure 4.11). Negative statistically significant correlation was identified between SUVm and age in the AKU group ($p<0.001$). The control group also has a negative correlation with age however this was not statistically significant ($p>0.05$). The youngest patients consistently have the highest SUVms and the oldest have the lowest values. Again, as seen in the lumbar vertebrae the SUVms of the control patients have higher SUVms compared to the AKU patients across the ages and no significant difference was found between the two groups (independent t-test, $p>0.05$). In terms of change in SUVms across the visits there appears to be no obvious change from V1 to V5.

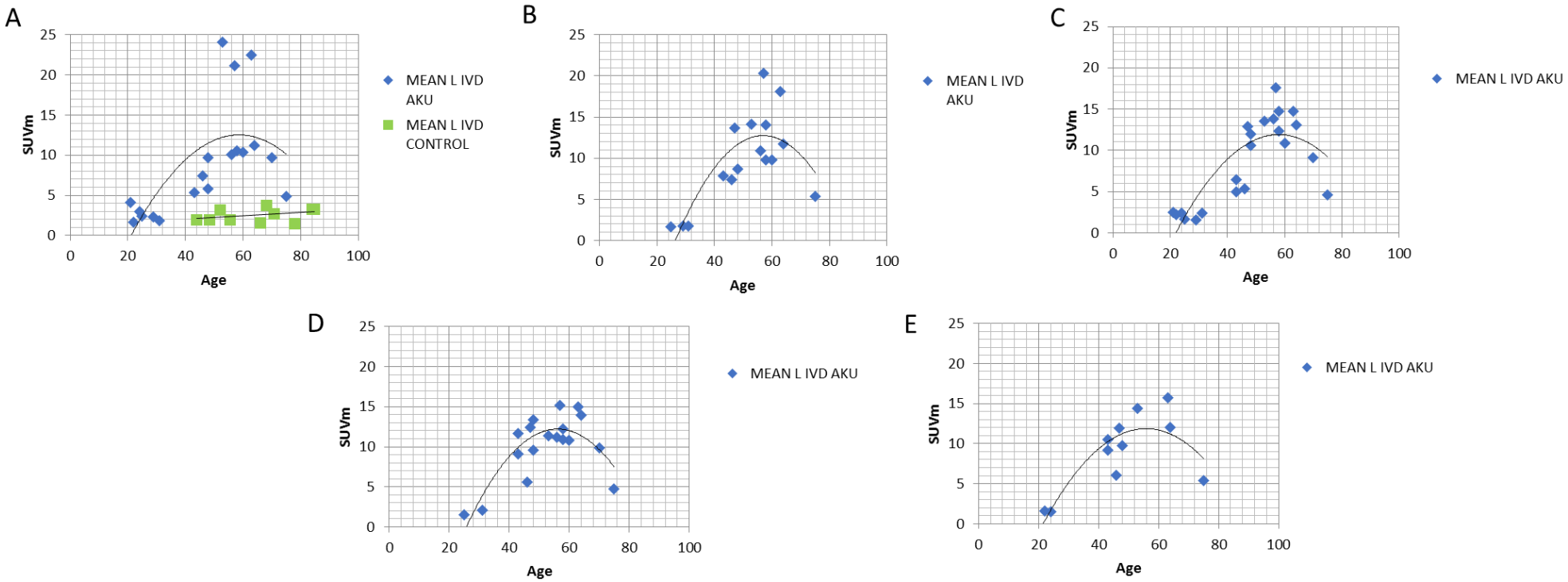

Figure 5.3 Mean lumbar IVD SUVm with age in individual AKU and control patients across 5 visits. A – baseline (visit one-V1), B – V2, C – V3, D – V4, E– V5. MEAN L IVD – SUVm of mean lumbar IVD (L5/S1, T3/T4, L1/L2). Polynomial (order 2) regression lines = A (R^2=0.446), B (R^2=0.634), C (R^2=0.683), D (R^2=0.690), E (R^2=0.721). Linear regression line - Control (R^2= 0.133). Independent t-test and Wilcoxon-Mann-Whitney test revealed a significant difference between the AKU mean lumbar IVD SUVm and the control ($p< 0.01$) (Figure A). n=22 AKU patients (9 females, 13 males, mean age 47, SD±16.05, range 21-75). V1 n=19, V2 n=16, V3 n=22, V4 n=18, V5 n=11.

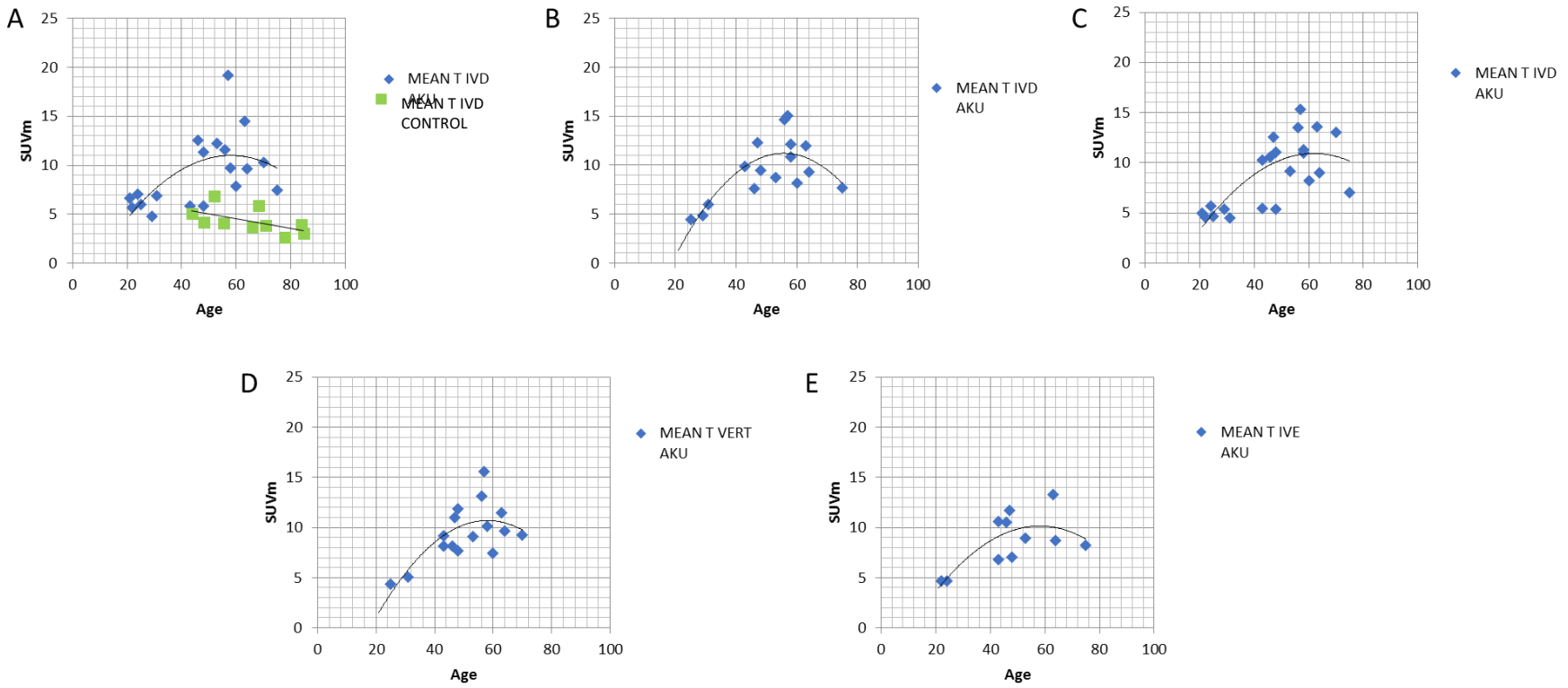

Figure 5.4 Mean thoracic IVD SUVm with age in individual AKU and control patients across 5 visits. A – baseline (visit one-V1), B – V2, C – V3, D – V4, E – V5. MEAN T IVD – SUVm of mean thoracic IVD (T12/L1, T6/T7, T1/T2). Polynomial (order 2) regression lines = A (R^2=0.362), B (R^2=0.603), C (R^2=0.535), D (R^2=0.505), E (R^2=0.552). Linear regression line - Control (R^2= 0.331). Independent t-test and Wilcoxon-Mann-Whitney test revealed a significant difference between the AKU mean thoracic IVD SUVm and the control ($p< 0.01$) (Figure A). n=22 AKU patients (9 females, 13 males, mean age 47, SD±16.05, range 21-75). V1 n=19, V2 n=16, V3 n=22, V4 n=18, V5 n=11.

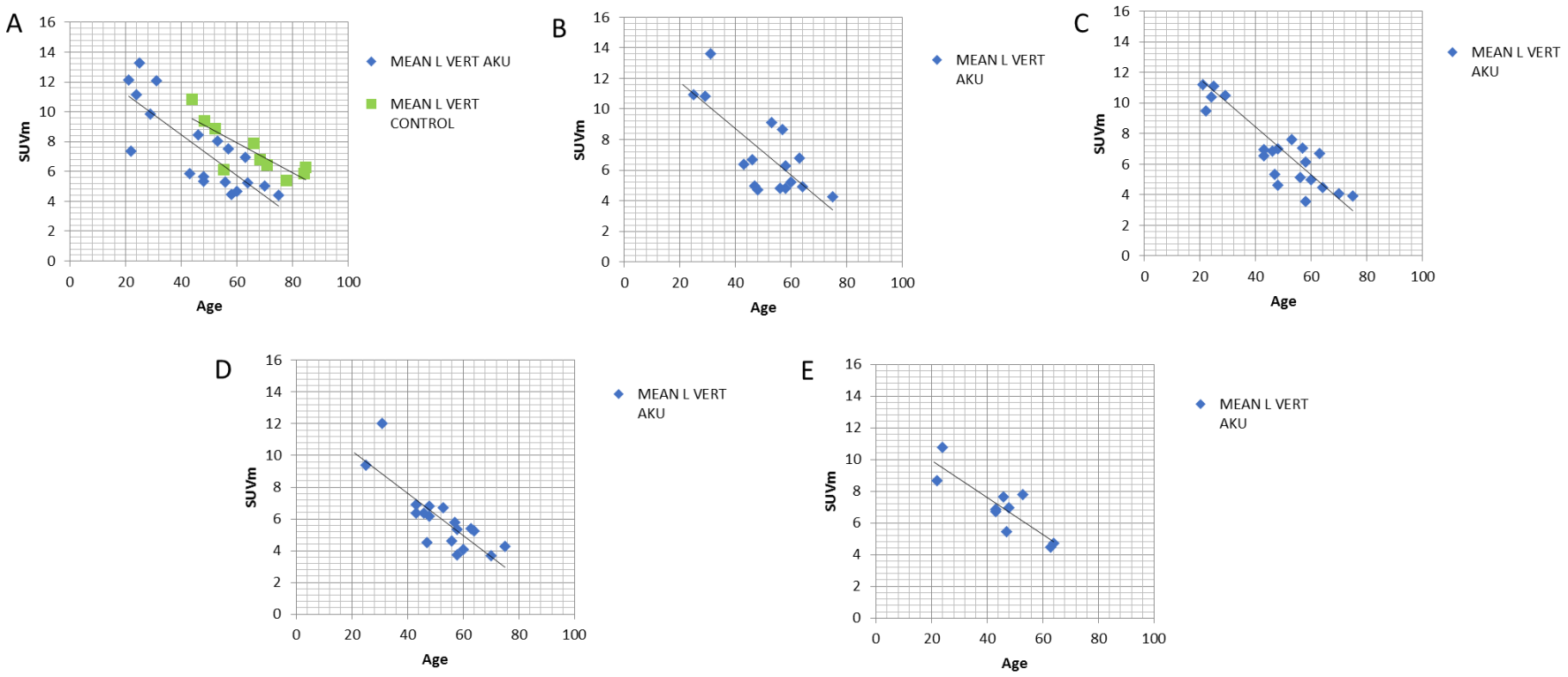

Figure 5.5 Mean lumbar vertebrae SUVm with age in individual AKU and control patients across 5 visits. A – baseline (visit one-V1), B – V2, C – V3, D – V4, E – V5. MEAN L VERT – SUVm of mean lumbar vertebrae (L5, L3, L1). Negative statistically significant correlation identified in both AKU ($r=-0.809$, $p<0.001$) and control ($r=-0.831$, $p<0.01$). Independent t-test revealed no significant difference between the AKU mean lumbar vertebrae SUVm and the control ($p>0.05$) (Figure A). n=22 AKU patients (9 females, 13 males, mean age 47, SD±16.05, range 21-75). V1 n=19, V2 n=16, V3 n=22, V4 n=18, V5 n=11.

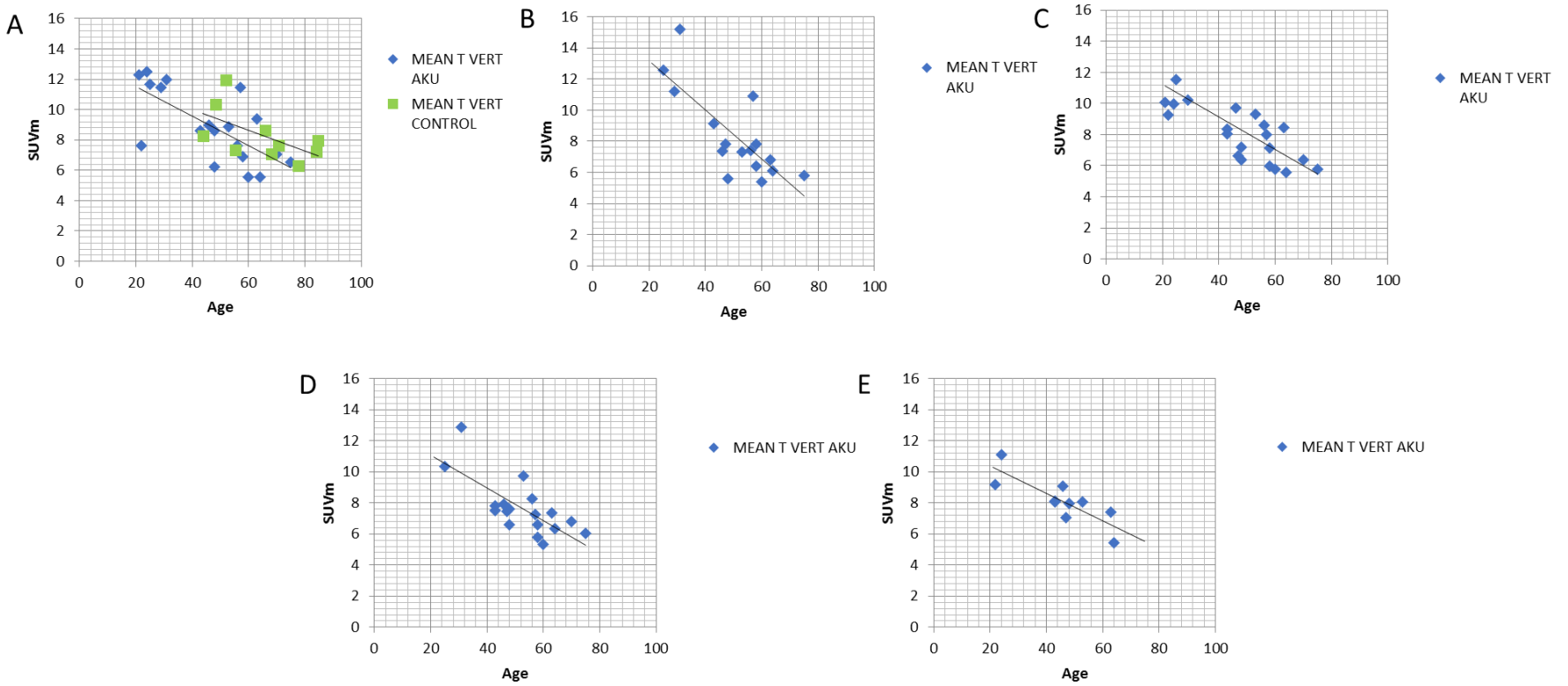

Figure 5.6 Mean thoracic vertebrae SUVm with age in individual AKU and control patients across 5 visits. A – baseline (visit one-V1), B – V2, C – V3, D – V4, E – V5. MEAN T VERT – SUVm of mean thoracic vertebrae (T12, T6, T1). Negative statistically significant correlation identified in the AKU group (r=-0.696, p<0.001). Negative correlation also identified in the control group (r=-0.588, p>0.05). Independent t-test revealed no significant difference between the AKU mean thoracic vertebrae SUVm and the control (p>0.05) (Figure A). n=22 AKU patients (9 females, 13 males, mean age 47, SD±16.05, range 21-75). V1 n=19, V2 n=16, V3 n=22, V4 n=18, V5 n=11.

5.3.3 INDIVIDUAL CHANGE IN SUVm ACROSS 5 VISITS

The AKU patients were divided into four age groups; 20-31 years, 40-49 years, 50-59 years, 60+ years, to look at the individual change in SUVm over five visits in the thoracic and lumbar vertebrae and IVDs. Figure 5.7 demonstrates the mean lumbar IVD SUVm across the five visits in the four age groups. The age dependent trend (inverted 'U' trend) in SUVm is evident across the four graphs as seen in Figures 5.3 and 5.4. The inverted 'U' trend reflects the youngest age group (21-30) having the lowest SUVms (Figure 5.7A), the 50-59 age group reaching the highest (Figure 5.7C), and the oldest age group having reduced SUVms (Figure 5.7D). When looking at the change in SUVm in the mean lumbar IVDs across the five visits in the individual patients there appears to be no direct trend (Figure 5.7). When the IVD SUVm is high initially it appears to always come down across the visits in most cases. Generally, there is little change in the mean lumbar IVD SUVm in the youngest patients across the five visits (Figure 5.7A). In the 40-49 and the 50-59 age groups, the SUVm fluctuates across the five visits, with generally little change between V1 and V5 (Figure 5.7B and C). The SUVm in the oldest age group (60+ Figure 5.7D) is generally consistent across each of the visits.

Figure 5.8 shows the mean thoracic IVD SUVm in the four age groups. There is a small reduction in SUVm across the five visits in the youngest patients (Figure 5.8A). In the patients aged 40-49 (Figure 5.8B) there appears to be fluctuations in SUVms across the visits again with little difference between the values at V1 and V5. The patients in the oldest two age groups (Figures 5.8 C and D) generally have consistent SUVms across the five visits with minimal change between visits.

Figure 5.9 demonstrates the mean lumbar vertebrae SUVm in the four age groups across the five visits. A reduction in SUVm can be seen across the four age groups (Figures 5.9 A-D) with the youngest patients reaching the highest SUVms (Figure 5.9A) and the oldest patients having the lowest SUVms (Figure 5.9D) as seen in Chapter 4 (Figure 4.10). Generally, the SUVms across the five visits are very consistent with little change between the visits in each of the patient groups.

The same trends are seen in the thoracic vertebrae (Figure 5.10) with the youngest patients reaching the highest SUVms (Figure 5.10A) and the oldest having the lowest SUVms (Figure 5.10D) as seen in the previous chapter (Figure 4.11). Again, there is little change in SUVm across the five visits (Figures 5.10).

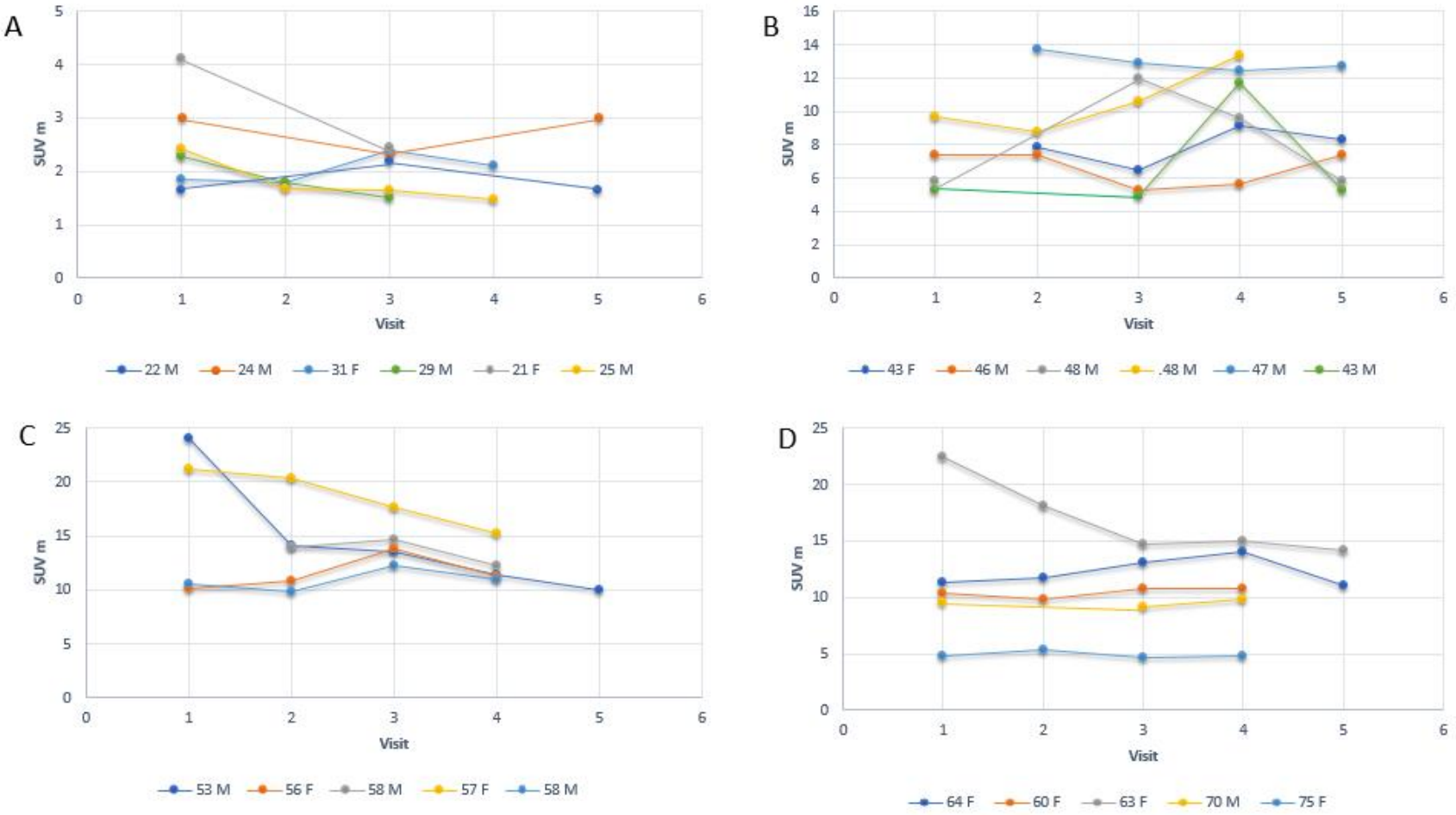

Figure 5.7 Mean lumbar IVD SUVm across 5 visits in individual patients grouped by age. A – age 20-31 (n=6), B – age 40-49 (n=6), C - age 50-59 (n=5), D – age 60+ (n=5). The key defines the age and gender of each patient.

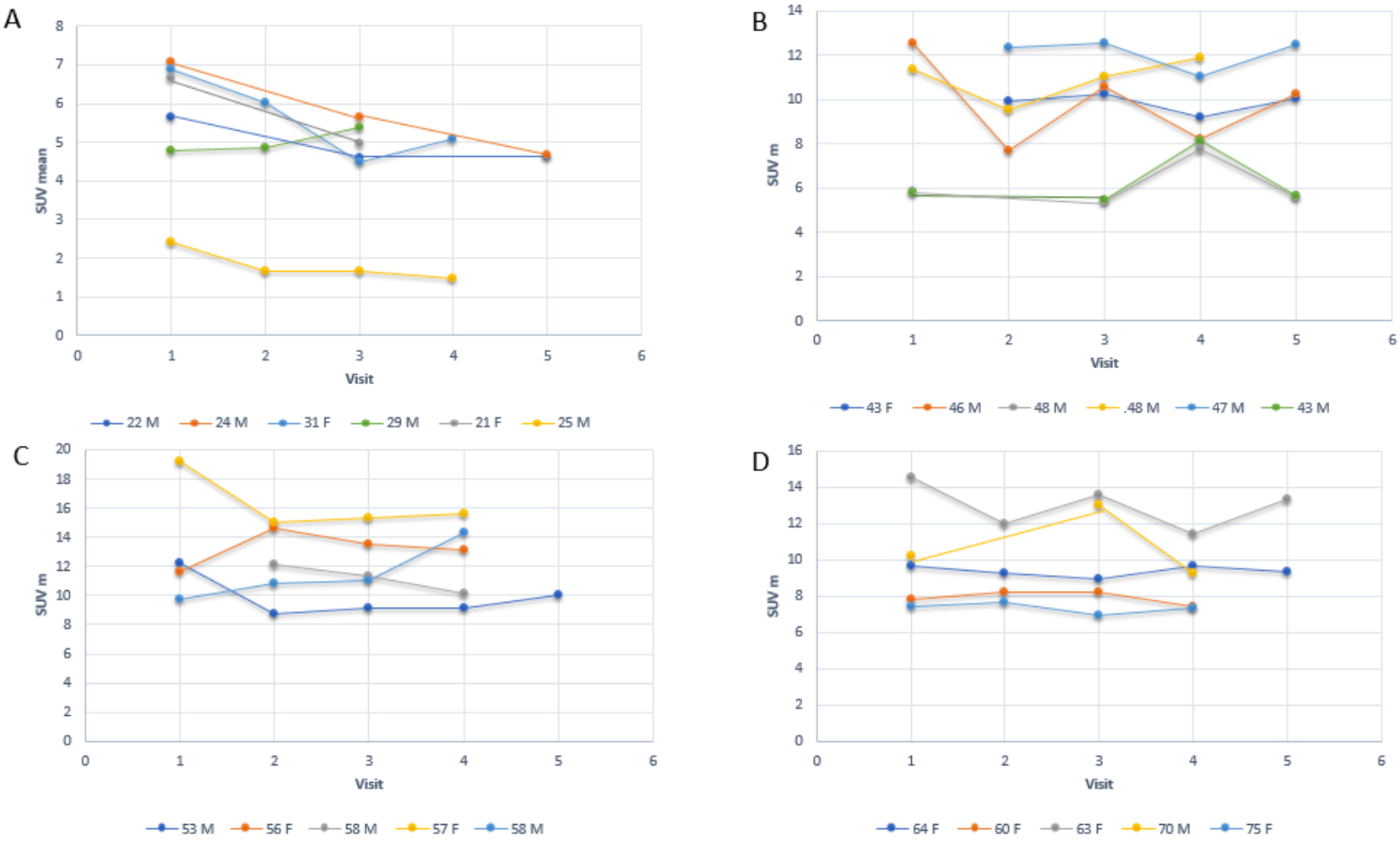

Figure 5.8 Mean thoracic IVD SUVm across 5 visits in individual patients grouped by age. A – age 20-31 (n=6), B – age 40-49 (n=6), C - age 50-59 (n=5), D – age 60+ (n=5). The key defines the age and gender of each patient.

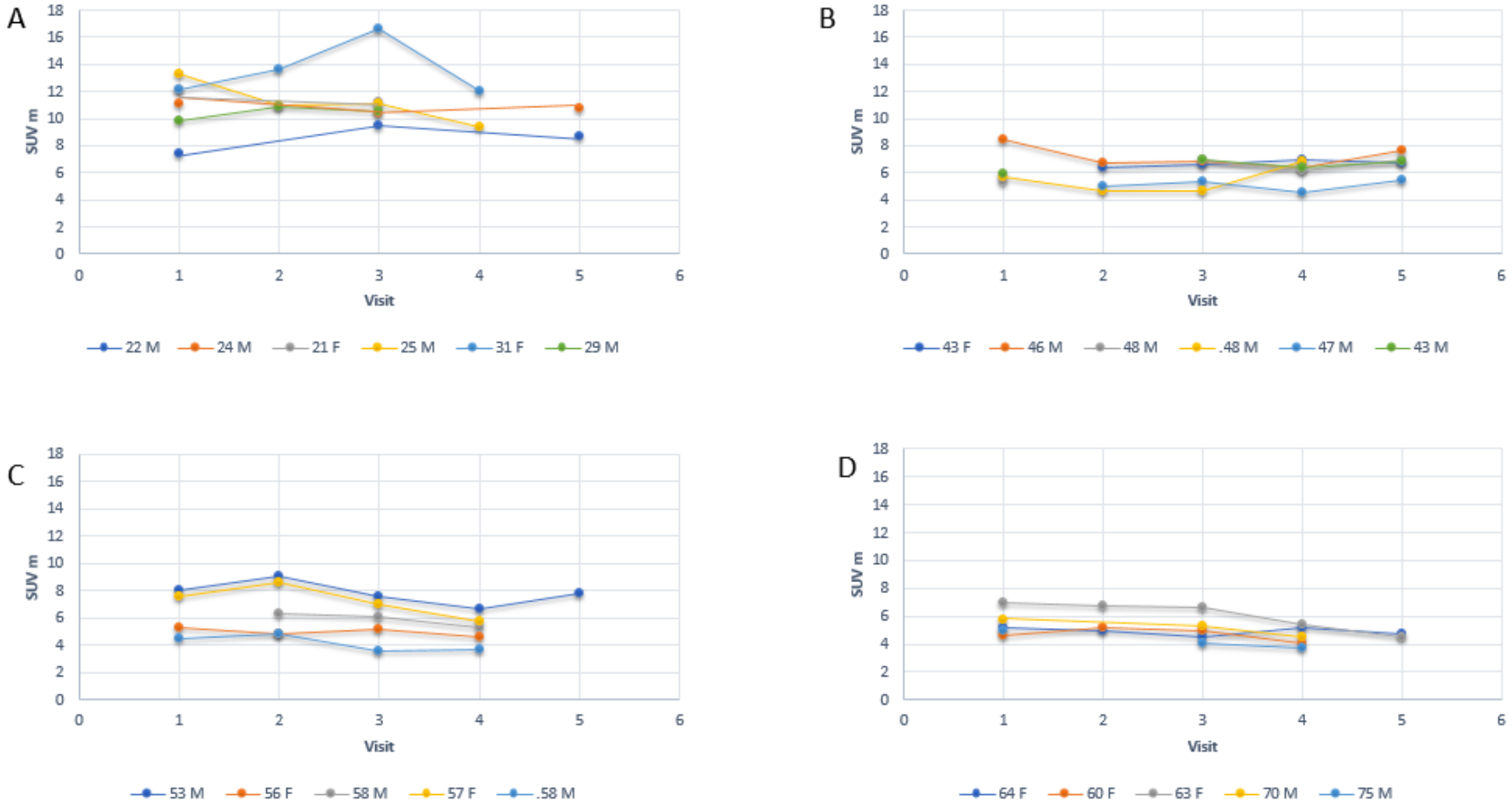

Figure 5.9 Mean lumbar vertebrae SUVm across 5 visits in individual patients grouped by age. A – age 20-31 (n=6), B – age 40-49 (n=6), C - age 50-59 (n=5), D – age 60+ (n=5). The key defines the age and gender of each patient.

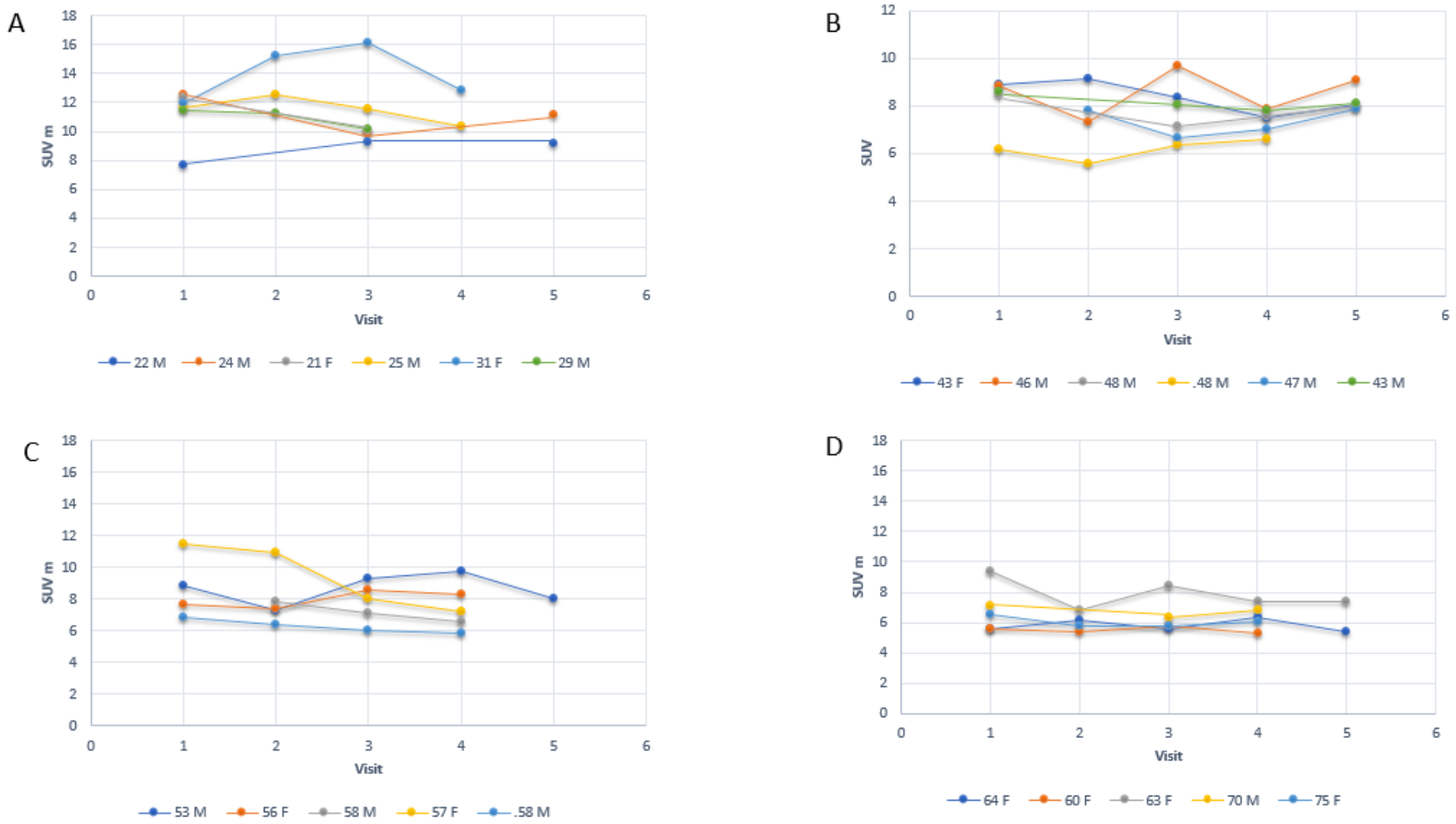

Figure 5.10 Mean thoracic vertebrae SUVm across 5 visits in individual patients grouped by age. A – age 20-31 (n=6), B – age 40-49 (n=6), C - age 50-59 (n=5), D – age 60+ (n=5). The key defines the age and gender of each patient.

5.3.4 SUVm CORRELATION WITH CLINICAL AND ANATOMICAL THRESHOLD SCORES

All the following correlations are based on baseline data (visit 1). The average lumbar and thoracic IVD and vertebrae SUVm were plotted against the clinical score and anatomical threshold scores (as described in section 2.4.6 - 2.4.9). The clinical score is based on the AKUSSI where a nuclear medicine clinician scores 10 large joints; the shoulder, elbow, wrist and hands, hip, knee, ankle, foot, lumbar, thoracic and cervical spine, based on those areas having increased tracer uptake or not. The clinical score does not distinguish between left and right joints therefore ranges from 0-10. The bone and cartilage anatomical threshold (AT) scores (B-AT and C-AT) differentiate between bone and cartilage and are both a summation of the totality of the bones or joints scored in Chapter 3 utilising the thresholding method (described in 2.4.4 - 2.4.7).

Figure 5.11 demonstrates the correlation between the total clinical score and the mean lumbar and thoracic IVD SUVm. A positive statistically significant correlation was observed ($r= 0.585$, $p<0.01$) demonstrating that low SUVms correlate with low clinical scores and high SUVms correlate with higher clinical scores. This suggests that two methodologies display the same trend providing evidence of a robust method. Figure 5.12 demonstrates a negative statistically significant correlation ($r=-0.762$, $p<0.01$) between the total clinical score and the mean lumbar and thoracic vertebrae SUVm. Interestingly a negative correlation suggests that in the vertebrae, high SUVms are associated with low clinical scores and lower SUVms are associated with high clinical scores. The same trends were observed when the total anatomical threshold (AT) score was correlated with IVD and vertebrae SUVm. The total AT score is

described in section 2.4.8. This score is directly comparable to the total clinical score in terms of the joints scored therefore also has a maximum of 10. Figure 5.13 demonstrates a positive statistically significant correlation (r=0.658, p<0.01) between the total AT score and the mean thoracic and lumbar IVD SUVm as seen in Figure 5.11. Figure 5.14 demonstrates a negative statistically significant correlation (r=-0.612, p<0.01) between the total AT score and the mean lumbar and thoracic vertebrae SUVm as seen in Figure 5.12.

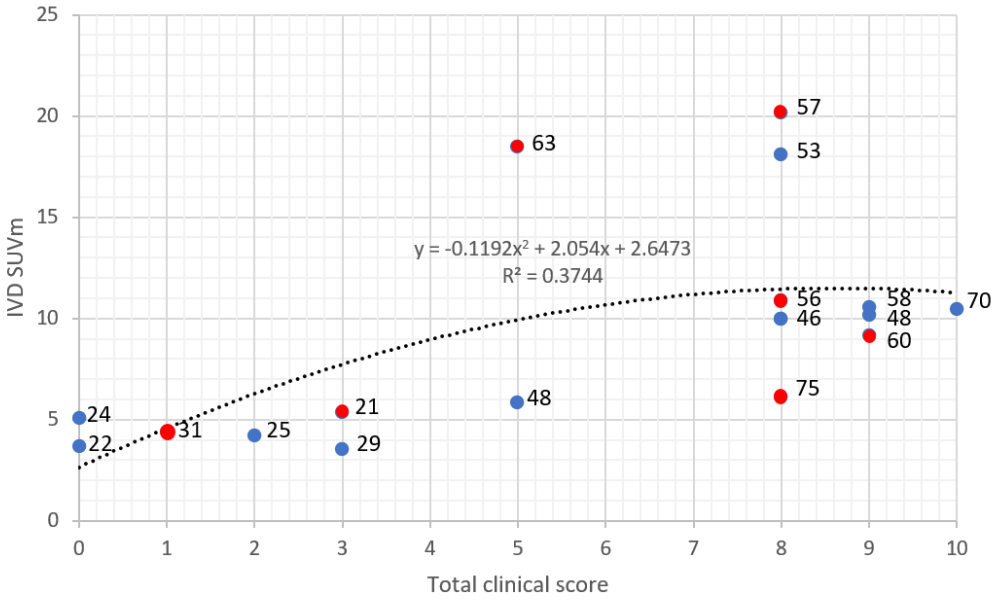

Figure 5.11 Scatter graph demonstrating a positive correlation between the mean lumbar and thoracic IVD SUVm with the total clinical score for visit 1. The ages are represented next to each point. Positive statistically significant correlation (r= 0.585, p<0.01). Males are plotted in blue, females in red.

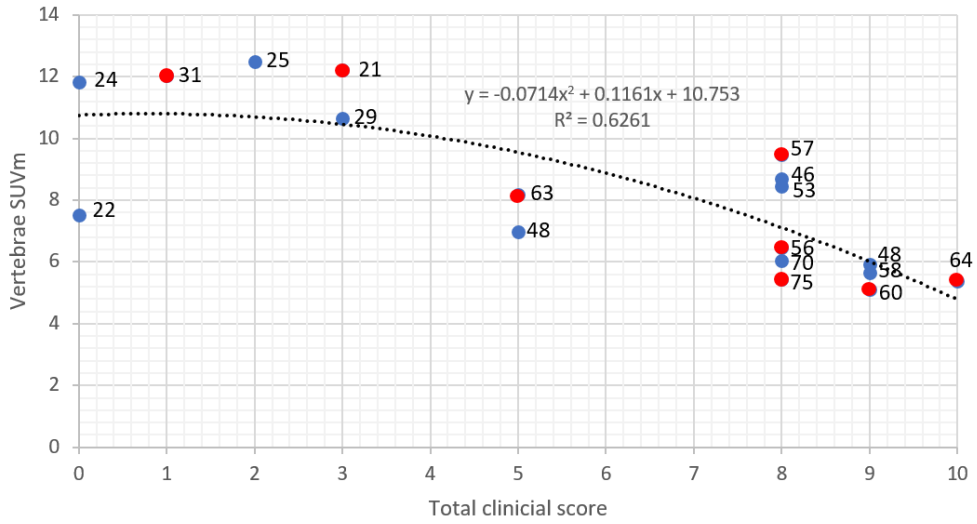

Figure 5.12 Scatter graph demonstrating a negative correlation between the mean lumbar and thoracic vertebrae SUVm with the total clinical score for visit 1. Ages represented next to each point. Negative statistically significant correlation (r= -0.762 p<0.01). Males are plotted in blue, females in red.

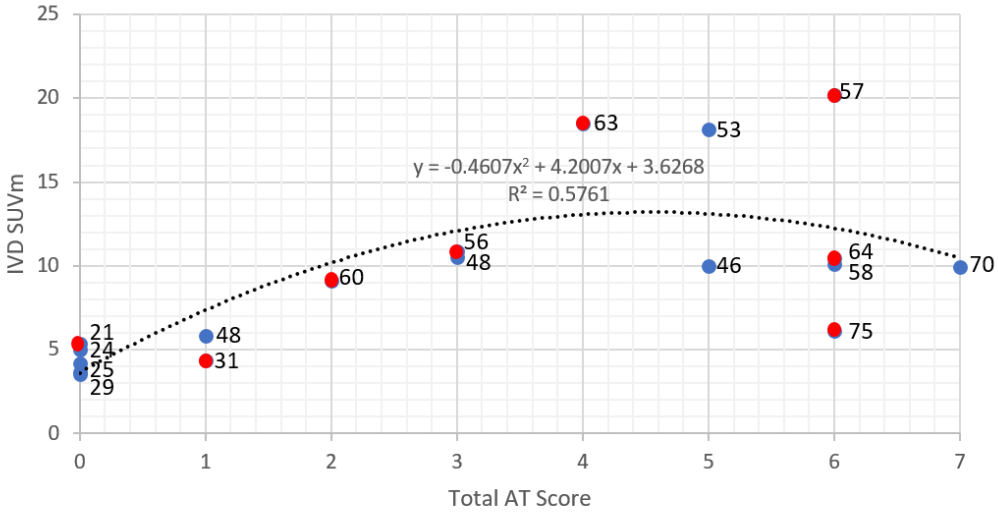

Figure 5.13 Scatter graph demonstrating the correlation between the mean lumbar and thoracic IVD SUVm with the total anatomical threshold for visit 1. The ages are represented next to each point. Positive statistically significant correlation (r= 0.658, p<0.01). Males are plotted in blue, females in red.

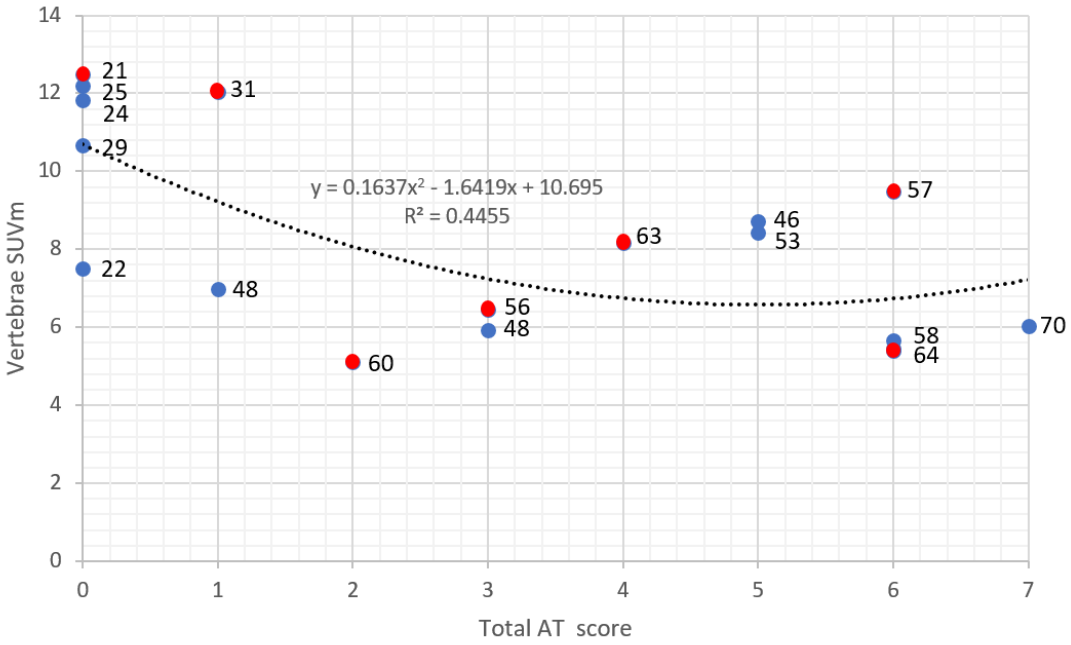

Figure 5.14 Scatter graph demonstrating the correlation between the mean lumbar and thoracic vertebrae SUVm with the total anatomical threshold score for visit 1. The ages are represented next to each point. Negative statistically significant correlation (r=-0.612, p<0.01). Males are plotted in blue, females in red.

Correlations were also made between the total C-AT score and total B-AT score with the mean thoracic and lumbar IVD SUVm and vertebrae SUVm respectively. The C-AT and B-AT scores differentiate between bone and cartilage (described in sections 2.4.6, 2.4.7). Figure 5.15 demonstrates no correlation between the mean lumbar and thoracic IVD SUVm with the C-AT score (r= 0.09, p>0.05). Figure 5.16 also demonstrates no correlation between the mean lumbar and thoracic vertebrae SUVm with the B-AT score (r=-0.169, p>0.05).

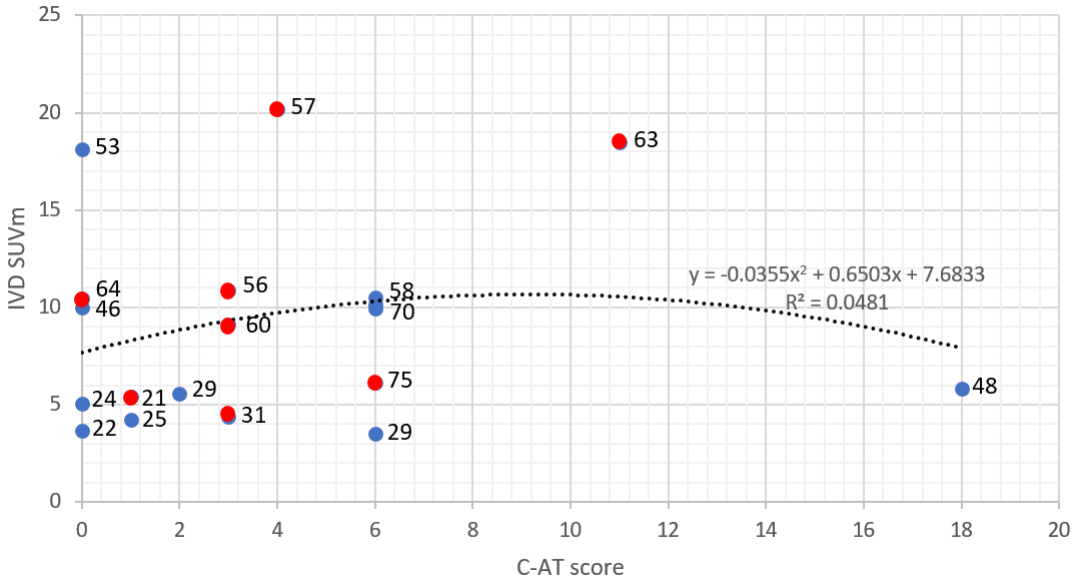

Figure 5.15 Scatter graph between the mean lumbar and thoracic IVD SUVm with the cartilage anatomical threshold score for visit 1. The ages are represented next to each point. No correlation (r= 0.09, p>0.05). Males are plotted in blue, females in red.

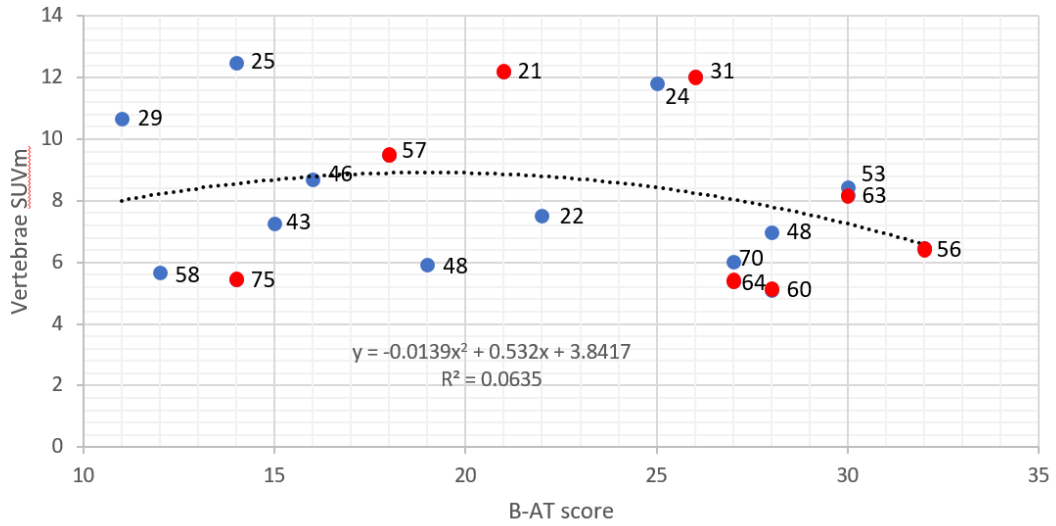

Figure 5.16 Scatter graph between the mean lumbar and thoracic vertebrae SUVm with the bone anatomical threshold score for visit 1. The ages are represented next to each point. No correlation (r=-0.169, p>0.05). Males are plotted in blue, females in red.

5.3.5 LUMBAR SPINE QUANTITATIVE COMPUTER TOMOGRAPHY

The next variable to be investigated was QCT T-scores. QCT measures BMD. Correlations between SUVm and BMD were made to investigate if BMD had an effect of SUVm, it was suggested that low SUVms may reflect low BMD, due to less hydroxyapatite available for ^{18}F to bind to. Firstly, BMD (represented as T-score- described in section 1.6.3.2 and Table 1.4) and age were correlated in AKU males and females. Figure 5.17 demonstrates the lumbar (L1-L3) QCT T-score and age in males and females. A negative statistically significant correlation ($r= -0.682$, $p<0.01$) was found in both males and females. Independent t-tests revealed no significant differences between the lumbar QCT T-score in males and females ($p>0.05$). The next set of analysis looked at the correlation between SUVm with QCT T-score. Figure 5.18 demonstrates a negative statistically significant correlation between the lumbar (L1-L3) QCT T-score with the average lumbar IVD SUVm in males and females ($r= -0.470$, $p>0.05$). This reveals that normal BMD T-scores are associated with low IVD SUVm, and low BMD T-scores are associated with higher IVD SUVms.

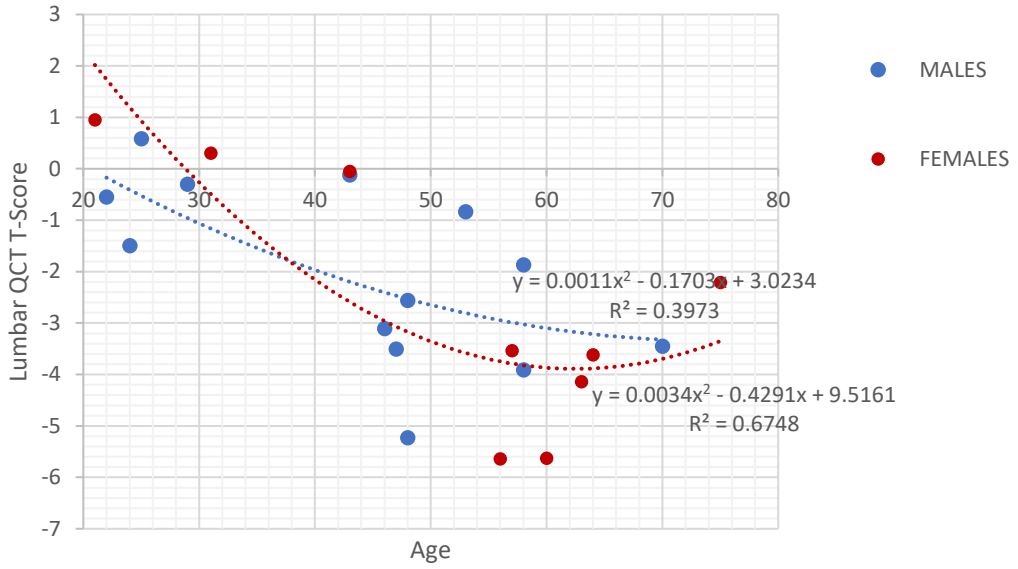

Figure 5.17 Scatter graph demonstrating correlation between lumbar (L1-L3) Quantitative Computer Tomography T-score and age in males and females (visit 1). Negative statistically significant correlation (r= -0.682, p<0.01).

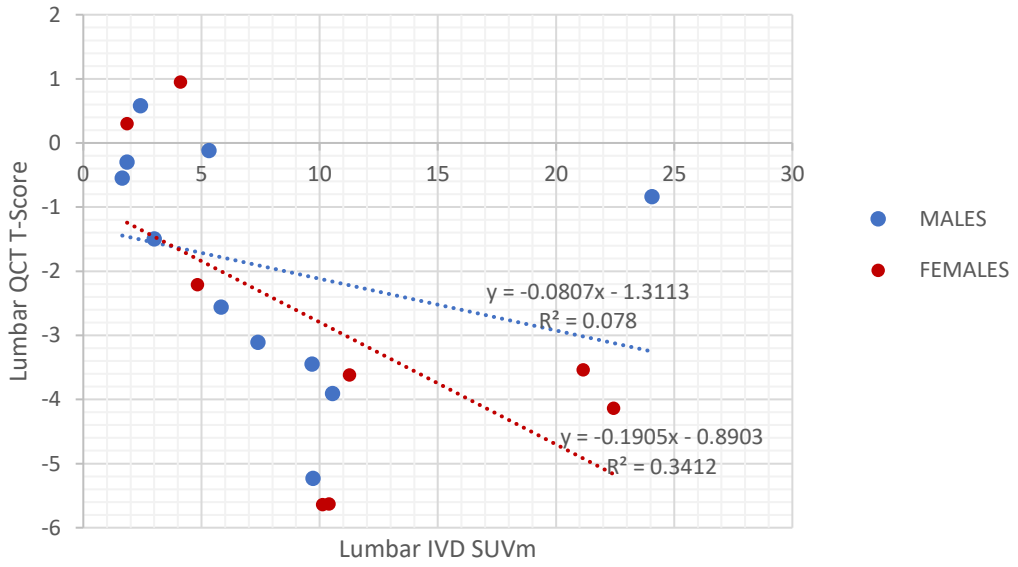

Figure 5.18 Scatter graph demonstrating correlation between lumbar (L1-L3) Quantitative Computer Tomography T-score and the average lumbar IVD SUVm in males and females (visit 1). Negative statistically significant correlation (r= -0.470, p<0.05).

Figure 5.19 demonstrates the correlation between the lumbar QCT T-score and the average lumbar vertebrae SUVm. Interestingly a positive statistically significant correlation was found between lumbar QCT T-score and lumbar vertebrae SUVm in both males and females (r=0.735, p<0.01) (Figure 5.19). Low lumbar QCT T-scores are associated with low lumbar vertebrae SUVm suggesting that patients with low bone density in the vertebrae have low uptake of ^{18}F in that region.

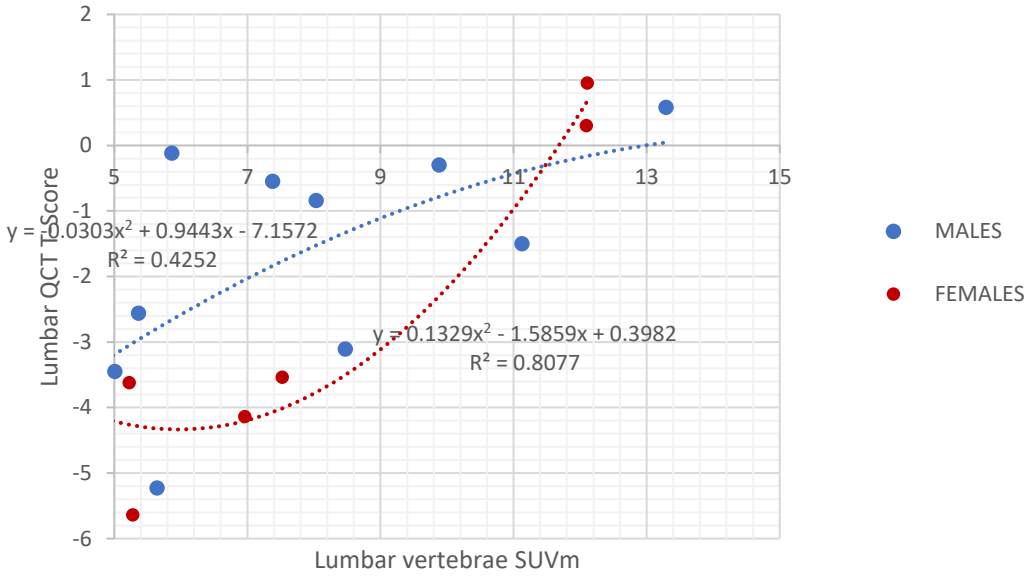

Figure 5.19 Scatter graph demonstrating correlation between lumbar (L1-L3) Quantitative Computer Tomography T-score and the average lumbar vertebrae SUVm in males and females (visit 1). Positive statistically significant correlation (r= -0.735, p<0.01.

5.3.6 FEMUR QUANTITATIVE COMPUTER TOMOGRAPHY

The femur QCT was also performed on the AKU patients. Figure 5.20 demonstrates a comparison between lumbar spine and femur T-scores with age. Negative statistically significant correlations with age can be seen in both the lumbar spine ($r=-0.682$, $p<0.01$) and femur ($r=-0.757$, $p<0.01$). Notably the femur T-scores are consistently higher than the lumbar spine T-scores across all ages. Paired t-test revealed a significant difference ($p<0.01$) between the spine QCT T-score and the femur QCT T-score.

A positive statistically significant correlation was identified between spine QCT T-scores and femur QCT T-scores ($r=0.718$, $p<0.01$) demonstrating that they both follow the same trend (Figure 5.21).

The following correlations are equivalent to what was compared with the lumbar T-scores. Figure 5.22 demonstrates a negative statistically significant correlation between Femur T-score and the average lumbar IVD SUVm in both males and females ($r= -0.642$, $p<0.01$) as seen in Figure 5.18, ochronosis being the common factor. A positive statistically significant correlation was found when correlating the femur QCT T-score with the average lumbar vertebrae SUVm in both males and females ($r=0.503$, $p<0.05$) (Figure 5.23) as seen in Figure 5.19, the amount of bone being the common factor.

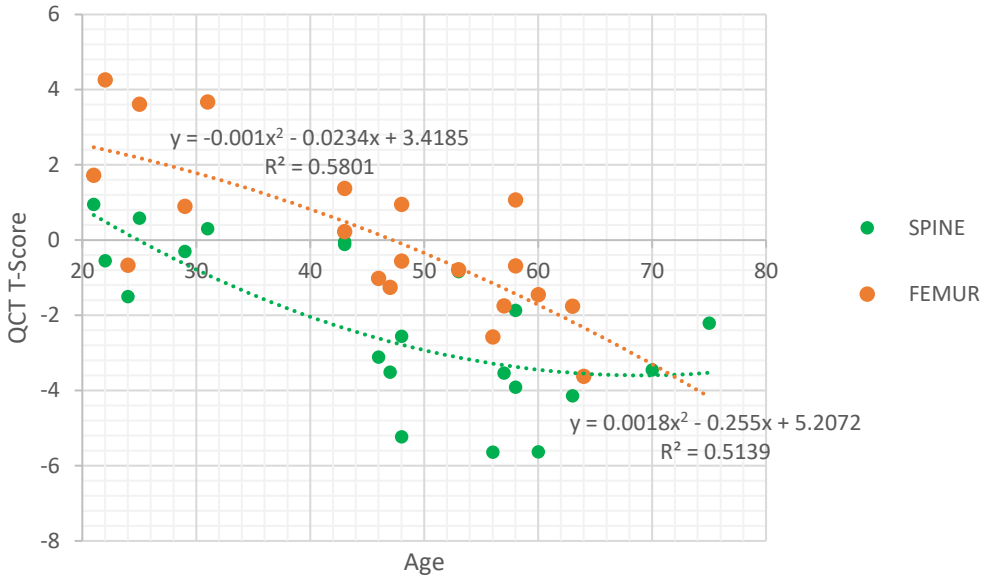

Figure 5.20 Scatter graph demonstrating a correlation between lumbar spine and femur QCT T-score with age (visit 1). Negative statistically significant correlations identified; spine (r=-0.682, p<0.01), femur (r=-0.757, p<0.01).

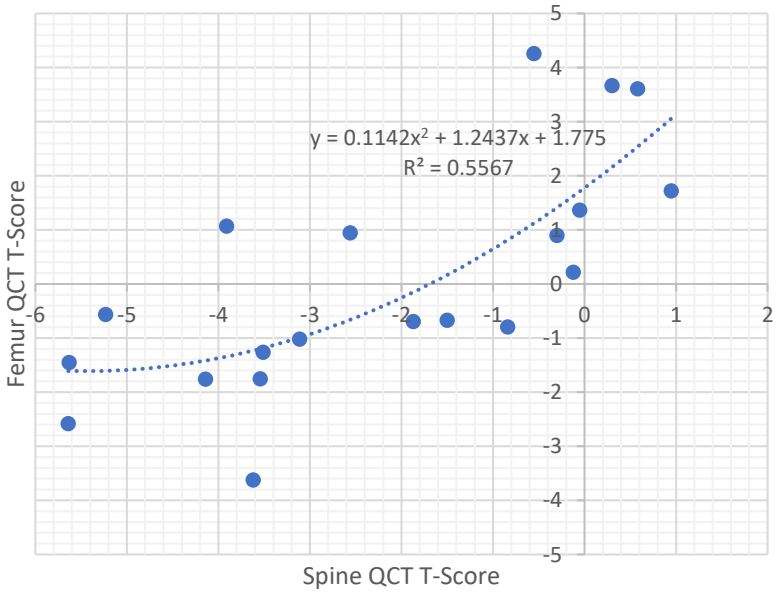

Figure 5.21 Correlation between spine and femur QCT T-scores (visit 1). Positive statistically significant correlation identified (r=0.718, p<0.01).

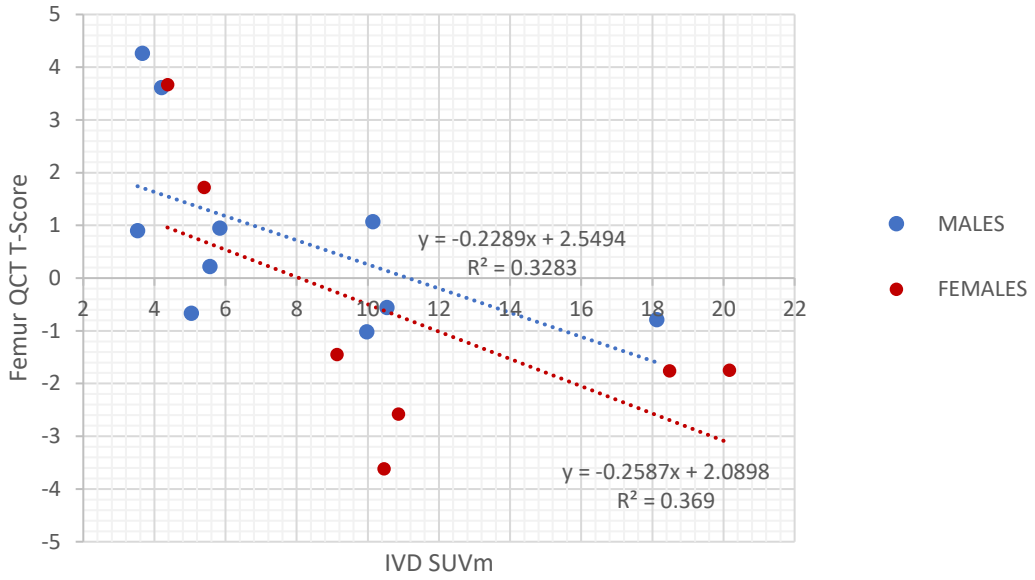

Figure 5.22 Scatter graph demonstrating correlation between femur QCT T-score and the average lumbar IVD SUVm in males and females (visit 1). Negative statistically significant correlation (r= -0.642, p<0.01).

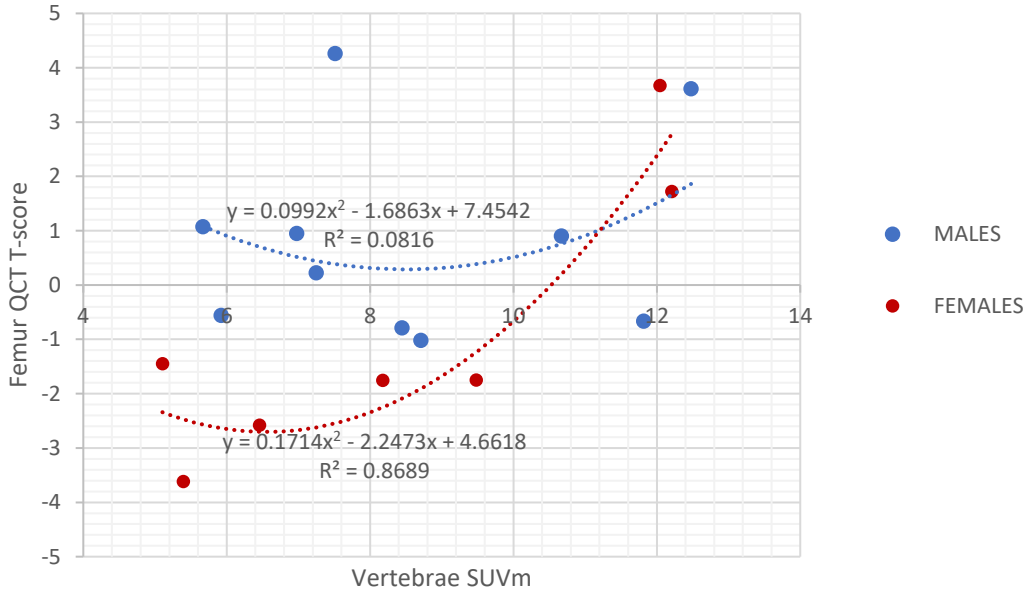

Figure 5.23 Scatter graph demonstrating correlation between femur QCT T-score and the average lumbar vertebrae SUVm in males and females (visit 1). Positive statistically significant correlation (r= 0.503, p<0.05).

5.3.7 C-TERMINAL TELOPEPTIDE 1 (CTX-1) BONE MARKER

Serum CTX-1 (ug/L) is a marker of bone resorption and is a by-product of collagen degradation. This section looks to see if there is any correlation between CTX-1 and vertebrae and IVD SUVm. Firstly, Figure 5.24 demonstrates the correlation between CTX-1 and age in males and females of which no statistically significant correlation was identified ($r=0.0008$, $p>0.05$). Independent t-tests revealed no significant difference between CTX-1 measurements in males and females ($p>0.05$).

Figure 5.25 demonstrates the correlations between CTX-1 measurements and the spine and femur QCT T-scores. No correlation was identified in both the spine ($r=0.148$, $p>0.05$) and femur ($r=0.110$, $p>0.05$) when QCT T-score was correlated with CTX-1 concentration. No statistically significant correlations were identified when correlating CTX-1 with the average lumbar and thoracic IVD SUVm in males and females ($r=0.243$, $p>0.05$) (Figure 5.26). No correlation was observed between CTX-1 concentration and the average lumbar and thoracic vertebrae SUVm in males and females ($r=0.225$, $p>0.05$) (Figure 5.27).

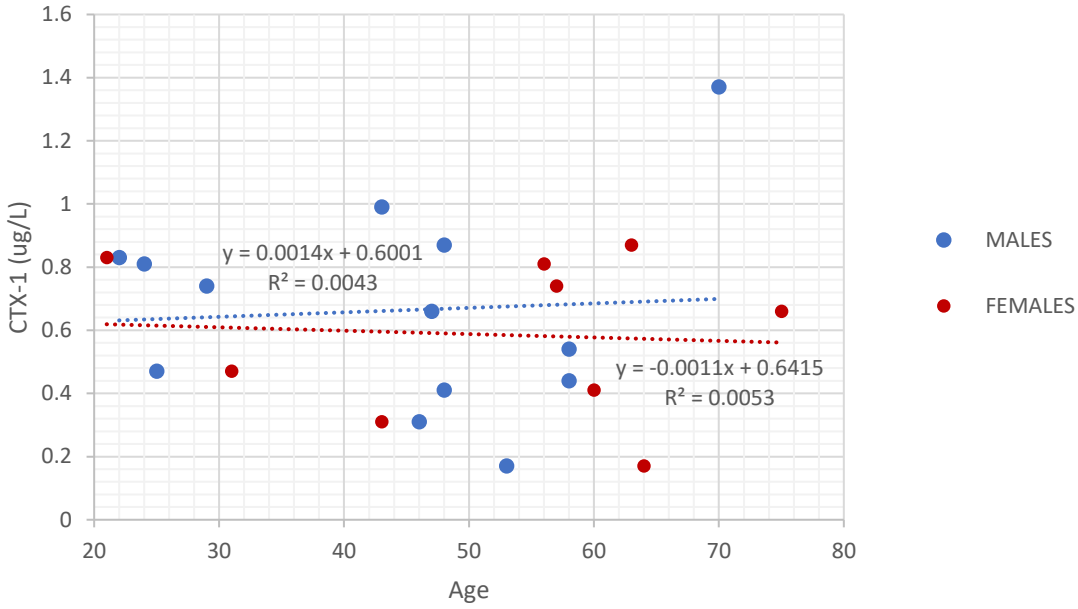

Figure 5.24 Scatter graph demonstrating the correlation between serum CTX-1 with age in males (R^2= 0.004) and females (R^2= 0.005) for visit 1. No correlation was observed (r=0.0008, p>0.05).

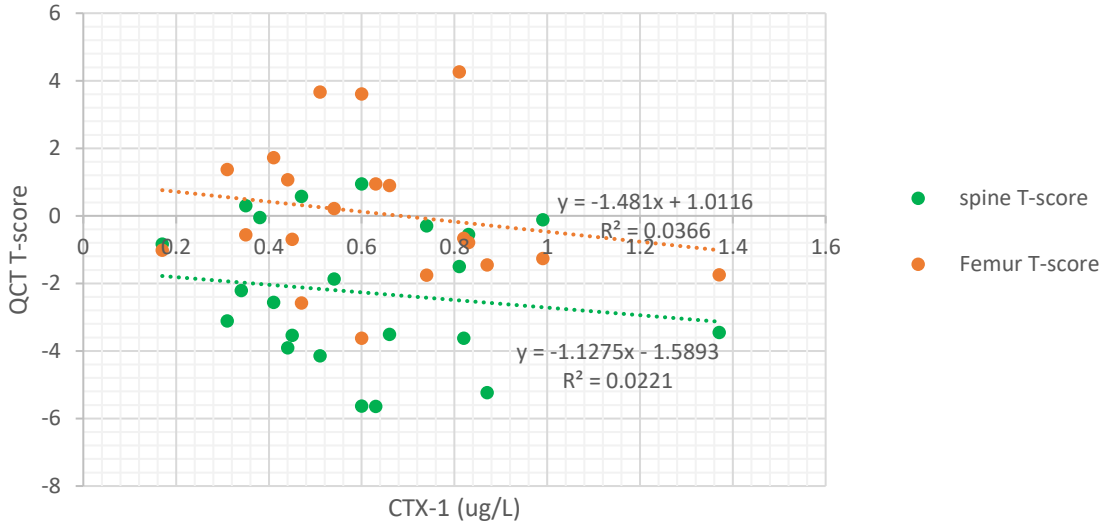

Figure 5.25 Scatter graph demonstrating the correlation between spine and femur T-scores with CTX-1 bone resorption marker. No correlations identified between spine QCT score and CTX-1 (r=0.148, p>0.05), and femur QCT T-score and CTX-1 (r=0.110, p>0.05).

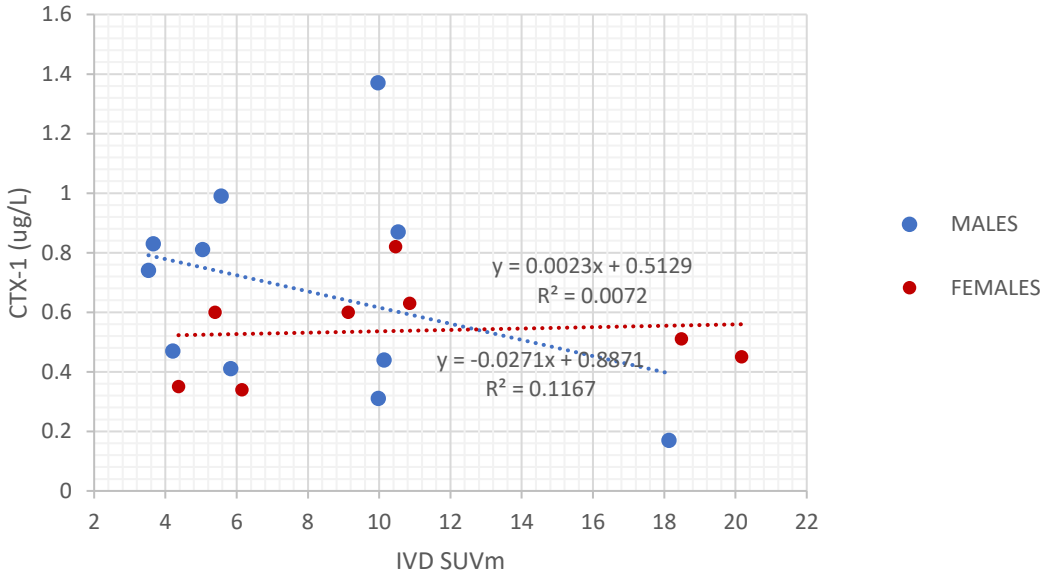

Figure 5.26 Correlation between CTX-1 and average lumbar and thoracic IVD SUVm in males and females at visit 1. No statistically significant correlation observed in both males and females (r=0.243, p>0.05).

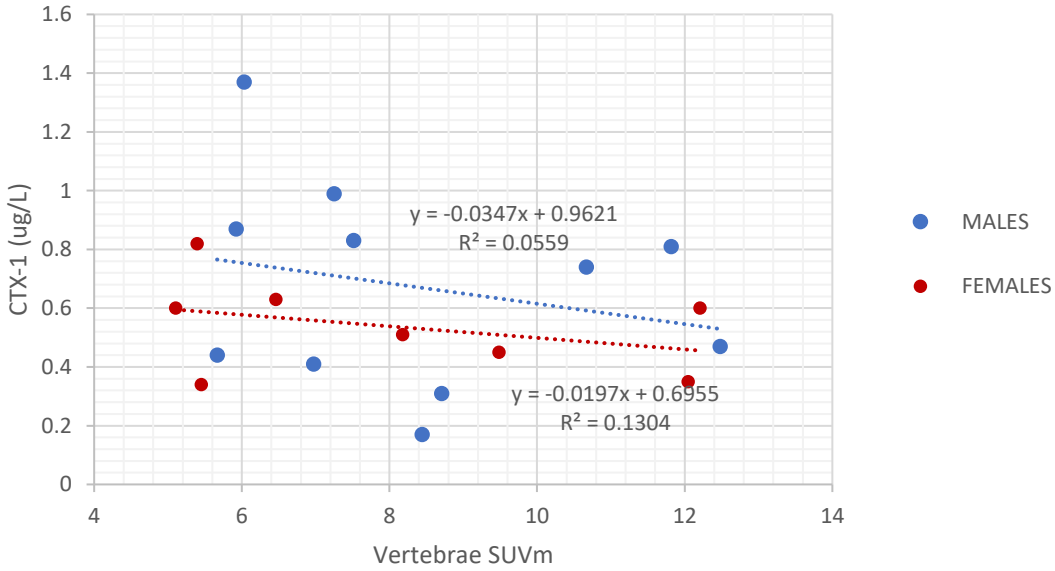

Figure 5.27 Correlation between CTX-1 and average lumbar and thoracic vertebrae SUVm in males and females at visit 1. No statistically significant correlation observed in both males and females (r=0.225, p>0.05).

5.3.8 LUMBAR AND THORACIC PAIN SCORES

As part of the NAC patient questionnaire, the NAC patients are asked to score pain in the lumbar and thoracic spine on a scale of 0-10, where zero equals no pain and ten equals severe pain. The lumbar and thoracic pain scores were correlated with age (Figure 5.28). Positive statistically significant correlation was observed between lumbar pain score and age ($r=0.584$, $p<0.01$). The correlation between thoracic pain score and age also shows the same trend however was not statistically significant ($r=0.441$, $p>0.05$). Low pain scores correlate with the younger patients, pain can be seen increasing with age up to around the age of 50-60 years of age. The polynomial trend line demonstrates that pain decreases in the oldest patients. Paired t-tests revealed a significant difference between lumbar and thoracic pain scores ($p<0.01$) suggesting that AKU patient's lumbar spine is affected to a higher extent compared to the thoracic spine.

Pain scores were correlated with IVD and vertebrae SUVms. Figure 5.29 demonstrates a positive statistically significant correlation ($r=0.601$, $p<0.01$) between lumbar pain score and the average lumbar IVD SUVm. Low lumbar pain scores are associated with low lumbar IVD SUVms. Lumbar pain can be seen increasing with increasing lumbar IVD SUVms before plateauing towards the higher SUVms. Lumbar pain can then be seen reducing in the highest SUVms (Figure 5.29).

Figure 5.30 demonstrates a positive statistically significant correlation ($r=0.608$, $p<0.01$) between thoracic pain score and the average thoracic IVD SUVm. Interestingly when the lumbar and thoracic pain scores were correlated with lumbar

and thoracic vertebrae SUVms the opposite trend was seen. Figure 5.31 demonstrates a negative statistically significant correlation between lumbar spine pain score and the average lumbar vertebrae SUVm (r= -0.587, p<0.05). Figure 5.32 also demonstrates a negative correlation between thoracic pain scores and thoracic vertebrae SUVm however this was not significant (r=-0.491, p>0.05). This was also the trend seen previously when the total clinical score and T-AT scores were correlated with IVD and vertebrae SUVm. A positive correlation was observed in both the total clinical score and the T-AT score with IVD SUVm (Figures 5.11 and 5.13), and negative correlations were observed when correlating these scores with vertebrae SUVm (Figures 5.12 and 5.14).

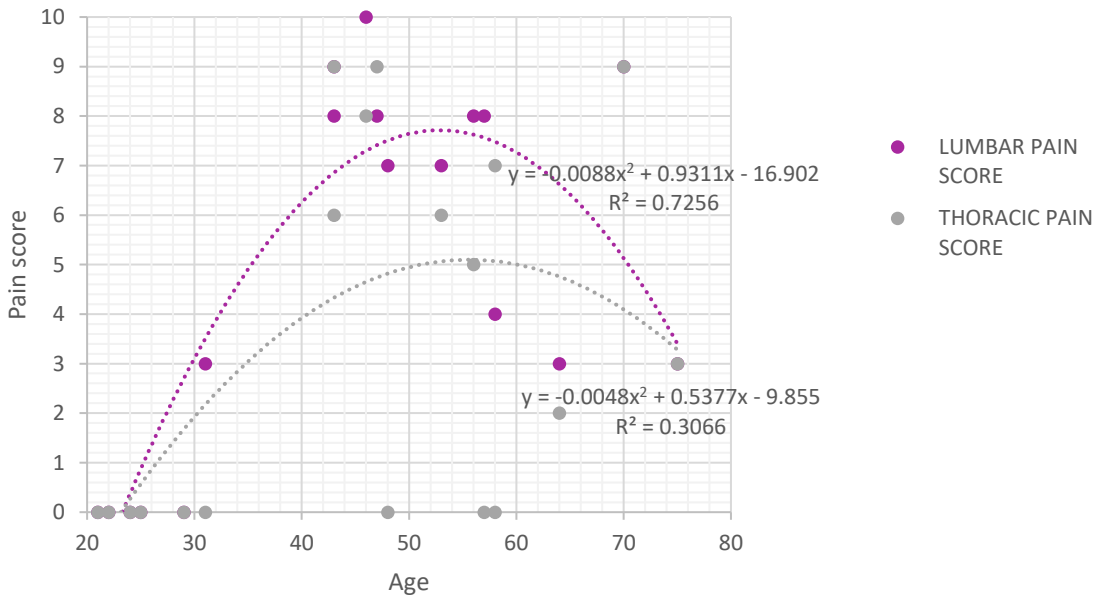

Figure 5.28 Correlation between the lumbar and thoracic pain scores with age at visit 1. Positive statistically significant correlation was observed between lumbar spine pain score with age (r=0.584, p<0.01). No statistically significant correlation was observed between thoracic pain score and age (r=0.441, p>0.05).

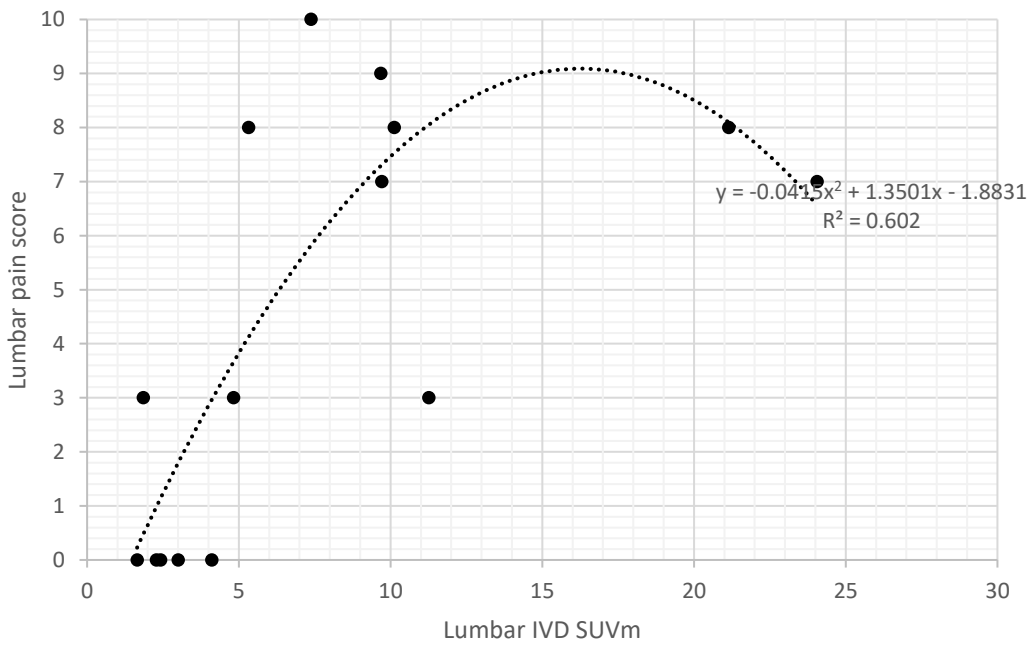

Figure 5.29 Correlation between average lumbar IVD SUVm with lumbar pain score at visit 1. Positive statistically significant correlation was observed (r=0.601, p<0.01).

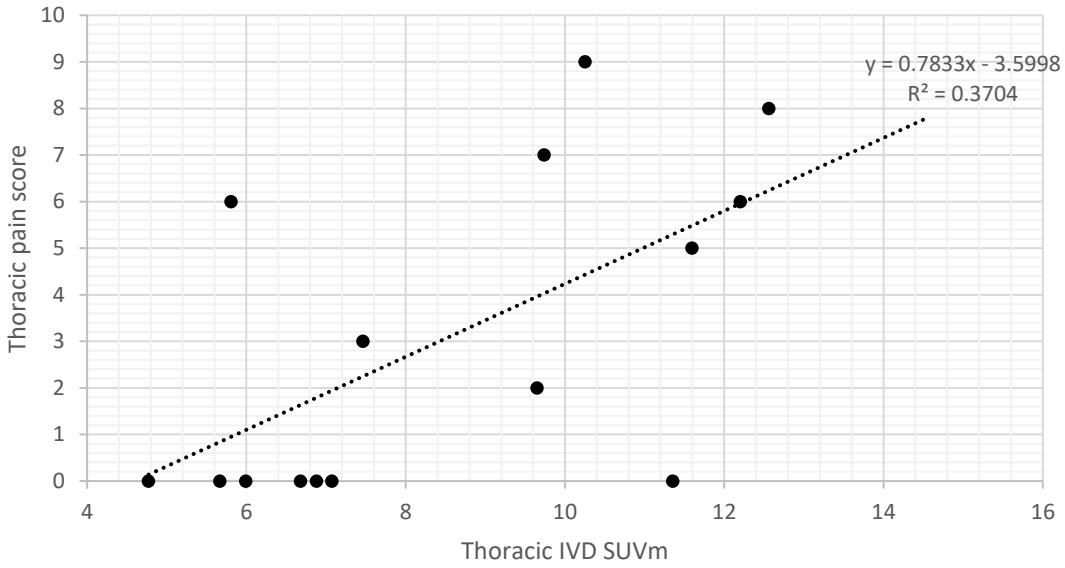

Figure 5.30 Correlation between the average thoracic IVD SUVm with thoracic pain score at visit 1. Positive statistically significant correlation was observed (r=0.608, p<0.01).

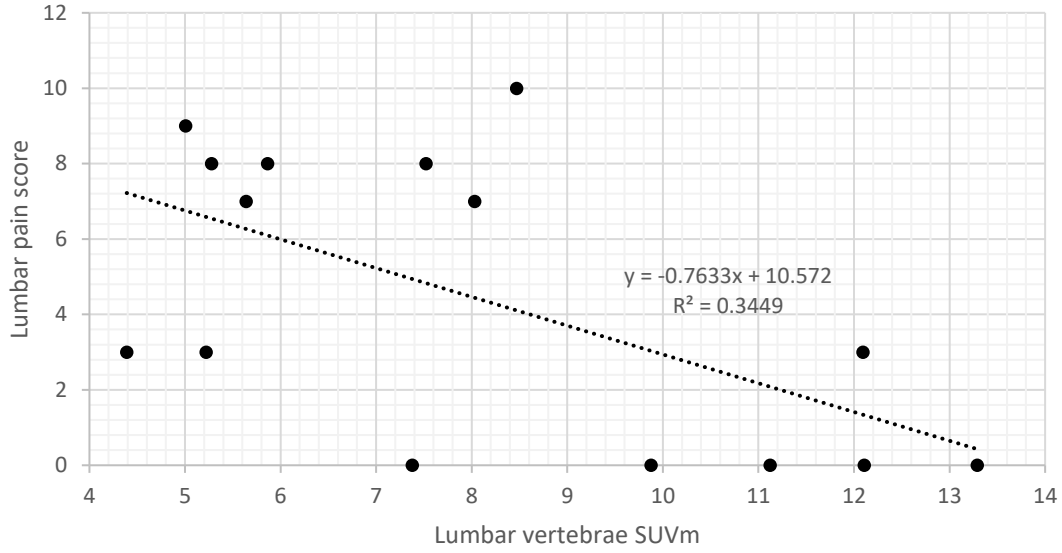

Figure 5.31 Correlation between average lumbar vertebrae SUVm with lumbar pain score at visit 1. Negative statistically significant correlation was observed (r=-0.587, p<0.05).

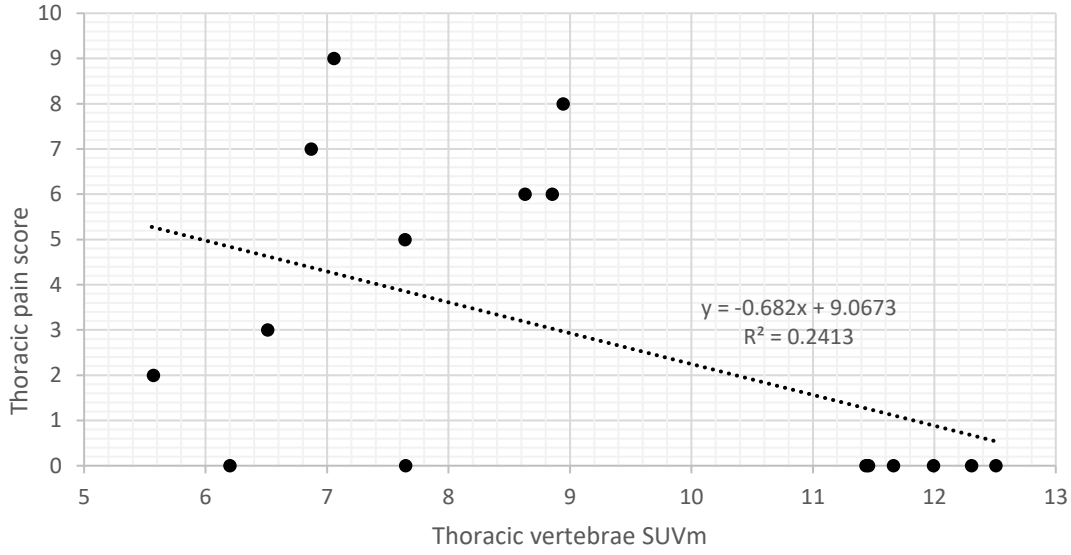

Figure 5.32 Correlation between average thoracic vertebrae SUVm with thoracic pain score at visit 1. Negative statistically significant correlation was observed (r=-0.584, p<0.01).

5.4 DISCUSSION

This chapter aims to assess the progression of spinal arthropathy, over a period of five years, in response to nitisinone, the potentially disease modifying therapy monitored by ^{18}F-NaF SUVm.

5.4.1 COMPARISON BETWEEN LUMBAR AND THORACIC VERTEBRAE AND IVD SUVms

In this chapter, the analysis described in Chapter 4 has been repeated on a different patient group, this chapter reporting on the NAC patients and Chapter 4 reporting on the SONIA 2 patients. The main difference between the two patient groups being that the NAC patients included in this analysis have attended the NAC 5 times, each with a year in between, compared to just 2 visits for SONIA 2 (with one year in between). Another main difference is that all the NAC patients have been prescribed nitisinone (2mg daily) in contrast to the SONIA 2 patients where half received 10mg of nitisinone in a blinded design. This chapter aims to look at the longitudinal change in SUVm over a period of five years in response to nitisinone.

When looking at the comparison between the lumbar and thoracic vertebrae and IVDs in the NAC patients (Figure 5.1) the results were slightly different compared to the SONIA 2 patients (Figure 4.9). For the SONIA 2 patients the mean SUVm for the vertebrae was 7.4, and for the IVDs was 11.6 with significant differences identified at every level (except T1/ T1/T2). For the NAC patients, no significant differences were found between the vertebrae and IVDs at every level. The mean SUVm across the vertebrae was 8.2, and the mean SUVm across the IVDs was 9.0. The proposed reason for the similar results between the SUVm of the vertebrae and IVDs in the NAC

patients may be due to the age range of the patients. In the SONIA 2 patient group, 41 patients were analysed (16 females, 25 males, mean age 51 SD±10.9, range 30-68), in the NAC patient group, 22 patients were analysed (9 females, 13 males, mean age 47, SD±16.05, range 21-75). The age range of patients in the NAC patient group starts almost 10 years younger (21 years compared to 30 in the SONIA 2). As identified the youngest patients have low IVD SUVms (Figures 4.12, 4.13, 5.3 and 5.4) and high vertebral SUVms (Figures 4.10, 4.11, 5.5 and 5.6). It is proposed that these younger patients have resulted in the means of the vertebrae and IVDs to fall closer together. The SONIA 2 patient age range starts from the age of 30, by the age of 40 the SUVm are almost 3 times that of the youngest patients, with almost double the number of patients in this group.

5.4.2 ANNUAL CHANGE IN SUVm IN THE VERTEBRAE AND IVDs

The main purpose of this chapter was to look at the annual change in SUVm over a period of 4 years. Figure 5.2 demonstrates the mean AKU lumbar and thoracic vertebrae and IVD SUVm across the 5 visits. It is evident that there is very little change in SUVm across the 5 visits for the lumbar and thoracic vertebrae and IVDs. Paired t-tests revealed no statistically significant differences between V1 and V5 in both lumbar and thoracic IVD and vertebrae SUVms. This supports what was found in the previous chapter where there was very little change in SUVm over a period of 1 year. At the very most nitisinone is thought to arrest ochronosis and or slow progression of the disease, it is widely agreed that it is very unlikely for nitisinone to reverse ochronosis. Figure 5.2 demonstrates small changes in SUVm across the visits with a

small reduction seen in the lumbar vertebrae, thoracic vertebrae and thoracic IVDs from V1 to V5. Unfortunately, a control group could not be used as a comparison longitudinally, as we only had data representative of a single visit for each control patient. The control patients were non-metastatic breast cancer patients that only had one scan to determine bony metastasis. This would have been useful as a control group would have provided an insight into normal change in SUVm across a period of 5 years. It is therefore not possible to comment on the effectiveness of nitisinone on SUVm in this group at this stage.

5.4.3 SUVm WITH AGE

The SUVm was plotted against age in the thoracic and lumbar vertebrae and IVDs for each of the five visits for comparison with the SONIA 2 data (Figures 5.3 – 5.6). Significant differences were identified between the AKU and control groups when comparing both the mean lumbar and thoracic IVD SUVms (independent t-test $p<0.01$ for both comparisons; Figures 5.3 and 5.4). This demonstrates that AKU IVD SUVms are significantly different to that of the control group. When analysing the difference between AKU mean lumbar and thoracic vertebrae SUVms compared to that of the control no significant differences were found (Figures 5.5 and 5.6). The trend with age for the AKU vertebrae SUVms supports the findings described in the previous chapter (Figure 4.10 and 4.11). The SUVm in AKU vertebrae decreases with age (Figures 5.5 and 5.6), supporting the idea that this is due to reduced bone mass with ageing (145). Reduced bone mass results in less hydroxyapatite for ^{18}F to bind to, therefore resulting in lower SUVms. Additionally this process could be

exacerbated by AKU as Aliberty, *et al*. (148) described ochronotic patients have an imbalance in bone metabolism, resulting in osteopenia and osteoporosis.

The SUVm in AKU IVDs also followed the same trend as what was found in the previous chapter; the inverted 'U' curve (Figures 4.12, 4.13, 5.5.3 and 5.4). From the age of 40 an exponential increase can be seen, which corresponds to the onset of arthropathy, of which the spine is widely affected. The results of this chapter support the suggested reason for this explained in Chapter 4. It is proposed that the increase in SUVm could be due to deposition of hydroxyapatite / calcium pyrophosphate dehydrate crystals of which the plateau corresponds to complete calcification of the IVD, and the reduction in SUVm corresponds to reduced turnover due to fusion of the vertebrae.

5.4.4 INDIVIDUAL CHANGES IN SUVm ACROSS THE FIVE VISITS

It is clear from Figure 5.2 that when the mean SUVms are plotted for the lumbar and thoracic vertebrae and IVDs across the five visits, little change is observed from one year to the next. Small fluctuations are observed, however the SUVm at V1, compared to the SUVm at V5 are very similar. As in Chapter 4, the next step was to plot individual patient changes to see if any trends could be identified with age. Figures 5.7 – 5.10 represent the individual changes across the five visits in the lumbar and thoracic vertebrae and IVDs in four age groups (20-31, 40-49, 50-59, 60+). These graphs try to shed light on what is happening to the SUVm over 4 years on an individual basis. No definitive trends were identified in any of the patients, generally the SUVms remain stable across the visits with very little change in the values. The lumbar and thoracic vertebrae SUVms are particularly stable (Figures 5.9 and 5.10)

reflecting a robust methodology. These results may also demonstrate the stabilisation of the disease by nitisinone. The SUVm of the lumbar and thoracic IVDs were slightly more variable. Especially so, in the 40-49 age group where the SUVm can be seen fluctuating, however when comparing the SUVms at V1 and V5, they were very similar. It was noted that if the SUVm was high at V1, it can be seen reducing across the visits in a few patients (Figure 5.7 C and D and 5.8 C). The effect of nitisinone on IVD and vertebrae SUVm cannot be confirmed due to fact that no AKU control group (no treatment group) was available for comparison to elucidate normal changes in SUVm across a period of 4 years. However, it can be commented that it would not be unreasonable to have expected an increase in IVD SUVm that reflects disease progression especially over a period of 4 years in those patients aged 40 and over. Vertebrae SUVm was expected to decrease as we have shown this occurs with age. Future work includes comparing these results with an AKU non-treatment group to investigate changes without nitisinone.

The systemic effects of nitisinone have been widely studied in terms of HGA levels in urine and in serum (44,45). Nitisinone (2.1 mg/day) has been shown to reduce urinary HGA down by 98% (from 5.1 to 0.125 g/day) and mean plasma HGA levels down by 95% from 5.74 to 0.306 mg/l (44). The SONIA 1 clinical trial revealed a clear dose response relationship between nitisinone and urinary HGA. The five dosages given were 0,1,2,4 and 8mg/day, with the 8mg dose reducing urinary HGA from 31.53mmol to 0.15mmol after 4 weeks (45). The long-term safety and efficacy of nitisinone has not fully been elucidated hence why the 2mg dose is routinely prescribed currently. HGA is the culprit molecule in AKU and nitisinone has been shown to effectively

reduce this down to negligible levels. This chapter has found no clear trends in SUVm over the four-year period in the 22 patients analysed. It is proposed that changes in response to nitisinone, measured by fluoride uptake in cartilage and bone, cannot be elucidated until a no treatment group is analysed. It may also be questioned whether four years is enough time to see any definite changes in ^{18}F uptake in the spine. Changes to cartilage and bone in AKU occur over many years, continued polymerisation of HGA in cartilage leads to osteoarthropathy. In terms of monitoring fluoride uptake as a measure of radioactivity and detecting osteoarthropathy, this method is capable of identifying arthritic changes in the spine. However, it could be proposed that for the effect of nitisinone on the spine to be elucidated, many more years of data will be required to assess the long-term effects. This method may demonstrate the effect of nitisinone on cartilage in AKU if a comparison was made between a group of patients that have been taking nitisinone for decades compared to a group of patients with no treatment. The increased SUVms may occur much younger in the non-treatment group compared to the treatment group.

5.4.5 CORRELATION BETWEEN SUVm AND CLINICAL AND ANATOMICAL THRESHOLD SCORES

The average lumbar and thoracic IVD and vertebrae SUVms were plotted against the total clinical score (described in section 2.4.9). A positive statistically significant correlation was identified ($r=0.585$, $p<0.01$) between the total clinical score and the average lumbar and thoracic IVD SUVm before plateauing at the higher total clinical scores (Figure 5.11). This demonstrates that higher IVD SUVms are associated with

higher total clinical scores. In Chapter 3 it was reported that the total clinical score had a positive correlation with age (Figure 3.15). Additionally, in Chapter 4 it was reported the age-related trend in IVD SUVm (Figure 4.12 and 4.13) that occurs with disease progression (the inverted 'U' curve) where SUVm increases up to around the age of 40 then stabilises and then reduces back down in the oldest patients. This trend was proposed to be due to calcification of the IVDs that occurs with disease progression. These two previous findings are reflected in these results (Figure 5.11). The patients with the highest total clinical scores are associated with the oldest patients as the more joints are affected. The lowest IVD SUVms and low clinical scores are associated with the younger patients less affected by the disease. This trend was also observed when correlating the total anatomical threshold score (explained in section 2.4.8) with IVD SUVm (Figure 5.13) suggesting that both the clinical and anatomical threshold methods are robust and demonstrate the same trend.

Interestingly, the opposite trend was seen when plotting vertebrae SUVms with the total clinical score. A negative statistically significant correlation was observed when correlating the total clinical score with the average lumbar and thoracic vertebrae SUVm (Figure 5.12, $r=-0.762$, $p<0.001$) demonstrating that high vertebrae SUVms are associated with low total clinical scores, and these patients were identified as the youngest. This supports what was described in Chapter 4, where a reduction in the mean lumbar and thoracic vertebrae SUVm was identified with age (Figures 4.10 and 4.11). The oldest patients have the highest total clinical scores and lower vertebrae SUVms. As described in Chapter 4, high SUVms in the vertebrae of younger patients reflects active bone remodelling that reduces with age, this is due to reduced bone

turnover and often reduced BMD with age. Again, the same trend was identified when correlating the average lumbar and thoracic vertebrae SUVm with the total anatomical threshold score (Figure 5.14).

5.4.6 SUVm WITH LUMBAR SPINE AND FEMUR QCT T-SCORE

It is widely recognised that changes in cartilage composition as seen in AKU have direct implications to bone. QCT was therefore performed on these patients to assess BMD. In AKU it is proposed that chronic arthritis can impair bone architecture which then may predispose AKU patients to fractures (89). Aliberti *et al*. (148) reported an imbalance in bone metabolism in 7 AKU patients, leading to osteopenia and osteoporosis. It was hypothesised that HGA deposition in bone matrix and osteocytes may play a pathophysiological role in accelerating bone loss in AKU (148).

QCT measures BMD using an X-ray computed tomography scanner containing a calibration standard to convert Hounsfield units into BMD values. The sites most commonly measured to determine BMD are the lumbar spine and hip (95). QCT has the ability to spatially separate highly responsive cortical bone from less responsive trabecular bone. This is useful because osteoarthropathy affects the trabecular bone earlier and to a greater degree than cortical bone. QCT is therefore likely to detect low BMD earlier in the spine than DEXA. Artificially high BMD has been identified in DEXA reports of spinal arthropathy patients due to calcification and osteophyte formation, resulting in unusually high T-values (148). This is because DEXA estimates the amount of total mineral in the path of the X-ray beam in the region of L2-L4. This can be avoided in QCT as this method specifically measures volumetric trabecular

BMD and does not include the IVDs unlike DEXA (94). QCT imaging often results in lower T-scores than that of the DEXA in cases of spinal arthropathy due to the increased mineral content of the calcified IVDs and/or bony osteophtyes. The lower T-scores of QCT compared to DEXA may be due to a variety of factors such as the physiological effects of ageing and the menopause (that affects trabecular bone first), therefore QCT can detect changes earlier than DEXA (96). The size of the patient also affects DEXA scores as DEXA cannot exclude soft tissue, therefore obese patients have higher T-scores, volumetric measurements of QCT are not affected by size (94).

Although QCT has many benefits over DEXA it is important to note that QCT T-scores are not comparable to DEXA T-scores and are not used to diagnose osteopenia or osteoporosis from the WHO definition of T-scores (a DEXA T-score of -2.5 equates to a QCT T-score of -3.4) (96). At present DEXA is the only modality accepted as the leading method in clinical decision making. However, as discussed QCT may provide a more accurate measure of BMD in patients with spinal arthropathy in AKU. This chapter explores the trends between QCT T-score and SUVms as it was proposed that low BMD may be the reason for low SUVms in the vertebrae a result of less hydroxyapatite available for ^{18}F to bind to.

Firstly, a negative statistically significant correlation was identified between the lumbar spine QCT T-score with age ($r= -0.682$, $p<0.01$) (Figure 5.17). Independent t-test revealed no significant difference between the lumbar QCT T-scores of males and females ($p>0.05$). It is widely agreed that bone deteriorates in composition, structure and function with age. Peak BMD is reached around the age of 20 in women and slightly older in men, after this bone turnover continues at a slower rate resulting in

a steady reduction in BMD (145,146). Lumbar spine QCT and femur QCT T-scores were also found to correlate well ($r=0.718$, $p<0.01$) (Figure 5.21) demonstrating that both anatomical areas of obtaining BMD scores demonstrate the same trends. However, when lumbar spine and femur QCT T-scores were plotted with age, femur T-scores were consistently higher than T-scores from the lumbar spine (Figure 5.20) in AKU patients. When the spine QCT T-scores were statistically compared to femur QCT T-scores a significant difference was found (paired t -test $p<0.01$). This supports the idea that the spine is one of the first areas affected in AKU and is often associated with pain. Discordance in T-scores has been discussed in the literature between the hip and spine. Trabecular bone (typical of the lumbar spine) is known to have a more rapid rate of deprivation compared to cortical bone (typical of the proximal femur) which may explain the increased T-scores observed in the femur compared to the hip.

In terms of SUVm correlations, a negative statistically significant correlation was observed between lumbar spine QCT T-score with the average lumbar IVD SUVm ($r= -0.470$, $p<0.05$). Low lumbar IVD SUVms are associated with high lumbar QCT T-scores, which follows a negative trend (Figure 5.18). This is also the case when correlating the femur QCT T-score with the lumbar IVD SUVm (Figures 5.22) of which a negative statistically significant correlation was observed ($r= -0.642$, $p<0.01$). It is proposed that this effect is related to ageing as previously shown that young patients have high BMD compared to older patients (Figure 5.17). It has also been shown that the youngest patients have low IVD SUVms that increases with age before plateauing around middle age before decreasing back down in the oldest patients (Figures 4.12

and 4.13). It was expected that patients that have high BMD (i.e. the younger patients) will have low SUVms in the IVD as they will be less affected by the disease in terms of progression with age. The patients with low BMD (i.e. the older patients) will have higher SUVms due to calcification and spinal degeneration.

When analysing vertebrae SUVms, the opposite trend was seen. Positive statistically significant correlations were identified when the lumbar vertebrae SUVm was correlated with both lumbar QCT T-score ($r= 0.735$, $p<0.01$) and femur QCT T-score ($r=0.503$, $p<0.05$) (Figures 5.19 and 5.23 respectively). This demonstrates that low BMD correlates with low SUVms and high BMD correlates with high SUVms. It is proposed that reduced BMD reflects reduced hydroxyapatite available for ^{18}F to bind this therefore results in lower SUVms. It was also described in Chapter 4 that SUVm reduces with age in the vertebrae (Figures 4.10 and 4.11). BMD also reduces with age so it is proposed that this trend reflects the ageing vertebrae.

5.4.7 C-TERMINAL TELOPEPTIDE 1 (CTX-1) BONE MARKER

In recent year's extracellular components of bone matrix have been identified and categorised as either markers of bone formation or resorption that can be used to reflect the rate of bone turnover. Many clinical investigations have provided evidence that these biomarkers correlate with the rate of bone loss and fracture risk demonstrating their utility in biomedical research and clinical practice (152). The WHO has defined osteoporosis as a BMD measured by DEXA, as 2.5 standard deviations (SD) or more below that of the mean peak bone mass of premenopausal females (T-score ≤ -2.5 SD). DEXA T-scores are used to define osteopenia and

osteoporosis however, as discussed in 5.4.7 they may not always represent true BMD. Markers of bone resorption could therefore be used as an additional tool alongside DEXA to report on bone turnover (153).

The majority of bone resorption markers are degradation products of collagen. C-terminal telopeptide 1 (CTX-1) of type I collagen is the marker of choice for bone resorption. CTX-1 is generated by cathepsin K activity. Cathepsin K is a major catalytic enzyme expressed and secreted by osteoclasts and plays a predominant role in in the degradation of type I collagen (153). A negative correlation has been reported between bone turnover markers and BMD in the literature (152). No correlation was identified in this chapter when the femur and spine QCT T-scores were correlated with CTX-1 (Figure 5.25) suggesting that there is no correlation between BMD and CTX-1 concentration. No correlation was identified between CTX-1 and the average lumbar and thoracic vertebrae and IVD SUVm (Figures 5.26 and 5.27). It was proposed that CTX-1 concentration would increase with age in AKU reflecting increased bone resorption with disease progression. Figure 5.24 demonstrates CTX-1 with age in males and females of which no correlation was identified ($r=0.0008$, $p>0.05$). Independent t-test revealed that there is no significant difference between CTX-1 concentration in males and females ($p>0.05$). An increase in CTX-1 concentration with an increase in IVD SUVm was also expected reflecting increased bone resorption due to spinal degeneration however no correlations were identified in this group of patients.

No correlation was identified between CTX-1 and vertebrae SUVms (Figure 5.27). High CTX-1 concentration was expected to be associated with lower vertebrae SUVms

as this is thought to reflect reduced bone turnover associated with ageing. This assumption seems sensible as increased bone resorption markers reflect reduced BMD, and reduced BMD is associated with reduced SUVm as there is less bone for fluoride to bind to. However, this trend is not obvious here. When analysing IVD SUVms against CTX-1, no correlation was identified (Figure 5.26). High CTX-1 concentrations were expected to be associated with low IVD SUVms. High IVD SUVms are associated with advanced spinal osteoarthropathy, and increased CTX-1 is representative of increased bone resorption. It was therefore expected that CTX-1 would correlate with high IVD SUVms for this reason, however this was not the case here.

There are many factors that affect the concentration of CTX-1. CTX-1 and other markers of bone resorption have been reported to exhibit marked circadian variation. Increased bone resorption occurs at night compared to a lower rate in the day. This variation is independent of age, gender, ethnicity, menopausal state, osteoporotic stage and antiresorptive therapy. The cause of circadian variation remains unknown but it has been speculated that calcium homeostasis is crucial (152). All bone markers are also significantly lower in a fed state, this may be due to several factors including the clearance rate of markers which may be partly explained by a variation in serum insulin (151). CTX-1 is therefore measured after fasting and tested early in the morning as and where possible. Bone turnover markers also varies with the menstrual cycle, where bone resorption is decreased during the luteal period and increased during the follicular phase. Fractures also increase levels of all bone markers and these may remain elevated for up to one year (151). Inter-patient

variability also proves a problem when comparing between patients as bone metabolism rates vary between males, females, pubertal stage, menopausal stage, as well as age. Antiresorptive therapy will also reduce CTX-1 concentration. All these factors should be taken into account when analysing the results.

In terms of AKU CTX-1 is used as an additional measurement reflecting bone turnover that can be used to compare between visits. This data is representative of the baseline visit pre-nitisinone, therefore these CTX-1 concentrations are not representative of the effect of nitisinone.

5.4.8 LUMBAR AND THORACIC PAIN SCORES

Clinical pain scores were extracted from the patient questionnaires at baseline (pre-nitisinone). The patients were asked to score pain on a scale of 0-10 where zero equals no pain, and ten equals severe pain, in the thoracic and lumbar spine. The spine has been described as the first region to experience pain in AKU. Pain was scored in both the lumbar and thoracic regions. Interestingly paired t-test revealed a significant difference between lumbar and thoracic pain scores. Figure 5.28 demonstrates that lumbar pain reaches higher pain scores, therefore suggesting that the lumbar spine is affected to a higher degree compared to the thoracic spine. This is thought to be due to the increased mechanical stress that the lumbar spine experiences.

An interesting correlation was identified with age in both the lumbar and thoracic pain scores that is proposed to be representative of spinal degeneration and progression with age (Figure 5.28). A positive statistically significant correlation was

identified between the lumbar pain score and age ($r=0.584$ $p<0.01$). With a polynomial trend line applied, pain can be seen increasing with age with the highest pain scores observed around the mid 40's, from here pain can be seen decreasing from around the mid 50's. This is representative of what was described in Figures 4.12 and 4.13 that demonstrates the trend between the IVD SUVm with age. In Chapter 4 an inverted 'U' trend was described between age and IVD SUVm where SUVm is low in the youngest patients, SUVm then increases up to around the age of 50 where it then stabilises before reducing back down in the oldest patients between 60 and 70 (Figures 4.12 and 4.13). It is proposed that Figure 5.28 pain scores reflect the trend in IVD SUVm with age. The reduction in both IVD SUVm and pain in the oldest patients reflects the end-point of spinal arthropathy which is spinal fusion that has been associated with reduced pain. To support this a positive statistically significant correlation ($r=0.601$, $p<0.01$) was observed between the lumbar IVD SUVm and lumbar pain scores (Figure 5.29). A positive statistically significant correlation was also identified between thoracic IVD SUVm and thoracic pain ($r=0.608$, $p<0.01$) (Figure 5.30). These graphs demonstrate that the highest SUVms are representative of calcified IVD and disc degeneration, this undoubtedly results in high pain scores.

In contrast, negative statistically significant correlations were observed between the lumbar and thoracic pain scores with vertebrae SUVms (Figure 5.31 and 5.32). Again, this supports what was described in Chapter 4 (Figures 4.10 and 4.11) where a reduction in SUVm can be seen with age. Therefore, the youngest patients have high SUVms reflecting active bone turnover and have low pain scores. Low SUVms have

been shown to be associated with older patients, with reduced bone turnover and increased pain.

5.4.9 SUMMARY

This chapter has confirmed the findings identified in Chapter 4, and confirmed the repeatability and validity of the SUVm methodology. This chapter has revealed differences between AKU and control SUVms in the spine. This was most strikingly observed in the IVDs where the SUVms were significantly higher than the control. The proposed explanation for this is that in AKU, deposition of calcifications in the IVDs occurs with disease progression, which levels out around the sixth decade due to reduced turnover seen in advancing spinal disease. The SUVm then reduces in the oldest patients due to spinal fusion. It has also been identified that bone metabolism in the spine of AKU patients is normal and in-line with age matched controls. Age related changes in the SUVms of AKU vertebrae were reported, where the SUVm reduces with age due to reduced bone turnover, and BMD with ageing. However, the longitudinal changes in SUVm in response to nitisinone were not significant and very small. It is proposed that four years on nitisinone may not be long enough to identify any changes in fluoride uptake, therefore for the effect of nitisinone on the spine to be elucidated, many more years of data will be required to assess the long-term effects. Additionally, when the SONIA 2 clinical trial is complete longitudinal data will be available on a non-treatment AKU group for comparison which is key to understanding if nitisinone is having an effect.

Positive correlations were described between IVD SUVm with the total clinical score and the T-AT scores, demonstrating that increased IVD SUVms represent disc degeneration which is related to age. The opposite negative trend was identified when correlating vertebrae SUVm with the total clinical score, total anatomical threshold score and pain scores demonstrating that high vertebrae SUVms are associated with active bone turnover in the youngest patients. High IVD SUVms were also associated with low QCT T-scores reflecting osteoarthritic spine with disease progression. The opposite was seen when correlating QCT T-scores with vertebrae SUVms where high vertebrae SUVms correlated with high T-scores. High vertebrae SUVms reflect active bone remodelling and normal BMD. The trend in spinal pain when correlated with IVD and vertebrae SUVms also confirmed what was described previously. An increase in spinal pain was associated with increased IVD SUVm up to around middle-age before plateauing and decreasing in the oldest patients. In contrast, a negative correlation was identified when correlating pain with vertebrae SUVm. Therefore, SUVm in the spine and IVDs could also be used as an indicator of pain.

5.4.10 FURTHER WORK

The next step will be to correlate the SONIA 2 SUVm data from Chapter 4 with other data extracted from the clinical trial site files such as urine and plasma HGA levels, spinal flexion and DEXA and Cobb angle measurements. This will determine if the SUVm measurements correlate well with other data that has been extracted from the SONIA 2 patients.

6.0 SUVm CORRELATION WITH SONIA 2 CLINICAL DATA

6.1 INTRODUCTION

Chapter 4 demonstrates the utility of SUVms to identify active arthropathy in the spine and to quantify disease state in the SONIA 2 patient group. Chapter 5 demonstrates the repeatability and validity of the method in the NAC patient group, as well as reported some interesting correlations in this patient group with other data obtained at the NAC. This chapter aims to look at the correlations between the SONIA 2 SUVm data reported in Chapter 4 with other patient data obtained as part of the clinical trial at visit one (baseline; pre-nitisinone). Correlations made with other data obtained from the same patient group is important to analyse to observe if the data follows similar trends, this provides evidence of a robust methodology.

Serum and urine HGA levels were recorded at baseline (pre-nitisinone). Serum HGA (s-HGA) concentration provides a measure of HGA that is circulating around the body. Urine HGA (u-HGA) concentration provides a measure of HGA that is excreted out of the body. As explained previously HGA is the culprit molecule in AKU that is deposited in connective tissues resulting in ochronosis that ultimately leads to early onset osteoarthropathy.

Cobb angles are used to standardise spinal curvatures. Obtaining Cobb angles of thoracic kyphosis, lumbar lordosis and scoliosis provide the clinician with detailed information regarding the curvatures of the spine, and these can be assessed annually to observe if there are any changes. The spine has naturally three curvatures: cervical lordosis, thoracic kyphosis, lumbar lordosis. Normal thoracic kyphosis is said to range from 20-45 degrees, hyper kyphosis is defined as more than 45 degrees and the most common reason for this being osteoporosis (122). Lumbar

lordosis is characterised by increased inward curving of the lumbar spine. There is no definition of normal lumbar lordosis or is there a definition for lumbar hyperlordosis as many factors affect this angle such as muscular strength, flexibility and BMI (123). Scoliosis is defined as a lateral spinal curvature of 10 degrees or more to the right or left (124). Measurements of lumbar side flexion and cervical rotation measured in cm by the physiotherapist were also obtained to assess spinal flexibility.

6.2 DESIGN OF STUDY

6.2.1 PATIENT GROUP

41 adult patients (16 females, 25 males, mean age 51, SD±1.09, range 30-68) from the SONIA 2 clinical trial (see section 2.2.2) underwent a series of tests and examinations in 2014/15. This chapter is based on the baseline data obtained at visit 1 (pre-nitisinone). Each patient underwent ^{18}F-NaF PET/CT, X-ray, MRI and DEXA imaging. Physiotherapy assessments were carried out to assess spinal motion and flexibility and blood and urine was extracted to measure circulating and excreted HGA. These data were used to correlate with the SUVms reported in Chapter 4.

6.2.2 MEASURING THE SUVms

Hermes hybrid viewer (see section 2.5.1) was used to measure SUVms (section 2.5.2). The SUVm was obtained from the centre of three lumbar (L5, L3, L1) and three thoracic (T1, T6, T12) vertebral bodies, and from the centre of the corresponding IVDs below (L5-S1, L3/L4, L1/L2, T12/L1, T6/T7, T1/T2). The SUVms utilised in this chapter were obtained from the baseline visit; visit 1 (pre-nitisinone).

6.2.3 PATIENT DATA OBTAINED

The DEXA images were accessed on the PACS system at the RLBUHT computer and the data from visit 1 was recorded (for more information regarding DEXA see section 1.6.3.1). Table 1.4 demonstrates the WHO definitions of BMD. X-ray images were also accessed on the PACS system and the Cobb angles were measured using this software

(method explained in section 6.2.3.1 and 6.2.3.2). The physiotherapy measurements of lumbar side flexion and cervical rotation were obtained from the site files at the RLBUHT and visit 1 data was recorded. Urine and serum HGA levels for visit 1 were analysed in the biochemistry lab at the RLBUHT and were provided by the lab in an excel file.

6.2.3.1 X-RAY AND MRI COBB ANGLE MEASURMENTS

Whole body posterioanterior (PA) X-Ray view was selected to analyse scoliosis. Using the Cobb angle tool the end vertebrae of the curve were selected and lines were drawn to demarcate the vertebrae that lie at the upper and lower limits of the curve (the vertebrae that tilt the most towards the apex of the curve) (Figure 2.11A). The Cobb angle was automatically generated measuring the intersection of the two lines drawn.

Lateral X-ray view was selected to measure the thoracic kyphosis and lumbar lordosis Cobb angles. Using the Cobb angle tool, the lower border of the twelfth thoracic vertebrae (T12) and the upper border of the fourth thoracic vertebrae (T4) were selected (Figure 2.11B). The Cobb angle was automatically generated by measuring the intersection between the lines selected. Normal kyphosis ranges from 20-45 degrees, hyper kyphosis is defined as more than 45 degrees (122). Lumbar lordosis was measured from the lower border of the fifth lumbar (L5) vertebrae and the upper border of the first lumbar vertebrae (L1). Lumbar hyperlordosis is not defined by a Cobb angle (Figure 2.11B).

Thoracic kyphosis and lumbar lordosis Cobb angles were also measured on MRI (Figure 2.11C). The MRI whole spine was selected using the PACS and the methodology of measuring thoracic kyphosis and lumbar lordosis was exactly as described as above.

6.2.3.2 LUMBAR SIDE FLEXION AND CERVICAL ROTATION MEASUREMENTS

Lumbar side flexion was measured by a senior physiotherapist at the RLBUHT. The patient was asked to stand up straight against the wall with their feet 12 inches apart. Firstly, the distance was measured (in cm) between the tip of the middle finger to the floor with the patient standing up straight on both the right and left sides. The patient was then asked to side flex to the right with the physiotherapist applying over pressure to push the patient further into the range and the distance between the tip of the middle finger to the floor was measured again. This was then repeated on the left. The difference between the two measurements was calculated and this value reflects the passive lumbar side flexion of the patient in cm (126,127).

Cervical spine rotation was measured by a senior physiotherapist. The patient was asked to stand up straight against the wall with shoulders back in a neutral position with the head facing forwards. The distance between the gnathion of the chin to the lateral aspect of the acromion was measured with the head looking straight forward on both the right and left sides. The patient was then asked to look over to the right with the physiotherapist applying over pressure to push the patient further into the range, and this distance was re-measured. This was then repeated on the left side.

The difference between the two values was then calculated to obtain the value of passive cervical spine rotation (126,127).

6.2.3.3 SERUM AND URINE HGA

A fasting blood sample and acidified 24-hour urine sample (25mL of 5 N sulphuric acid added to 2.5 L urine collection bottle) were collected at visit 1 (pre-nitisinone). Blood samples were collected into plain serum tubes from all subjects in a fasting state, centrifuged and serum acidified with perchloric acid (5.8 M, at a ratio of 1:11). The acidified urine and serum were analysed for HGA using liquid chromatography tandem mass spectrometry methodology (LC-MS/MS). Serum HGA is HGA concentration (µmol/L), urine HGA is total HGA output in 24 hours (µmol/24hr).

6.3 RESULTS

6.3.1 SERUM HGA CORRELATIONS

AKU patients have elevated serum-HGA (s-HGA) concentrations compared to the reference range. The mean s-HGA (µmol/L) in the AKU group was 33.2 µmol/L at visit 1 (pre-nitisinone) compared to the reference range of <3.1 (154). Independent t-tests found no statistical significance between the s-HGA concentrations in males and females ($p>0.05$). There appears to be a weak positive correlation with age in both males and females, however this was not statistically significant ($r=0.290$, $p>0.05$) (Figure 6.1). Weak correlations were also identified between s-HGA (µmol/L) and the average lumbar and thoracic vertebrae SUVm ($r=0.0781$, $p>0.05$) with females having a slight negative correlation and males having no correlation (Figure 6.2).

Serum HGA (µmol/L) was also correlated with the average lumbar and thoracic IVD SUVm (Figure 6.3). This graph demonstrates more of an interesting trend where both males and females follow an inverted 'U' trend, with low s-HGA concentrations correlating with low and high IVD SUVms and the high s-HGA concentrations correlating with the middle of the range IVD SUVms. This correlation however was not significant ($r=0.0174$, $p>0.05$)

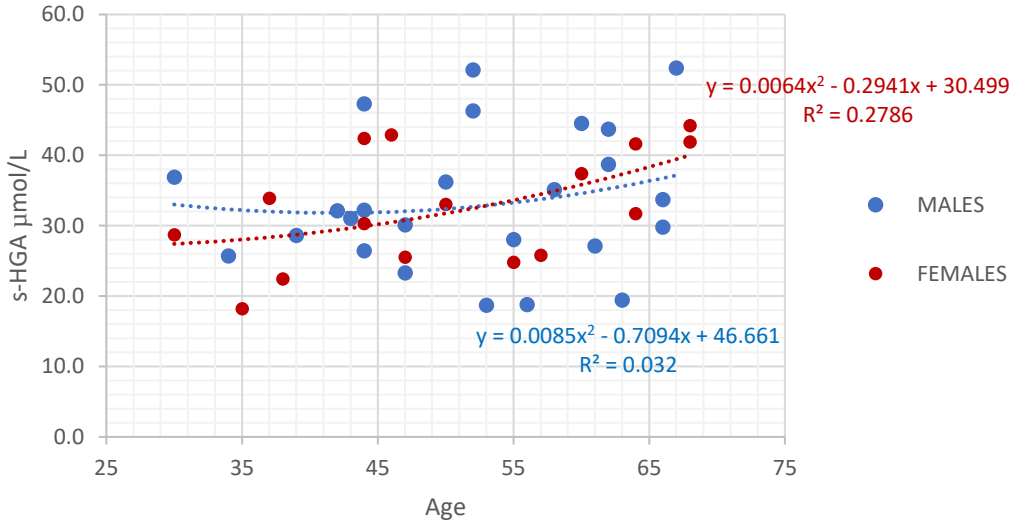

Figure 6.1 Correlation between serum HGA pre-nitisinone (µmol/L) with age in males and females at visit 1. Weak positive correlation identified in males (R^2=0.032) and females (R^2=0.279). No statistically significant correlation identified (r=0.290, p>0.05).

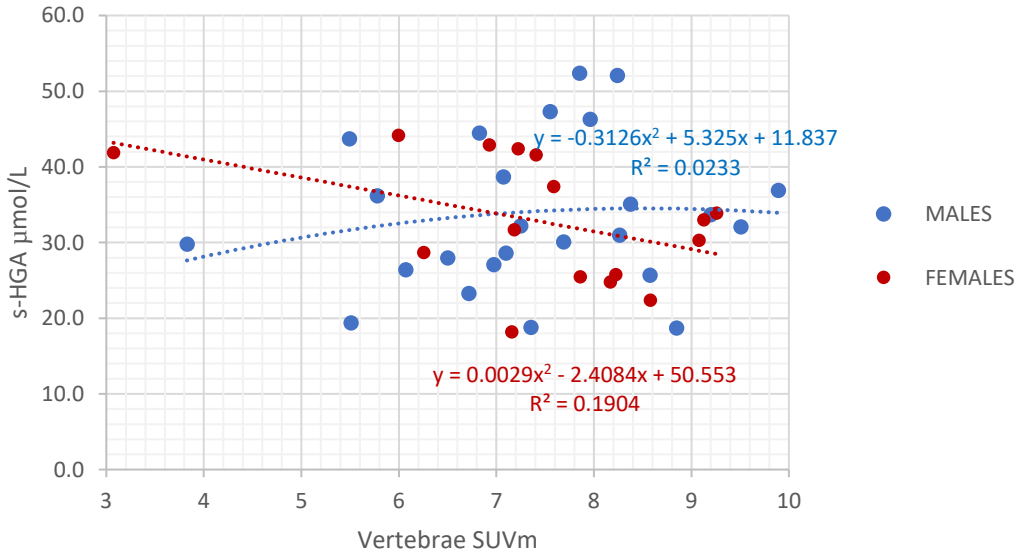

Figure 6.2 Correlation between serum HGA µmol/L (pre-nitisinone) with the average lumbar and thoracic vertebrae SUVm at visit 1 in males and females. No correlation in males (R^2=0.02) and weak negative correlation in females (R^2=0.19). No statistically significant correlation identified (r=0.0781, p>0.05).

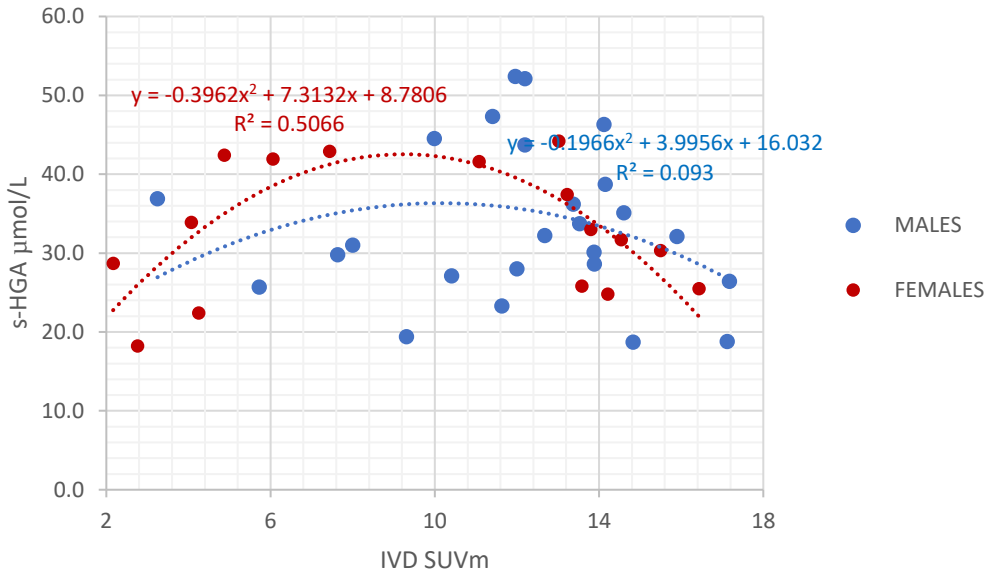

Figure 6.3 Correlation between serum HGA µmol/L (pre-nitisinone) with the average lumbar and thoracic IVD SUVm at visit 1 in males and females. Correlation coefficient in males (R^2=0.09) and females (R^2=0.51). No statistically significant correlation identified (r=0.0174, p>0.05).

6.3.2 TOTAL URINE HGA CORRELATIONS

The total urine HGA (u-HGA) is a measure of total HGA output in 24 hours (µmol/24hr). AKU patients have elevated urine HGA concentrations compared to the reference range. The average u-HGA (µmol/24hrs) in the AKU group was 27035 µmol/24hrs at visit 1 (pre-nitisinone) compared to the reference range of <2.92 umol/24hrs (154). Independent t-tests revealed statistically significant differences between the u-HGA (µmol/24hrs) of males and females (p<0.01) with males having higher mean u-HGA concentrations (30546 umol/24hr) than females (21556 umol/24hr). When correlated with age there was no statistically significant correlation (r=0023, p>0.05). Males and females both demonstrated variable trends,

with males following a weak inverted 'U' trend and females following a weak 'U' shaped trend (Figure 6.4).

Total u-HGA was then correlated with the average lumbar and thoracic vertebrae SUVm in males and females (Figure 6.5). No statistically significant correlation was found (r=0.014, p>0.05). Females showed a weak negative correlation that plateaus at high SUVms, whereas males showed a weak positive correlation. Total u-HGA was correlated with the average lumbar and thoracic IVD SUVm (Figure 6.6). No statistically significant correlation was observed in both males and females (r=0.03, p>0.05).

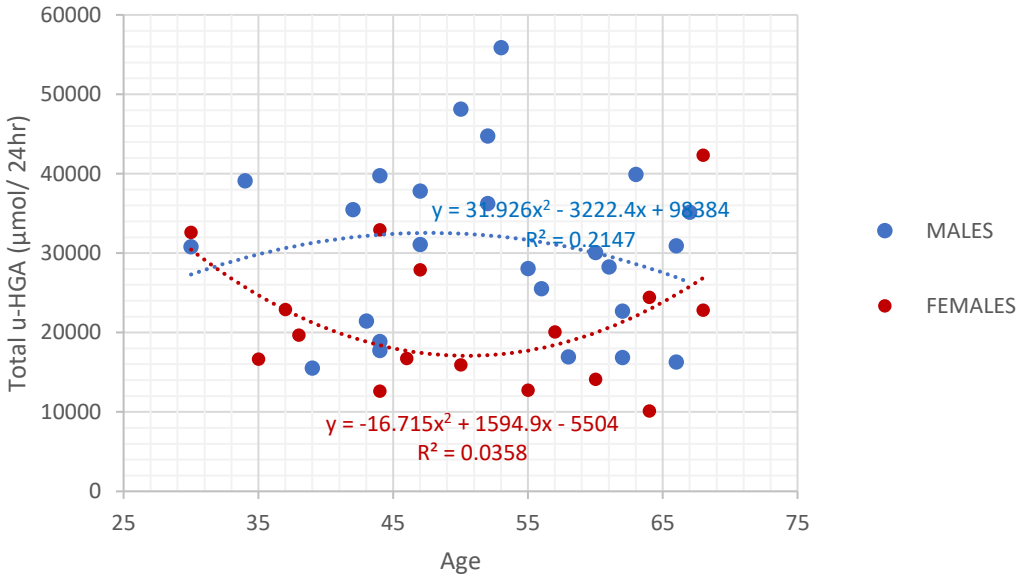

Figure 6.4 Correlation between total urine HGA pre-nitisinone with age in males and females at visit 1. Correlation coefficient in males (R^2=0.21) and females (R^2=0.04). No statistically significant correlation identified (r=0.023, p>0.05).

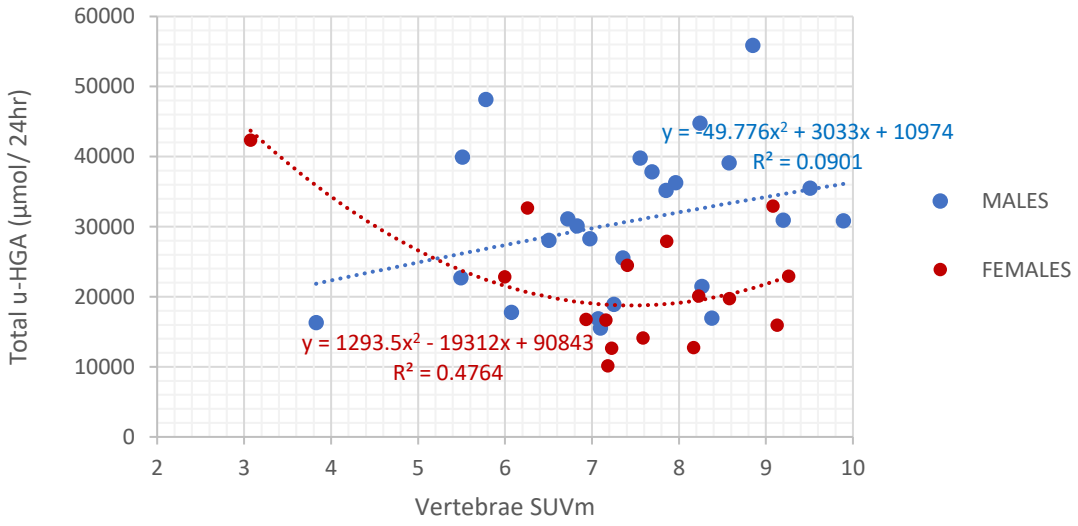

Figure 6.5 Correlation between total urine HGA pre-nitisione with the average lumbar and thoracic vertebrae SUVm at visit 1 in males and females. Correlation coefficient in males (R^2=0.09) and females (R^2=0.48). No statistically significant correlation identified (r=0.014, p>0.05).

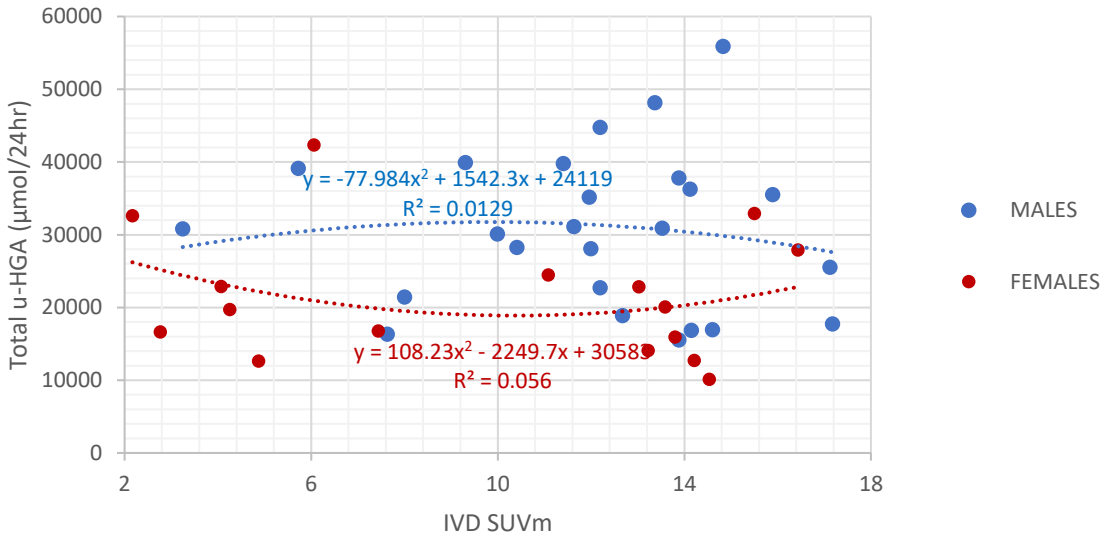

Figure 6.6 Correlation between total urine HGA pre-nitisione with the average lumbar and thoracic IVDs SUVm at visit 1 in males and females. Correlation coefficient in males (R^2=0.01) and females (R^2=0.06). No statistically significant correlation identified (r=0.03, p>0.05).

6.3.3 LUMBAR SIDE FLEXION CORRELATIONS

Lumbar side flexion (cm) was measured by a senior physiotherapist at the RLBUHT. Negative correlations were identified in both males and females when lumbar side flexion was correlated with age (Figure 6.7 A and B). A negative statistically significant correlation was identified ($r=-0.850$, $p<0.001$) between right passive lumbar side flexion and age (Figure 6.7A). Right passive lumbar side flexion was highest in the younger patients and this decreased linearly with age in both males and females with the oldest patients having the smallest range of motion in the spine. The same trend can be seen when correlating passive lumbar side flexion on the left side with age in both males and females (Figure 6.7B). A negative statistically significant correlation was identified between left passive lumbar side flexion with age ($r=-0.806$, $p<0.001$). Independent t-tests found no statistically significant differences between the lumbar side flexion (cm) on both the right and left sides between males and females.

Interestingly, when lumbar side flexion was plotted against the average lumbar and thoracic vertebrae SUVm, positive correlations were identified in both males and females (Figure 6.8 A and B). A positive statistically significant correlation was observed between the right passive lumbar side flexion and the average lumbar and thoracic vertebrae SUVm ($r=0.588$, $p<0.05$). A positive statistically significant correlation was also identified between the left passive lumbar side flexion and the average lumbar and the average lumbar and thoracic vertebrae SUVm ($r=0.616$, $p<0.05$). This trend supports what has been described in Chapter 4 and 5 with high vertebrae SUVms being associated with the younger patients with increased range of motion in the spine.

Weak inverted ‘U’ shaped trends were identified when correlating lumbar side flexion with the average lumbar and thoracic IVD SUVm in both males and females (Figure 6.9 A and B). Suggesting that reduced lumbar flexion is associated with middle of the range IVD SUVms, and that high and low IVD SUVms are associated with increased lumbar side flexion. However, this was not statistically significant on both the right and left sides.

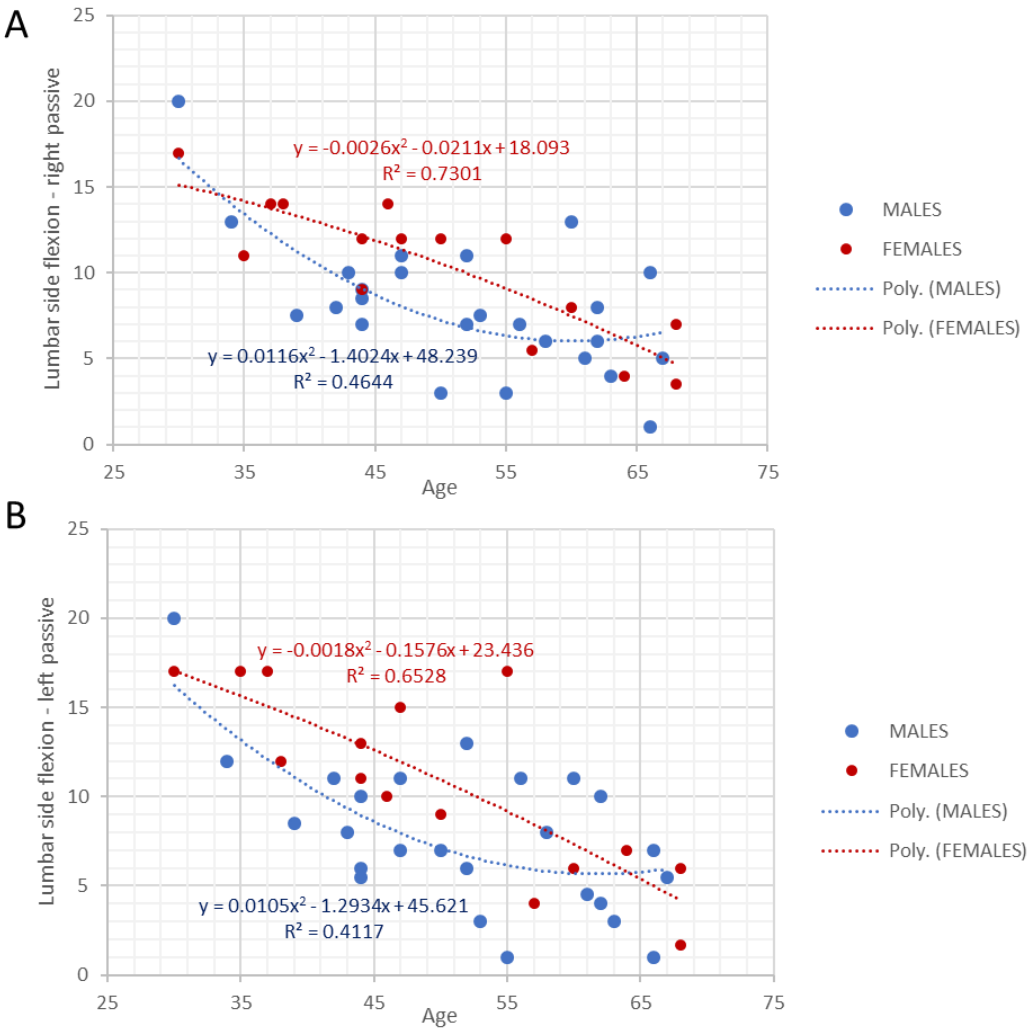

Figure 6.7 Correlation between lumbar side flexion (cm) with age in males and females at visit 1. A- right passive lumbar side flexion (cm) with age. B- left passive lumbar side flexion (cm) with age. Negative statistically significant correlations were observed; A- (r=-0.850, p<0.001), B- (r=-0.806, p<0.001).

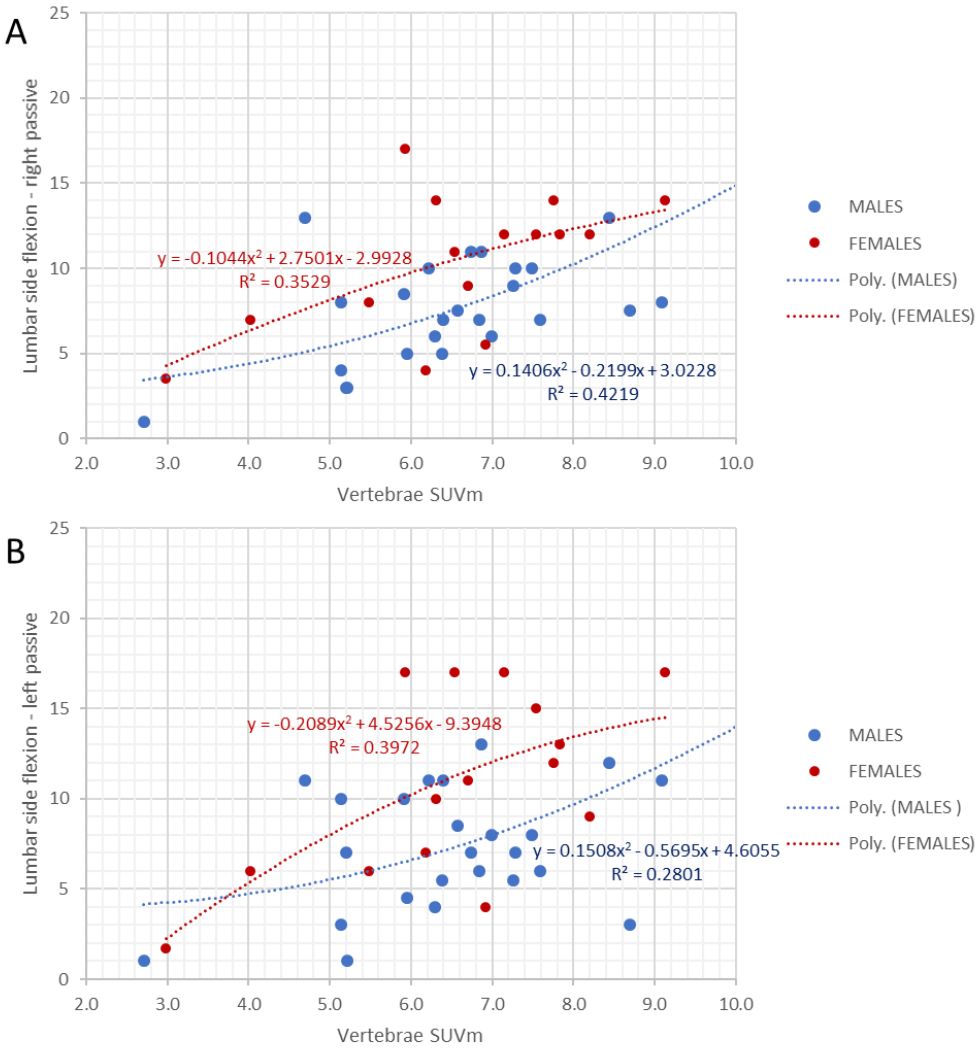

Figure 6.8 Correlation between lumbar side flexion (cm) with average lumbar and thoracic vertebrae SUVm in males and females at visit 1. A- right passive lumbar side flexion (cm) with vertebrae SUVm. B- left passive lumbar side flexion (cm) with vertebrae SUVm. Positive statistically significant correlations were observed; A- ($r=0.588$, $p<0.05$), B- ($r=0.616$, $p<0.05$).

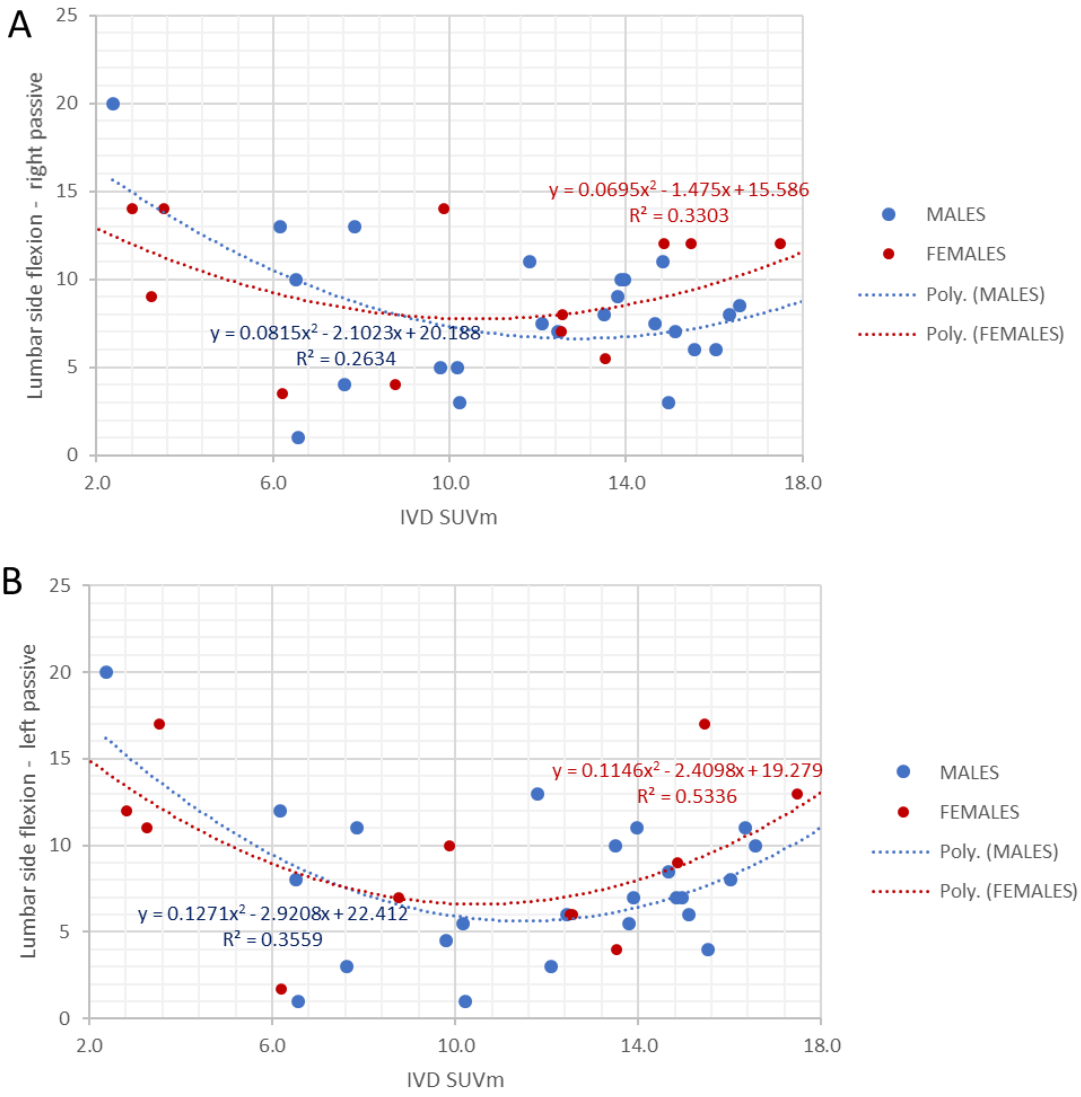

Figure 6.9 Correlation between lumbar side flexion (cm) with average lumbar and thoracic IVD SUVm in males and females at visit 1. A- right passive lumbar side flexion (cm) with IVD SUVm. B- left passive lumbar side flexion (cm) with IVD SUVm. No statistical significant correlations identified; A- ($r=0.160$, $p>0.05$), B-($r=0.0312$, $p>0.05$).

6.3.4 CERVICAL SPINE ROTATION CORRELATIONS

Cervical spine rotation (cm) was measured by a senior physiotherapist at the RLBUHT. No statistically significant correlations were identified in both males and females when cervical spine rotation was correlated with age. Figure 6.10A demonstrates no correlation between right passive cervical spine rotation with age ($r=0.175$, $p>0.05$). Figure 6.10B shows no correlation between left passive cervical spine rotation with age ($r=0.113$, $p>0.05$). No correlations were also identified between cervical spine rotation and vertebrae and IVD SUVm in both males and females on both the right and left sides (Figure 6.11 A and B, and 6.12 A and B).

Independent t-tests revealed significant differences between cervical spine rotation (cm) on the right and left sides in males and females ($p<0.01$, and $p<0.05$ respectively). Males can be seen having increased cervical rotation compared to females on both the right and left sides (mean cervical rotation on the right males = 12.08, females = 9.96, mean cervical rotation on the left males = 11.97, females = 10.31).

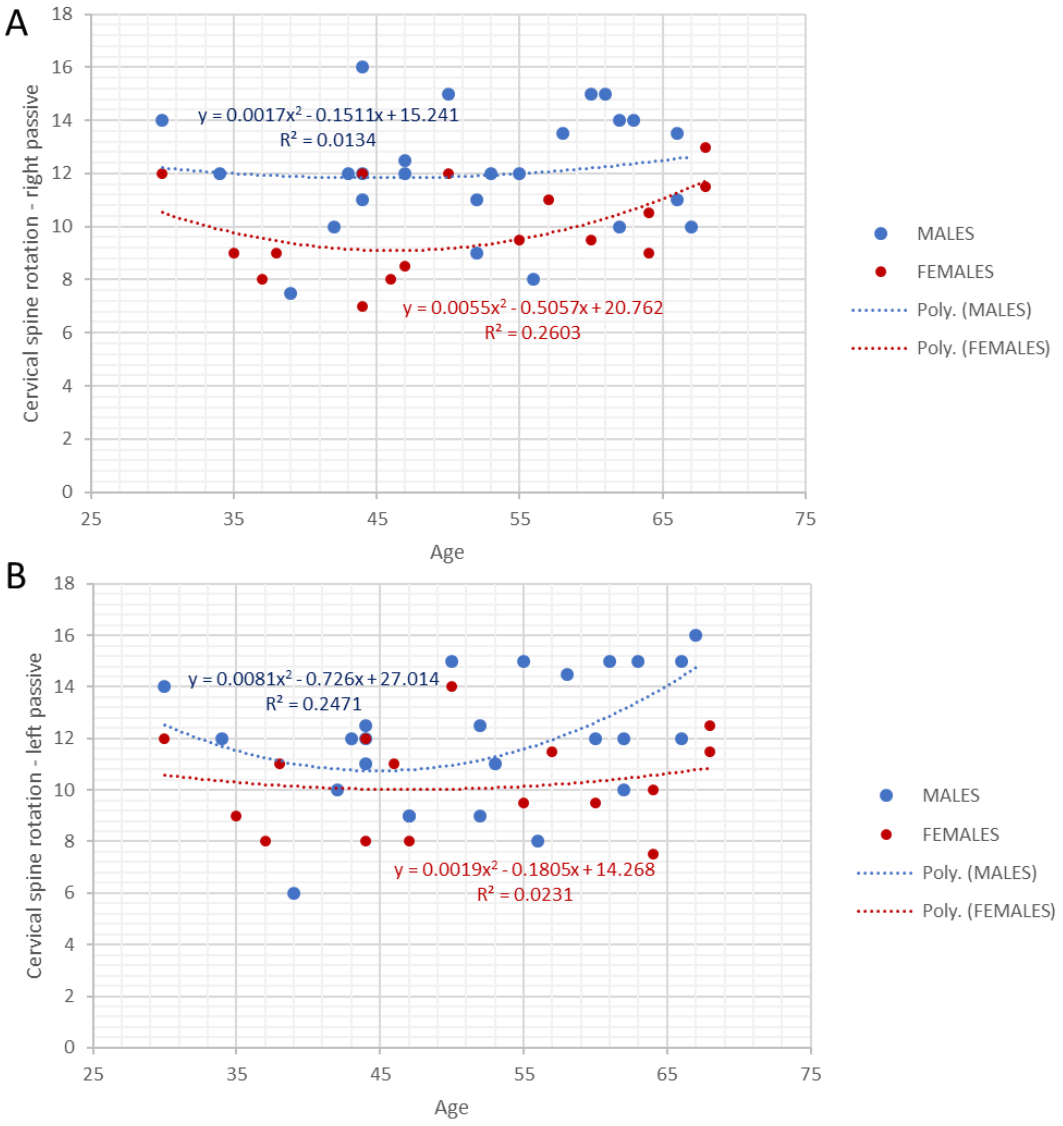

Figure 6.10 Correlation between cervical spine rotation with age in males and females at visit 1. A- right passive cervical spine rotation (cm) with age. B- left passive cervical spine rotation (cm) with age. No statistical significant correlations identified; A- (r=0.175, p>0.05), B- (r=0.113, p>0.05).

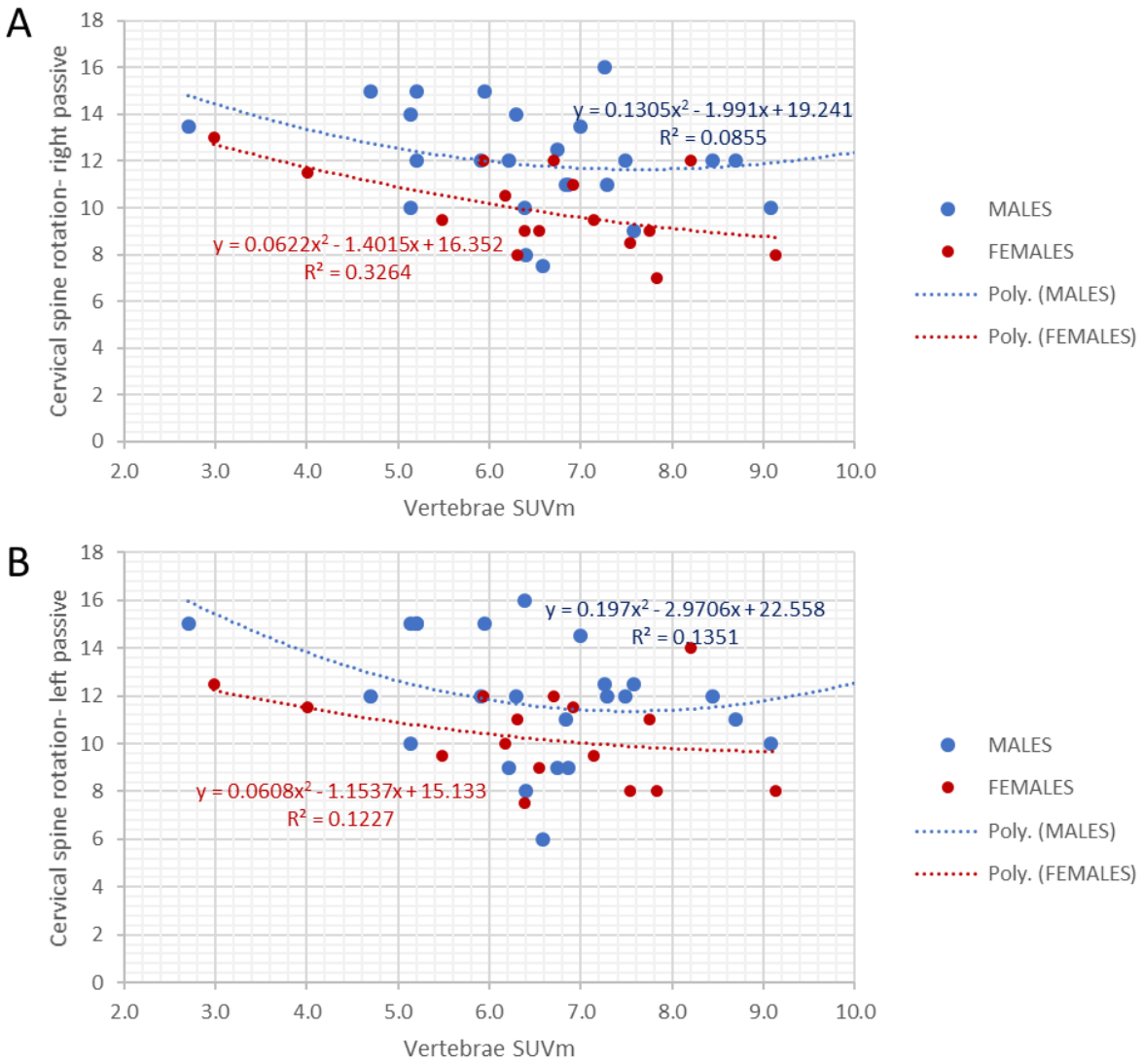

Figure 6.11 Correlation between cervical spine rotation with the average lumbar and thoracic vertebrae SUVm in males and females at visit 1. A- Right passive cervical spine rotation (cm) with average vertebrae SUVm, B- Left passive cervical spine rotation (cm) with average vertebrae SUVm. No statistical significant correlations identified; A- ($r=0.258$, $p>0.05$), B- ($r=0.248$, $p>0.05$).

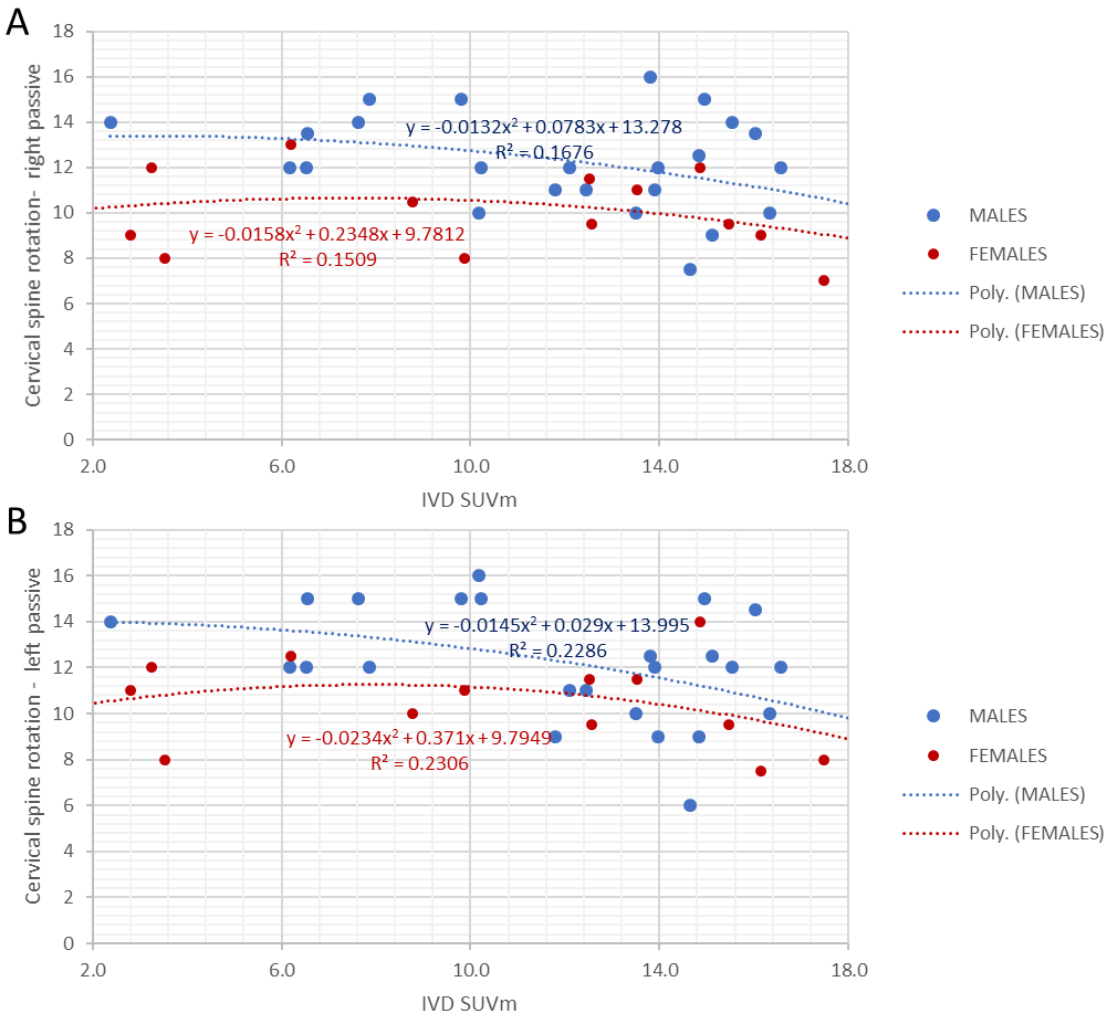

Figure 6.12 Correlation between cervical spine rotation with the average lumbar and thoracic IVD SUVm in males and females at visit 1. A- Right passive cervical spine rotation (cm) with average IVD SUVm, B- Left passive cervical spine rotation (cm) with average IVD SUVm. No statistical significant correlations identified; A- (r=0.026, p>0.05), B-(r=0.231, p>0.05).

6.3.5 COBB ANGLE CORRELATIONS WITH SUVm

Correlations were made between spinal Cobb angles obtained from X-ray images and vertebrae and IVD SUVms. Figure 6.13 demonstrates the correlation between the average thoracic vertebrae SUVm with thoracic kyphosis Cobb angles. No correlation was identified ($r=0.204$, $p>0.05$) between the normal thoracic kyphosis Cobb angles that range from 20-45 degrees (blue) with the thoracic vertebrae SUVm. However, the hyperkyphosis Cobb angles (>45 degrees- red) demonstrate a negative statistically significant correlation with the thoracic vertebrae SUVms ($r=-0.850$, $p<0.01$). Figure 6.14 demonstrates the correlation between lumbar vertebrae SUVm and the lumbar lordosis Cobb angle. No statistically significant correlation was identified ($r=0.068$, $p>0.05$).

Cobb angles were also correlated with IVD SUVms. Figure 6.15 demonstrates the correlation between the average thoracic IVD SUVm with the thoracic kyphosis Cobb angle. No correlation was identified ($r=0.035$, $p>0.05$) between the normal thoracic kyphosis Cobb angles that range from 20-45 degrees (blue) with the thoracic IVD SUVm. However, the hyperkyphosis Cobb angles (>45 degrees- red) demonstrate a negative statistically significant correlation with the thoracic IVD SUVms ($r=-0.723$, $p<0.01$). Figure 6.16 demonstrates the correlation between the lumbar IVD SUVm with the lumbar lordosis Cobb angle, no correlation was identified ($r=0.004$, $p>0.05$).

Scoliosis Cobb angles were also correlated with the mean lumbar and thoracic IVD and vertebrae SUVms (Figures 6.17 and 6.18). No correlations were identified even when assessing the patients with a scoliosis angle greater than 10 degrees (clinical definition of scoliosis >10 degrees).

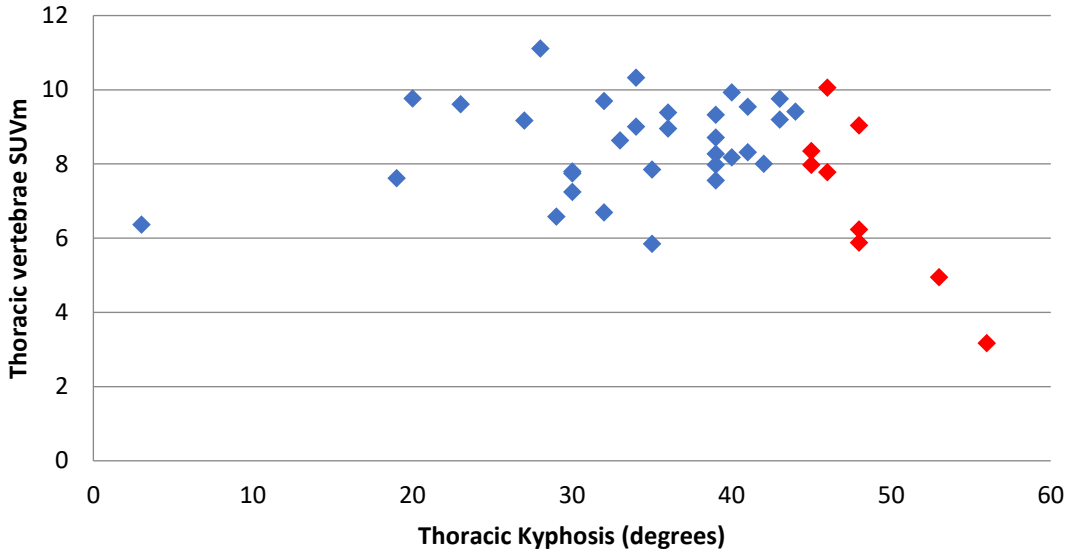

Figure 6.13 Correlation between the average thoracic vertebrae SUVm with thoracic kyphosis X-Ray Cobb angle in AKU patients at visit 1. No statistical significant correlation identified between the normal range of Cobb angles (20-45° blue) and thoracic vertebrae SUVm ($r=0.204$, $p>0.05$). Negative statistically significant correlation between the hyperkyphosis Cobb angles (>45° red) and thoracic vertebrae SUVm ($r=-0.850$, $p<0.01$).

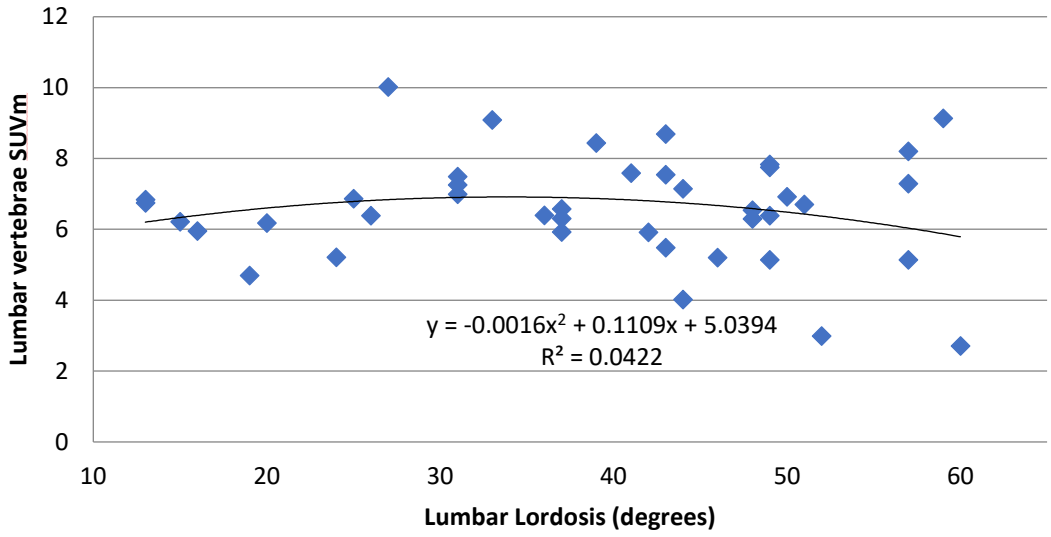

Figure 6.14 Correlation between average lumbar vertebrae SUVm with lumbar lordosis X-Ray Cobb angle in AKU at visit 1. No statistical significant correlation identified (r=0.068, p>0.05).

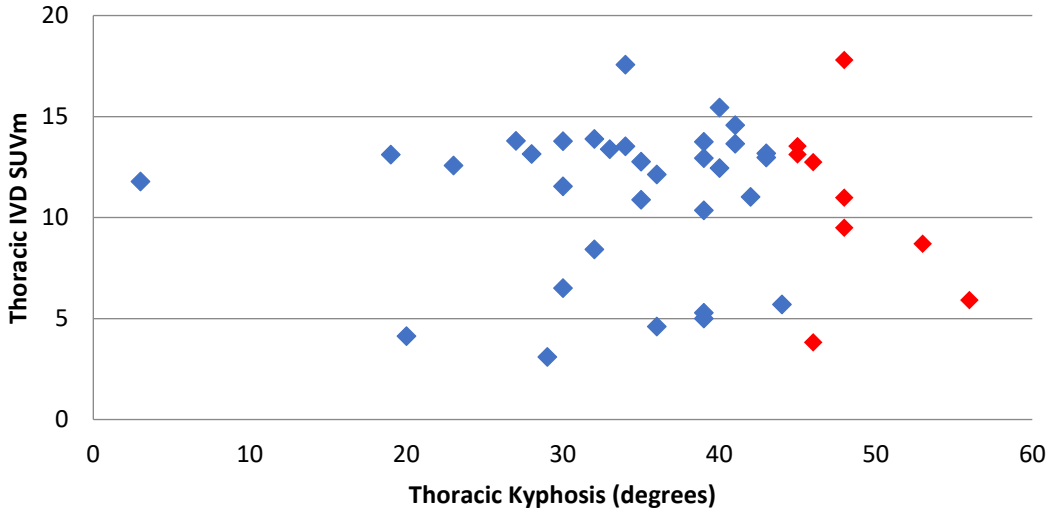

Figure 6.15 Correlation between average thoracic IVD SUVm with thoracic kyphosis X-Ray Cobb angle in AKU patients at visit 1. No statistical significant correlation between the normal thoracic kyphosis Cobb angles (20-45˚-blue) with the thoracic IVD SUVm (r=0.035, p>0.05). Negative statistically significant correlation between the hyperkyphosis Cobb angles (>45˚red) and thoracic IVD SUVm (r=-0.723, p<0.01).

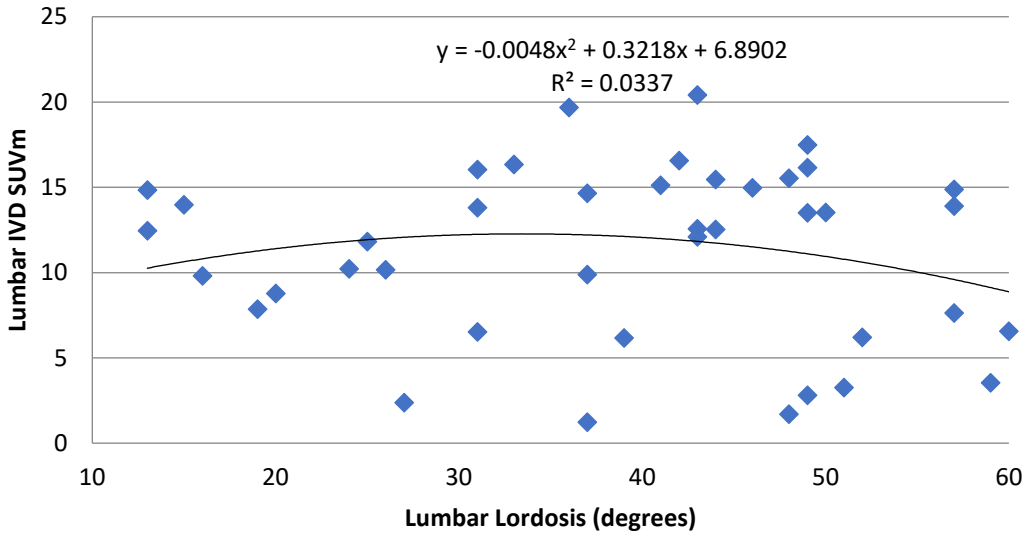

Figure 6.16 Correlation between average lumbar IVD SUVm with lumbar lordosis X-Ray Cobb angle in AKU patients at visit 1. No statistical significant correlation identified (r=0.004, p>0.05).

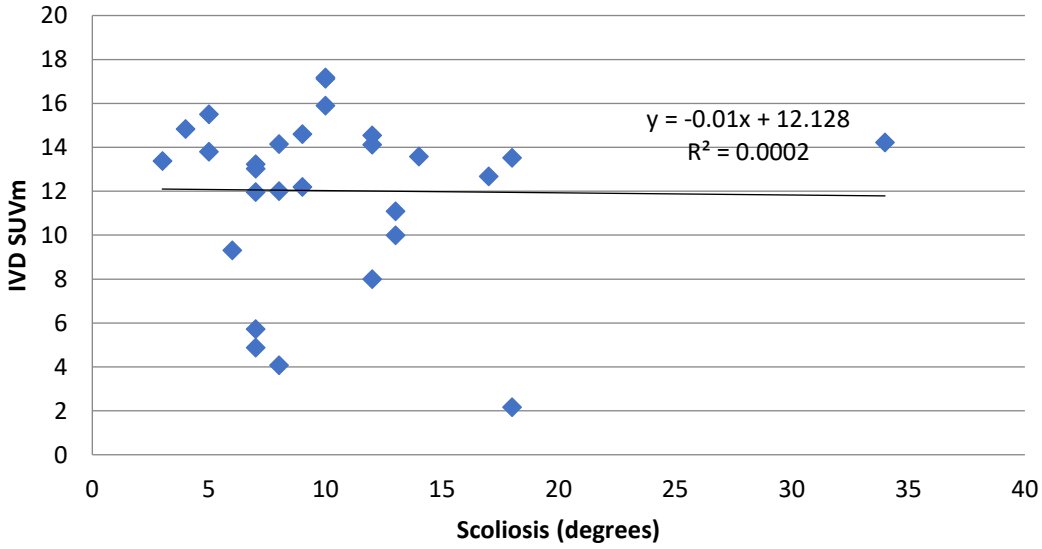

Figure 6.17 Correlation between average thoracic and lumbar IVD SUVm with scoliosis X-Ray Cobb angle in AKU patients at visit 1. No statistical significant correlation identified (r=0.01, p>0.05).

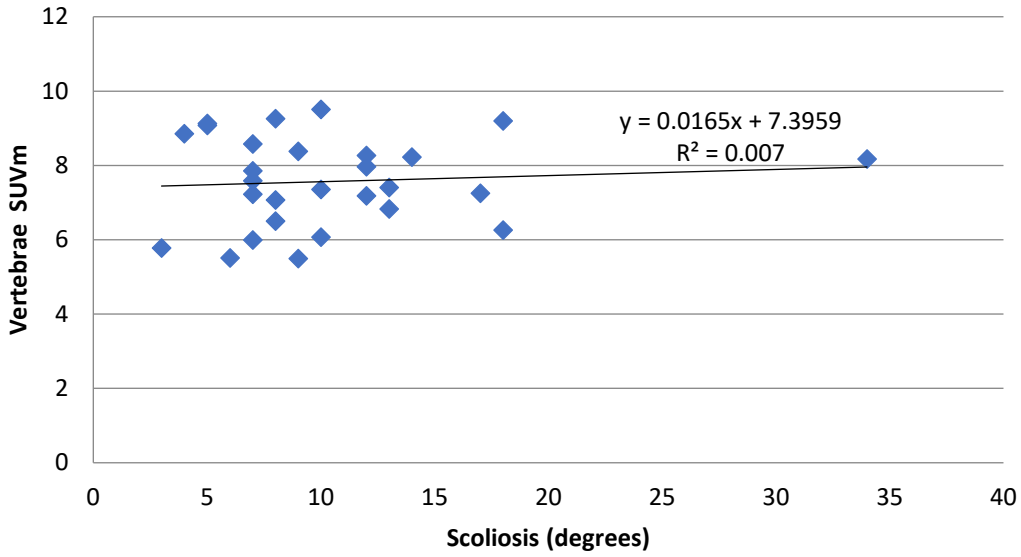

Figure 6.18 Correlation between average thoracic and lumbar vertebrae SUVm with scoliosis X-Ray Cobb angle in AKU patients at visit 1. No statistical significant correlation identified (r=0.08, p>0.05).

6.3.6 COBB ANGLE MRI vs X-RAY

The Cobb angles presented in section 6.3.5 were measured using the conventional X-Ray method (see section 2.6 for more information). This section investigates the difference between Cobb angles obtained from conventional X-Ray imaging and those obtained from MRI scans. A traditional chest X-ray is obtained whilst the patient is standing. It is known that standing up (weight bearing) accentuates kyphosis and is therefore used for clinical assessments. It is widely agreed that IVDs reduce in height from morning to night due to the forces and weight that passes through them throughout the day. MRI is performed with the patient lying supine, therefore it was questioned whether there would be a difference between measurements taken from the two modalities. The methodology used to measure

the Cobb angles was the same (described in sections 2.6.2 and 2.6.3) for both the X-Ray and MRI images.

Positive statistically significant correlations were identified between both thoracic kyphosis and lumbar lordosis Cobb angles when correlating X-ray and MRI techniques. This suggests that the two modalities of measuring Cobb angles both generate similar results and correlate well (Figures 6.19 and 6.20). Table 6.1 demonstrates the mean thoracic kyphosis and lumbar lordosis Cobb angles obtained from MRI and X-ray imaging modalities with the difference and statistical significance of the correlation included**.** Correlations were also made between thoracic kyphosis and lumbar lordosis Cobb angles to see if they show the same trends. No statistical significant correlation was identified between the lumbar lordosis Cobb angle and thoracic kyphosis Cobb angle using both the X-Ray imaging and MRI modalities.

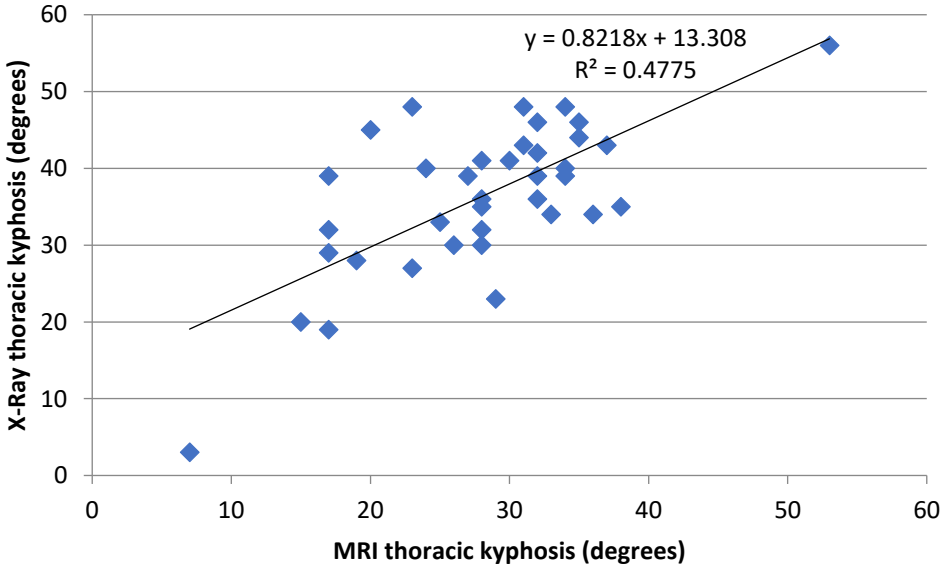

Figure 6.19 Correlation between X-Ray and MRI thoracic kyphosis Cobb angles in AKU patients at visit 1. Positive statistically significant correlation was observed ($r=0.691$, $p<0.001$).

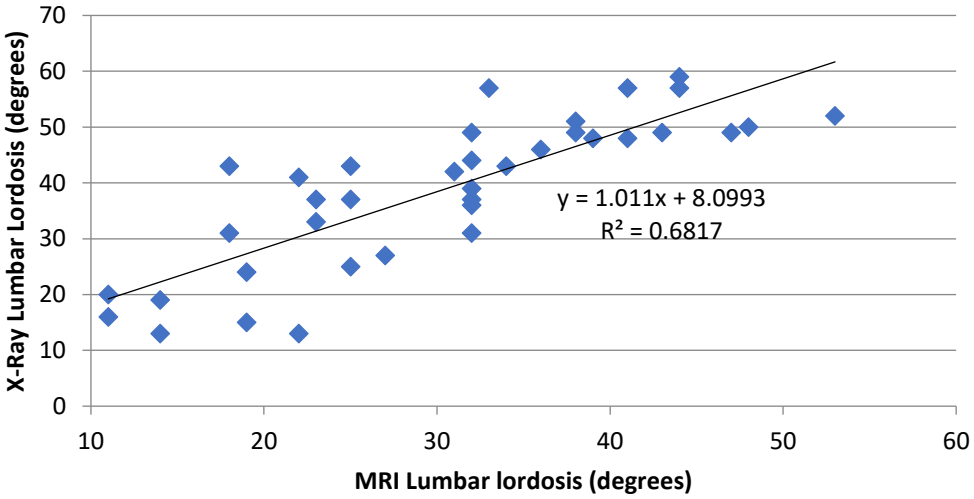

Figure 6.20 Correlation between X-Ray and MRI lumbar lordosis Cobb angles in AKU patients at visit 1. Positive statistically significant correlation was observed (r=0.825, p<0.001).

Table 6.1 Thoracic kyphosis and lumbar lordosis mean Cobb angles obtained from MRI and X-ray imaging modalities. All angles are given in mean degrees (standard deviation).

	MRI	X-Ray	Difference	Correlation
Thoracic Kyphosis	27.9 (8.4)	36.3 (9.9)	9.14 (6.25)	r=0.691, p<0.001
Lumbar Lordosis	30.2 (10.9)	38.6 (13.4)	9.29 (6.44)	r=0.825 p<0.001

6.3.7 DEXA LUMBAR SPINE T-SCORE

The next set of analysis was to explore lumbar spine bone density utilising data obtained from DEXA scans in the form of T-scores. DEXA T-scores of the lumbar region were measured at the L2-L4 spinal level. Table 1.4 describes the WHO definitions of bone mineral density. Figure 6.21 demonstrates the correlation between DEXA lumbar spine T-scores with age in males and females. No statistically significant correlation was identified in both males and females (males $r=0.006$, $p>0.05$, females $r=0.419$, $p>0.05$). The trend lines demonstrate from around the age of mid-40's there is a general reduction in lumbar spine T-score with age in both males and females. This supports what was reported in the previous chapter were QCT was correlated with age (Figure 5.15). Interestingly however, DEXA T-scores show a slight positive correlation with age up to around the mid-40's demonstrated but the inverted 'U' shaped curves in Figure 6.21. Additionally, females appear to have slightly reduced T-scores compared to men after the age of around 45. Independent t-tests however revealed no statistically significant differences between male and female lumbar spine T-score ($p>0.05$).

Figure 6.22 demonstrates the correlation between the DEXA lumbar spine T-score and the mean lumbar vertebrae SUVm. A statistically significant positive correlation was identified in the female group ($r=0.345$, $p<0.05$) where low lumbar spine T-scores are associated with low lumbar vertebrae SUVms. This supports what was reported when analysing QCT with vertebrae SUVm in the previous chapter (Figure 5.17). However, there was no statistically significant correlation in the male group ($r=0.117$, $p>0.05$).

Figure 6.23 displays the correlation between the DEXA lumbar spine T-score with the mean lumbar IVD SUVm. Positive statistically significant correlations were identified in males ($r=0.428$, $p<0.05$). However, the correlation was not significant in the female group ($r=0.361$, $p>0.05$). The trend demonstrates that high lumbar spine T-scores are associated with high lumbar IVD SUVms. This does not support what was found in the previous chapter where lumbar QCT was correlated with lumbar IVD SUVm (Figure 5.16) this will be discussed later.

Correlations were made between T-scores and spinal Cobb angles to investigate whether changes in spinal curvatures correlate with changes in bone density. Figure 6.24 demonstrates the correlation between DEXA lumbar spine T-score and the thoracic kyphosis Cobb angle in males and females. No correlation was identified in males ($r=0.032$, $p>0.05$), and a negative correlation was identified in females ($r=-0.403$, $p>0.05$) however this was not statistically significant. Additionally, this graph illustrates that males have a much wider range of thoracic kyphosis angles ranging from 3-53 degrees, compared to females that ranged from 29-56 degrees. However, independent t-tests revealed no statistical significant difference between the thoracic kyphosis Cobb angles of males and females ($p>0.05$).

Lastly, lumbar lordosis Cobb angles were correlated with the average DEXA lumbar spine T-scores (Figure 6.25). No statistically significant correlations were identified in both males and females (males $r=0.056$, $p>0.05$, females $r=0.164$, $p>0.05$) with no definitive trends being identified. As described in the Figure 6.24 males had a much wider range of lumbar lordosis Cobb angles ranging from 13-60 degrees, whereas females ranged from 37-59 degrees. However, there was no statistical difference

between the lumbar lordosis Cobb angles of males and females (independent t-test p>0.05).

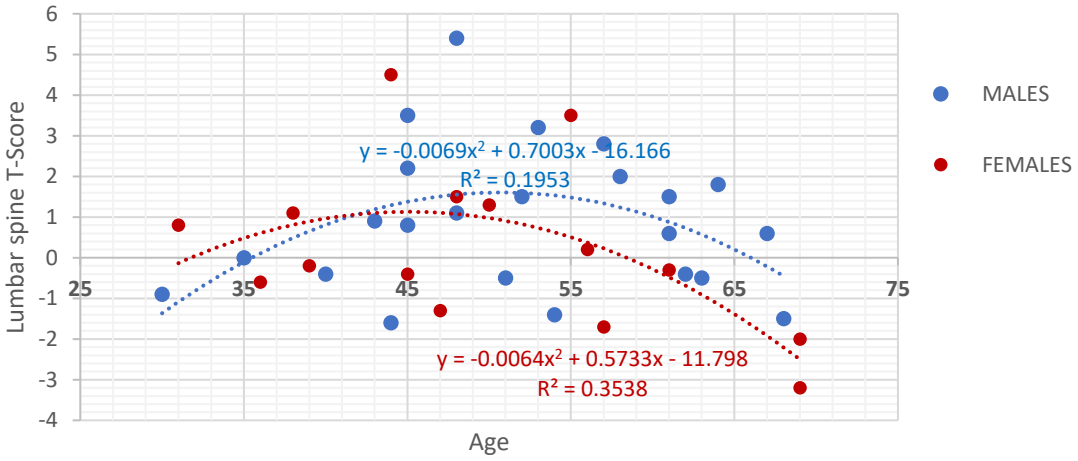

Figure 6.21 Correlation between DEXA lumbar spine (L2-L4) T-score and age in males and females at visit 1. No statistically significant correlation observed (males r=0.006, p>0.05, females r=0.419, p>0.05).

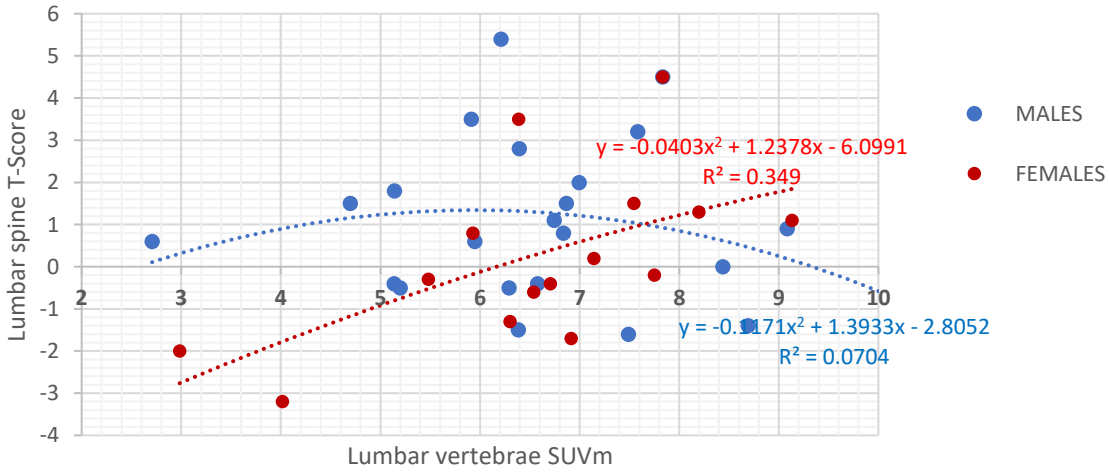

Figure 6.22 Correlation between DEXA lumbar spine T-score and mean lumbar vertebrae SUVm at visit 1 in males and females. Positive statistically significant correlation identified in the female group (r=0.345, p<0.05). No statistically significant correlation observed in the male group (r=0.117, p>0.05).

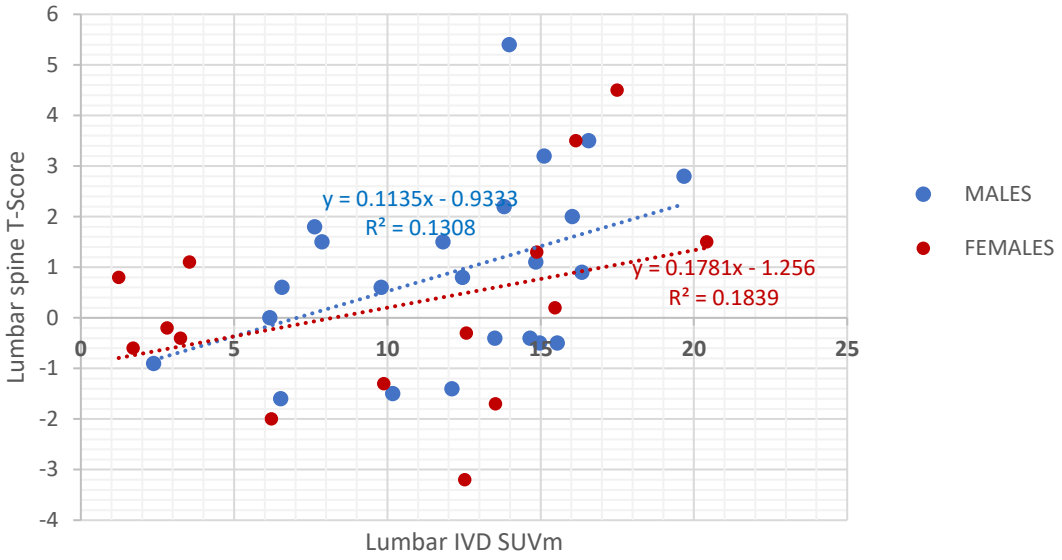

Figure 6.23 Correlation between DEXA lumbar spine T-score and the mean lumbar IVD SUVm at visit 1 in males and females. Positive statistically significant correlation observed in males (r=0.428, p<0.05). No significant correlation identified in females (r=0.361, p>0.05).

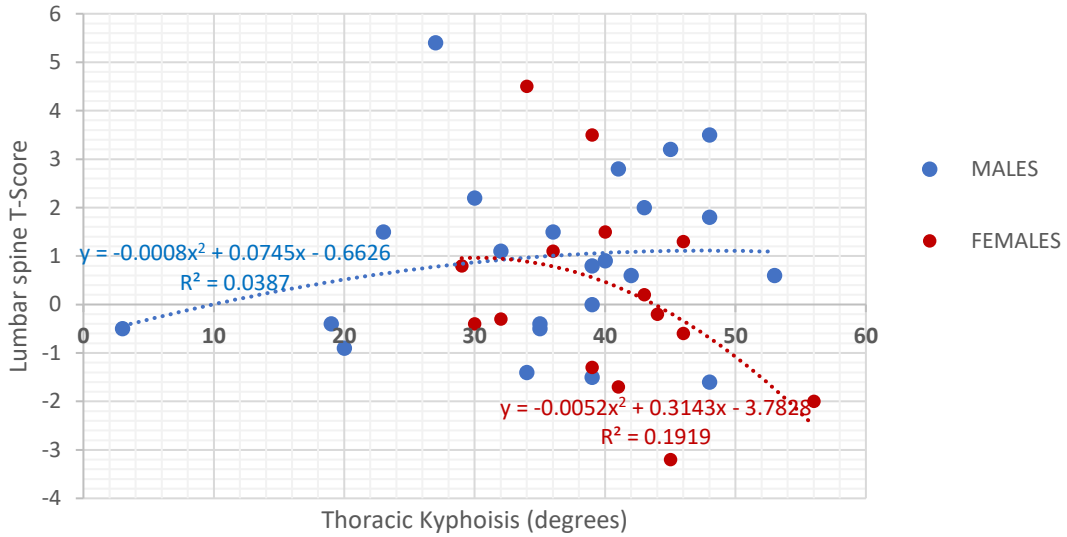

Figure 6.24 Correlation between DEXA lumbar spine T-score and the thoracic kyphosis Cobb angle in males and females. No statistically significant correlation observed in both males (r=0.032, p>0.05) and females (r=-0.403, p>0.05).

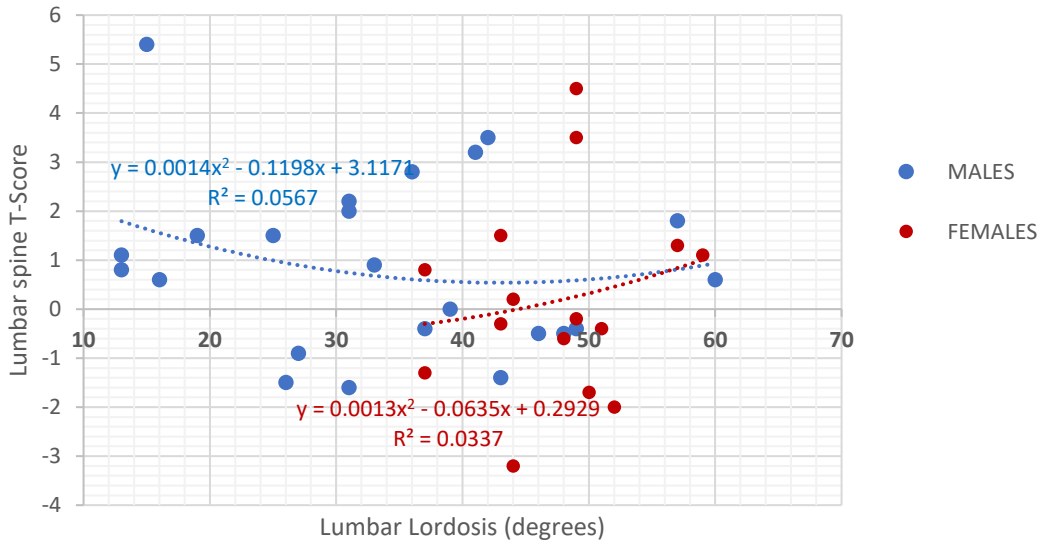

Figure 6.25 Correlation between DEXA lumbar spine T-score and the lumbar lordosis Cobb angle in males and females. No statistically significant correlation observed in both males and females (males r=0.056, p>0.05, females r=0.164, p>0.05).

6.3.8 DEXA FEMUR T-SCORE

Correlations were also made with femur DEXA T-scores to investigate if the same trends were identified as seen in the previous section (section 6.3.7) in a different anatomical region. Figure 6.26 demonstrates the correlation between the DEXA femur T-score and the mean lumbar vertebrae SUVm in males and females. No significant correlation was identified (males r=0.345 p>0.05, females r=0.331 p>0.05). However, similar trends were identified as seen in Figure 6.22, demonstrating a general increase in lumbar SUVm with increased femur T-score. Independent t-scores revealed no significant differences between the femur T-score in males and females

(p>0.05). Notably, the T-score values are much lower in the femur, ranging from -3.1 to 1.4, compared to -3.1 to 5.2 in the lumbar spine.

Figure 6.27 demonstrates the correlation between the DEXA femur T-score and the mean lumbar IVD SUVm in males and females. A negative statistically significant correlation was identified in females ($r=-0.496$, $p<0.05$), with no statistically significant correlation identified in the male group ($r=0.250$, $p>0.05$). This trend however demonstrates that higher femur T-scores are associated with low lumbar IVD SUVms. This does not support what was found when lumbar IVD SUVm was correlated with lumbar spine T-scores (Figure 6.23) that represents a weak positive trend. Again, it is clear that the T-scores in the lumbar spine reach much higher values, a maximum of 5.4 compared to the maximum femur T-score value of 1.3.

Figure 6.28 demonstrates the correlation between DEXA femur T-score with age. A negative correlation was identified, supporting what was found in Figure 6.21. DEXA lumbar spine T-score was plotted alongside the femur data, illustrating that the lumbar spine T-scores are much higher (average T-score= 0.62) than the femur (average T-score=-1.53). The data of the spine and femur T-scores below the age of 40 overlaps, however after approximately the age of 45 the spine T-scores are generally much higher than the femur T-scores. Paired t-tests and Wilcoxon signed rank sum tests revealed a significant difference between the lumbar spine and femur T-scores ($p<0.01$).

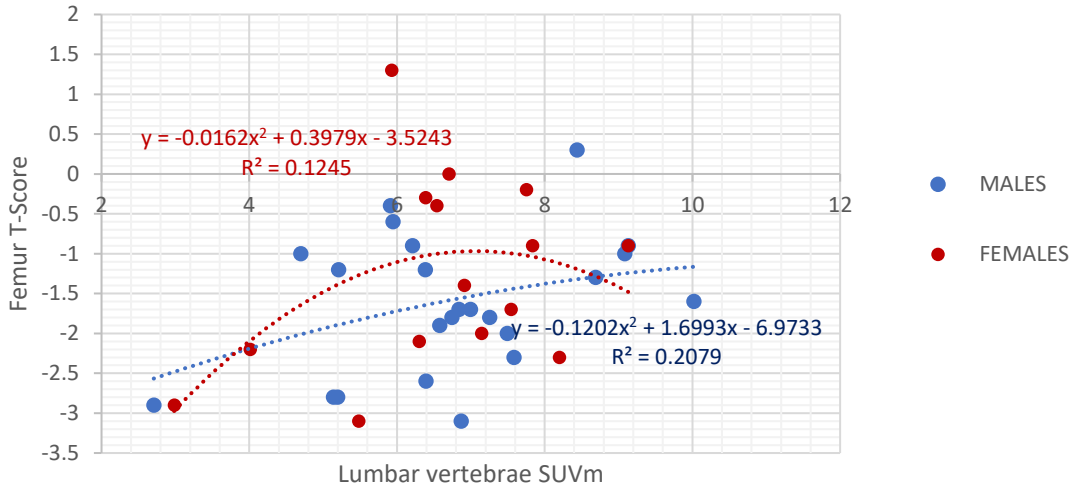

Figure 6.26 Correlation between DEXA femur T-score and the average lumbar vertebrae SUVm at visit 1 in males and females. No statistically significant correlation observed in both males and females (males r=0.345, p>0.05, females r=0.331, p>0.05).

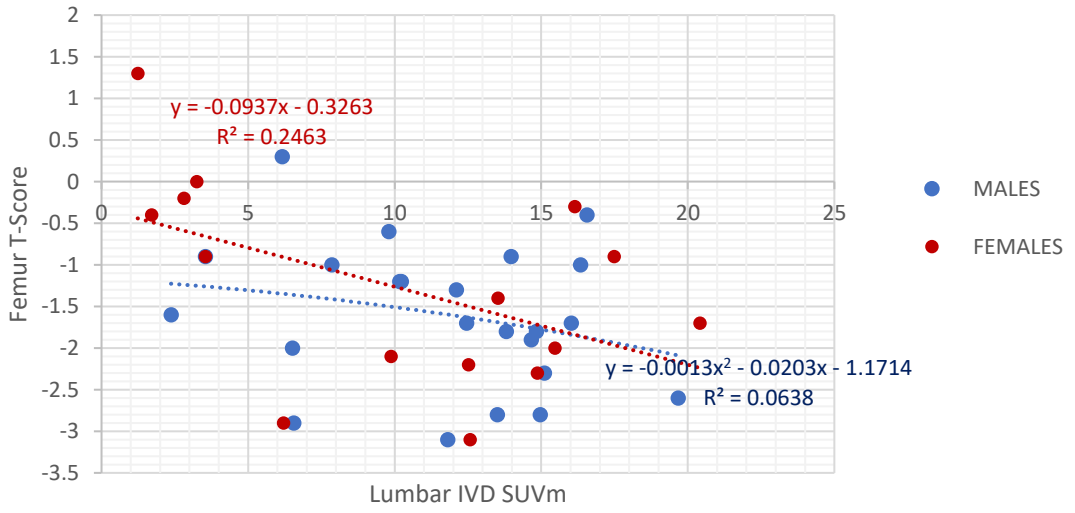

Figure 6.27 Correlation between DEXA femur T-score and the average lumbar IVD SUVm at visit 1 in males and females. Negative statistically significant correlation observed in females (r=0.496, p<0.05). No statistically significant correlation identified in males (=0.250, p>0.05).

6.3.8.1 Comparison between DEXA and QCT results

Figure 5.20 in the previous chapter reported QCT T-scores of the spine and femur. Figure 6.28 reports DEXA T-scores of the spine and femur. The mean spine QCT T-score was -2.27 ranging from -5.63 to 0.95, compared to the mean DEXA T-score of 0.62 ranging from -3.2 to 5.4. The QCT femur T-score had a mean of 0.08 ranging from -2.58 to 4.26 compared the mean DEXA femur T-score of -1.5 ranging from -3.1 to 1.3. Independent t-test revealed a statistically significant difference between the spine T-scores obtained from DEXA and QCT ($p<0.001$). The femur T-scores were not statistically different between QCT and DEXA.

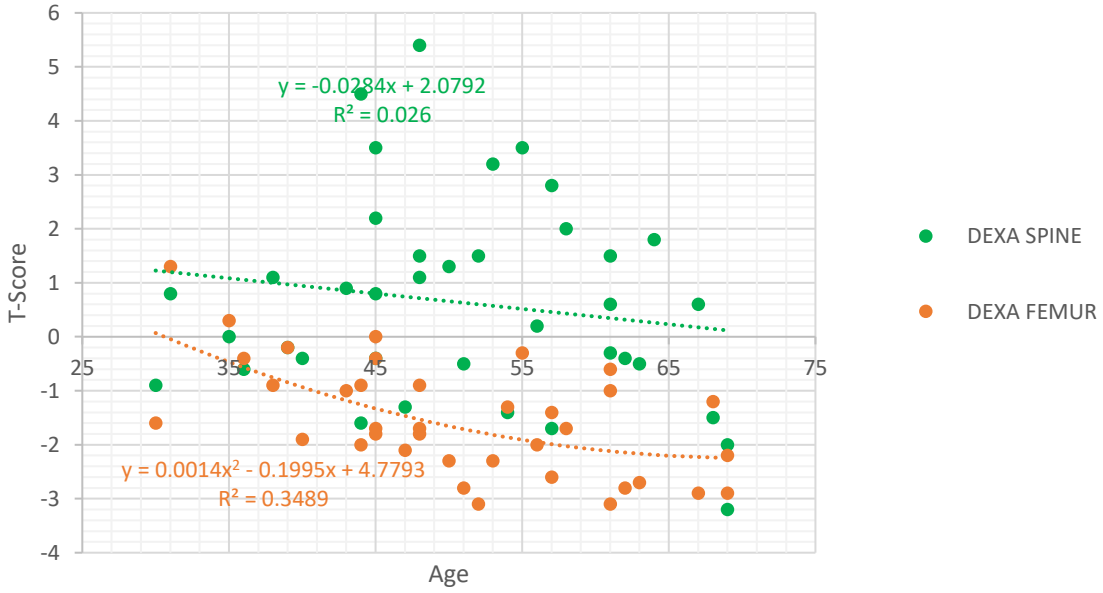

Figure 6.28 Correlation between DEXA spine T-score and femur T-score with age in AKU patients at visit 1. Negative statistically significant correlation identified; femur ($r=-0.309$, $p<0.01$), no significant correlation in the spine ($r=0.01$, $p>0.05$). Paired t-test and Wilcoxon signed rank sum tests revealed statistically significant difference between lumbar spine and femur T-scores ($p<0.01$).

6.4 DISCUSSION

This chapter has focused on correlating the vertebrae and IVD SUVm with other clinical data obtained from the clinical trial site files from SONIA 2. Correlating other data such as, serum and urine HGA concentrations, spinal flexibility, spinal curvature angles and DEXA T-scores with the SUVm method will allow us to find common trends between types of examination and imaging methods as well as allowing us to see if these show any statistical relationships.

6.4.1 SERUM HGA CORRELATIONS

The serum HGA (s-HGA) concentration was obtained from a fasting blood sample collected at visit 1 pre-nitisinone using LC-MS/MS by a biochemist at the RLBUHT. After plotting the data provided by the biochemistry lab, AKU patients clearly have elevated s-HGA concentrations (33.2umol/L) compared to the reference range (<3.1umol/L) pre-nitisinone, which was one of the important findings reported in the SONIA 1 clinical trial (45). When analysing male and female s-HGA there was no significant difference between the two groups (independent t-test $p>0.05$). The difference between male and female s-HGA in AKU has not been reported in the literature and this data has revealed no significant differences suggesting that the concentration of HGA in serum of patients with AKU is not affected by gender. Weak positive correlations were reported between s-HGA and age in both males and females (Figure 6.1) suggesting that age does not influence s-HGA concentration significantly. The weak positive correlation however may represent reduced renal function with age. It has been recognised for decades that there is an age associated loss of kidney function associated with progressive decreases in glomerular filtration

rate and renal blood flow. In AKU this would result in increased HGA circulating in the blood due to reduced efficiency of the kidneys (155).

It is clear that s-HGA concentration is elevated in AKU patients without treatment. The SONIA 1 clinical trial elucidated a clear dose response relationship with increasing dosages of nitisinone (1,2,4 and 8mg) with the highest dose reducing HGA by 99.4% (45). Serum HGA concentrations in the SONIA 1 group went from 30.3 umol/L at baseline to 0.7umol/L after one year on nitisinone. Without treatment s-HGA remains elevated demonstrating the effectiveness of the drug at lowering the culprit molecule HGA (45).

Correlations were also made between s-HGA and the average lumbar and thoracic IVD and vertebrae SUVm (Figures 6.2 and 6.3). No statistically significant correlations were identified between both the s-HGA and the vertebrae SUVm ($r=0.0781$, $p>0.05$) (Figure 6.2), or the s-HGA and IVD SUVm ($r=0.0174$, $p>0.05$) (Figure 6.3). This suggests that the concentration of HGA that is circulating in the blood, pre-treatment at visit 1, does not correlate with the SUVms. This may be because s-HGA concentration does not appear to be affected by age and remains relatively stable across the population. Whereas in contrast we have seen how the SUVm changes with age in both the vertebrae and IVDs due to the progression of the disease (Figures 4.10- 4.13). Additionally, s-HGA represents the concentration of s-HGA circulating in the blood at a single time-point, before treatment. The SUVm is a measure of fluoride uptake that represents years of HGA accumulation in the spine. Therefore, it is not the circulating s-HGA concentration that is important, it is the life-long exposure to HGA that is key in AKU ochronosis that results in osteoarthropathy.

6.4.2 URINE HGA CORRELATION

Acidified 24-hour urine samples were obtained from all SONIA 2 patients at visit 1, pre-nitisinone. The acidified urine was analysed for HGA using LC-MS/MS by a biochemist at the RLBUHT and is representative of the total amount of HGA excreted in 24 hours. The data was provided by the biochemistry lab and was plotted against age. AKU patients have elevated urine HGA (u-HGA) (27035 umol/L) compared to the reference range (<2.9 umol/L) which again was one of the main findings in the SONIA 1 clinical trial (45). Interestingly there was a statistical significant difference between the u-HGA of males and females with males having a higher mean u-HGA (30546 umol/24hr) than females (21556 umol/24hr). This may be due to the increased dietary intake of protein in males compared to females. It is known that dietary intake of tyrosine/phenylalanine results in the accumulation of HGA. The more tyrosine/phenylalanine ingested, the more HGA is therefore produced and excreted. It is widely agreed that males are generally larger than females and require more calories and more fluid, and they therefore excrete more urine which may represent why males have increased u-HGA umol/24hrs.

As in section 6.4.1 no statistically significant correlations were identified between u-HGA and the average lumbar and thoracic vertebrae and IVD SUVms. This suggests that the total urinary HGA output in 24hrs does not correlate with fluoride uptake in the vertebrae and IVDs. This is not unexpected as it is not the amount u-HGA that is excreted that is important in terms of ochronosis and arthropathy of the spine but it is the amount that is bathing the tissues over many years that results in ochronosis and spinal arthropathy.

6.4.3 LUMBAR SIDE FLEXION CORRELATION

A senior physiotherapist at the RLBUHT measured lumbar side flexion (for more information see section 2.7.1) on all SONIA 2 patients at visit 1, pre-nitisinone. Lumbar side flexion measurements can be used as a standardised measurement to quantify spinal flexibility. Lumbar side flexion provides a good picture of spinal flexibility in contrast to lumbar flexion (forward bending) as it is not augmented by hip joint movement. Additionally, practically it is often easier to ask patients with back pain to flex to the side rather than bend forwards (156). When correlating lumbar side flexion on the right and left sides with age, negative statistically significant correlations were identified ($p<0.001$ on both the left and right sides) with no statistical difference between males and females (Figure 6.7 A and B). Lumbar side flexion was highest in the younger patients and lower in the older patients. As expected younger patients have increased flexibility compared to older patients. It is widely agreed that with increasing age, BMD reduces, that is associated with increased risk of fractures. Collagen production reduces with age meaning response to repair is reduced. Tendons and ligaments become stiffer and elasticity is reduced and muscles supporting the joints become weak. All these factors contribute to reduction in flexibility with age.

In AKU raised HGA levels in plasma and extracellular fluid lead to ochronosis. HGA polymers are deposited in connective tissues such as cartilage, tendons and ligaments. The affected tissues often become weak and brittle, and prone to bone fracturing, and tendon snapping. This ultimately reduces flexibility and impacts on mobility due to pain and discomfort of the major joints such as the spine, hip and

knees (36). This clearly explains why there is a reduction in lumbar side flexion with age in AKU. This trend would also be expected in a control population. However, the slope on Figure 6.7 A and B would be expected to be shifted over to the right as AKU patients suffer from pain and arthropathy decades before that of control patients. Physiotherapy is routine practice for most AKU patients and it is encouraged that all patients participate in exercises set by the physiotherapist to try to increase flexibility and range of motion at the joint and to try to keep joints supple, reducing pain (157).

Interestingly, positive statistically significant correlations were identified between lumbar side flexion (on both the right and left sides) and the average lumbar and thoracic vertebrae SUVm in both males and females (Figure 6.8 A and B). This demonstrates that increased spinal flexibility is associated with increased vertebrae SUVms. This trend reflects what has been described in Chapter 4, where SUVm can be seen decreasing with age due to reduced BMD with age (Figures 4.10 and 4.11). Younger patients are associated with high vertebrae SUVms and high BMD due to increased hydroxyapatite for ^{18}F to bind. Older patients are associated with low SUVms and low BMD as there is less bone turnover with age. These findings reflect that younger patients have increased flexibility; higher BMD values therefore have increased SUVms. In contrast the older patients have reduced spinal flexibility, reduced BMD and reduced SUVms.

No statistical correlations were identified when correlating the lumbar side flexion (on the right and left sides) with the average lumbar and thoracic IVD SUVm in both males and females which was disappointing. It was expected that with increased IVD SUVm there would be a reduction in lumbar side flexion, as increased IVD SUVm

reflects calcification of the IVDs and it would be assumed that calcified IVDs would be less flexible due to pain and or spinal fusion.

6.4.4 CERVICAL SPINE ROTATION CORRELATION

Cervical spine rotation is a measure of range of motion of the neck. No statistically significant correlations were identified between cervical spine rotation (on the right and left sides) with age. Suggesting that cervical flexibility is not influenced by age (right side r=0.175, left side r=0.113). This is surprising as although the cervical spine is not weight bearing and is not one of the major regions affected in AKU, cervical mobility has been reported to be reduced in AKU along with cervical disc space narrowing, spinal cord compression and disc herniations at the cervical level (158). It was therefore expected that cervical flexibility would be reduced in the older AKU patient's as it is one of the regions where these patients report pain. No correlations were identified between cervical spine rotation and lumbar and thoracic vertebrae and IVD SUVms suggesting that lumbar side flexion may be a better indicator of disease state and progression compared to cervical rotation.

6.4.5 COBB ANGLE CORRELATION WITH SUVm

The Cobb angle is a standardised measure of spinal curvature. Cobb angles are used clinically to measure thoracic kyphosis, lumbar lordosis and scoliosis, if present. In AKU patients these measurements are repeated annually to assess if there are any changes to the curvatures of the spine. The data presented in this chapter was from visit 1, pre-nitisinone. Normal thoracic kyphosis ranges from 20-45 degrees and

hyperkyphosis is defined as more than 45 degrees (122). Clinically there is no range for normal lumbar lordosis neither is there an angle to define hyper or hypo-lordosis as there are many factors that influence the lumbar spine such as muscular strength, flexibility and BMI (123). Scoliosis is defined as a spinal curvature of 10 degrees or more to the left or the right (124). No statistically significant correlations were identified between lumbar lordosis and age ($r=0.01$, $p>0.05$) or thoracic kyphosis and age ($r=0.07$, $p>0.05$).

Correlations were made between the spinal Cobb angles and vertebrae and IVD SUVms to see if there was a relationship between spinal curvature and bone and or IVD ^{18}F uptake. When the thoracic kyphosis Cobb angle and the thoracic vertebrae SUVm was correlated no correlation was identified between the normal thoracic kyphosis Cobb angles that range from 20-45 degrees, and the thoracic vertebrae SUVm. Looking at the graph (Figure 6.13) the normal thoracic kyphosis Cobb angles all have SUVm that are higher up the scale ranging from 6-11 suggesting that normal thoracic curvatures are associated with uptake of fluoride consistent with the younger less affected patients. As we have previously reported there is a negative trend with vertebrae SUVm with age (see Figures 4.10 and 4.11). Interestingly it can be seen in Figure 6.13 that the hyperkyphosis Cobb angles (>45°) demonstrate a negative correlation with thoracic vertebrae SUVm and this was found to be statistically significant ($r=-0.850$, $p<0.01$). This suggests that the patients with increasingly hyperkyphotic spines have reduced thoracic vertebrae SUVms. This supports what we have seen previously in Figures 4.10 and 4.11 where a negative trend was identified between vertebrae SUVm and age. It was proposed that this

reduction in vertebrae SUVm was due to reduced BMD with age. It is also proposed that this is what this trend is demonstrating (Figure 6.13), that the hyperkyphotic spines have low BMD which is one of the main reasons for this hyperkyphotic curvature (125). Hyperkyphosis also may result from either muscle weakness and degenerative disc disease, leading to vertebral fractures all of which are common in AKU patients (125).

Interestingly, when the hyperkyphotic Cobb angles were correlated with thoracic IVD SUVms (Figure 6.15) a negative statistically significant correlation was identified ($r=-0.723$, $p<0.01$). This suggests that increasingly hyperkyphotic spines have reduced thoracic IVD SUVms. The negative correlation of the hyperkyphosis Cobb angles with thoracic IVD SUVm supports what has been presented previously in Figure 4.13. Figure 4.13 demonstrates the inverted 'U' shaped trend of thoracic IVD SUVms with age. It is clear in the oldest patients, around the age of 55-60, that there is a reduction in IVD SUVm with age. It is proposed that this reduction in SUVm is likely to be due to reduced deposition of hydroxyapatite/calcium pyrophosphate dihydrate crystals into the IVDs that occurs as part of AKU disease pathophysiology. This reduction in deposition may be due to complete calcification of the IVD and or spinal fusion. Once this has been achieved deposition of hydroxyapatite/calcium pyrophosphate dihydrate crystals into the IVDs stops. It is understood that ^{18}F binds preferentially to newly laid down hydroxyapatite due to the higher availability of binding sites, once new hydroxyapatite / calcium pyrophosphate dihydrate crystals stop being laid down ^{18}F does not preferentially bind to those regions therefore the SUVms in those regions reduce.

When analysing the correlations between lumbar lordosis Cobb angles and the lumbar vertebrae and IVD SUVm no correlations were identified (Figures 6.14 and 6.16). There is no clinical definition of lumbar hyper or hypo lordosis in terms of using a Cobb angle. Clinicians often visually assess lumbar lordosis by assessing the arch and pelvic tilt (159). Lumbar lordosis is a unique structural characteristic of the normal human spine and phylogenetically is considered the key structural adaptation to bipedalism. An increased lumbosacral angle is known to augment the pressure on the posterior ligaments and facet joints of the spine, and ultimately causes lower back pain. Most clinicians advise their patients to abolish lumbar lordosis by carrying out flexion exercises to strengthen the muscles. Interestingly, a loss of lumbar lordosis is the most distinctive finding of the aging spine (160), and it is widely known the prevalence of lower back pain increases with age (161). Therefore, a positive correlation was expected between lumbar lordosis Cobb angle and lumbar vertebrae SUVm. Demonstrating that lower lumbar lordosis Cobb angles correlate with lower vertebrae SUVms, associated with older patients. However, when age was correlated with lumbar lordosis in this group no correlation was identified ($r=0.01$, $p>0.05$) which may explain why these results were not found.

Lastly scoliosis Cobb angles were correlated with the IVD and vertebrae SUVms of which no correlations were identified (Figures 6.17 and 6.18). Scoliosis is characterised by a lateral deviation of the spine in the coronal plane and is clinically defined as a spinal curvature of ten degrees or more (124,162). The prevalence of adult scoliosis in the USA has been reported as ranging from 2%-32% (163). In the SONIA 2 AKU patient group, 32.5% of the patients have clinically defined

degenerative scoliosis. Degenerative scoliosis is a deformity that develops from a previously straight spine, caused by accelerated degeneration of the spine with progressive disc and facet degeneration (163). In AKU it is understood that the spine degenerates with radiological signs such as reduced IVD height, IVD calcifications, osteophyte formation and in severe cases spinal fusion. These changes to the spine, if more severe on one side compared to another, can lead to degenerative scoliosis. It was expected therefore that the scoliosis Cobb angle would be associated with increased IVD SUVms due to calcification of the IVDs resulting in spinal changes. Additionally, it was expected that higher scoliosis Cobb angles would also be associated with reduced vertebrae SUVms as this would reflect reduced BMD in the vertebrae with disease progression.

6.4.6 COBB ANGLE MRI vs X-Ray

Standing plain radiographs remain the gold standard for measuring spinal curvatures. Clinicians utilise the Cobb angle methodology to obtain measurements of scoliosis, thoracic kyphosis and lumbar lordosis. Several studies have shown the variability and reliability of Cobb angle measurements. Loder *et al*. (164) described the interobserver variance of 11.8° and intraobserver variance of 9.6° when using the Cobb angle method to measure scoliosis using plain radiographs. Carman *et al*. (165) described that interobserver variations for measurements of the Cobb angle on radiographs of patients who had kyphosis (3.3°) were comparable with those on the radiographs of patients who had scoliosis (3.8°). It has been investigated in the literature whether alternative imaging modalities may be superior to the conventional X-Ray in obtaining more accurate measurements. In the literature, idiopathic scoliosis is the

deformity that has been investigated in terms of utilising alternative imaging methodologies as scoliosis is common in developing children and it is of concern that these patients are exposed to repeated ionizing radiation. Lee *et al*. (166) demonstrated the relationship between adolescent idiopathic scoliosis Cobb angle measurements obtained with standing plain radiographs and standard supine magnetic resonance images (MRI). They found that Cobb angles measured from supine MRI of the spine can be directly translated to Cobb angle measurements obtained from plain radiographs with an acceptable degree of accuracy. They proposed that this method could significantly reduce radiation exposure to these patients (166).

Tauchi *et al*. (167) discussed that measuring Cobb angles with X-rays is difficult as the resolution of the images makes it difficult to define the appropriate end plates of the vertebrae to measure. They stated that 3D-CT can provide more detailed images and hypothesised that Cobb angles in congenital scoliosis can be measured more accurately using this technique. This study concluded that Cobb angles assessed using the X-ray method produced similar variances as 3D-CT images suggesting that plain X-rays are clinically useful. However, they concluded that 3D-CT can provide more detailed images and can contribute greatly to the development of strategies for surgical treatment but exposes the patient to high levels of radiation.

Vavruch *et al*. (168) commented that 3D imaging is needed for the assessment of scoliosis due to the 3D nature of the disorder. The advantage of MRI is that it does not use radiation, however this method is time consuming and expensive. CT is superior to conventional radiographs however requires relatively high radiation

doses. They correlated the Cobb angles obtained from low dose CT and that measured from radiographs and found that the correlation was strong.

As presented, the literature primarily focuses on using scoliosis Cobb angles to compare different imaging modalities such as the conventional radiography with MRI and CT. In this chapter, thoracic kyphosis and lumbar lordosis were used to compare the Cobb angles obtained from X-ray and MRI images to see if standing and lying down alters the spinal measurements. The results obtained from the SONIA 2 group at visit one are consistent with the literature. Figure 6.19 demonstrates a positive statistically significant correlation between the thoracic kyphosis Cobb angle obtained from MRI and plain X-ray ($r=0.691$, $p<0.001$) and the difference being 9.14º between the two modalities (Table 6.1). A positive statistically significant correlation was also identified between the lumbar lordosis Cobb angles obtained from plain X-ray and MRI ($r=0.825$, $p<0.001$) (Figure 20). These results reflect that obtaining the thoracic kyphosis and lumbar lordosis Cobb angles from both MRI and plain X-ray both show very similar results and the pros and cons of both imaging modalities should be assessed to determine what modality is best for the patient.

6.4.7 BONE MINERAL DENSITY T-SCORE COMPARISONS

The assessment of BMD in AKU is important to measure as it is widely understood that arthritic changes to the IVDs with disease progression has direct implications to the bony vertebrae. It has also been hypothesised that in AKU HGA deposition in bone matrix and osteocytes may play a pathophysiological role in accelerating bone loss (148). DEXA is the gold standard for obtaining BMD T-scores and the WHO

classification to determine BMD is based solely on the DEXA assessment. The 'T-score' is a statistical definition which indicates the difference between patient's BMD and mean bone density of normal population in the age of 20 – 30. T-scores under the value of -2.5 are considered as osteoporotic, between -1 and -2.5 are defined as osteopenia and values of -1 and above are classed as normal (Table 1.4) (169). QCT is an alternative method of obtaining BMD that is obtained from CT imaging and has been proposed to be superior to DEXA for the assessment of accurate BMD T-scores.

All patients attending the NAC undergo QCT to determine BMD and the SONIA 2 clinical trial patients all undergo DEXA scanning to obtain BMD values. Chapter 5.4.6 discussed the pros and cons of both of these two methodologies and suggested that QCT may be superior, especially in AKU as this method has the ability to specifically measure volumetric trabecular bone in the spine, avoiding the IVDs that are often calcified (94). Artificially high BMD has been reported in DEXA reports of spinal arthropathy patients due to calcification of the IVDs and osteophyte formation resulting in high T-scores (148). This is because DEXA estimates the total amount of mineral in the path of the X-ray beam in the region of L2-L4 including the cortical and trabecular bone as well as the IVDs. Therefore, QCT imaging often results in lower T-scores than that of DEXA. QCT is also said to detect BMD changes earlier than DEXA due to the physiological effect of ageing and/or the menopause that affects trabecular bone first (96). Interestingly, the data analysed in this Chapter demonstrates these predictions.

In Chapter 5 it was shown (Figure 5.20) that the femur QCT T-scores reached higher values (ranging from -2.58 to 4.26) compared to the spine QCT T-scores (ranging from

-5.63 to 0.95). This suggests that the spine is affected by a loss of BMD to a higher extent than the femur which is consistent to what has been reported in the literature. This could be due to several reasons. The difference between velocities of bone loss in different parts of human body could be the main reason. Trabecular bone, found in the lumbar spine is known to have a more rapid rate of bone loss compared to cortical bone, typical of proximal femur. In addition, the hip is primarily weight bearing, which can result in increased BMD that has been shown to affect the hip and head of femur (169).

When T-scores of the spine and femur obtained from DEXA were plotted the range of T-scores were statistically different from the T-scores obtained from QCT. Figure 6.28 demonstrates the spine and femur T-scores obtained from DEXA. It is clear that the spine T-scores obtained from DEXA reach much higher values compared to that of the femur which is the opposite to what was found in Figure 5.20. The Spine T-scores range from -3.2 to 5.4 compared to -3.1 to 1.3 in the femur.

Importantly, independent t-tests revealed a significant difference ($p<0.001$) between the spine T-scores obtained from DEXA and QCT. The spine QCT T-scores are much lower (ranging from -5.63 – 0.95) than the DEXA spine T-scores (ranging from -3.2 – 5.4) which supports what has been stated in the literature. This increase in spine T-scores obtained from DEXA evident in Figure 6.28 is thought to represent IVD calcification and spinal arthropathy in AKU. It is clear in the literature that BMD measured by DEXA is variable depending on the site measured with significant differences identified between the T-scores obtained from the hip and spine (170). Increased calcification within the laminae and facet joints and increased

development of vascular calcifications, spondylophytes and endplate sclerosis is thought to render DEXA scanning of the lumbar spine unreliable (170). Discordance has also been reported between hip and spine BMD using DEXA that can affect overall diagnosis of osteoporosis (171). Because of this discordance in 2000, the WHO updated the guidelines stating that diagnostic use of T-scores should be reserved for the use of hip DEXA BMD measurements only and no other T-scores are to be used to diagnose osteoporosis. BMD measurements at sites other than the hip can be used however to assess relative risks of osteoporosis and fracture risk (172). These finding suggests that maybe QCT imaging is most appropriate to determine true hip and lumbar vertebrae BMD in AKU.

6.4.8 DEXA LUMBAR SPINE T-SCORE

It is agreed in the literature that BMD reduces with age in both males and females (145). Peak BMD is reached in women around the age of 20, and slightly older in men. Women experience a more rapid decline in BMD compared to males around the onset of the menopause as it is understood that reduction in oestrogen levels results in increased bone resorption and decreased BMD (146). Figure 6.21 demonstrates that in AKU after the age of around 45 there is a steady decline in the lumbar spine T-score with females having lower T-scores compared to males. This supports what has been stated in the literature. This was also found when the lumbar T-scores obtained from QCT were plotted with age where a statistically significant correlation was found ($r= -0.682$, $p<0.01$) (Figure 5.17).

It has been hypothesised that reductions in SUVm in the vertebrae may be due to reductions in BMD. Reduced BMD reflects a reduction in hydroxyapatite, reducing the amount available for ^{18}F to bind. When the lumbar spine T-score was correlated with the lumbar vertebrae SUVm a positive correlation was identified (Figure 6.22). However, this was only statistically significant in the female group ($r=0.345$, $p<0.05$). This supports what was found in Chapter 5 when QCT lumbar T-score was correlated with lumbar vertebrae SUVm (Figure 5.19). This supports the hypothesis that a reduction in BMD is associated with lower SUVms.

If reduced BMD in the vertebrae is associated with reduced SUVms it is therefore assumed that high SUVms in the IVDs would be associated with reduced BMD in the vertebrae. This assumption is supported by the results described in previous chapters where calcified IVDs are associated with age and disease progression, and with age there is a reduction in BMD therefore reduced amount of hydroxyapatite resulting in lower SUVms. This is what was found in the previous chapter where a negative statistically significant correlation was identified between the lumbar spine QCT T-score and the average lumbar spine IVD SUVm ($r= -0.470$, $p<0.05$) (Figure 5.18). Interestingly, this trend was not identified when the lumbar spine DEXA T-score was correlated with the average lumbar IVD SUVm (Figure 6.23), of which positive correlations were identified. In males, this positive correlation was statistically significant ($r=0.428$, $p<0.05$). This suggests that high lumbar BMD obtained from DEXA is associated with high IVD SUVms. High IVD SUVms suggests that there is calcification in the IVDs and therefore reflects an osteoarthritic spine. This confirms that lumbar DEXA T-scores of the spine are overestimated due to the IVD

calcifications as DEXA estimates the total mineral in the path in the region of L2-L4. This confirms what has been discussed in the literature that lumbar spine DEXA T-scores are unreliable in patients with spinal arthritis.

Correlations were also made to investigate if BMD correlated with thoracic kyphosis and lumbar lordosis Cobb angles. Figure 6.24 demonstrates the correlation between the DEXA lumbar spine T-score with thoracic kyphosis of which no statistically significant correlation was observed in both males and females. This was surprising as it was expected that a reduction in BMD would correlate with increased thoracic kyphosis Cobb angle as it is well documented that an osteoporotic spine undergoes structural changes characterised by an excessive thoracic kyphosis (known as Dowagers hump). Figure 6.24 does however demonstrate that males have a wider range of thoracic kyphosis Cobb angles ranging from 3-53 degrees compared to 29-56 degrees in females, although no statistical difference was found between male and female thoracic kyphosis Cobb angles (independent t-test $p>0.05$). Hyperkyphosis is defined as a Cobb angle of more than 45 degrees, normal thoracic kyphosis ranges from 20-45 degrees, (122). All females are within the normal and hyperkyphotic range (29-56 degrees). Although the males range from 3 to 53 degrees, Figure 6.24 demonstrates that only 2 patients lie in the hypokyphotic range the rest of the group fall around the normal and hyperkyphotic range.

When lumbar lordosis Cobb angle was plotted against the DEXA lumbar spine T-score again no correlation was identified in both males and females suggesting that BMD does not affect the lumbar lordotic curvature. Additionally, when male and female

lumbar lordosis Cobb angles were statistically compared no statistical difference was identified (independent t-test $p>0.05$). This is not consistent with what has been described in the literature. Hay *et al*. (173) described that females had a statistically significant greater curvature than males. The deeper lordosis among females was proposed to be due to the female lumbar curve being positioned more dorsally to reduce stress on the vertebral elements during pregnancy and nursing (173).

6.4.9 DEXA FEMUR T-SCORES

The DEXA femur T-scores were also correlated with the vertebrae and IVD SUVms to see if the same trends were identified as in the lumbar T-scores. Figure 6.26 demonstrates a positive correlation between the DEXA femur T-score and the lumbar vertebrae SUVm. This supports the trend observed between the DEXA lumbar spine T-score and the lumbar vertebrae SUVm (Figure 6.22) as well as the trend identified in Chapter 5 where the femur T-score was obtained from QCT (Figure 5.23). This supports the theory that high BMD is associated with increased ^{18}F uptake into bone due to the availability of hydroxyapatite for ^{18}F to bind to.

Figure 6.27 demonstrates a negative correlation between the DEXA femur T-score and the IVD SUVm. This supports the findings in Figure 5.22 where a low T-score is associated with high IVD SUVms. This supports the theory that low BMD would be associated with increased uptake in the IVDs due to disease progression and calcification. Older patients have reduced BMD and have increased IVD SUVm for this reason.

6.4.10 SUMMARY

This chapter aimed to investigate the correlations between the SONIA 2 SUVms reported in Chapter 4 with other patient data obtained from the clinical trial at visit 1, pre-nitisinone. This chapter focuses on the baseline data (pre-nitisinone) to exclude trends that may be associated with the drug nitisinone. The data used to correlate with the SUVms included serum and urine HGA concentrations, spinal flexibility measurements obtained from the physiotherapist, spinal curvature Cobb angles and DEXA BMD scores.

No statistically significant correlations were identified when correlating serum HGA with vertebrae and IVD SUVms. Serum HGA also did not correlate with age suggesting that the concentration of circulating HGA is not affected by disease progression with no differences identified between males and females. It is important to note that serum HGA represents the concentration of circulating HGA in the blood at a single time point, whereas age, vertebrae and IVD SUVms all represent lifelong exposure to HGA that is key to the progression of the disease. This was proposed to explain why no significant correlations were identified between these parameters. Correlations with urine HGA also did not show any significant correlations with SUVm suggesting that the total urinary output of HGA in 24 hours does not correlate with fluoride uptake in the vertebrae or IVDs. Again, it was proposed that it is not the amount of excreted HGA that is important in terms of disease progression it is the amount circulating and bathing the tissues over many years that is key to ochronosis hence why no correlations were identified.

When analysing spinal flexibility measurements obtained from the physiotherapist, negative statistically significant correlations were identified between lumbar side flexion and age. This reduction in flexibility with age is thought to represent reduced elasticity of tendons and ligaments due to deposition of HGA polymers rendering them stiff and brittle as well as solidifying IVDs. Interestingly positive statistically significant correlations were identified between lumbar side flexion and vertebrae SUVm supporting the hypothesis that SUVm decreases with age due to reduced BMD that will result in reduced spinal flexibility which are both linked to age. No statistically significant correlations were identified between cervical rotation with age or with vertebrae and IVD SUVms suggesting that lumbar side flexion may be a better indicator of disease state and progression.

In addition to this when the hyperkyphosis Cobb angles were correlated with thoracic vertebrae SUVm a negative trend was identified. This suggests that patients with hyperkyphotic spines have reduced thoracic vertebrae SUVms and this was proposed to be due to the reduction in BMD with age as reduced BMD in the spine is one of the main reasons for hyperkyphosis. When the hyperkyphotic Cobb angles were correlated with thoracic IVD SUVms a negative statistically significant correlation was found suggesting that hyperkyphosis is associated with reduced thoracic IVD SUVms. This supports the theory that the older patients have the most severe spinal deformity reflected by reduced IVD SUVms due to reduced deposition of calcium into the IVDs at the late stage of spinal arthropathy. This is characterised by complete calcification and spinal fusion and once this has been achieved it is thought that

calcium deposition stops therefore ^{18}F uptake stops hence the reduction in IVD SUVm.

Furthermore, positive correlations were also identified between the DEXA lumbar vertebrae T-score and lumbar vertebrae SUVm this supports the theory that reductions in SUVm is due to reductions in BMD. This was also the case when the DEXA femur T-score was correlated with lumbar vertebrae SUVm supporting this further that high BMD is associated with increased ^{18}F uptake into bone due to the availability of binding sites for ^{18}F to attach to. Additionally, negative correlations were found between the DEXA femur T-score and the IVD SUVm which supports the theory that low BMD is associated with increased uptake of ^{18}F into the IVDs due to disease progression and calcification.

Some interesting comparisons were also made in this chapter. This chapter included an investigation into whether Cobb angles obtained from conventional X-ray imaging and that obtained from MRI that showed a strong correlation. Thoracic kyphosis and lumbar lordosis Cobb angles were measured using the same technique on both X-ray and MRI modalities. Interestingly and in support of what has been documented in the literature a strong statistically significant correlation was identified between X-ray and MRI imaging modalities when both the lumbar lordosis and thoracic kyphosis Cobb angles were measured. It can be commented that it was easier to see the margins of bone using MRI compared to X-ray therefore, it could be said that it was easier to calculate the Cobb angles using MRI. However, the pros and cons of both modalities should be considered to determine which modality is best for the patient.

Another interesting comparison was made in this chapter between T-scores obtained from DEXA and QCT. It was described in Chapter 5 that QCT may be superior to DEXA in obtaining accurate BMD T-scores especially in AKU, as QCT can specifically measure volumetric trabecular bone in the spine avoiding the IVDs. This is particularly beneficial in AKU as the IVDs become calcified and this has been shown to result in artificially high BMD T-scores obtained from DEXA reports. This is thought to be because the DEXA scan estimates the total amount of mineral in the path of the X-ray beam in the region of L2-L4 including trabecular and cortical bone as well as the IVDs. In this chapter when T-scores of the spine obtained from DEXA were compared with that obtained from QCT the results were significantly different. The DEXA spine T-scores reached much higher values compared to that obtained from QCT and this is thought to represent the IVD calcification in AKU. It was suggested that the imaging modality QCT may be more appropriate to use in AKU for this reason.

This chapter has demonstrated the validity of the SUVm as a measure of arthropathy by providing evidence that this method correlates with other clinical manifestations of AKU.

7.0 GENERAL DISCUSSION

Early onset osteoarthropathy is an inevitable consequence of AKU resulting in considerable pain and suffering in peak adult-hood. Weight bearing joints are thought to be predominantly affected due to increased mechanical damage (1). The purpose of Chapter 3 was to investigate the natural history of AKU using the novel imaging modality ^{18}F-NaF PET. The anatomical distribution of increased tracer uptake was assessed by analysing the various bones and joints of the skeleton. Areas of increased tracer uptake in cartilage were considered areas associated with degeneration. Areas of increased tracer uptake in bone reflects active bone metabolism. Chapter 3 demonstrates the various bones and joints involved in AKU related degeneration across a broad range of ages. Cross sectional analysis across the ages enabled the natural history of the disease to be elucidated.

The bones associated with the highest incidences of increased tracer uptake were the hip, sacrum, lumbar and thoracic vertebral bodies (Figure 3.1). These bones are primarily weight bearing and involved in transferring load through the skeleton. The link between mechanical stress and ^{18}F uptake has been investigated in the literature. It is thought that mechanical stress results in bone formation via purinergic signalling, and bone formation results in new hydroxyapatite for ^{18}F to bind to. The lowest incidence of increased tracer uptake was identified in the bones of upper limb supporting the theory that bones associated with increased mechanical loading have increased tracer uptake. Interestingly the percentage incidence of ^{18}F uptake in bone decreased with age that is proposed to be due to reduced bone turnover associated with ageing. This data supports what has been published in the literature by Win *et al*. (117) who described that the uptake of ^{18}F in various skeletal sites is variable in a

control population. They found that different skeletal sites have different amounts of fluoride uptake in healthy control patients and described that ^{18}F tends to have greater deposition in the axial skeleton (e.g. vertebrae and pelvis) than in the appendicular skeleton. This supports the results described in Chapter 3 where the highest incidences were found in the hip, sacrum and lumbar and thoracic spine.

When the cartilaginous joints were analysed high incidences of ^{18}F uptake was found in the hip, knee, shoulder and joints of the foot (Figure 3.7). Interestingly, the incidence of ^{18}F uptake was found to increase with age in the shoulder, hip and knee and reached up to 100% in the oldest age group (61-70 years old) (Figure 3.10). These results all support the hypothesis that it is the weight bearing joints / very heavily used joints that are primarily affected in AKU.

When the cartilage scores were summated from all the joints scored for each patient (C-AT score explained in 2.4.6) and plotted against age a positive statistically significant correlation was found (Figure 3.11). It is clear that in AKU there was increased involvement in cartilage with age thought to be due to calcification within the cartilage, resulting in increased uptake of ^{18}F. This trend was also evident when the total clinical score (based on the AKUSSI consultant scoring) was plotted against age (Figure 3.15). When the anatomical threshold score was correlated with the clinicians score (Figure 3.13) a statistically significant correlation was found providing evidence that the methodology utilised in Chapter 3 was reliable and shows the same trend as the clinician's report.

Chapter 3 demonstrates the sensitivity of ^{18}F-NaF PET scans in detecting the distribution of increased ^{18}F uptake in AKU to determine the joints most affected by the disease. This data supports what has previously been published in the literature on the uptake of ^{18}F in various skeletal sites in a control population. The significant correlation with the clinical score implies that this methodology is reliable and demonstrates the same trend as the clinical reports therefore, is a suitable methodology to measure distribution of ^{18}F in bone and cartilage. Improvements to this method included obtaining a purely quantitative methodology; by obtaining measurements of radioactivity instead of measuring pixel values. The methodology described in Chapter 3 utilised the 'pixels above the threshold value' method to determine increased uptake. This threshold value was determined by the darkest pixels in the image based on analysing the histogram plot. An improvement would be to utilise the uptake of ^{18}F instead of the intensity. Another improvement was to utilise PET/CT images instead of the MIP PET images, which have superior spatial resolution and anatomical localisation, ensuring accurate placement of the ROIs.

Chapter 4 employed these improvements by utilising PET/CT imaging for improved anatomical localisation and obtaining the standardised uptake value as a measure of ^{18}F uptake. Uptake measurements are used to assess response to therapies and to distinguish degree of pathology (114). The mean standardised uptake value (SUVm) is a common method of expressing the uptake of PET tracers. The SUVm is a measure of radioactivity in a region of interest, normalised against the injected activity and the subject's body weight. The SUVm is defined as the activity concentration in the ROI (kBq/mL) divided by the decay corrected injected dose of ^{18}F-NaF, divided by the

patient body weight (kg) (116). Larger SUVms represent proportionally higher concentrations of radiotracer.

Chapter 4 introduced for the first time, quantitative SUVm measurements of bone and cartilage to identify active arthropathy and to quantify disease state in a clinical trial group with AKU (SONIA 2). This methodology revealed a striking variation between AKU and control SUVms in the IVDs thought to represent calcification of the IVDs in AKU. The mechanism proposed is that calcium hydroxyapatite or calcium pyrophosphate dihydrate are deposited in the fibrocartilaginous IVDs in AKU due to biochemical alterations of the disease. ^{18}F binds to the calcium deposits resulting in high SUVms compared to the control. The SUVms obtained from the vertebrae in both AKU and control patients are similar across the lumbar and thoracic spine suggesting that generalised rates of bone turnover in AKU and control patients are comparable. The vertebrae SUVms were also found to be in line with what has been published in the literature (117), providing confidence in the method and quality of results. Longitudinal information was also elucidated when the SUVms were plotted against age.

With age the AKU SUVms of the IVDs followed an interesting trend (the inverted 'U' shaped trend, Figures 4.12 and 4.13) that was strikingly different to that of the control group, that appears to remain stable with age. It is proposed that the AKU trend demonstrates the process of disc degeneration. The SUVm increases as calcium deposits get laid down, the plateau represents maximum calcification and reduced deposition due to no more free binding sites available for ^{18}F to bind, and the

reduction in SUVm represents vertebral fusion, complete calcification and/or reduced turnover (^{18}F binds preferentially to newly laid down and active bone). The initial increase in SUVm with age in the cartilage of AKU patients supports what was found in Chapter 3 where an increase in percentage incidence of ^{18}F uptake was found with age. In the bony vertebrae there was an age-related decline in SUVm in both AKU and control groups that is thought to represent reduced bone turnover with age. This also supports what was found in Chapter 3 where the percentage incidence of ^{18}F uptake in bone decreases with age. However, the vertebrae SUVms in the AKU group were lower compared to the control group. The proposed reason for this being that they have reduced BMD compared to controls of the same age. This is thought to be due to AKU patients having an imbalance in bone metabolism resulting in loss of BMD (148).

In summary, Chapter 4 introduced for the first time a quantitative measure of ^{18}F uptake in cartilage and bone of AKU patients. This data has provided new insights into bone metabolism and IVD degeneration in AKU and can be used to identify active arthropathy in the spine. The utility of SUVms in a clinical setting could provide clinicians with a quantitative tool to aid visual interpretation of PET images and to assess inter and intra patient differences.

Chapter 5 utilised the vertebrae and IVD SUVm methodology to assess a group of NAC patients that had visited the centre annually for four consecutive years. Visit one was baseline data, and thereafter the patients were all prescribed 2mg of nitisinone daily. The aim of this chapter was to utilise this quantitative measurement to track disease

progression in AKU longitudinally in response to nitisinone. The results described in this chapter support what was found in the previous chapter based on the SONIA 2 patients. The differences between AKU and control SUVms in the spine were reminiscent of what was seen in Chapter 4. The inverted 'U' trend was observed in the AKU group with age where the SUVms of the IVDs reached significantly higher values in the AKU group compared to the control (Figures 5.3 and 5.4). The negative trend observed when the vertebrae SUVms were plotted against age (Figures 5.5 and 5.6) was also observed in this chapter providing evidence of the repeatability and validity of the SUVm methodology.

The longitudinal changes in SUVms did not show any significant changes across the visits from baseline. The effect of nitisinone could not be fully elucidated as there was no AKU no-treatment control group to draw a comparison to. However, this result could be demonstrating that nitisinone is stabilising the progression of the disease. When the SONIA 2 clinical trial is complete longitudinal data will be available on a no-treatment AKU group for comparison allowing this important comparison to be made. It was also proposed that four years on nitisinone may not be long enough to identify any changes in ^{18}F uptake into bone and cartilage since years of HGA exposure causes ochronosis over a period of many years. At the very least, nitisinone could be expected to slow the progression of the AKU. Therefore, for the effect of nitisinone on the spine to be further investigated, many more years of data will be required to assess the long-term effects of the drug.

Correlations were made between the IVD and vertebrae SUVms with the total clinical score and the total anatomical threshold score (method used in Chapter 3). Positive statistically significant correlations were identified between both the total clinical and total anatomical threshold scores with the IVD SUVms. Negative statistically significant correlations were identified when the vertebrae SUVms were correlated with the total clinical and total anatomical threshold scores. These correlations suggest that the 3 methodologies all demonstrate the same trends.

Spinal pain scored by the patient was also correlated with IVD and vertebrae SUVms. Increased IVD SUVms were associated with increased spinal pain as well as the total clinical and anatomical threshold scores and is hypothesised to be due to disc calcification and degeneration with age. In contrast a negative correlation was identified between spinal pain and vertebrae SUVms. High vertebrae SUVms are associated with low pain scores and lower total clinical and total anatomical threshold scores proposed to be due to active bone remodelling in a healthy spine.

BMD was also investigated to determine if AKU patients had altered bone metabolism. Interestingly high IVD SUVms correlated with low lumbar QCT T-scores reflecting an osteoarthritic spine with calcified IVDs. Conversely high vertebrae SUVms correlated with high lumbar T-scores reflecting active bone remodelling and normal BMD.

Chapter 5 demonstrated the repeatability of the SUVm methodology and confirmed the potential use of this method in a clinical setting as a quantitative measure of

arthropathy in the spine. Chapter 5 also revealed that the methodology correlates well with the clinician's report, the anatomical threshold methodology as well as patient pain scores. The aim of Chapter 6 was to utilise the SONIA 2 SUV data to correlate with other patient data obtained as part of the SONIA 2 clinical trial. Chapter 6 focused on baseline data (pre-nitisinone) to exclude trends that may be associated with nitisinone. The clinical data used to correlate with the SUV data included serum and urine HGA concentrations, spinal flexibility measurements, spinal curvature Cobb angles and DEXA BMD scores.

A reduction in spinal flexibility was found with age, thought to represent reduced elasticity of tendons, ligaments and IVDs due to the deposition of HGA in AKU rendering them stiff and brittle. Interestingly, when correlated with the SUVm data a positive correlation was identified between lumbar side flexion and vertebrae SUVm. This supports the hypothesis that the SUVm decreases with age due to reduced BMD with age and this is associated with reduced spinal flexibility. Lumbar side flexion was concluded to be a good indicator of disease progression in contrast to cervical spine rotation that found no clinical significant correlations.

To support this, hyperkyphotic Cobb angles demonstrated a negative correlation with thoracic vertebrae SUVms suggesting that patients with hyperkyphotic spines have reduced thoracic SUVms proposed to be due to reduced BMD with age, as reduced BMD in the spine is one of the main reasons for hyperkyphosis. The hyperkyphosis Cobb angle also demonstrated a negative correlation with the thoracic IVD SUVm suggesting that the hyperkyphosis is associated with reduced IVD SUVms. This

supports the hypothesis that older patients have the most severe spinal degeneration reflected by reduced IVD SUVms.

When DEXA lumbar vertebrae T-score and the lumbar vertebrae SUVm was correlated, a statistically significant positive correlation was observed supporting the theory that reductions in vertebrae SUVm may be due to reductions in BMD. This correlation was also identified in Chapter 4 where the lumbar QCT T-score demonstrated a positive correlation with the lumbar vertebrae SUVm. A comparison was also made between DEXA and QCT to determine what imaging modality was superior in terms of measuring BMD. DEXA scores were found to reach much higher T-scores in the spine compared to QCT. The proposed reason for this being due to calcification of the IVDs. It was concluded that QCT may be superior to DEXA as QCT measures volumetric trabecular bone unlike DEXA that measures all the mineral in the path of the X-ray beam in the region of L2-L4 including the IVDs. Chapter 6 has demonstrated the validity of the SUVm as a measure of arthropathy by providing evidence that this method correlates with other clinical manifestations of AKU.

All in all this thesis has provided new insights into spinal arthropathy in AKU, the utilisation of novel quantitative techniques demonstrated in this thesis can be used to aid in clinical interpretation of PET scans as well as providing a measure of disease severity and to analyse disease progression and response to therapy.

8.0 REFERENCES

1. Ranganath LR, Jarvis JC, Gallagher JA. Recent advances in management of alkaptonuria (invited review; best practice article). J Clin Pathol. 2013 May;66(5):367–73.
2. Taylor AM, Boyde A, Wilson PJM, Jarvis JC, Davidson JS, Hunt JA, et al. The role of calcified cartilage and subchondral bone in the initiation and progression of ochronotic arthropathy in alkaptonuria. Arthritis Rheum. 2011 Dec;63(12):3887–96.
3. Gallagher J, Taylor A, Boyde A, Jarvis J, Ranganath L. Recent advances in understanding the pathogenesis of ochronosis:Najnowsze postępy w zrozumieniu patogenezy ochronozy. Reumatologia. 2012 Sep50(4):316-323.
4. Fisher AA, Davis MW. Alkaptonuric ochronosis with aortic valve and joint replacements and femoral fracture: a case report and literature review. Clin Med Res. 2004 Nov;2(4):209–15.
5. Stenn F, Milgram J, Lee S, Weigand R, Veis A. Biochemical identification of homogentisic acid pigment in an ochronotic egyptian mummy. Science. 1977 Aug;197(4303):566-568.
6. Lee SL, Stenn FF. Characterization of Mummy Bone Ochronotic Pigment. JAMA J Am Med Assoc. 1978 Jul;240(2):136.
7. Aquaron R. Alkaptonuria: A very rare metabolic disorder. Vol. 50, Indian Journal of Biochemistry and Biophysics. 2013 Oct;50(5):339–44.
8. Mistry JB, Bukhari M, Taylor AM. Alkaptonuria. Rare Dis. 2013 Dec;18;1.e27475. DOI: 10.4161/rdis.27475.
9. Phornphutkul C, Introne WJ, Perry MB, Bernardini I, Murphey MD, Fitzpatrick DL, et al. Natural History of Alkaptonuria. N Engl J Med. 2002 Dec;347(26):2111–21.
10. Benedek TG. Rudolph virchow on ochronosis. Arthritis Rheum. 1966 Feb;9(1):66–71.
11. Scriver CR. Garrod's Croonian Lectures (1908) and the charter 'Inborn Errors of Metabolism': Albinism, alkaptonuria, cystinuria, and pentosuria at age 100 in 2008. J Inherit Metab Dis. 2002 Oct;31(5):580-98.
12. Garrod AE, Oxon MA. The Incidence of Alkaptonuria: A Study in Chemical Individuality 1902. Yale J Biol Med. 2002 Jul-Aug;75(4):221–31.
13. Gallagher JA, Dillon JP, Sireau N, Timmis O, Ranganath LR. Alkaptonuria: An example of a “fundamental disease”-A rare disease with important lessons for more common disorders. Semin Cell Dev Biol. 2016 Apr;52(3):53–7.
14. Suwannarat P, O’Brien K, Perry MB, Sebring N, Bernardini I, Kaiser-Kupfer MI, et al. Use of nitisinone in patients with alkaptonuria. Metabolism. 2005 Jun;54(6):719–28.
15. Zatková a, de Bernabé DB, Poláková H, Zvarík M, Feráková E, Bosák V, et al. High frequency of alkaptonuria in Slovakia: evidence for the appearance of multiple mutations in HGO involving different mutational hot spots. Am J Hum Genet. 2000 Nov;67(5):1333–9.

16. Al-Sbou M, Mwafi N. Nine cases of Alkaptonuria in one family in southern Jordan. Rheumatol Int. 2012 Mar;32(3):621–5.

17. Mannoni A, Selvi E, Lorenzini S, Giorgi M, Airò P, Cammelli D, et al. Alkaptonuria, Ochronosis, and Ochronotic Arthropathy. Vol. 33, Seminars in Arthritis and Rheumatism. 2004 Feb;33(4):239–48.

18. Al-Sbou M. Novel mutations in the homogentisate 1,2 dioxygenase gene identified in Jordanian patients with alkaptonuria. Rheumatol Int. 2012 Jun;32(6):1741–6.

19. Granadino B, Beltran-Valero de Bernabe D, Fernandez-Canon JM, Penalva MA, Rodriguez de Cordoba S. The human homogentisate 1,2-dioxygenase (HGO) gene. Genomics. 1997 Jul;43(2):115–22.

20. Zatkova A, Nemethova M. Genetics of alkaptonuria – an overview. Acta Fac Pharm Univ Comenianae. 2015 May;62(11):27–32.

21. Zatkova A. An update on molecular genetics of Alkaptonuria (AKU). J Inherit Metab Dis. 2011 Dec;34(6):1127–36.

22. Vilboux T, Kayser M, Introne W, Suwannarat P, Bernardini I, Fischer R, et al. Mutation spectrum of homogentisic acid oxidase (HGD) in alkaptonuria. Human Mutat. 2009 Dec;30(12): 1611–9.

23. Nemethova M, Radvanszky J, Kadasi L, Ascher DB, Pires DE V, Blundell TL, et al. Twelve novel HGD gene variants identified in 99 alkaptonuria patients: focus on “black bone disease” in Italy. Federica Genov Jozef Rovensky Eur J Hum Genet. 2016 Jan;24(1):66–72.

24. Martin JP, Batkoff B. Homogentisic acid autoxidation and oxygen radical generation: implications for the etiology of alkaptonuric arthritis. Free Radic Biol Med. 1987 Jun;3(4):241–50.

25. Kotob SI, Coon SL, Quintero EJ, Weiner RM. Homogentisic acid is the primary precursor of melanin synthesis in Vibrio cholerae, a Hyphomonas strain, and Shewanella colwelliana. Appl Environ Microbiol. 1995 Apr;61(4):1620–2.

26. Kahveci R, Ergüngör MF, Günaydin A, Temiz A. Alkaptonuric patient presenting with “black” disc: A case report. Acta Orthop Traumatol Turc. 2013 May;47(2):134–8.

27. O’Brien WM, La Du BN, Bunim JJ. Biochemical pathologic and clinical aspects of alcaptonuria, ochronosis, and ochronotic arthropathy: Review of World Literature (1584–1962). Am J Med. 1963 Dec;36(6):813–38.

28. Acar MA, Erkocak ÖF, Aydin BK, Altan E, Şenaran H, Elmadağ NM. Patients with black hip and black knee due to ochronotic arthropathy: Case report and review of literature. Oman Med J. 2013 Nov;28(6):448–9.

29. Wilke A, Steverding D. Ochronosis as an unusual cause of valvular defect: a case report. J Med Case Rep. 2009 Nov;27(3):9302.

30. Ozmanevra R, Guran O, Karatosun V, Gunal I. Total knee arthroplasty in ochronosis: a case report and critical review of the literature. Eklem Hastalik Cerrahisi. 2013 Mar;24(3):169–72.

31. Helliwell TR, Gallagher JA, Ranganath L. Alkaptonuria - A review of surgical and autopsy pathology. Histopathology. 2008 Nov;53(5):503–12.

32. Hannoush H, Introne WJ, Chen MY, Lee SJ, O'Brien K, Suwannarat P, et al. Aortic stenosis and vascular calcifications in alkaptonuria. Mol Genet Metab. 2012 Feb;105(2):198–202.

33. Taylor AM, Fraser WD, Wilson PMJ, Ranganath LR, Gallagher JA. Ultrastructural studies on the binding of ochronotic pigment to collagen fibres in cartilage and bone in vivo and in vitro. Calcif Tissue Int. 2009 Aug;85(2):187.

34. Taylor AM, Wlodarski B, Prior IA, Wilson PJM, Jarvis JC, Ranganath LR, et al. Ultrastructural examination of tissue in a patient with alkaptonuric arthropathy reveals a distinct pattern of binding of ochronotic pigment. Rheumatology (Oxford). 2010 Jul;49(7):1412–4.

35. Taylor AM, Boyde A, Wilson PJM, Jarvis JC, Davidson JS, Hunt JA, et al. The role of calcified cartilage and subchondral bone in the initiation and progression of ochronotic arthropathy in alkaptonuria. Arthritis Rheum. 2011 Dec;63(12):3887–96.

36. Gallagher J, Taylor A, Boyde A, Jarvis J. Recent advances in understanding the pathogenesis of ochronosis. Reumatologia. 2012 Sep;50(4):316-323.

37. Introne WJ, Gahl WA. Alkaptonuria. GeneReviews. University of Washington, Seattle; 1993-2018. Available from https://www.ncbi.nlm.nih.gov/books/NBK1454/

38. Gallagher JA, Dillon JP, Sireau N, Timmis O, Ranganath LR. Alkaptonuria: An example of a "fundamental disease"-A rare disease with important lessons for more common disorders. Semin Cell Dev Biol. 2016 Apr;52:53–7.

39. Sealock RR, Galdston M, Steele JM. Administration of Ascorbic Acid to an Alkaptonuric Patient. Exp Biol Med. 1940 Jun;44(2):580–3.

40. Wolff JA, Barshop B, Nyhan WL, Leslie J, Seegmiller JE, Gruber H, et al. Effects of ascorbic acid in alkaptonuria: alterations in benzoquinone acetic acid and an ontogenic effect in infancy. Pediatr Res. 1989 Aug;26(2):140–4.

41. De Haas V, Carbasius Weber EC, de Klerk JB, Bakker HD, Smit GP, Huijbers WA, et al. The success of dietary protein restriction in alkaptonuria patients is age-dependent. J Inherit Metab Dis. 1998 Dec;21(8):791–8.

42. Morava E, Kosztolányi G, Engelke UFH, Wevers RA. Reversal of clinical symptoms and radiographic abnormalities with protein restriction and ascorbic acid in alkaptonuria. Ann Clin Biochem. 2003 Jan;40(1):108–11.

43. McKiernan PJ. Nitisinone for the treatment of hereditary tyrosinemia type I. Expert Opin Orphan Drugs. 2013 Apr;1(6):491–7.

44. Introne WJ, Perry MB, Troendle J, Tsilou E, Kayser MA, Suwannarat P, et al. A 3-year randomized therapeutic trial of nitisinone in alkaptonuria. Mol Genet Metab. 2011 Aug;103(4):307–14.

45. Hall AK, Ranganath LR, Milan A, Hughes A, Olsson B, Szamosi J, et al.

Suitability Of Nitisinone In Alkaptonuria 1 (SONIA 1): Results of a dose-response study of once-daily nitisinone on 24-hour urinary homogentisic acid excretion (u-HGA 24) in patients with alkaptonuria. Ann Rheum Dis. 2016 Feb;75(2):362-7.

46. Cox TF, Ranganath L. A quantitative assessment of alkaptonuria. J Inherit Metab Dis. 2011 Dec;34(6):1153–62.

47. Welcome To The Alkaptonuria Society - AKU Society [Internet]. [cited 2017 Mar 19]. Available from: http://www.akusociety.org.

48. Lock E, Ranganath LR, Timmis O. The Role of Nitisinone in Tyrosine Pathway Disorders. Curr Rheumatol Rep. 2014 Nov;16(11):457

49. Partners in DevelopAKUre [Internet] Retrieved from http://pathlabs.rlbuht.nhs.uk/developakure.pdf.

50. DevelopAKUre Home [Internet]. [cited 2017 Mar 19]. Available from: http://www.developakure.eu/.

51. Cucchiarini M. Biological Systems: Open Access The Biology of Articular Cartilage: An Overview? Biol Syst Open Access. 2013;2(1):104-105.

52. Ulrich-Vinther M, Maloney MD, Schwarz EM, Rosier R, O'Keefe RJ. Articular cartilage biology. J Am Acad Orthop Surg. 2003 Nov-Dec,11(6):421–30.

53. Martini FH, NathJL, Bartholomew EF. Fundamentals of Anatomy and Physiology, ninth edition; Pearsons Eduction;2012.

54. Sophia Fox AJ, Bedi A, Rodeo SA. The basic science of articular cartilage: structure, composition, and function. Sports Health. 2009 Nov;1(6):461–8.

55. Poole CA. Articular cartilage chondrons : form, function and failure. J Anat. 1997 Jul;191(1):1–13.

56. Alexopoulos LG, Setton L a, Guilak F. The biomechanical role of the chondrocyte pericellular matrix in articular cartilage. Acta Biomater. 2005 May;1(3):317–25.

57. Sobol E, Shekhter A, Guller A, Baum O, Baskov A. Laser-induced regeneration of cartilage. J Biomed Opt. 2011 Aug;16(8):80902.

58. Poole, C A, Ayad S, Gilbert RT. Chondrons from Articular Cartilage. J Cell Sci. 1992 Sep;103(4):1101–10.

59. Akkiraju H, Nohe A. Role of Chondrocytes in Cartilage Formation, Progression of Osteoarthritis and Cartilage Regeneration. J Dev Biol. 2015 Dec;3(4):177–92.

60. Liacini A, Sylvester J, Li WQ, Huang W, Dehnade F, Ahmad M, et al. Induction of matrix metalloproteinase-13 gene expression by TNF-α is mediated by MAP kinases, AP-1, and NF-κB transcription factors in articular chondrocytes. Exp Cell Res. 2003 Aug;288(1):208–17.

61. Hochberg MC, Yerges-Armstrong L, Yau M, Mitchell BD. Genetic epidemiology of osteoarthritis: recent developments and future directions. Curr Opin Rheumatol. 2013 Mar;25(2):192–7.

62. Chen D, Shen J, Zhao W, Wang T, Han L, Hamilton JL, et al. Osteoarthritis: toward a comprehensive understanding of pathological mechanism. Bone Res. 2017 Jan 17;5:16044.

63. Lindahl A. From gristle to chondrocyte transplantation: treatment of cartilage injuries. Philos Trans R Soc London B Biol Sci. 2015 Oct;19(370):1680.

64. Gelse K, Pöschl E, Aigner T. Collagens--structure, function, and biosynthesis. Adv Drug Deliv Rev. 2003 Nov;55(12):1531–46.

65. Hulmes DJS. Collagen diversity, synthesis and assembly. In: Collagen: Structure and Mechanics. 2008. p.15–47.

66. Kini U, Nandeesh BN. Physiology of Bone Formation, Remodeling, and Metabolism. In: Radionuclide and Hybrid Bone Imaging. Berlin, Heidelberg: Springer Berlin Heidelberg; 2012. p.29–57.

67. Buckwalter JA, Glimcher MJ, Cooper RR, Recker R, A Buckwalter BJ, Iowa City Md, et al. Bone Biology Bone Biology Part I: Structure, blood supply, Cells, Matrix, and Mineralisation. J Bone Jt Surg J Bone Jt Surg Am. 1995;77:1256–75.

68. Standring S. Gray's Anatomy: The Anatomical Basis of Clinical Practice. Vol. 2, Development. 2008. p.1389-1406.

79. You L, Temiyasathit S, Lee P, Kim CH, Tummala P, Yao W, et al. Osteocytes as mechanosensors in the inhibition of bone resorption due to mechanical loading. Bone. 2008 Jan;42(1);172-9.

70. Bonewald LF, Johnson ML. Osteocytes, mechanosensing and Wnt signaling. Vol. 42, Bone. 2008. p.606–15.

71. Rucci N. Molecular biology of bone remodelling. Clin Cases Miner Bone Metab. 2008 Jan-Apr;5 (1):49–56.

72. Castañeda S, Roman-Blas JA, Largo R, Herrero-Beaumont G. Subchondral bone as a key target for osteoarthritis treatment. Biochem Pharmacol. 2012 Feb;83(3):315–23.

73. Wen C, Lu WW, Chiu KY. Importance of subchondral bone in the pathogenesis and management of osteoarthritis from bench to bed. J Orthop Transl. 2014 Jan;2(1):16–25.

74. Gallagher JA, Ranganath LR, Boyde A. What does the arthropathy of alkaptonuria teach us about disease mechanisms in osteoarthritis and ageing of joints? Rheumatology (Oxford). 2016 Jul;55(7):1151–2.

75. Boyde A, Davis GR, Mills D, Zikmund T, Cox TM, Adams VL, et al. On fragmenting, densely mineralised acellular protrusions into articular cartilage and their possible role in osteoarthritis. J Anat. 2014 Oct;225(4):436–46.

76. Wang F, Cai F, Shi R, Wang X-H, Wu X-T. Aging and age related stresses: a senescence mechanism of intervertebral disc degeneration. Osteoarthr Cartil. 2016 Mar;24(3):398–408.

77. Urban JPG, Roberts S. Degeneration of the intervertebral disc. Arthritis Res

Ther. 2003;5(3):120–30.

78. Ouyang Z-H, Wang W-J, Yan Y-G, Wang B, Lv G-H. The PI3K/Akt pathway: A critical player in intervertebral disc degeneration. Oncotarget. 2015 Jun;8(34):57870-57881.

79. Etzkorn E, Oliver AM. Not just another case of low back pain. BMJ Case Rep. 2014 Apr. DOI 10.1136/bcr-2014-204085.

80. Kohn MD, Sassoon AA, Fernando ND. Classifications in Brief: Kellgren-Lawrence Classification of Osteoarthritis. Clin Orthop Relat Res. 2016 Aug;474(8):1886–93.

81. Siemens AG, Healthcare. Background Information: The History of Computed Tomography at Siemens. [Internet]. [cited 2017 April 15]. Available from: https://www.siemens.com/press/pool/de/feature/2015/healthcare/2015-07-ct-40/background-history-ct-siemens-e.pdf

82. Cierniak R. Some Words About the History of Computed Tomography. In: X-Ray Computed Tomography in Biomedical Engineering. 2011. p.1–14.

83. Bradley WG. History of medical imaging. Proc Am Philos Soc. 2008 Sep;152(3):349–61.

84. Scatliff JH, Morris PJ. From Roentgen to magnetic resonance imaging: the history of medical imaging. N C Med J. 2014 Mar;75(2):111–3.

85. Hayashi D, Roemer FW, Jarraya M, Guermazi A. Imaging of osteoarthritis. In: Geriatric Imaging. 2013. p.93–121.

86. Suetens P. Fundamentals of medical imaging. In: Fundamentals of Medical Imaging. 2009. p.128–58.

87. Herr KD. Radiology 101: The Basics and Fundamentals of Imaging, 3rd ed. Acad Radiol. 2010. p.269-275.

88. Lisle D. Imaging for students. Hodder Arnold; 2007. p.283.

89. Vinjamuri S, Ramesh CN, Jarvis J, Gallagher JA, Ranganath LL. Nuclear medicine techniques in the assessment of alkaptonuria. Nucl Med Commun. 2011 Oct;32(10):880–6.

90. Mandl P, Kainberger F, Friberg Hitz M. Imaging in osteoporosis in rheumatic diseases. Best Pract Res Clin Rheumatol. 2016 Aug;30(4):751–65.

91. Oei L, Koromani F, Rivadeneira F, Zillikens MC, Oei EHG. Quantitative imaging methods in osteoporosis. Quant Imaging Med Surg. 2016 Dec;6(6):680–98.

92. Toombs RJ, Ducher G, Shepherd JA, De Souza MJ. The Impact of Recent Technological Advances on the Trueness and Precision of DXA to Assess Body Composition. Obesity. 2012 Jan;20(1):30–9.

93. Yu W, Glüer CC, Fuerst T, Grampp S, Li J, Lu Y, et al. Influence of degenerative joint disease on spinal bone mineral measurements in postmenopausal women. Calcif Tissue Int. 1995 Sep;57(3):169–74.

94. Li N, Li X-M, Xu L, Sun W-J, Cheng X-G, Tian W. Comparison of QCT and DXA:

Osteoporosis Detection Rates in Postmenopausal Women. Int J Endocrinol. 2013 Mar 27;2013:895474.

95. Oei L, Koromani F, Rivadeneira F, Zillikens MC, Oei EHG. Quantitative imaging methods in osteoporosis. Quant Imaging Med Surg. 2016 Dec;6(6):680–98.

96. Kabayel DD, Kabayel D. The role of quantitative computed tomography and magnetic resonance imaging in diagnosis and follow-up of osteoporosis: A review. Turk J Phys Med Rehab. 2016;62(3):288–95.

97. Fallis A. Computed Tomography- Principles, Design, Artifacts, and Recent Advances. Vol. 53, Journal of Chemical Information and Modeling. 2013. p.1689-1699.

98. Hashefi M, Curiel R. Future and upcoming non-neoplastic applications of PET/CT imaging. Ann N Y Acad Sci. 2011 Jun;1228(1):167–74.

99. Boesen M, Ellegaard K, Henriksen M, Gudbergsen H, Hansen P, Bliddal H, et al. Osteoarthritis year in review 2016: imaging. Osteoarthr Cartil. 2017 Feb;25(2):216–26.

100. Rahmim A, Zaidi H. PET versus SPECT: strengths, limitations and challenges. Nucl Med Commun. 2008 Mar;29(3):193–207.

101. Rich DA. A brief history of positron emission tomography. J Nucl Med Technol. 1997 Mar;25(1):4–11.

102. Carlson S. A Glance At The History Of Nuclear Medicine. Acta Oncol (Madr). 1995 May;34(8):1095–102.

103. Portnow LH, Vaillancourt DE, Okun MS. The history of cerebral PET scanning: From physiology to cutting-edge technology. Neurology. 2013 Mar;80(10):952–6.

104. Kim EE, Inoue T, Lee MC, Wong WH. Clinical PET and PET/CT: Principles and applications. Clinical PET and PET/CT: Principles and Applications. 2013. p.1-398.

105. Raichle ME. Positron Emission Tomography. Nature. 1985 Oct;317(6):574–575.

106. Mick CG, James T, Hill JD, Williams P, Perry M. Molecular imaging in oncology: (18)F-sodium fluoride PET imaging of osseous metastatic disease. AJR Am J Roentgenol. 2014 Aug;203(2):263–71.

107. Grant FD, Fahey FH, Packard AB, Davis RT, Alavi A, Treves ST. Skeletal PET with ^{18}F-fluoride: applying new technology to an old tracer. J Nucl Med. 2008 Jan;49(1):68–78.

108. Dahlbom M, Hoffman EJ, Hoh CK, Schiepers C, Rosenqvist G, Hawkins RA, et al. Whole-body positron emission tomography: Part I. Methods and performance characteristics. J Nucl Med. 1992 Jun;33(6):1191–9.

109. Raynor W, Houshmand S, Gholami S, Emamzadehfard S, Rajapakse CS, Blomberg BA, et al. Evolving Role of Molecular Imaging with ^{18}F-Sodium Fluoride PET as a Biomarker for Calcium Metabolism. Curr Osteoporos Rep.

2016 Aug;14(4):115–25.

110. Blake GM, Siddique M, Frost ML, Moore AEB, Fogelman I. Imaging of Site Specific Bone Turnover in Osteoporosis Using Positron Emission Tomography. Curr Osteoporos Rep. 2014 Dec;12(4):475–85.

111. Czernin J, Satyamurthy N, Schiepers C. Molecular mechanisms of bone ^{18}F-NaF deposition. J Nucl Med. 2010 Dec;51(12):1826–9.

112. Wong KK, Piert M. Dynamic bone imaging with 99mTc-labeled diphosphonates and ^{18}F-NaF: Mechanisms and applications. J Nucl Med. 2013 Apr;54(4):590–9.

113. Segall G, Delbeke D, Stabin MG, Even-Sapir E, Fair J, Sajdak R, et al. SNM Practice Guideline for Sodium ^{18}F-Fluoride PET/CT Bone Scans 1.0. J Nucl Med. 2010 Nov;51(11):1813–20.

114. Thie JA. Understanding the standardized uptake value, its methods, and implications for usage. J Nucl Med. 2004 Sep;45(9):1431–4.

115. Kobayashi N, Inaba Y, Tateishi U, Yukizawa Y, Ike H, Inoue T, et al. New application of ^{18}F-fluoride PET for the detection of bone remodeling in early-stage osteoarthritis of the hip. Clin Nucl Med. 2013 Oct;38(10):379-83.

116. Win AZ, Aparici CM. Factors Affecting Uptake of NaF-18 by the Normal Skeleton. J Clin Med Res. 2014 Dec;6(6):435–42.

117. Win AZ, Aparici CM. Normal SUV values measured from Na^{18}F- PET/CT bone scan studies. Boswell CA, editor. PLoS One. 2014 Sep 25;9(9):108429.

118. Kinahan PE, Fletcher JW. Positron emission tomography-computed tomography standardized uptake values in clinical practice and assessing response to therapy. Semin Ultrasound CT MR. 2010 Dec;31(6):496–505.

119. Zasadny KR, Wahl RL. Standardized uptake values of normal tissues at PET with 2-[fluorine-18]-fluoro-2-deoxy-D-glucose: variations with body weight and a method for correction. Radiology. 1993 Dec;189(3):847–50.

120. Kobayashi N, Inaba Y, Yukizawa Y, Ike H, Kubota S, Inoue T, et al. Use of ^{18} F-fluoride positron emission tomography as a predictor of the hip osteoarthritis progression. Mod Rheumatol. 2015 Sep;25(6):925–30.

121. National Institute of Health. ImageJ [Internet]. [cited 2017 May 31]. Available from: https://imagej.nih.gov/ij/

122. Lafage V, Schwab F, Patel A, Hawkinson N, Farcy J-P. Pelvic Tilt and Truncal Inclination. Spine (Phila Pa 1976). 2009 Aug;34(17):E599–606.

123. Chernukha K V, Daffner RH, Reigel DH. Lumbar lordosis measurement. A new method versus Cobb technique. Spine (Phila Pa 1976). 1998 Jan;23(1):74-80.

124. Kim H, Kim HS, Moon ES, Yoon C-S, Chung T-S, Song H-T, et al. Scoliosis Imaging: What Radiologists Should Know. RadioGraphics. 2010 Nov;30(7):1823–42.

125. Katzman WB, Wanek L, Shepherd JA, Sellmeyer DE. Age-related hyperkyphosis: its causes, consequences, and management. J Orthop Sports

Phys Ther. 2010 Jun;40(6):352–60.

126. Clarkson H GG 1989. Musculoskeletal Assessment: Joint Range of Motion and Manual Muscle Strength. Williams Wilkins, Balt. 2000; p.158–160.

127. Levangie PK, Norkin CC. Joint Structure and Function: A Comprehensive Analysis. F A Davis Co. 2005; p.393–436.

128. Wong KK, Piert M. Reply: Regarding Dynamic Bone Imaging with 99mTc-Labeled Diphosphonates and ^{18}F-NaF: Mechanisms and Applications. J Nucl Med. 2013 Dec;54(12):2190–1.

129. Watanabe T, Takase-Minegishi K, Ihata A, Kunishita Y, Kishimoto D, Kamiyama R, et al. (18)F-FDG and (18)F-NaF PET/CT demonstrate coupling of inflammation and accelerated bone turnover in rheumatoid arthritis. Mod Rheumatol. 2016 Jul;26(2):180–7.

130. Frost ML, Cook GJR, Blake GM, Marsden PK, Benatar NA, Fogelman I. A prospective study of risedronate on regional bone metabolism and blood flow at the lumbar spine measured by ^{18}F-fluoride positron emission tomography. J Bone Miner Res. 2003 Dec;18(12):2215–22.

131. Rutkovskiy A, Stenslokken K-O, Vaage IJ. Osteoblast Differentiation at a Glance. Med Sci Monit Basic Res. 2016 Sep;26(22):95–106.

132. Kim JH, Liu X, Wang J, Chen X, Zhang H, Kim SH, et al. Wnt signaling in bone formation and its therapeutic potential for bone diseases. Ther Adv Musculoskelet Dis. 2013 Feb;5(1):13–31.

133. Sanchez C, Pesesse L, Gabay O, Delcour JP, Msika P, Baudouin C, et al. Regulation of subchondral bone osteoblast metabolism by cyclic compression. Arthritis Rheum. 2012;64(4):1193–203.

134. Puri T, Frost ML, Curran KM, Siddique M, Moore AEB, Cook GJR, et al. Differences in regional bone metabolism at the spine and hip: a quantitative study using ^{18}F-fluoride positron emission tomography. Osteoporos Int. 2013 Feb;24(2):633–9.

135. Riggs BL, Wahner HW, Dunn WL, Mazess RB, Offord KP, Melton LJ. Differential changes in bone mineral density of the appendicular and axial skeleton with aging: relationship to spinal osteoporosis. J Clin Invest. 1981 Feb;67(2):328–35.

136. Gallagher JA, Ranganath LR, Boyde A. Lessons from rare diseases of cartilage and bone. Curr Opin Pharmacol. 2015 Jun;22:107–14.

137. Abhishek A, Doherty M. Pathophysiology of articular chondrocalcinosis—role of ANKH. Nat Rev Rheumatol. 2011 Feb;7(2):96–104.

138. Gürkanlar D, Daneyemez M, Solmaz I, Temiz C. Ochronosis and lumbar disc herniation. Acta Neurochir (Wien). 2006 Aug;148(8):891–4.

139. Palazzi C, D'Angelo S, Leccese P, Nigro A, Olivieri I. Ochronotic arthropathy of the spine limited to the thoracic section. Rheumatology (Oxford). 2013 May;52(5):799.

140. Chakraverty JK, Lawson TM, Herdman G. Not just simple degenerative disc disease (alkaptonuria). Spine J. 2013 Aug;13(8):985–6.

141. Khan UN, Wenokor C, Altschuler EL. Back Pain in a Middle-Aged Man. Am J Phys Med Rehabil. 2015 May;94(5):42.

142. Jebaraj I, Chacko BR, Chiramel GK, Matthai T, Parameswaran A. A simplified staging system based on the radiological findings in different stages of ochronotic spondyloarthropathy. Indian J Radiol Imaging. 2013 Jan;23(1):101–5.

143. Tarihi G, Aktafi I, Akgün K, Çakmak B. Intervertebral disc calcification in the elderly: a case report. Turkish J Geriatr. 2007 Oct;10(1):37–9.

144. Kaneta T, Ogawa M, Daisaki H, Nawata S, Yoshida K, Inoue T. SUV measurement of normal vertebrae using SPECT/CT with Tc-99m methylene diphosphonate. Am J Nucl Med Mol Imaging. 2016 Sep;6(5):262–8.

145. Demontiero O, Vidal C, Duque G. Aging and bone loss: new insights for the clinician. Ther Adv Musculoskelet Dis. 2012 Apr;4(2):61–76.

146. Daly RM, Rosengren BE, Alwis G, Ahlborg HG, Sernbo I, Karlsson MK. Gender specific age-related changes in bone density, muscle strength and functional performance in the elderly: a-10 year prospective population-based study. BMC Geriatr. 2013 Jul; 6(1);13:71.

147. Chen W-T, Shih TT-F, Chen R-C, Lo S-Y, Chou C Te, Lee J-M, et al. Vertebral Bone Marrow Perfusion Evaluated with Dynamic Contrast-enhanced MR Imaging: Significance of Aging and Sex. Radiology. 2001 Jul;220(1):213–8.

148. Aliberti G, Pulignano I, Schiappoli A, Minisola S, Romagnoli E, Proietta M. Bone metabolism in ochronotic patients. J Intern Med. 2003;254(3):296–300.

149. Adams MC, Turkington TG, Wilson JM, Wong TZ. A systematic review of the factors affecting accuracy of SUV measurements. AJR Am J Roentgenol. 2010 Aug;195(2):310–20.

150. Kinahan PE, Fletcher JW. Positron emission tomography-computed tomography standardized uptake values in clinical practice and assessing response to therapy. Semin Ultrasound CT MR. 2010 Dec;31(6):496–505.

151. Wheater G, Elshahaly M, Tuck SP, Datta HK, van Laar JM. The clinical utility of bone marker measurements in osteoporosis. J Transl Med. 2013 Aug 29;11(1):201.

152. Leeming DJ, Alexandersen P, Karsdal MA, Qvist P, Schaller S, Tankó LB. An update on biomarkers of bone turnover and their utility in biomedical research and clinical practice. Eur J Clin Pharmacol. 2006 Oct;62(10):781–92.

153. Garnero P. The Utility of Biomarkers in Osteoporosis Management. Mol Diagn Ther. 2017 Aug;21(4):401–18.

154. Davison AS, Milan AM, Hughes AT, Dutton JJ, Ranganath LR. Serum concentrations and urinary excretion of homogentisic acid and tyrosine in normal subjects. Clin Chem Lab Med. 2015 Feb;53(3):81-3.

155. Weinstein JR, Anderson S. The Aging Kidney: Physiological Changes. Adv Chronic Kidney Dis. 2010 Jul;17(4):302–7.

156. Jonsson E, Ljungkvist I, Hamberg J. Standardized Measurement of Lateral Spinal Flexion and Its Use in Evaluation of the Effect of Treatment of Chronic Lower Back Pain. Ups J Med Sci. 1990 Mar;95(1):75–86.

157. Laxon S, Ranganath L, Timmis O. Living with alkaptonuria. BMJ. 2011 Sep;29;343:d5155.

158. Rana AQ, Saeed U, Abdullah I. Alkaptonuria, more than just a mere disease. J Neurosci Rural Pract. 2015 Apr-Jun;6(2):257–60.

159. Chun S-W, Lim C-Y, Kim K, Hwang J, Chung SG. The relationships between low back pain and lumbar lordosis: a systematic review and meta-analysis. Spine J. 2017 Aug;17(8):1180–91.

160. Takeda N, Kobayashi T, Atsuta Y, Matsuno T, Shirado O, Minami A. Changes in the sagittal spinal alignment of the elderly without vertebral fractures: a minimum 10-year longitudinal study. J Orthop Sci. 2009 Nov;14(6):748–53.

161. Dionne CE, Dunn KM, Croft PR. Does back pain prevalence really decrease with increasing age? A systematic review. Age Ageing. 2006 May 1;35(3):229–34.

162. Ohrt-Nissen S, Cheung JPY, Hallager DW, Gehrchen M, Kwan K, Dahl B, et al. Reproducibility of thoracic kyphosis measurements in patients with adolescent idiopathic scoliosis. Scoliosis Spinal Disord. 2017 Feb;21(1):12-4.

163. Kotwal S, Pumberger M, Hughes A, Girardi F. Degenerative Scoliosis: A Review. HSS Journal. 2011 Oct;7(3):257–64.

164. Loder RT, Urquhart A, Steen H, Graziano G, Hensinger RN, Schlesinger A, et al. Variability in Cobb angle measurements in children with congenital scoliosis. J Bone Joint Surg Br. 1995 Sep;77(5):768–70.

165. Carman DL, Browne RH, Birch JG. Measurement of scoliosis and kyphosis radiographs. Intraobserver and interobserver variation. J Bone Joint Surg Am. 1990 Mar;72(3):328–33.

166. Lee MC, Solomito M, Patel A. Supine magnetic resonance imaging cobb measurements for idiopathic scoliosis are linearly related to measurements from standing plain radiographs. Spine (Phila Pa 1976). 2013 May;38(11):656-61.

167. Tauchi R, Tsuji T, Cahill PJ, Flynn JM, Flynn JM, Glotzbecker M, et al. Reliability analysis of Cobb angle measurements of congenital scoliosis using X-ray and 3D-CT images. Eur J Orthop Surg Traumatol. 2016 Jan;26(1):53–7.

168. Vavruch L, Tropp H. A Comparison of Cobb Angle: Standing Versus Supine Images of Late-onset Idiopathic Scoliosis. Polish J Radiol. 2016 Jun;81:270–6.

169. Moayyeri A, Soltani A, Tabari NK, Sadatsafavi M, Hossein-neghad A, Larijani B. Discordance in diagnosis of osteoporosis using spine and hip bone densitometry. BMC Endocr Disord. 2005 Dec 11;5(1):3.

170. Lo HC, Kuo DP, Chen YL. Impact of beverage consumption, age, and site dependency on dual energy X-ray absorptiometry (DEXA) measurements in perimenopausal women: A prospective study. Arch Med Sci. 2017 Aug;13(5):1178–87.

171. El Maghraoui A, Mouinga Abayi DA, Rkain H, Mounach A. Discordance in Diagnosis of Osteoporosis Using Spine and Hip Bone Densitometry. J Clin Densitom. 2007 Aug;10(2):153–6.

172. Kanis JA, Glüer CC. An update on the diagnosis and assessment of osteoporosis with densitometry. Committee of Scientific Advisors, International Osteoporosis Foundation. Osteoporos Int. 2000 Feb;11(3):192–202.

173. Hay O, Dar G, Abbas J, Stein D, May H, Masharawi Y, et al. The lumbar lordosis in males and females, revisited. PLoS One. 2015 Aug;10(8):e0133685.